



The
University
Of
Sheffield.

Advanced Titanium Welding in Particle Physics and Aerospace Engineering

Michalis Benakis

A thesis submitted in partial fulfilment of the requirements for the degree of

Doctor of Philosophy in Applied Physics

The University of Sheffield
Faculty of Science
Department of Physics and Astronomy

December 2020

This thesis is dedicated to my true teachers – my parents – Soteris and Georgia.

Thank you for being the best one could ask for.

Acknowledgements

First of all I would like to express my gratitude to my main academic and industrial supervisors, Prof. Davide Costanzo and Dr. Alin Patran, for trusting in me and for providing their guidance and support throughout the project. Both of them went over and beyond the extra mile when unforeseen events were obstructing progression.

I would also like to thank my secondary supervisors Dr. Richard French, Dr. Christopher Lane, Dr. Sampan Seth and Matthew King for the opportunity to work with them and for their input in several stages of the project. I would also like to express my gratitude to my co-authors Dr. Chunling Du and Dr. Hector Marin-Reyes for their patience and for the wealth of technical knowledge they provided.

I should also thank the team of the Sheffield ATLAS and ESIM group, Paul, Sam and Ben first for the laughs and then for their technical support.

From ARTC I would like to thank the team of Aerospace Remanufacturing: Leon for teaching me the broad universe of welding, Davide and Norman for their guidance in metallography, and Helene and Chris for their support. Special thanks to my lunch-crew from the Intelligent Product Verification group, Sean, Wei Yi, Bisma, Zhang Zhen, Andy, Mato, Zhen Zhen and Shaowei. Also to the rest of the team that turned my time in Singapore in an exciting experience, Buenaventura and the Ang Mos Amir, Alberto, Dejanira and Luc.

My outermost gratitude is expressed to my parents Soteris and Georgia, for all their blood, their sweat and their sacrifices in supporting my journey in life. I would like to also thank my sister Tonia and my brother Andreas for understanding my absence all these years.

Last but not least, I want to thank my αρφούι, Xiaohui, for being the one to share this journey with since its very first days.

Abstract

The quest for answers that will unlock the mysteries of the cosmos and broaden our perception and understanding of the physical laws that govern the universe, demands studying particle collisions of high energies at particle accelerators. Monitoring of these collisions requires complex detectors whose development pushes the boundaries of engineering. In the present study advanced titanium welding is explored in the development of the new ATLAS Inner Tracker detector to be installed in line with the High-Luminosity Large Hadron Collider at CERN. Pulsed welding currents are employed to join thin titanium pipes used in the detector's evaporative CO₂ cooling system.

The benefits of the low heat input enabled by the welding process are utilised in the repair and remanufacturing industry of aerospace applications. Wire arc additive manufacturing is applied in the regeneration of aerospace components providing successive material deposition on a layer-upon-layer manner. To this extent investigations and implementations related to Pulsed Gas Tungsten Arc Welding are explored in the presented work aiming to further understand, implement and advance the welding process.

Assurance of the weld quality is furthered studied, as the outcome of the process depends on maintaining input parameters and welding conditions at optimum levels for the whole duration of the process. By implementing process monitoring methodologies, invaluable data are recorded whose analysis can be utilised in the detection of process disturbances and weld quality assessment.

Table of Contents

Acknowledgements.....	i
Abstract.....	ii
Table of Contents.....	iii
List of Figures	vi
List of Tables	viii
Declaration.....	ix
1 Introduction	1
1.1 Motivation and Problem Statement	1
1.2 Industry-Academia Collaboration	1
1.3 Work and Thesis Contribution	2
1.4 Project Chronology and Author Contributions	2
1.5 Thesis Content and Outline.....	4
2 Titanium Precision Engineering: Development of the ATLAS Detector and Links with Aerospace Engineering	5
2.1 Large Hadron Collider and the ATLAS Experiment	5
2.2 High Luminosity and the ATLAS Upgrade	6
2.3 Inner Tracker Cooling System Development	8
2.3.1 Pixel and Strips Cooling Loops	9
2.3.2 Material Selection and Requirements	10
2.3.3 The Need for Orbital Welding.....	11
2.3.4 Non-Destructive Evaluation and the Need for Welding Process Monitoring.....	12
2.4 Aerospace Engineering	13
2.4.1 Titanium in the Aerospace Industry.....	13
2.4.2 Additive Manufacturing in Aerospace Engineering	14
2.4.3 Aeroengines MRO	16
2.5 ATLAS ITk development and Aerospace Engineering Overlaps	18
2.6 Conclusion.....	18
3 Gas Tungsten Arc Welding (GTAW)	19
3.1 Arc Welding Introduction.....	19
3.1.1 Welding – Definition and Classification	19
3.1.2 Arc Welding Processes	20
3.1.3 Geometry of a Weld.....	21
3.1.4 Welding Parameters and Welding Procedure Specifications	22

3.1.5	Physics of Welding	22
3.2	Pulsed GTAW.....	26
3.3	Pulsing Utilisation.....	29
3.3.1	Orbital Welding	29
3.3.2	ATLAS ITk Development	30
3.3.3	Welding Defects in Orbital Welding.....	33
3.4	Conclusion.....	34
4	Welding-Based Additive Manufacturing.....	35
4.1	Additive Manufacturing and Remanufacturing	35
4.2	Wire Arc Additive Manufacturing	36
4.3	Desired bead geometry in Wire Arc Additive Manufacturing	36
4.4	Pulsed Wire Arc Additive Manufacturing	38
4.4.1	Materials and Methods.....	38
4.4.2	Effects in Geometry and Heat Affected Zone	43
4.4.2.1	Effects in geometry	44
4.4.2.2	Effects in heat affected zone	49
4.4.3	Current Mode Evaluation.....	51
4.4.4	Pulsing Effects on Bead Shape and Weld Pool Dynamics	52
4.4.5	Application of the results in Wire Arc Additive Manufacturing.....	55
4.5	Conclusion.....	56
5	Robotic Aerospace Remanufacturing System Development.....	58
5.1	Compressor Blades Regeneration.....	58
5.2	Benefits of the Robotic Solution	59
5.3	Robotic System Development.....	60
5.3.1	Designing of the System Process Management.....	60
5.3.2	Industry 4.0 Design Principles.....	62
5.3.3	Implementation of the Design Principles.....	63
5.4	Deposition Process.....	66
5.5	Welding Procedure Specifications	67
5.6	Evaluation of the First Results	68
5.7	Project Completion	71
5.8	Conclusion.....	71
6	Welding Process Monitoring.....	72
6.1	Definition and Systems Classification	72

6.2	Monitoring Sensor Technologies and Methodologies	73
6.2.1	Arc Sensors.....	73
6.2.2	Vision-Based Systems.....	74
6.2.3	Infrared Sensors	76
6.2.4	Ultrasonic Sensors.....	78
6.2.5	Other Process Monitoring Techniques	80
6.2.5.1	Spectroscopy.....	81
6.2.5.2	Acoustic Emissions	81
6.2.5.3	X-ray Radiography.....	82
6.2.6	Industrial Adoption Barriers.....	82
6.3	Welding Monitoring for ATLAS and Aerospace Remanufacturing.....	83
6.4	Fault Detection and Quality Assurance.....	84
6.4.1	Materials and Methods.....	84
6.4.2	Extracted Features Correlations	88
6.4.3	Supervised Classification.....	90
6.5	Conclusion.....	92
7	Technology Transfer	93
7.1	Welding 4.0 – The Future of Welding	94
7.1.1	Red Queen Hypothesis.....	94
7.1.2	Applied Industry 4.0 Principles	94
7.2	Nuclear Reactor Pressure Vessels Fabrication.....	96
7.3	The Need for Process Monitoring in In-Space Manufacturing	100
8	Conclusions	101
8.1	Overview and Project Outcomes	101
8.2	Outcome of Industry-Academia collaboration	102
8.3	Future Work.....	102
	Publications.....	104
	Author’s Publications to Date	104
	Glossary of Terms, Abbreviations and Acronyms	105
	References	107
	Appendix A: The Need for Process Monitoring in In-Space Manufacturing.....	118

List of Figures

Figure 2.1 – The ATLAS detector.....	6
Figure 2.2 – Particle tracking in different detector layers.	6
Figure 2.3 – The LHC/ATLAS running and update schedule.....	7
Figure 2.4 – Quarter view of the ATLAS ITk proposed layout.....	7
Figure 2.5 – ATLAS Inner Detector and ITk radiation length of different materials within the detector versus pseudorapidity.....	8
Figure 2.6 – Pixel half-ring assembly.....	9
Figure 2.7 – End-cap petal and barrel stave components for the Strip silicon sensors.....	9
Figure 2.8 – The cooling loops embedded in the support structures of an end-cap petal and a barrel stave.....	10
Figure 2.9 – Internal structure schematic of the stave core, including the silicon sensors and ASICs.	10
Figure 2.10 – Titanium fitting and electrical break developed for the Insertable B-Layer (IBL).....	11
Figure 2.11 – Diagram of a Strip stave cooling loop and the six welded joints on each loop.	12
Figure 2.12 – Vacuum leak test for the completed welded Strip stave cooling loops.....	13
Figure 2.13 – Totals for the overall market for additively manufactured parts in civil aviation, forecasted for the next ten years.	15
Figure 2.14 – Additively manufactured GE Aviation jet engine fuel nozzle.....	16
Figure 2.15 – Additively manufactured aerospace parts to replace their traditionally manufactured counterparts.	16
Figure 3.1 – Classification diagram of welding processes according to the latest British Standards... ..	19
Figure 3.2 – Gas Tungsten Arc Welding diagram and torch schematic.	21
Figure 3.3 – Root, fusion penetration, weld junction and zones of typical welds.....	21
Figure 3.4 – Forces in the Gas Tungsten Arc Welding Process.	23
Figure 3.5 – Plasma region forces: plasma jet force and electromagnetic force.	23
Figure 3.6 – Conceptual representation of the plasma jet and the Lorentz force by arc current and its self-induced magnetic field.....	24
Figure 3.7 – Convective current flow forces in the weld pool region.....	25
Figure 3.8 –Heiple-Roper theory for variable weld penetration.	26
Figure 3.9 – Thermal pulsing waveform.	27
Figure 3.10 – High frequency pulsing waveform.	27
Figure 3.11 – High and low frequency dual pulsing.....	28
Figure 3.12 – Variations in the welding positions along an orbital welding path.....	29
Figure 3.13 – VBCie HMS IP50 welding machine and Polysoude UHP closed chamber welding head.....	30
Figure 3.14 – Pixel cooling semi-circular loop demonstrator welding.....	31
Figure 3.15 – Custom-build jig structure for tube alignment.	32
Figure 3.16 – Ceramic electrical isolator.....	33
Figure 4.1 – Bead-on-plate welding process with its corresponding cross section.....	37
Figure 4.2 – Weld bead geometries characteristics for Wire Arc Additive Manufacturing (WAAM)... ..	38
Figure 4.3 – Experimental setup used for GTAW-based WAAM.	39
Figure 4.4 – Welding current modes with corresponding mean current calculations.	40
Figure 4.5 – Examples of linear bead-on-plate welds produced by each current mode.....	43
Figure 4.6 – Metallographic observations on etched cross sections of IN718/SS316L linear welds....	44
Figure 4.7 – Metallographic observations on etched cross sections of Ti-6-4 linear welds.	44

Figure 4.8 – Penetration depth versus bead width for IN718 on SS316L plates.	45
Figure 4.9 – Electric charge input versus bead width for IN718 on SS316L plates.	46
Figure 4.10 – Electric charge input results on penetration depth for IN718 on SS316L plates.	46
Figure 4.11 – Reinforcement cap and bead width for IN718 on SS316L plates.	47
Figure 4.12 – Total weld bead height as a combination of the penetration depth and the reinforcement cap for all the IN718 beads on SS316L plates.	47
Figure 4.13 – Electric charge input versus total height-to-penetration ratio for IN718 on SS316L plates.	48
Figure 4.14 – Electric charge input versus bead width for Ti-6-4.	48
Figure 4.15 – Reinforcement cap and bead width for Ti-6-4.	49
Figure 4.16 – HAZ measurements.	49
Figure 4.17 – Heat affected zone width results on Ti-6-4.	50
Figure 4.18 – Heat affected region shapes on different current modes.	50
Figure 4.19 – Heat affected zone shape changes on weld with similar heat input.	51
Figure 4.20 – Process outcome comparison on bead width for IN718/SS316L against Ti-6-4.	52
Figure 4.21 – Process outcome comparison on reinforcement cap for IN718/SS316L against Ti-6-4.	52
Figure 4.22 – Pulsing effects on bead shape and witnessed evidences of possible turbulences within the melt pool.	53
Figure 4.23 – Double circulation flow in melt pool.	55
Figure 4.24 – Combination of continuous current root pass with pulsed-current build-up passes in WAAM (Ti-6-4).	56
Figure 4.25 – Circular root and built-up passes on wire arc additive manufacturing.	56
Figure 5.1 – Jet engine sections and stages.	58
Figure 5.2 – Compressor blade tip-repair using GTAW-based material deposition.	60
Figure 5.3 – The concept’s process flow for compressor blades re-manufacturing.	61
Figure 5.4 – Different modules and subsystem forming the network of the robotic solution.	63
Figure 5.5 – Exchange of information between manufacturers, customers and service providers.	65
Figure 5.6 – Interconnection principle applied in the operational design of the robotic remanufacturing system.	66
Figure 5.7 – Schematic representation of the AM build-up process for the regeneration of a compressor blade.	67
Figure 5.8 – Thermal camera images that illustrate the gradual heat accumulation.	67
Figure 5.9 – Electric measurements during a material deposition pass.	68
Figure 5.10 – Material deposition root pass of a blade model tip-repair.	69
Figure 5.11 – 3D scanning modelling of a blade model before welding, after welding without additive material and after welding with additive material.	69
Figure 5.12 – 3D scanning of blade models with induced disturbances.	70
Figure 5.13 – Welded edge of compressor blade models and electrical signals analysis.	71
Figure 6.1 – Torch position sensing by through-the-arc electrical arc signal variations.	74
Figure 6.2 – Vision systems in welding monitoring.	75
Figure 6.3 – Diagram of ultrasonic probes arrangement used to monitor root-pass welds.	79
Figure 6.4 – Laser ultrasonic used for online inspection of a welding process.	79
Figure 6.5 – Ultrasonic reflections in resistance spot welding.	80
Figure 6.6 – Sensor box used for welding current and voltage measurements.	83
Figure 6.7 – Examples of square butt welds.	85

Figure 6.8 – Introducing Notches on SS316L plates using milling machining.....	85
Figure 6.9 – Welding conditions disturbances on SS316L square butt welds.	87
Figure 6.10 – Zones within a recorded welding signal corresponding to the different stages of the process.	88
Figure 6.11 – Current and voltage measurement mean values for individual welding condition disturbances.....	89
Figure 6.12 – Examples of SMRA and Waveform factor of current signals.	89
Figure 6.13 – Examples of voltage peak mean and standard deviation values.	90
Figure 6.14 – Voltage mean value vs. contamination.....	90
Figure 6.15 – Quality prediction accuracy on welds with and without induced disturbances.....	91
Figure 6.16 – Quality prediction accuracy with down-sampled signals.....	92
Figure 7.1 – Schematic representation of the technology transfer lifecycle.....	93
Figure 7.2 – Tube-to-tubesheet weld of a 316L test structure and power measurements.	97
Figure 7.3 – Defected (notch) tube-to-tubesheet weld and power measurements.	98
Figure 7.4 – Defected (grease contamination) tube-to-tubesheet weld and power measurements. .	98
Figure 7.5 – Defected (gas disturbances) tube-to-tubesheet weld and power measurements.....	99
Figure 7.6 – Welding power of test sample using the right and wrong filler wire.	99
Figure 7.7 – Welding power of contaminated test sample using the right and wrong filler wire.....	100

List of Tables

Table 4.1 – Chemical composition of welding wire Inconel 718.	40
Table 4.2 – Chemical composition of welding wire Ti-6-4.....	40
Table 4.3 – DOE Partial Factorial L27 Orthogonal Array.	42
Table 4.4 – Welding input parameters for IN718 wire on SS316L plates.	42
Table 4.5 – Welding input parameters for Ti-6-4 wire on Ti-6-4 plates.	42
Table 6.1 – Experiment Welding Parameters.	85
Table 6.2 – DOE Full Factorial L27 Orthogonal Array.....	86
Table 6.3 – Disturbance levels.	86
Table 6.4 – Definitions of Time-domain features.	87

Declaration

I, the author, confirm that the Thesis is my own work. I am aware of the University's Guidance on the Use of Unfair Means. This work has not been previously been presented for an award at this, or any other, university.

1 Introduction

1.1 Motivation and Problem Statement

Understanding the mysteries of the universe and the physical laws that govern the cosmos requires large-scale engineering projects where particles are accelerated at speeds close to the speed of light. Particle collisions at such high speeds allow the formation of new particles originating from the collision energies. Detecting and studying the properties of those particles requires complex detectors whose precision sensing abilities depend on silicon sensors. For optimum detection and reliable operation within the service lifetime the sensors need to operate in low temperature environments. In the case of the new ATLAS Inner Tracker detector that is developed for operation in line with the High-Luminosity Large Hadron Collider, the low temperatures will be achieved with an evaporative CO₂ cooling system. Thin titanium cooling pipes embedded in the structure of the detector are recruited to transport the coolant and remove the heat from the detector.

The joining of these pipes requires precise control of the heat input in order to minimize the effects on the material's microstructure that could affect the service life of the cooling circuit and in turn potentially compromise the detector's operation. This control can be achieved with the use of pulsing currents in the orbital welding process. Applications of this technology are also found in the aerospace repair and remanufacturing industry, where titanium is utilised due to its superior properties like high strength-to-weight ratio and corrosion resistance.

Welding process outcome relies heavily on maintaining input parameters and welding conditions at optimum levels for the whole duration of the process. Deviations beyond acceptable thresholds due to unforeseen reasons result in disturbances of the process that are reflected in the quality of the weld. To ensure and control the quality of the output, real-time welding process monitoring is explored allowing defect detection and quality prediction.

In the present doctoral thesis a series of investigations and implementations related to Pulsed Gas Tungsten Arc Welding are explored by the author under an industry-academia collaboration. The goal of these investigations was the understanding, wider implementation and advancement of the welding process, along with the establishment of a weld quality assurance mechanism based on process monitoring.

1.2 Industry-Academia Collaboration

The thesis is a result of an industry-academia collaboration between the Department of Physics and Astronomy at the University of Sheffield in United Kingdom and the Agency for Science, Technology and Research (A*STAR) Singapore through its Advanced Remanufacturing and Technology Centre (ARTC). Under the A*STAR Research Attachment Program (ARAP) students from participating universities in the United Kingdom undertake placements of a duration between 12-24 months at one of the A*STAR Research Institutes (RI).

The ATLAS group at the University of Sheffield has been actively involved in the development, operation and monitoring of the ATLAS detector at CERN. The group is also involved in the analysis of the data acquired by the detector and the development of the new Inner Tracker detector that will replace the existing Inner Detector in view of the High Luminosity Upgrade.

The Advanced Remanufacturing and Technology Centre is a contemporary platform under the A*STAR, in partnership with the Nanyang Technological University, Singapore (NTU Singapore). Its membership consortium ranges from global multinational corporations (MNCs) to small and medium enterprises (SMEs) with more than 80 companies as members. The institute focuses on advanced manufacturing and remanufacturing and serves to accelerate the transfer of innovation from applied research to industrial applications.

1.3 Work and Thesis Contribution

Following the guidelines set by the industry-academia collaboration, since the inauguration of the present doctoral research project the author has been involved in three major research directions.

- The ATLAS Inner Tracker cooling system development via orbital welding and process evaluation.
- Robotic-assisted welding-based additive manufacturing for aerospace applications.
- Welding process monitoring applications for non-destructive evaluation within the Industry 4.0 concept.

The contributions that are presented in the current thesis include:

- Investigations on weld bead geometry and heat affected regions on wire arc additive manufacturing using high and low frequency pulsed currents on titanium and nickel-based alloys used in aerospace engineering.
- Identification of weld pool competing flow phenomena induced by high and low frequency pulsing in Gas Tungsten Arc Welding.
- Implementations of Industry 4.0 design principles in the process management and systems configuration of a robotic aerospace compressor blades remanufacturing system.
- Defect detection and weld quality prediction by means of process monitoring of in-situ voltage and current measurements, feature extractions and supervised machine learning.
- Additional to the applications on aerospace remanufacturing and cryogenic systems the author identifies and presents the technology transfer applications of the outcome of the present research in nuclear engineering and in-space manufacturing.

1.4 Project Chronology and Author Contributions

The A*STAR Research Attachment Program is set on a four-year doctoral research programme allowing the student to be hosted in A*STAR Research Institutes for a period of 12-24 months. At the beginning of this project the timeline was set as follows: the first year is spent at the University of Sheffield, then for the second and third year the research is to take place at ARTC, while for the fourth year the student returns to the University of Sheffield.

First Year

The author's engagement with the project was initiated in October 2016. A series of trainings and introductions to the subject were undertaken in line with the doctoral development needs. Ongoing projects within the department and the Enabling Sciences for Intelligent Manufacturing (ESIM) group allowed the author to get hands-on experience and be involved in the following research:

- *ATLAS Inner Tracker cooling loops welding (Chapter 3.3)*: The author was involved and trained in the ongoing orbital welding process for the joining. Through the participation and results the author contributed to the works and authorship of the manuscript presenting the joining

process at the 70th International Institute of Welding Annual Assembly and International Conference 2017 [1].

- *Nuclear components fabrication welding trials (Chapter 7.2)*: A series of welding trials related to tube-to-tubesheet orbital welding and manual welding were undertaken at the Nuclear AMRC. The author took part in the trials, contributing to the welding process monitoring and data acquisition, performed the data analysis and co-authored the manuscript that was published as a Chapter in the book “Advances in Ergonomics of Manufacturing: Managing the Enterprise of the Future” [2].
- *Robotic system development for aeroengine blade regeneration (Chapter 5)*: The project was at its first stages of development when the author joined the team. Individual contributions during the first year were related to the analysis of the repair process, generation of the concept design, process management steps and the various peripheral components configuration needed, as well as the process monitoring evaluation (introduction of the defects, analysis of the results). This work is reflected in a publication at the 2017 IEEE 5th International Symposium on Robotics and Intelligent Sensors (IEEE-IRIS) [3].

Second and Third Year

For the second and third year of the project the author relocated to Singapore and was part of the Advanced Remanufacturing and Technology Centre workforce. While at the ARTC the author was still part of the ESIM group and continued to be involved with the Robotic System Development contributing to parts of the analysis, configuration and manuscript authorship for a publication at the 2018 IEEE International Conference on Advanced Robotics and Mechatronics (IEEE-ARM) [4] and a Chapter in the book “Advances in Manufacturing, Production Management and Process Control” [5]. The work undertaken at ARTC included extensive training and hands on experience on industrial robotics, manual and automatic welding, metallurgy and metallography, destructive and non-destructive testing as well as instrumentation and data analytics. These skills were extensively implemented in the following works:

- *Welding process monitoring investigations (Chapter 6)*: The author performed extensive study on the current state related to methods of monitoring the welding process. A series of welding trials were subsequently performed on both good welds and welds with disturbed conditions. Data analysis on the acquired signals was developed and the extracted information were used in classifications of the weld quality. The author, designed and performed the experiments and acquired the related data, performed the analysis using data analytics methods developed by the Condition Monitoring team in ARTC, implemented the findings in the concept of Industry 4.0 (Chapter 7.1) and authored the manuscript that was presented at the 2019 IEEE 15th International Conference on Automation Science and Engineering (IEEE-CASE) [6].
- *Weld bead geometry and heat-affected zone control in wire arc additive manufacturing (Chapter 4)*: A series of investigations on the effects of welding current modes on bead geometry and heat affected zone were performed by the author in wire arc additive manufacturing. Individual contribution of the author in these investigations included the design and execution of the experiments, metallurgical sample preparation and metallographic observations, data analysis and authorship of a manuscript published in the Journal of Manufacturing Processes [7].

Fourth Year

The author relocated back to the University of Sheffield for the final year of the project to conclude the work and perform the writing of the present thesis. Concurrently, analysis of the research data

gathered in the previous years were analysed and led to the aforementioned Journal of Manufacturing Processes publication [7]. The lessons learned from the industrial exposure and involvement with process monitoring led to the recognition for need of implementation of the monitoring concept in in-space manufacturing where the author presented the idea with a manuscript at the 2019 70th International Astronautical Congress (IAC) [8].

1.5 Thesis Content and Outline

The wide nature of the presented work differentiate this doctoral thesis from traditional theses as it involves many different subjects, technologies and engineering implementations. Due to the multidisciplinary nature, this thesis expands into interdisciplinarity, and therefore a single literature review would be massive and confusing as many concepts would have to be introduced simultaneously. As such, concepts related to a topic are presented when necessary, with some concepts briefly introduced whereas others are explored in depth if directly related or implemented in the presented work.

Additionally, since this project is industry-related, some technical details had to be omitted due to confidentiality and non-disclosure agreements. This includes names and parts models related to specific research materials, company specific numbers and quantities reported, instrumentation configurations where commercialisation plans are pending along with data analytics tools in-depth representation. In addition, in a number of occasions within the thesis, the economic aspects of technology implementations are presented as in manufacturing industries the cost justification and return on investment needs to be highlighted.

Thesis Outline

- In Chapter 2 the rationale of this doctoral thesis and the justification for the industry-academia interdisciplinary collaboration is presented. The ATLAS detector is presented along with the needs and cooling system developments for the Inner Tracker module of the detector. The commonalities between titanium welding for the ATLAS detector and the aerospace sector are also presented.
- In Chapter 3 an introduction to the arc welding is followed by the principles of pulsing currents and the benefits of the process. Implementation of pulsed gas tungsten arc welding in the ATLAS Inner Tracker cooling system development is presented.
- Chapter 4 includes a series of investigations related to the current mode effects on weld bead geometry and heat affected zone in wire arc additive manufacturing.
- Chapter 5 follows the stages of development of a robotic welding robot that automates the process of compressor blade regeneration in the aerospace industry. Industry 4.0 design principles are applied taking advantage on the wealth of data generated at each stage of the process.
- In Chapter 6 the principles and methodologies of welding process monitoring are investigated with implementation in a series of experiments related to robotic welding. Data analysis of the acquired data is then presented.
- Chapter 7 focuses on the concept of technology transfer presenting three occasions within the project where the research outcome is implemented in other areas and disciplines.
- A summary of the project along with conclusions and future work is finalised at Chapter 8.

2 Titanium Precision Engineering: Development of the ATLAS Detector and Links with Aerospace Engineering

In this chapter an introduction to the ATLAS particle detector is presented, alongside the use of titanium in its cooling system development. Additionally, specific applications of titanium in the aerospace industry and additive manufacturing are also presented. Similar challenges exist both in the use of titanium for the cooling system of the particle detector and within the aerospace applications engineering. These overlaps are highlighted and they constitute the rationale upon which the present work was based.

2.1 Large Hadron Collider and the ATLAS Experiment

Particle physics, also known as high energy physics, is the branch of physics that studies the elementary constituents of matter and their interactions [9]. The term high energy physics derives from the high amounts on energy required for the observation of subatomic particles. The Heisenberg's uncertainty principle in quantum mechanics (Eq. 1) prohibits the simultaneous prediction of both position (x) and momentum (p) of a particle from initial conditions.

$$\Delta x \cdot \Delta p \geq \hbar \quad (1)$$

If a resolution ' d ' is needed to observe a particle, then a 'probe' of specific momentum is required (Eq. 2), that doesn't violates the uncertainty principle [10].

$$d \cdot p_{probe} \simeq h \rightarrow p_{probe} \simeq \frac{h}{d} \quad (2)$$

Therefore 'probes' of short wavelength ($\lambda = h/p$) and subsequently high energies are required. Such energies are in the magnitudes of eV for atomic scales and MeV for nuclear scales, whereas for particle scales energies of GeV and TeV are required. Additionally, some of these elementary particles have high masses, therefore requiring high energies to be created and studied. Hence the term high energy physics, and in order to achieve these energies, particle accelerators are employed.

The largest particle accelerator in the world currently in operation is the Large Hadron Collider (LHC) located at CERN, in Switzerland. At ~ 100 m underground, a tunnel ring measuring 27 km in circumference hosts the circular accelerator where protons accelerate at high speeds, achieving beams of ~ 7 TeV of energy. Opposing parallel-running beams collide head-on one-another at four intersecting points along the ring, resulting in combining energies of 14 TeV, at a rate of about one billion collisions per second. At these intersections, four major experiments are running, named ALICE, ATLAS, CMS and LHCb. ATLAS and CMS use massive particle detectors of general purpose, whereas ALICE and LHCb use detectors specialised for studying specific phenomena.

The ATLAS Experiment (Figure 2.1), one of the two general-purpose detectors at the LHC measuring 25 meters in diameter and 44 meters in length [11]. This hybrid detector, uses an onion-like configuration for detection, utilising different detector technologies at successive layers (Figure 2.2). The collisions occur at the centre of the detector where the Inner Detector lies. Silicon sensors in overlapping layers inside the Inner Detector are used for tracking the particles scattered via the collision. The particles are then entering the successive layers of electromagnetic calorimeters where photons and electrons interact. Subsequent particle interactions occur in the hadron calorimeters,

and then with detectors in muon chambers at the outermost layers. Magnetic fields generated by a 2 Tesla solenoid and a 1 Tesla toroid located inside the detector allow particles of different charge to follow different trajectories. As a result of this configuration the ATLAS detector is used to detect, track and measure particles generated by the collisions.

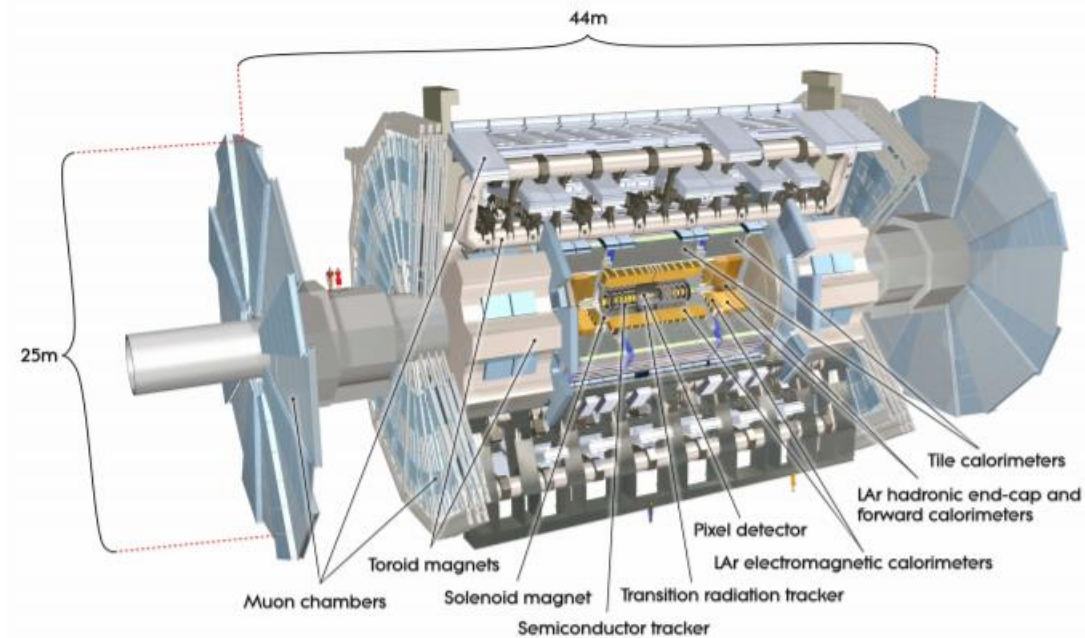


Figure 2.1 – The ATLAS detector [11].

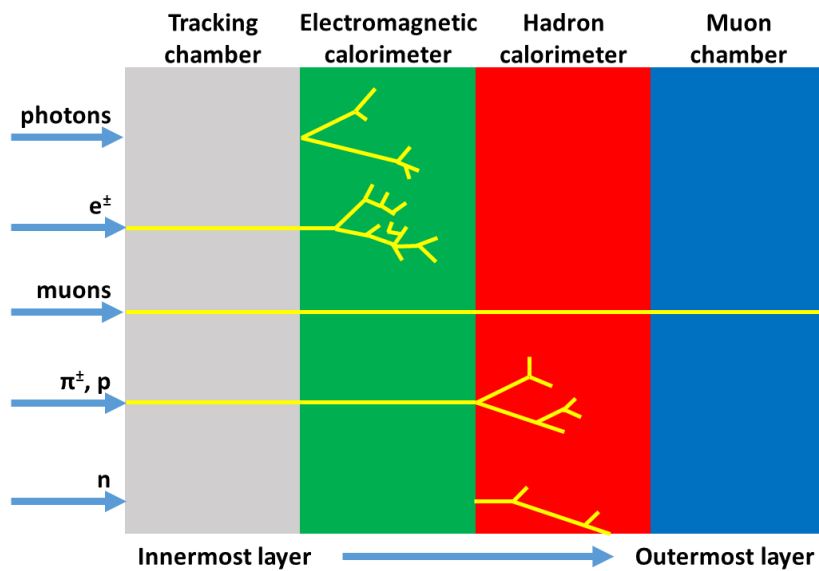


Figure 2.2 – Particle tracking in different detector layers.

2.2 High Luminosity and the ATLAS Upgrade

The high luminosity upgrade of the LHC (HL-LHC) scheduled for 2024 (Figure 2.3) is expected to achieve a factor of 10 luminosity¹ increase (higher rate of collisions). In order for ATLAS to be compatible with the HL-LHC, various detector upgrades are required. During the third planned major ATLAS upgrade

¹ See Glossary.

(Phase-II), an entirely new all-silicon inner detector named Inner Tracker (ITk) will replace the existing Inner Detector.

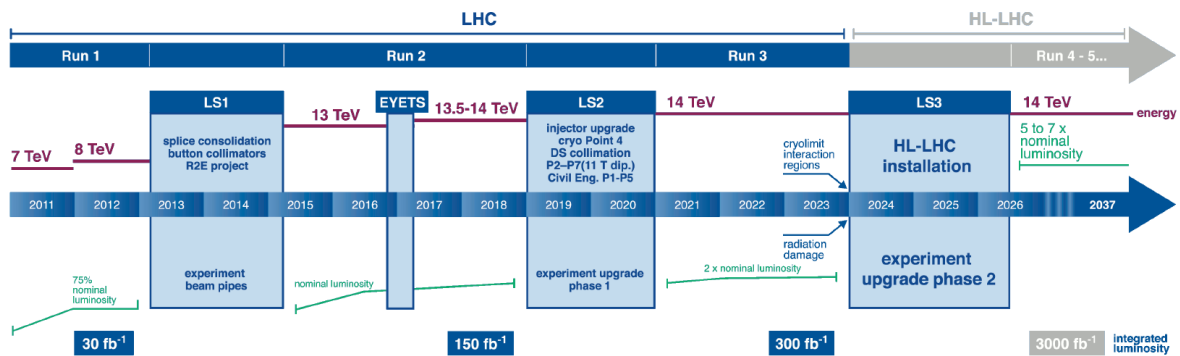


Figure 2.3 – The LHC/ATLAS running and update schedule [12].

An order of magnitude increase in the number of proton interactions per bunch crossing require higher capabilities in track reconstruction, and therefore a new detector layout will be followed. As shown in the quarter view of the detector in Figure 2.4, different layers of Pixel (red) and Strip (blue) sensors are arranged in parallel and perpendicular alignments along the beam pipe around which the detector is symmetrical. Pixel sensors are used in the regions closest to the beam-pipe where the track density is high. At larger radii, lower track density allows the use of Strip sensors at a lower cost without sacrificing performance.

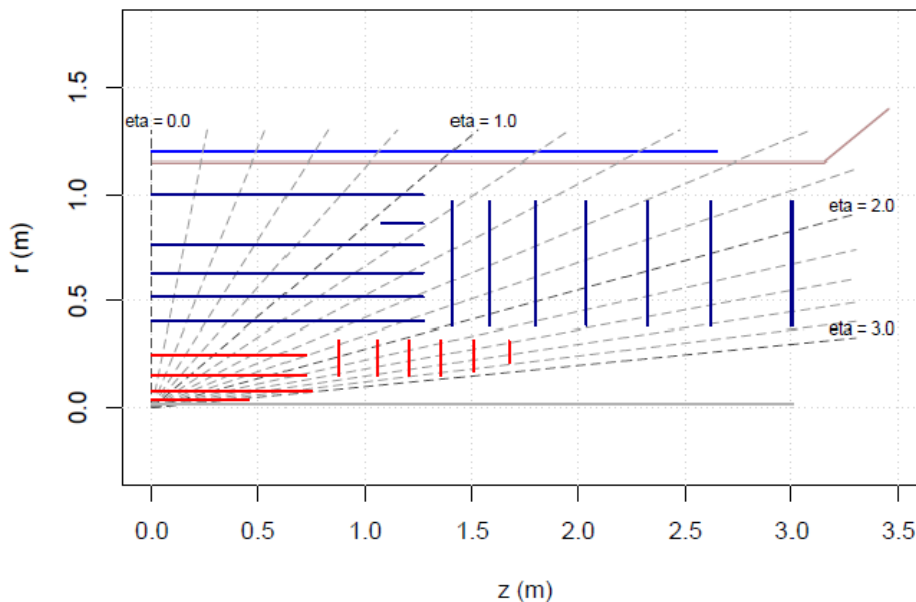


Figure 2.4 – Quarter view of the ATLAS ITk proposed layout [12]. The collisions are occurring at the lower left corner (0,0). Red lines represent the Pixel detectors and blue lines the Strip detectors.

The materials existing within the detector volume has direct impact on the detector tracking performance, affecting electron and photon measurements, fluences, and total ionizing doses. In order to reduce unwanted particle interaction for optimum particle tracking the new design aims for a lower detector mass. A new challenge arises as the new sensors are required to withstand radiation doses of approximately an order of magnitude higher than the present levels inside the inner detector,

while at the same time the radiation length, should be kept at the current level or lower. Radiation length is a property of a material relating to the energy loss of a particle while electromagnetically interacting with that material and longer radiation lengths correspond to more chances of the particles surviving the interaction. Simulations that compare the current (Run 2) radiation length in the Inner Detector with the proposed ITk design configuration reveal significant reduction in the volume of the material that the particles will travel through (measured in radiation lengths) as the new design allows lower mass at the corresponding pseudorapidity (spatial coordinate for the angle of a point relative to the beam axis marked as η/η in Figure 2.4). The new detector with less inactive material in the tracking volume results in less than one radiation length up to a pseudorapidity of 2.7 (Figure 2.5).

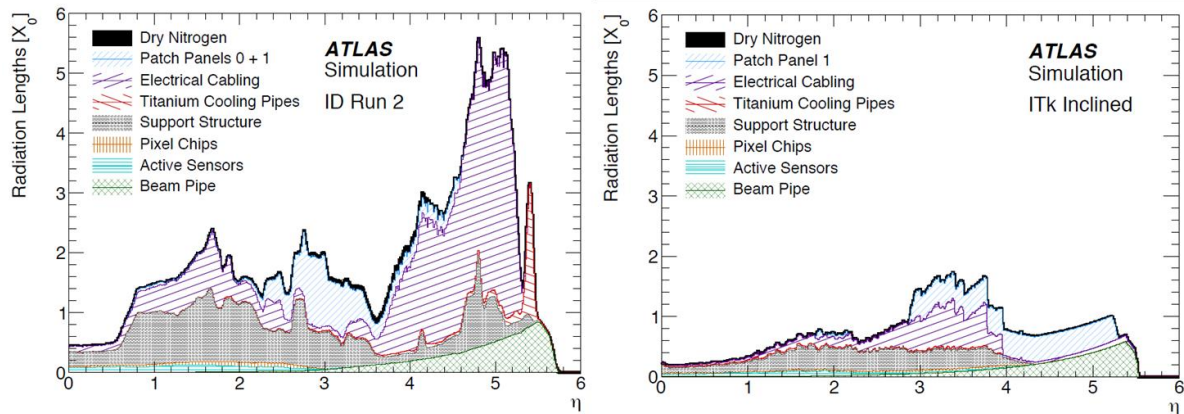


Figure 2.5 – ATLAS Inner Detector(left) and ITk (right) radiation length of different materials within the detector versus pseudorapidity (η) [12].

2.3 Inner Tracker Cooling System Development

The operation of the silicon sensors in the detector result in power dissipated in the detector in the form of heat. As a reference, in the existing ATLAS Inner Detector the front-end (FE) chips in the Pixel modules result in more than 15 kW dissipated into the detector volume, whereas the Semi-Conductor Tracker (SCT) Strip modules dissipate more than 25 kW. The temperature dependence of the reverse annealing of the silicon sensors requires the removal of this heat outside of the detector, to prevent the damaging of the sensors due to the defects formed in their lattices. Additionally, a lower operational temperature delays the continuous degradation of the silicon detectors and hence delays the increase in the device leakage current, allowing power savings in the overall operation.

To deal with the need for maintaining low temperatures inside the detector, complex cooling systems based on evaporative technology are employed. The systems' abilities have been demonstrated in the existing Inner Detector where thin-walled tubes integrated in both the support structures of the detector as well as the sensor modules are used to circulate bi-phase fluorocarbon refrigerant C_3F_8 . The decision to choose a two-phase evaporative cooling over single-phase liquid cooling was based on the higher heat transfer coefficient that allows the use of smaller pipes, and therefore reducing the total material inside the detector volume. Additionally the isothermal evaporation helps in maintaining more uniform and constant temperatures inside the detector.

During the Phase-II ATLAS Upgrade the cooling system that will be installed on the ITk will transition to the use of carbon dioxide (CO_2) as a coolant replacing the fluorocarbon liquids. The reasons behind the adoption of CO_2 are the low viscosity and high latent heat of evaporation of CO_2 that allows further reduction to the cooling pipe sizes, the much lower environmental impact compared to using

fluorocarbons and the significantly lower cost of fluid refilling. The CO₂-based cooling system has already been demonstrated by the ATLAS collaboration and the Insertable B-Layer (IBL) detector that was installed during the Phase-I upgrade is being cooled by CO₂ at a temperature of -35°C [13].

2.3.1 Pixel and Strips Cooling Loops

As presented previously in Figure 2.4 the ITk layout configuration comprises of barrel and disk shaped modules for both the Pixel and Strip sensors. In order for the cooling system to be effective the pipes should be in direct or indirect thermal contact with the sensor modules. At the same time the pipes should be positioned in such ways that will have the lowest possible interference with the tracked particles. To achieve that the cooling loops are embedded in the support structures of the modules and the detector depending on different layout configurations. In Figure 2.6 the position of the cooling loops of the Pixel modules are shown in the half-ring assemblies. Similarly the end cap petals and the barrel staves that compose the support components for the Strip sensors are shown in Figure 2.7. The cooling loops are directly embedded in the support structure, covered in carbon foam of high thermal conductivity (Figure 2.8). The carbon foam and cooling pipes combination is itself supported and maintained in position by a carbon-fibre honeycomb structure.

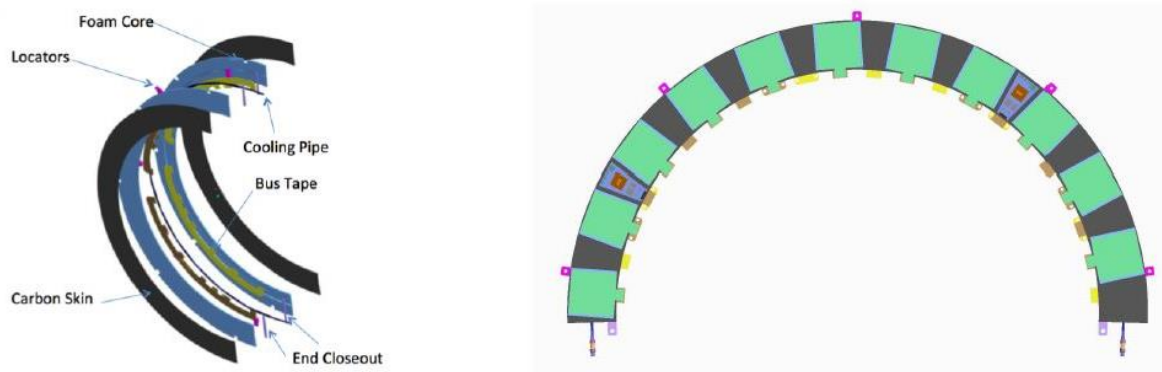


Figure 2.6 – Pixel half-ring assembly. Left: half-ring internal components. Right: Surface view of the half-ring with the Pixel modules (green). The cooling loops embedded in the structure are shown in blue colour (left) emerging from the center of both ends of the half-ring (right) [13].

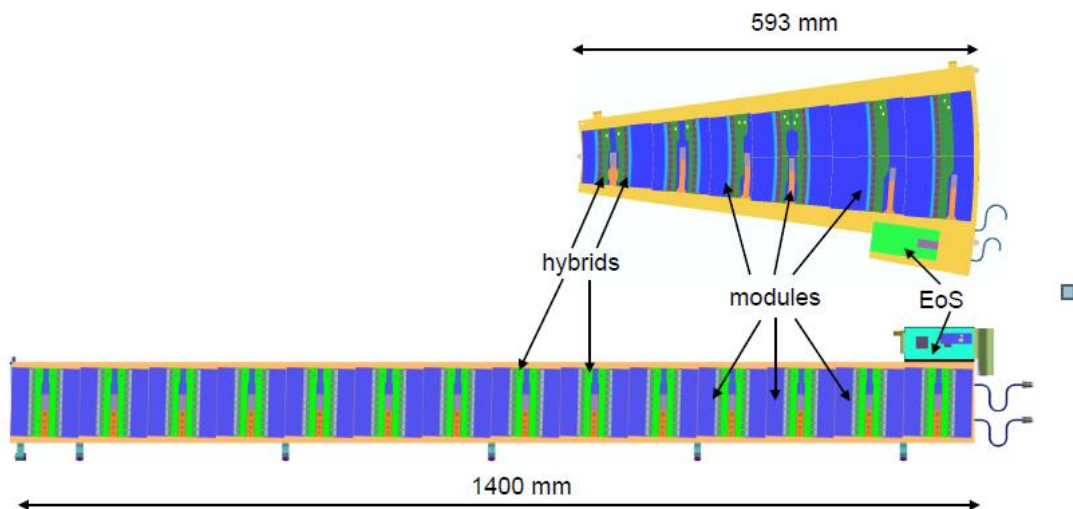


Figure 2.7 – End-cap petal (top) and barrel stave (bottom) components for the Strip silicon sensors [12].

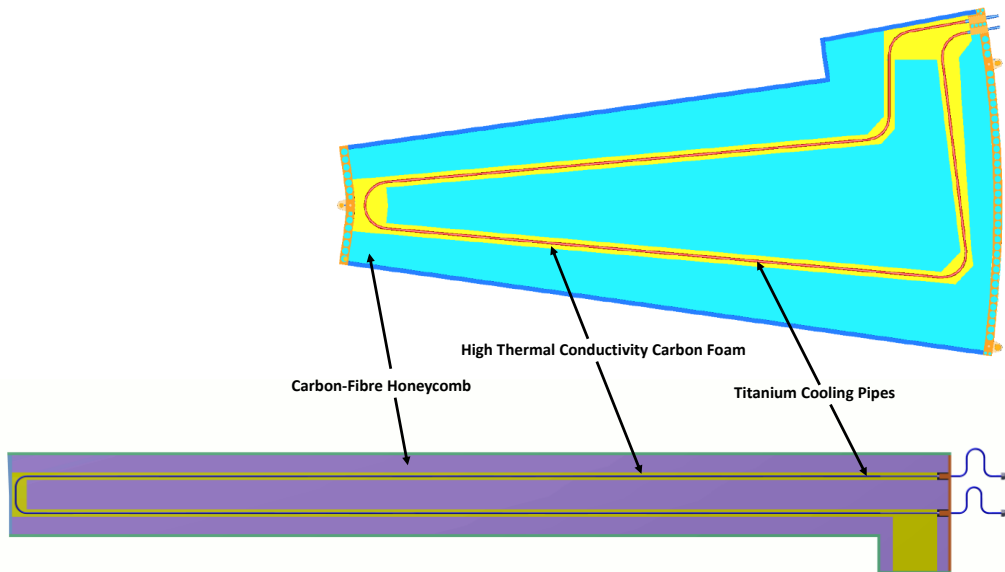


Figure 2.8 – The cooling loops embedded in the support structures of an end-cap petal (top) and a barrel stave (bottom). Titanium cooling pipes (red and blue), high thermal conductivity carbon foam (yellow and olive green) and carbon-fibre honeycomb (turquoise and purple) [12].

2.3.2 Material Selection and Requirements

As illustrated in Figure 2.9 the sensors follow a double-layer “sandwich-like” configuration, at the center of which are the cooling pipes. It is therefore required to have the lowest mass possible and as a result titanium was the material of choice. Commercially Pure Grade 2 (Ti CP2) titanium was selected because of its high strength-to-weight ratio (42% weight saving compared to stainless steel tubing with the same mass flow handling ability), its high resistance to corrosion, and its thermal expansion compatibility with carbon fibre reinforced plastics (CFRP). Additionally its radiation length matches with the design requirements of the ITk.

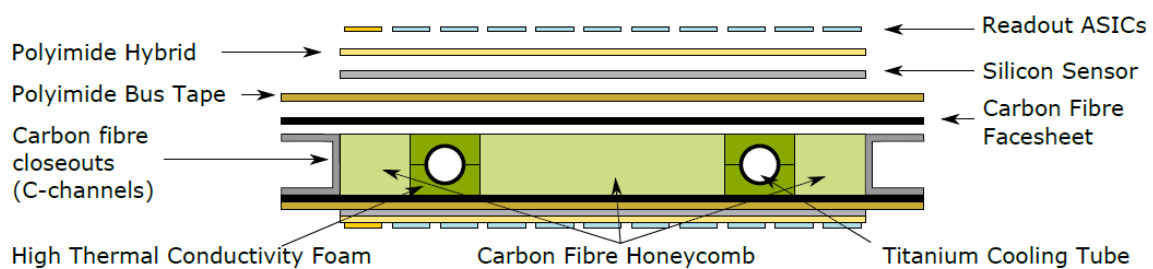


Figure 2.9 – Internal structure schematic of the stave core, including the silicon sensors and ASICs. Not to scale. Glue layers not shown [12].

The benefits of titanium in regards to strength-to-weight ratio are limited to inside the detector, since once the pipes are outside of the detector volume the need for material savings ceases. Therefore for cost saving reasons the material of choice for the outside piping changes to stainless steel from the manifolds to the distributor pumps and the heat exchangers. As a result a transitioning is required in the cooling system from titanium-to-stainless steel tubes. Additionally the cooling circuits have to be globally designed and placed in such way to prevent background electronics noise from being transmitted inside the detector. Appropriate electrical breaks are therefore needed to avoid inducing potential damage to the silicon modules. Experience gathered from the ATLAS Insertable B-Layer (IBL), which has been in operation since Phase-I upgrade, has shown both reliable operation of electrical

beaks and titanium/stainless-steel transitioning as shown in Figure 2.10. Electrical insulation is achieved by brazing of a short ceramic tube to the metallic component. Therefore this design is adapted to the designing of the ATLAS ITk cooling system.



Figure 2.10 – Left: Titanium fitting and electrical break developed for the Insertable B-Layer (IBL). Right: Electrical breaks in situ at the ends of the IBL staves [13].

2.3.3 The Need for Orbital Welding

For the ATLAS ITk cooling system, utilising the aforementioned benefits of the CO₂ evaporative system and of using Ti CP2, it was decided that 2.275 mm outer diameter (OD), 160 µm wall thickness titanium tubes will be used. The decision was made based on the tubes' ability to perform the task and their mechanical properties after testing. To further reduce the inactive material in the detector volume, it was decided that the bulky connectors traditionally used in joining the tubes to be replaced by weld joints. At such small scales the welding of the thin-walled tubes becomes extremely challenging, because of the high number of parameters that need to simultaneously and precisely be controlled as well as the difficulty in titanium weldability.

This challenge presented the opportunity for a collaboration between academia and industry to be formed. The ATLAS Group at the Department of Physics and Astronomy at the University of Sheffield in collaboration with the VBC Instrument Engineering Ltd (VBCie) developed a low current automatic orbital welding system based on pulsed Gas Tungsten Arc Welding technology (further details on the technology on Chapter 3). The demonstrated abilities of the system to deliver repeated results of high quality welds with low heat input led to the process being officially selected by the ATLAS Collaboration for the fabrication of the ITk cooling system. The ATLAS team at the University of Sheffield is now responsible for the fabrication of ~120 Pixel End-Cap cooling loops and ~600 barrel Strip stave loops. On each end of the loop a ceramic electrical break is welded followed by a VCR[®] connector² to be used in fitting during testing. Six welded joints are therefore needed on each loop, resulting in a total of ~3600 welded joints just for the Strip stave loops (Figure 2.11).

² See Glossary.

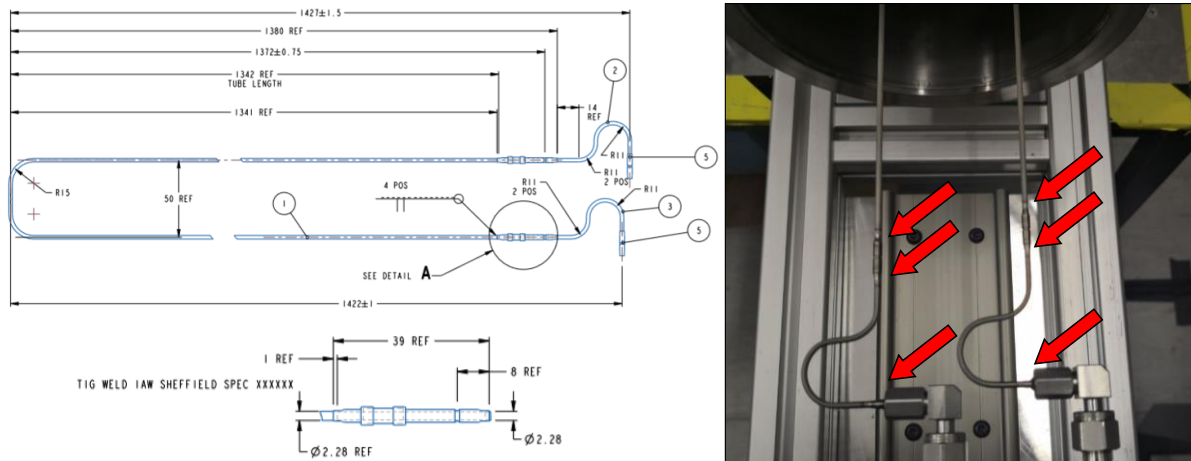


Figure 2.11 – Diagram of a Strip stove cooling loop (left) and the six welded joints on each loop (right).

2.3.4 Non-Destructive Evaluation and the Need for Welding Process Monitoring

When critical welds are performed in industrial applications such as nuclear and aerospace engineering the finished product undergoes a series of non-destructive tests to ensure the quality and properties of the welded joints matches the requirements defined by the quality control procedures. Depending on the material and applications the non-destructive testing techniques for weld inspection can vary from visual and magnetic particles inspection to ultrasonic testing and X-ray radiography among others. In the case of the ITk cooling system welded joints a series of barriers are restricting the extensive use of non-destructive testing:

- The large number of welds that need to be performed in a limited time-frame restrict the individual inspection of each weld using extensive time-demanding tests.
- The large number of in-situ welds that will be performed in confined spaces restrict the use of bulky testing equipment for in-situ evaluation.
- The very thin-walled pipes are below any existing welding procedure specification standards defined by the industry, and new testing procedures would need to be developed to test technologies in such scales.

The ATLAS collaboration decided to test the ITk cooling system via the following quality control procedure:

- Upon completion of a weld, visual inspection by the welder operator will ensure the absence of discoloration, dents, pin holes and visible defects, rippling of the bent tube and that weld dimensions are within limits avoiding undercuts and misalignments.
- Upon completion each loop is subjected to a series of vacuum leak tests (Figure 2.12). The tubes are submerged in a vacuum chamber and internal pressure is applied. The first leak test occurs at a pressure of 5-10 bars and then incremental increases follow in stages: first 50% then 5 X 10% to 190 bars. This max pressure is held for 30 mins then another leak check is performed at 5-10 bars.
- Multiple cooling loops connected simultaneously on a testing system will undergo hydraulic pressure testing at 200 bar.
- Using the same system additional vacuum leak checking on multiple loops will be done to a limit of 10^{-11} mbar 1 s^{-1} in parallel with the pressure testing. The leak test will be maintained for several hours.

During the last two tests the cooling loops will cycle at -60°C for a defined number of cycles. A fraction of the assembled cooling loops will be subject to further QA tests, comprised of thermal imaging evaluation of the cooling performance.

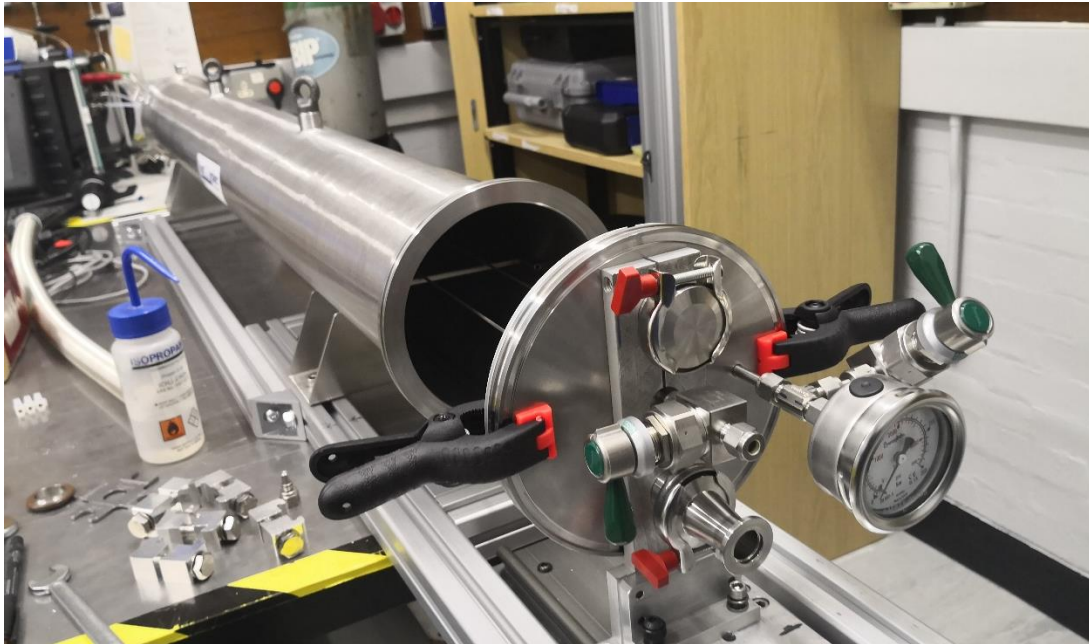


Figure 2.12 – Vacuum leak test for the completed welded Strip stove cooling loops.

While the proposed QC procedure is sufficient to ensure that the operational capabilities and working performance of the cooling system welded joints are matched, the possibility of faults detected during the tests closer to the completion stage would cause possible prolonged delays. In order to add another layer of quality assurance during the fabrication phase, the University of Sheffield developed a welding monitoring system able to detect disturbances while acquiring real-time voltage and current measurements during the welding process. The system, composed of a data acquisition module and a custom-built sensor box has been tested to successfully detect disturbances in the acquired signals when the welding process is subjected to surface contamination, surface integrity alterations, tube misalignments, gas flow disturbances and unexpected arc turn-offs due to electrode contamination (more on the welding process monitoring in Chapter 6).

2.4 Aerospace Engineering

Aerospace engineering refers to the collective efforts of science and engineering related to human flight in the atmosphere of the Earth and outer space. Technology and science of aerospace have grown exponentially since the first sustained piloted flights of the Wright Flyer in 1903. In the fast-paced modern society aerospace engineering research pushes the boundaries in the related ever-evolving topics that include vehicle design and materials, advanced propulsion systems and improved engine performance, safety and quality assurance, systems engineering and control.

2.4.1 Titanium in the Aerospace Industry

Titanium and its alloys are heavily used in the aerospace industry. More than 55% of the total titanium production of North America is used in the aerospace sector [14] for the same properties that made the material attractive for the ITk development.

The high strength-to-weight ratio offered by titanium (e.g. commercially pure grades), comparable to the strengths of stainless steels (e.g. annealed 300 series) but with 40% less density, enable significantly lighter aircrafts and therefore great fuel savings over operation, without sacrificing material strength and performance [15]. In tight regions where space limitations forbid the use of bulky lighter metals as aluminium, titanium is used as it provides greater strength using far less material (e.g. landing gear beams on Boeing 747 and 757, replacing aluminium) [16]. Titanium has a melting point of 1668°C and is used as aluminium replacement in applications where temperature exceeds the aluminium operating temperature of 130°C (e.g. areas in the Auxiliary Power Unit-APU and wing-anti-icing systems). Additionally, the high corrosion resistance that titanium exhibits – significantly higher than that of stainless steel – eliminate the need for further protective paint coatings where used, that otherwise add significant weight in the overall structure.

In the recent years, carbon fibre reinforced polymers (CFRP) composites in the airframes have been highly-adopted by the industry as they offer significant weight savings. Titanium's thermal expansion coefficient and stiffness is similar to that of CFRP composites. Titanium is also in electrochemical compatibility with carbon, capable of resisting galvanic corrosion as opposed to aluminium which is subjected to corrosion when in contact with CFRP polymers. Due to these properties the increase in the usage of titanium from the aerospace industry was greatly influenced by the increased use of CFRP composites.

Despite the wealth of benefits offered by the properties of titanium, the metal is not frequently the first material of choice and manufacturers try to limit its use because of its relatively high cost. While the titanium ore is not scarce at all as it is the ninth-most common element on our planet and the fourth-most abundant metal in the Earth's crust, the refining, processing and fabricating steps are what make it so expensive. To highlight the processing cost in comparison with aluminium, titanium is five times more expensive to refine and more than ten times as expensive to form into ingots and in fabrication of finished products. It is therefore a prerequisite that the use of titanium should be justified and supported by economic benefits. The price per kilogram of a material however is only a part of the full cost equation. Costs caused by maintenance, replacements and downtimes should be taken into account in high-value industries, making titanium a material of choice for applications where long and reliable service life are required.

In a study about the titanium industry, published by RAND Corporation in 2009, Seong et al. [17], identified five categories of emerging technologies with potentials of reducing the costs of titanium production and manufacturing. These categories include improvements on extraction and refinement, powder metallurgy, single-melt refining, solid freeform fabrication and improvements on machining. Solid freeform fabrication refers to the term of additive manufacturing (AM) or 3D-printing, where material is deposited in successive layers to build a three-dimensional part following a predesigned model. As it will be further explored in Chapter 4, metal AM processes have been evolved from welding processes, utilising the same expertise, knowledge, equipment and materials.

2.4.2 Additive Manufacturing in Aerospace Engineering

Metal parts fabricated via AM processes are revolutionising the aerospace manufacture industry. As an indication example of how established AM is getting in the industry, Boeing has installed more than 200 3D printed components across 10 different models of commercial and military jets since 2013 [18]. AM is currently experiencing high popularity, being regarded as one of the most studied

processes in recent times [19]. The rapid expansion of metal AM is projected on the forecasted revenue of \$7150M for 2026 with titanium parts expected to reach a \$1030M revenue in 2024 [20]. In the SmarTech Analysis' 2019 Report on Additive Manufacturing for Civil Aviation Part Production, the overall business of AM parts in civil aviation is forecasted to climb to \$7 billion per year during the next ten years (Figure 2.13) [21].

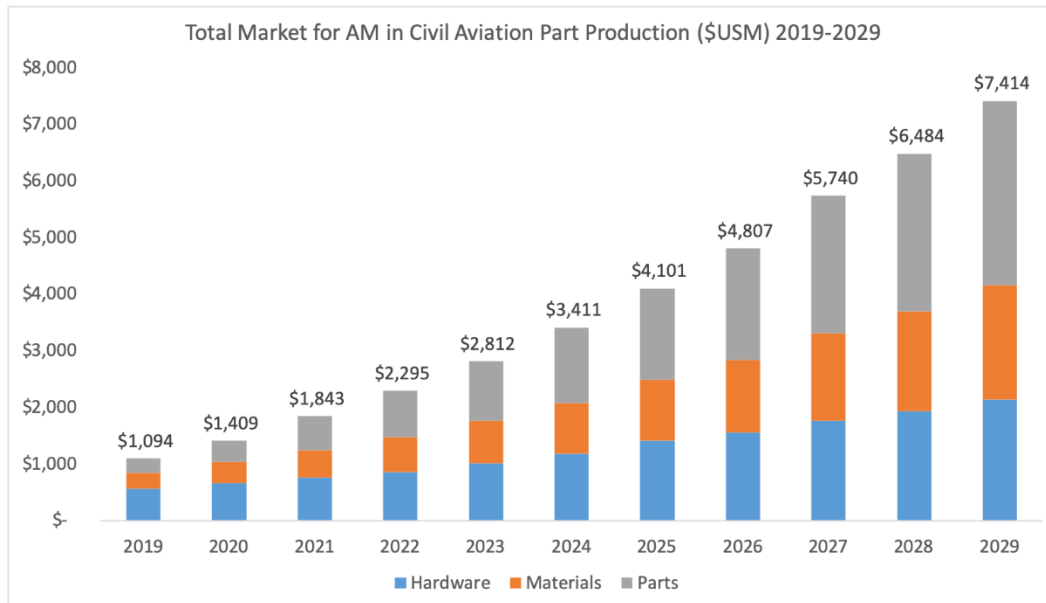


Figure 2.13 – Totals for the overall market for additively manufactured parts in civil aviation, forecasted for the next ten years [21]. (Credit: SmarTech Analysis).

The reason behind this increase of interest in the technology by the industry is highlighted by the attractive cost-saving benefits that AM offers.

The ability to fabricate parts on a layer-upon-layer manner allows the freedom to create complex geometries previously restricted by the traditional ways of manufacturing such as forging and subtractive technologies. This geometrical freedom of design results in lightweight construction, allowing two, three, and even more parts that were traditionally manufactured separately to be fused into a single part design. A notable example is the GE Aviation jet engine fuel nozzle that is additively manufactured, combining what was originally 20 separate parts into one (Figure 2.14) [22]. This flexibility provides the ability to define the force distribution within a component while keeping the component density under control and determining the microstructure quality. Furthermore, AM enables reduction in time to market from the steps of design to final product compared to traditional manufacturing, as specific steps can be skipped (e.g. cast forms creation) and working prototypes can easily be developed and tested. Additionally, the ability to print any part on-demand on decentralized locations eliminates the need for warehousing of spare parts that are rarely needed all over the world. AM has also been proven to shorten the time and cost of production up to 75%, by eliminating the need of specific construction tools [23]–[25].

An additional benefit of using AM in aerospace manufacturing is the higher utilization of material and reduction of waste. Subtractive processes can produce recyclable waste up to 75% of the initial material, whereas the 3D printed parts can have near net-shape results, with only about 5% of waste. Furthermore, the capability of producing calculated hollow and bionic (porous) structures increases

the material savings and decreases the structural weight without compromising its mechanical properties (Figure 2.15). AM is therefore highly attractive to industrial sectors that utilize expensive materials e.g. titanium alloys, superalloys (nickel-based alloys), such as aerospace, energy, medicine and defence [26]. Additionally, the freedom to explore more complex designs results in replacing compound structures with a single complex component, reducing weight and allowing fabrication of structures with lower buy-to-fly ratios³.



Figure 2.14 – Additively manufactured GE Aviation jet engine fuel nozzle [22]. (Credits: GE Aviation).

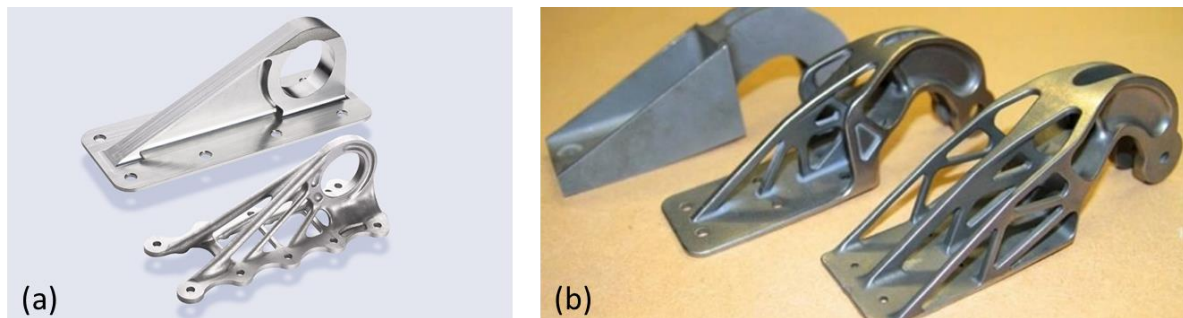


Figure 2.15 – Additively manufactured aerospace parts to replace their traditionally manufactured counterparts. a) wing brackets for Airbus A350 XWB; b) metal parts 3D printed for European Space Agency. (Credits: Airbus, European Space Agency).

2.4.3 Aeroengines MRO

Aircraft jet engines are highly complex structures that can be composed of up to approximately 30,000 individual components [27]. Component design materials selection and both manufacturing and in-service tolerances of each component drives optimum performance of the engine. However, harsh environmental and prolonged operational conditions result in physical wear of engine components, introducing a variety of defects. Operating in a high pressure/temperature environment, in combination with foreign object impact, leads to wear, distortion, dents and cracks on blades, vanes, blade-integrated disks (blisks) and such other components [28]. Introduction of such defects can lead to catastrophic events, resulting in huge costs, both societal and economic. In order to prevent such failures, aviation engines are required to be removed from the aircraft and overhauled after specific

³ See Glossary.

periods of operation, defined either by calendar time or their respective time between overhauls (TBO). Typically for a jet engine this TBO period lies between 3,000 and 6,000 running hours [29].

Maintenance, repair and overhaul (MRO) is defined as the process of ensuring that a system or equipment, continually performs its intended functions, with safety and reliability under acceptable constraints [30], [31]. The MRO operations that are required by complex products in the aerospace industry result in high MRO costs. Many manufacturing companies have altered their business strategy to support the servicing of their products through the entire lifecycle. The main reason behind this shift is to allow long, intensive operational periods of high cost engines to quickly yield a profit for the customer. To guarantee the lifespan of the engine, repairs on worn components and manufacturing spare parts is essential to ensure long term reliability [32].

The majority of rejected parts during overhaul inspections are both compressor and turbine blades and turbine vanes, due to the damages caused by ingested materials or damages occurring from elevated temperatures of operation [33]. Therefore these components are of particular interest to the aerospace companies. Their high value increases the need of repair instead of replacement. The blades of a turbofan engine are the most critical part, used in different stages of the engine with different sizes and roles. Their performance is solely based on their aerodynamic body, where small changes in the blade geometry can result in large changes on engine performance and efficiency. It is therefore of major importance to maintain the original shape of the engine blades, while the repaired component conforms to acceptable dimensional tolerance as defined by the original manufacturer. The traditional process for engine blade regeneration is mainly separated in four stages: pre-treatment, repair and material deposition, re-contouring and post-treatment. Stages of pre-inspection and post-inspection are also included before, in-between and after the aforementioned stages, to identify defects, select appropriate restoration procedures and ensure the quality of the restored component.

In regard to the second stage of the blade regeneration – the repair and material deposition process – techniques currently used for the repair vary according to the material and the damage of the blade. For patch-repairs plasma arc welding is used to weld the patch joint without additive material. Crack-repair on the blade's body is carried out through brazing or welding depending on the size of the crack. Tip-repair is done via additive arc welding with filler material or via material cladding using laser welding, due to low heat input requirements. The tip-repair, due to blades "sulfidation" (or sulphidation - chemical process that occurs in high temperature environments producing a sulfur compound on or under the metal/alloy surface) and crack formations during operation, occupies the majority of the volume repaired in aeroengine components [34].

In private communication of the author with a major aeroengines MRO service provider [35], it was reported that after the compressor and turbine blades undergo repair by means of gas tungsten arc welding, they present a variety of defects (mainly lack of fusion and porosity) at a rejection rate of about 15-20% of the total yield (30-40,000 blades annually). This corresponds to a faulty yield of 4500-8000 blades per year. Since the detection of the defects occurs on post-process inspection by means of X-ray radiography, the economic impact the company suffers increases when taking into consideration the time wasted in both re-repairing and inspecting the rejected blades. As a result a bottleneck effect is created in the MRO process and the need for an early detection of the defect using inline metrology and process monitoring would be advantageous.

2.5 ATLAS ITk development and Aerospace Engineering Overlaps

As presented in the previous sections, the numerous benefits in regards to material performance in harsh environments and its weight-to-strength ratio properties offering the ability to maintain low density without compromising strength, made titanium the material of choice for a series of applications in physics experiments and aerospace engineering.

The low heat input arc welding required in the joining of the cooling pipes for the development of the ATLAS ITk Detector overlaps with the low heat required in the repairs of high-value aeroengine components via arc welding processes. In both cases the pulsed current gas tungsten arc welding is the process of choice due to the benefits offered by the process (covered in Chapter 3).

The need for defect detection using real-time process monitoring technologies is highlighted in both the ITk cooling system development and the aerospace repair and overhaul industry, as critical welds should perform with integrity in harsh environments and extreme temperatures.

In both applications the design and operational restrictions allow little tolerance in deviation from the pre-set values and therefore fabrication precision and the process ability for repeatable results is highlighted.

The overlaps of the two titanium welding applications resulted in the Industry-Academia collaborations highlighted in the introduction and the doctoral project that this thesis is covering. In the following chapters the author's work in low-heat input joining is presented, along with additive manufacturing investigations using welding technologies and the process monitoring applications for defect detection and quality assurance.

2.6 Conclusion

In this chapter the need for use of titanium for the cooling system of the ATLAS ITk was highlighted by the demanding environments and extreme operational conditions in the particle detector. For the joining of the tubes, advanced welding technologies were selected that are used in the repair and overhaul industry of the aerospace sector. A series of overlapping challenges were identified in the two sectors highlighting the need for research and development in the fields of low-heat-input arc welding, additive manufacturing and welding process monitoring for defect detection.

3 Gas Tungsten Arc Welding (GTAW)

In this chapter an introduction to arc welding is presented with terms and definitions deemed necessary for the thesis comprehension. The physics and technology of pulsed tungsten inert gas welding are then presented followed by the applications of the technology on orbital welding for the ATLAS ITk development.

3.1 Arc Welding Introduction

3.1.1 Welding – Definition and Classification

Welding, or cohesion, is one of the major joining processes used in manufacturing, alongside fasteners, adhesives, brazing and soldering. It involves the joining of pieces of material by application of heat, pressure or both [36]. As presented in Figure 3.1, in the latest British Standards classification welding processes are divided into two major categories, welding with pressure and fusion welding, based on whether the process involves the application of pressure or not [37]. For the purposes of the present research the focus will be directed on fusion welding without pressure.

There is a variety of different fusion welding processes, classified based on the type of energy source they use in order to produce the heat required for melting the materials to be joined. The predominant type of fusion welding is arc welding, where an electric arc is formed between an electrode and the workpiece. Other types include electron beam welding, gas welding (combustible gas is mixed with oxygen and ignited, e.g. oxyacetylene welding), laser welding, thermit welding (exothermic reactions between aluminium and powders of metal oxide) and electro-slag welding (vertical joining of thick materials using electrical resistance of molten slag). Additional material fed into the melt pool to be fused with the base material is called filler metal. In the case where, during the fusion process, no filler metal is used, the welding process is called autogenous [38].

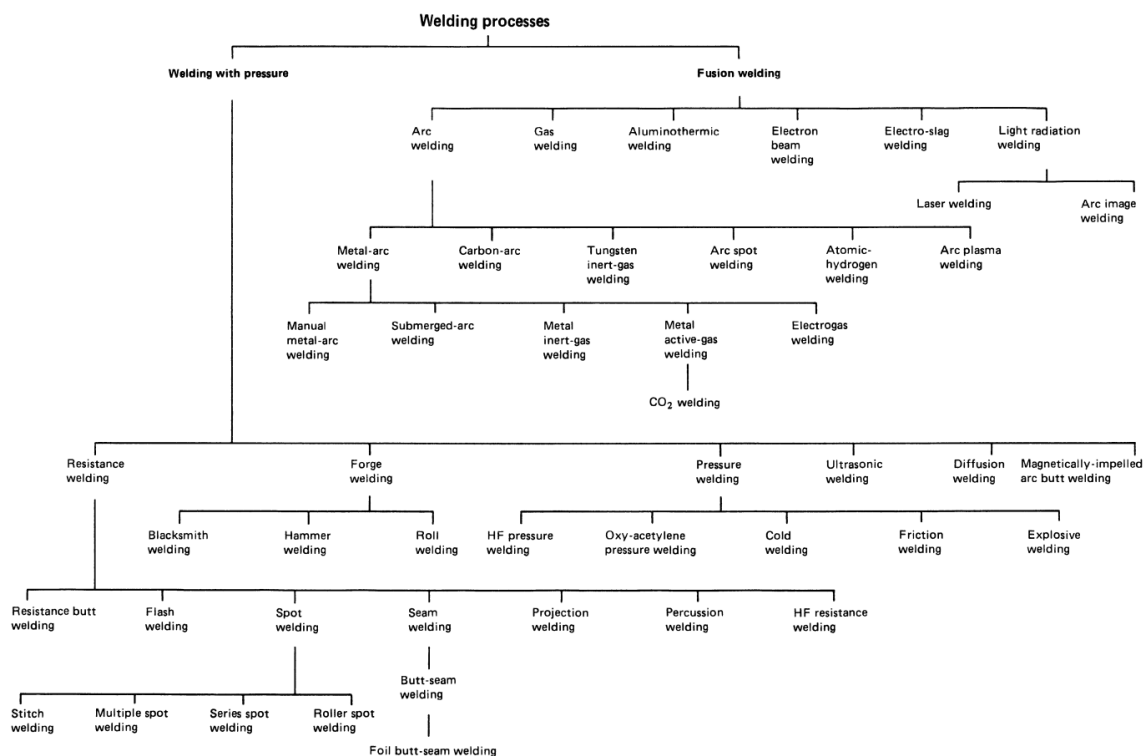


Figure 3.1 – Classification diagram of welding processes according to the latest British Standards [37].

3.1.2 Arc Welding Processes

In arc welding, an electric arc is formed between the base metal and an electrode. When the potential difference applied between the anode (the electrode or the workpiece) and the cathode is high enough to exceed the dielectric strength of the gas between them, an electric discharge is produced. The discharge causes ionization of the gas in the area leading in plasma formation. The generated heat causes melting of the local material. Subsequent solidification of the molten metal leads to fusion. The electrode can be either consumable – also serving as filler material – or non-consumable. A form of shielding is also required to protect the weld from atmospheric air and possible entrapment of oxides that affect the mechanical and chemical properties of the joint. The shielding can be in the form of an inert gas or protective coatings such as slag formed from fluxes. The different types of shielding methods and the different configurations of electrodes and filler materials allowed the evolution of different welding process, each presenting several advantages and disadvantages over specific applications. Some basic information of the most common arc welding processes are presented.

SMAW – Shielded Metal Arc Welding

Also known as manual metal arc welding or stick welding, SMAW is the most commonly used welding method. The arc is formed between a consumable electrode in the form of a rod and the workpiece. The electrode is covered by flux that when melted acts as a slag that protects the melt pool from atmospheric air. The low cost and simplicity of the equipment required, along with the convenience and portability provided as the need for shielding gas is eliminated, make SMAW a very popular welding method. SMAW is predominantly a manual welding process characterized by slower torch travel speeds and lower deposition rates compared to other processes.

SAW – Submerged Arc Welding

In the case of SAW the electrode is in the form of a wire and unfused granular particles comprise the flux that is supplied by a tube to the front of the path of the electrode. The electrode is submerged in the flux, making it invisible to the operator. High travel speeds and deep penetration can be achieved in SAW but its use is limited to flat and horizontal applications.

GMAW – Gas Metal Arc Welding

In GMAW, or Metal Inert Gas (MIG) welding, the weld pool is protected from the atmospheric air by a shielding gas (argon, helium or CO₂) and therefore no flux is required. The electrode is in the form of a wire, delivered through a nozzle in which the inert gas is blown coaxially. The arc is formed between the wire and the workpiece, causing the tip of the electrode to melt and a metal droplet to detach and fall in the melt pool. GMAW enables high travel speeds and easy control as the wire is fed directly in the weld while the torch is maintaining its distance from the workpiece.

GTAW – Gas Tungsten Arc Welding

GTAW, also known as Tungsten Inert Gas (TIG) welding, is a process similar to GMAW, but instead of the arc formed between the wire and the workpiece, a non-consumable electrode made mainly of tungsten is used. Shielding gas (mainly argon, helium or a mixture of both) is blown from the torch cup surrounding the electrode (Figure 3.2) to protect the weld-pool. As the electrode is non-consumable, GTAW can be used for the creation of both autogenous welds and welds with filler metal. The filler material can be delivered sideways of the torch, fed from the front of the welding direction. As opposed to MIG where the electrode is melting, the tungsten electrode allows a much more stable arc to be maintained, enabling welds of higher quality than MIG. Additionally, as the material transfer

is not occurring via the droplet transfer method, less spatter is witnessed and therefore cleaner welds are achieved. However, GTAW is a slower process and high skill is required as the operator needs both hands to control the torch and the filler material.

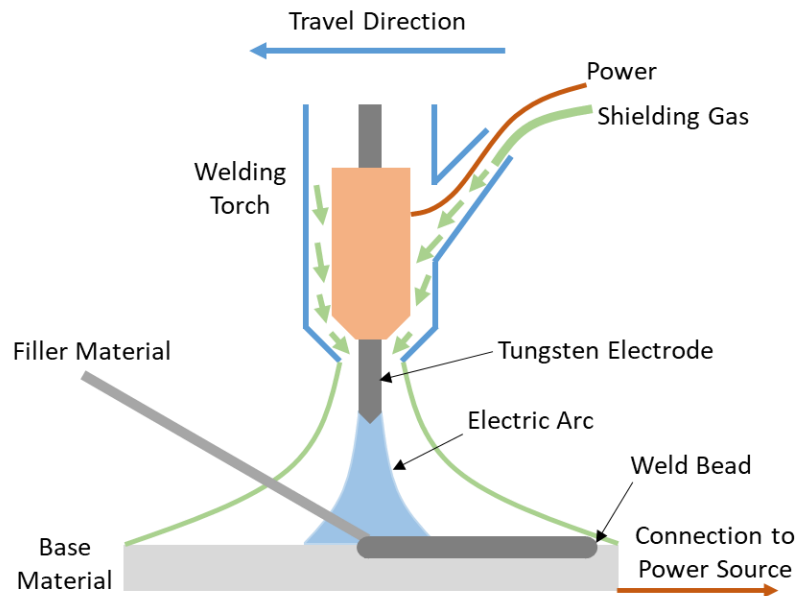


Figure 3.2 – Gas Tungsten Arc Welding diagram and torch schematic.

PAW – Plasma Arc Welding

PAW is similarly structured with GTAW, as it also uses a non-consumable tungsten electrode. In PAW however, ionized plasma gas is used in addition to the shielding gas. The arc with the ionized plasma are forced through a copper nozzle, providing higher energy density. This process allows higher travels speeds and deeper penetration than the aforementioned processes.

3.1.3 Geometry of a Weld

The geometry of a weld varies throughout different applications and different joint geometries. The geometrical features that characterize a weld and define its properties are the weld-bead shape and size, the depth of penetration and the properties of the heat-affected zone (HAZ). In Figure 3.3 an example of a cross-section of a weld is presented (V-shaped butt weld joint). The weld bead size and shape is what is defined as weld metal, composed by the filler material and the part of the parent metal that is melted and re-solidified (fusion zone).

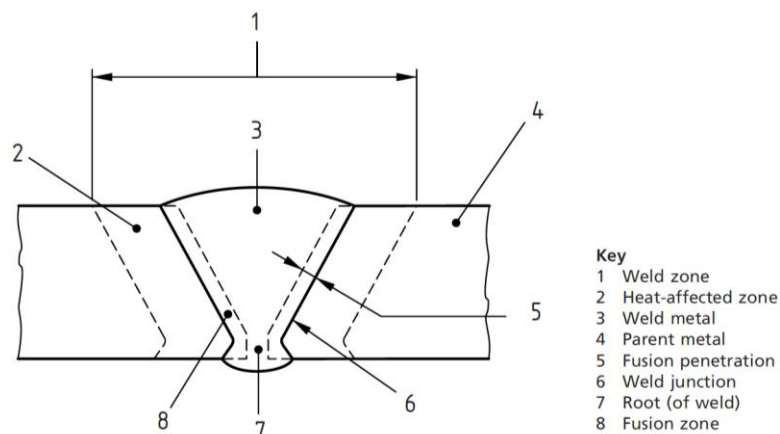


Figure 3.3 – Root, fusion penetration, weld junction and zones of typical welds [37].

The heat affected zone (HAZ) is the volume of base material at or near the weld where its properties have been altered due to the heat. As defined by the British Standards, HAZ is the area which is affected only by heat with no visible macroplastic deformation detectable by using optical microscopy. The fusion zone and the heat-affected regions are what compose the weld zone.

3.1.4 Welding Parameters and Welding Procedure Specifications

A series of welding process input parameters and conditions affect, directly or indirectly, the quality and the final outcome of a weld. With welding being a thermal process, the variables that contribute to the heat input of a weld are considered as the primary variables of a welding operation: current, voltage and travel speed. Additionally, primary variables can be considered the recipe and flow rate of the shielding gas, the wire feed speed (rate) and the electrode positioning (angle) [39], [40].

Selecting the right voltage, current, speed and recipe of gas should be good enough in order to achieve a good quality on a weld on a high level [41]. In general the welding current is the primary variable affecting the depth of penetration, while the voltage, related to the arc length, affects the width of the weld-bead. The travel speed affects the weld bead shape and the energy input [36]. However, welding is a complex process and for a given material there are a variety of additional factors that need to be considered in order to achieve the desired quality on a weld. These factors can range from the type of the current waveform provided from the power sources to the geometry of the weld groove and the joint preparation.

As means to achieve and maintain repeatable quality standards in a welding process, a welding engineer needs to generate a standard guideline to be followed. These guidelines, called welding procedure specifications, (WPS), contain a number of variables that affect, directly or indirectly, the quality of a weld. Fixed variables like the type of welding process, the type of the shielding gas and the shape of the electrode are maintained the same in all the individual welds following the specific WPS. Variables like current, voltage, travel speed and heat input are given values in a range, allowing some tolerance as long as the outcome is experimentally proven not to affect the quality of the weld.

3.1.5 Physics of Welding

In order to further elaborate on the advanced technologies that influence the weld bead geometries and heat affected zone and enable precision engineering for ATLAS and aerospace engineering, a brief analysis of the underlying principles and physical forces of arc welding is presented. As the author's work is related to GTAW the physical mechanisms presented are focusing only on this process. As shown in Figure 3.4 during GTAW a variety of forces are generated both within the plasma regions between the electrode and the workpiece as well as within the substrate weld pool.

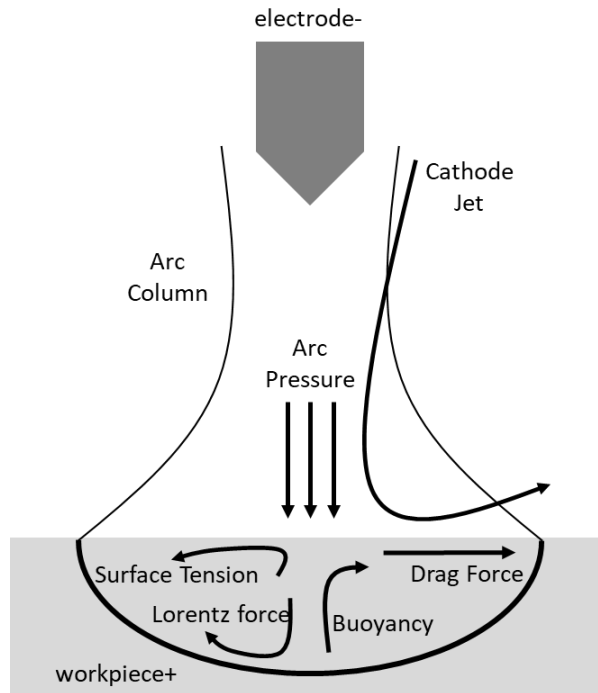


Figure 3.4 – Forces in the Gas Tungsten Arc Welding Process [42].

Forces: Plasma Region

The active force inside the plasma region is referred to as the arc force. Its main components are the electromagnetic force and the plasma jet force (Figure 3.5) [42], [43]. Some additional forces also contribute to the arc force (e.g. electron force) but their contribution is minimal compared to the two main forces.

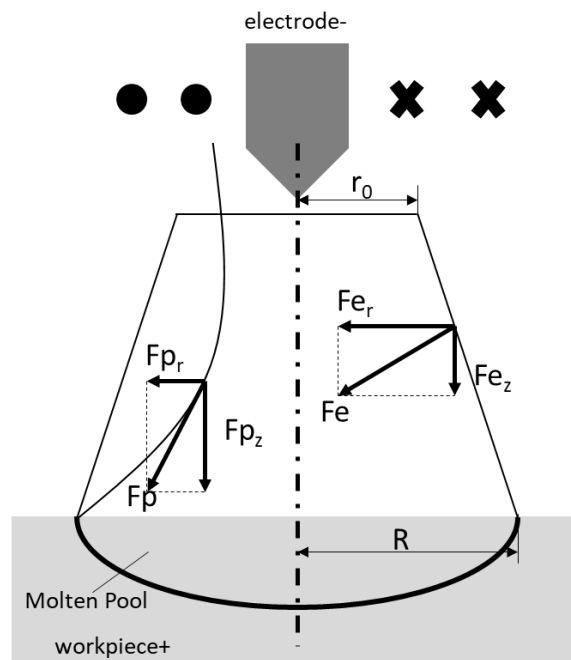


Figure 3.5 – Plasma region forces: plasma jet force (F_p) and electromagnetic force (F_e) [44].

The electromagnetic forces within the plasma region are a result of the welding current in the arc and the subsequent electromagnetic field produced by it. They are divided into the radial electromagnetic force (F_{e_r}) and the axial electromagnetic force (F_{e_z}):

$$F_{e_z} = \frac{\mu}{4\pi} I^2 \ln \frac{R}{r_0} \quad (3.1)$$

$$F_{e_r} = \frac{\mu}{4\pi} I^2 \ln \frac{R}{r_0} \cdot \frac{h}{R-r_0} \quad (3.2)$$

The plasma jet force is originating from the plasma flow, with a direction from the cathode region to the surface of the anode through the arc centre. This induced mass flow is a result of a phenomenon called “plasma pinching”, caused by the Lorentz force ($\vec{j} \times \vec{B}$) that is induced by the welding current. The magnetic field that is generated by the current narrows the arc plasma in the region close to the cathode resulting in the formation of a pressure gradient (Figure 3.6). At the surface of the anode the plasma jet changes to a radial direction, towards the periphery and the inertial force becomes the arc pressure. The plasma jet force is composed by the radial plasma jet force (F_{p_r}) and the axial plasma jet force (F_{p_z}).

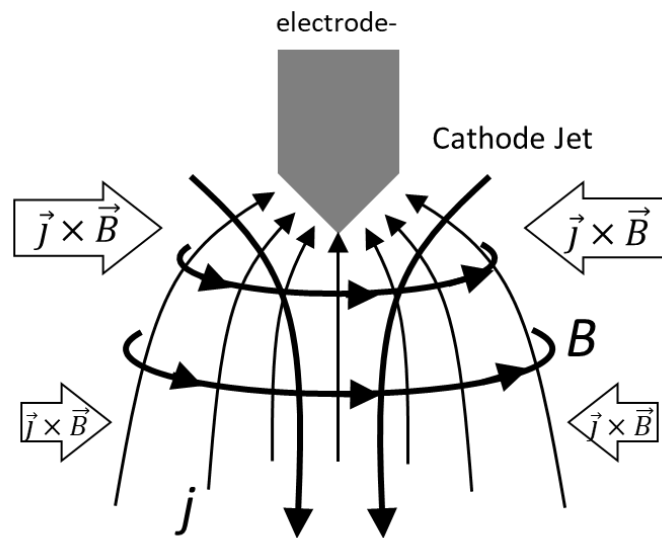


Figure 3.6 – Conceptual representation of the plasma jet and the Lorentz force ($j \times B$) by arc current and its self-induced magnetic field [45].

Forces: Weld Pool Region

The molten metal region resulting in the arc welding process is characterised as highly dynamic. A variety of forces act within the weld pool, all affecting the process’ final outcome. Differences between the weld joints geometries are mainly attributed to the differences in the convective current phenomena occurring within the weld pool. In relation to TIG welding, there are four main forces identified as the driving forces of these fluid flow convective currents. These forces are the buoyancy force, the electromagnetic force, the aerodynamic drag force and the surface tension (Figure 3.7).

The radial component of the aerodynamic drag force described above, caused by the plasma cathode jet, pushes the molten metal from the centre of the weld pool towards the edges. This weld pool drag force generates a surface fluid flow from the centre to the edge (outward flow) as shown in Figure 3.7a.

Similar to the electromagnetic forces in the plasma region, electromagnetic forces also act within the melt pool. The Lorentz forces are generated from the interaction of the induced magnetic field and from the current which is carried by the conductor [46]. The welding current within the melt pool

induces a magnetic field and the Lorentz force is acting inwards and downwards in the weld pool as shown in Figure 3.7b.

The buoyancy force is induced by the differences in density inside the melt pool as a result of the temperature gradient. An upward flow is therefore generated (Figure 3.7c).

The surface tension gradient of the molten pool induces forces related to the Marangoni effect. These Marangoni forces are thermocapillary forces whose resulting flow direction within the melt pool is defined by the material composition, predominantly the oxygen and sulphur concentrations. The large temperature gradient (order of 500 K/mm) between the centre of the molten pool and its edges suggests the generation of a large surface tension (γ) across the pool surface. As a result a Marangoni flow will occur from a region of low surface tension to a region of higher tension. Flows within the melt pool are subsequently generated as illustrated in Figure 3.7d and Figure 3.7e. For pure metals and metals with low contents of oxygen and sulphur such as iron and steels the tension is decreasing when the temperature increases. Therefore because of the low temperatures on the edges of the weld pool the surface tension is greater on the edges compared to the centre, causing a radial outward flow of that results in wide and shallow beads (Figure 3.8a). This outward radial flow is termed as negative Marangoni force (M-) because of the negative surface-tension-temperature coefficient. In metals with sulphur and oxygen concentrations greater than 60 parts per million (ppm), the surface tension is greater at the high-temperature central regions of the weld, resulting in a positive surface-tension-temperature coefficient and an inward radial flow (Figure 3.8b). A downward flow follows in the centre of the melt pool that pushes the molten metal deeper into the substrate. As a result a deeper and narrower weld bead is generated. In the cases where the positive tension-temperature reaches a maximum within a melt-pool temperature gradient a more complex flow is produced (Figure 3.8c) [47].

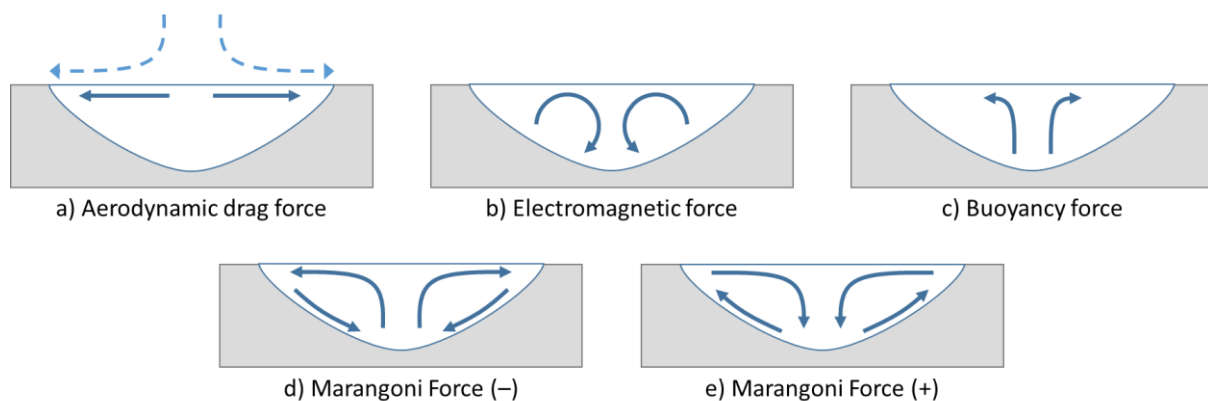


Figure 3.7 – Convective current flow forces in the weld pool region. a) aerodynamic drag forces resulting from plasma flow over the melt pool surface; b) electromagnetic forces (Lorentz) caused from the welding current and the magnetic field; c) buoyancy forces from density differences due to the temperature gradient; d) negative thermocapillary (Marangoni) forces; e) positive thermocapillary (Marangoni) forces.

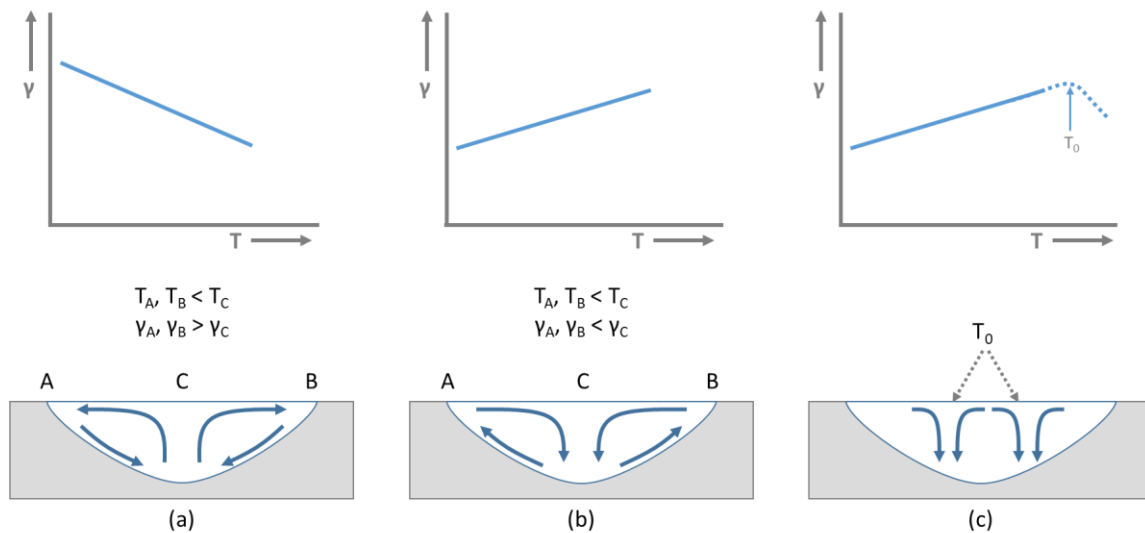


Figure 3.8 – Schematic diagram illustrating the Heiple-Roper theory for variable weld penetration [46]. a) Most pure metals with low O and S contents (including iron and steels); b) Fe-based metals with S (or O) > 60 ppm; c) systems that exhibit positive dy/dT reaching a maximum γ .

3.2 Pulsed GTAW

The majority of the aforementioned processes are described as traditional welding processes, which emerged when welding was still considered as a craft rather than a technological manufacturing process [48]. The need of improving the cost effectiveness and elimination of hazards in the welding environment led in great technological advances in the welding manufacturing processes. Applied intelligent automation and robotics are advancing the existing processes in order to increase weld quality and decrease the total cost effectiveness. New materials and new techniques are also being developed. Advances in GTAW include both basic process developments and automatic control of the process. Technologies on Arc initiation, power source modifications, wire feed alterations and inert gas combinations are transforming the traditional TIG welding process to a modern advanced manufacturing process. Relevant to the present research is the controlled heat management enabled by pulsed current power sources (Pulsed GTAW).

Pulsed-GTAW, is an advanced welding technology where the welding current undergoes modulation, switching between high and low preset values during regular intervals (pulses) [48], [49]. As a result of this technology greater control of the heat input is achieved, with subsequent regulation of the weld pool behavior and solidification. Newer inverter-based power sources with greater response times than the previous thyristor-based enabled the implementation of current modulation in the highest ends of sounding frequencies and ultrasonic frequencies [50].

Thermal Pulsing (Low Frequencies)

When the pulse frequency is low (1-10 Hz), thermal pulsing is occurring, enabling joining of materials with different thermal conductivity or dissimilar geometries, as well as difficult joints in thin materials. During the thermal pulse duration, the material is melting a single spot until the melt pool reaches the desired penetration. The current is then switched to the lower value, reducing the heat and allowing solidification to occur, while simultaneously providing sufficient energy to maintain the arc (Figure 3.9). The cycle is then repeated to the next point along the welding path, resulting in a series of overlapping identical single-spot welds [51]. By avoiding the excessive heat built-up that would have been accumulated with DC current mode, the thermal pulsing provides lower heat input and

subsequently reduced Heat Affected Zone (HAZ), while delivering the desired weld properties with uniformly penetration depth [50], [52], [53].

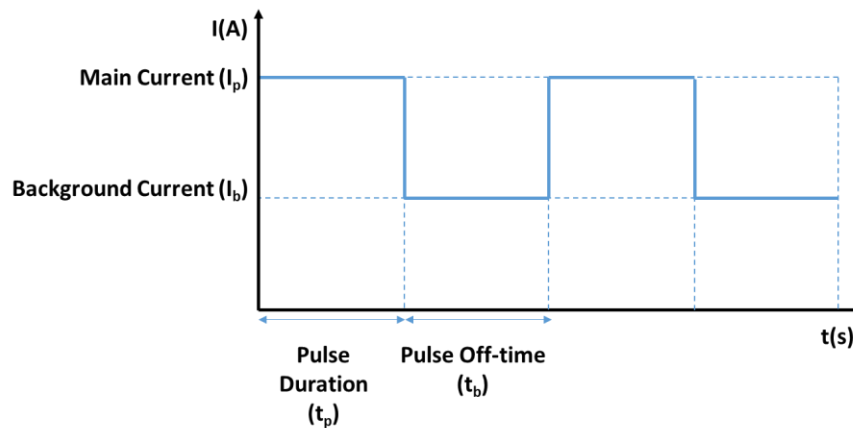


Figure 3.9 – Thermal pulsing waveform. The welding current is modulated between the pulse current (main) and the off-pulse current (background) during time intervals of low frequencies (1-10 Hz).

High frequency Pulsing

High frequency pulsing currents (>1 kHz), also referred to as InterPulse (Figure 3.10), have the ability to agitate the molten pool via forces generated as a result of the high frequency [50]. An arc root radius reduction witnessed in welding with high frequency current is resulting in narrower weld beads [54]. Studies on correlation between the arc root radius and the pulsing frequency have shown that with increasing frequencies the plasma root radius decreases [44], [55]. Additionally, with high frequency pulsed currents the arc force is significantly increased as the frequency increases [56]. This results in greater axial pressure, causing more depression of the weld pool surface and achieving increased weld penetration [55]. Higher energy density is also achieved, narrowing the HAZ and allowing higher welding speeds to be applied. Additionally, the arc stiffness is increased resulting in less arc wander [57], [58].

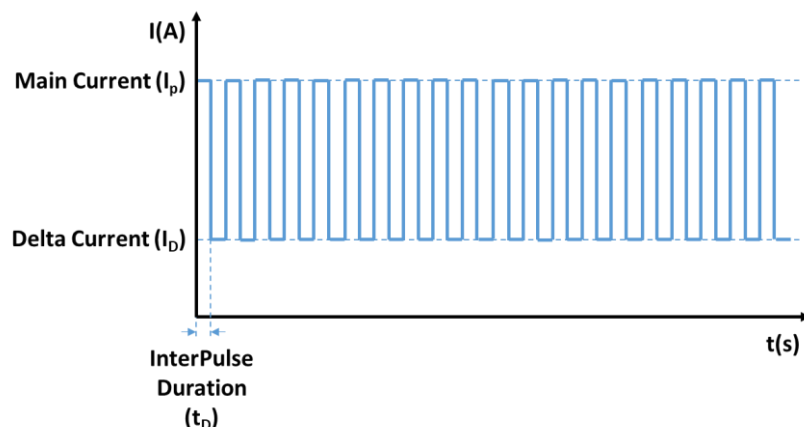


Figure 3.10 – High frequency (>1 kHz) pulsing waveform. The welding current is modulated between the main current and the delta current in InterPulse time intervals t_D .

The aforementioned properties can all be attributed to the plasma pinch effect that was presented in section 3.1.5. With high-frequency pulsing the axial electromagnetic force decreases where the radial electromagnetic force increases [44]. As this increased radial force, enhanced by the attenuation coefficient of the magnetic force, is imposed on the arc plasma, it results in further arc constriction [44]. With higher arc constriction the angle between the edge of the arc plasma and the sample area

increases resulting in less area under the arc shield. Therefore the arc root radius is reduced and larger arc pressure is imposed on the weld pool surface. It has been reported that, in the presence of arc constriction, the axial arc pressure increases in the area directly below the electrode center, up to a distance of 1.6 times the electrode diameter [44].

Because of the enhanced arc constriction, the high frequency GTAW process is also referred to as gas tungsten constricted arc welding (GTCAW).

Combination of high and low frequency pulsing

Technological developments related to power electronics and microcontrollers have enabled the development of modern power sources that can combine both the high and low frequency pulsing (Figure 3.11). This combination allows a process to benefit from the thermal pulsing heat input control properties while at the same time get advantage of the arc constriction properties enabled by the high frequency pulsing.

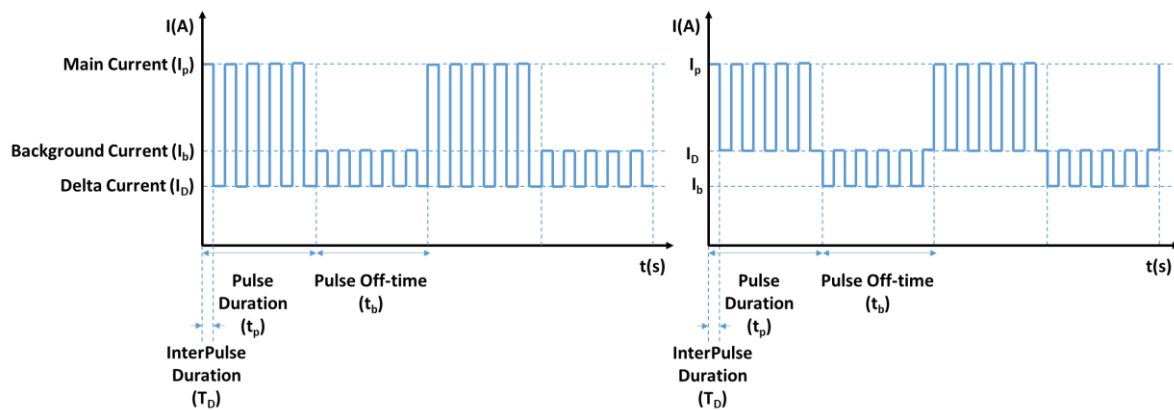


Figure 3.11 – Modern power sources allow the utilisation of combinations of high and low frequency pulsing. Left: high and low frequency pulsing with the InterPulse delta current lower than the background current; right: high and low frequency pulsing with the InterPulse delta current set between the main and background currents.

Changes in the microstructure

The solidification behavior of the weld pool, controls the resulting microstructure of the weld, and therefore plays a critical role in determining the ultimate strength of the joint [59]. In welding enhancing equiaxed (grains with axes of approximately same length) solidification is preferred [60]. Coarse columnar structures (elongated grains with uneven axes) are susceptible to hot cracking whereas other structures like finer grain or equiaxed are more resistant [61].

Notable changes have been reported in the microstructure of welds where high frequency pulsing was used in comparison with non-pulsed welds [50]. With the melt pool being agitated by the enhanced forces, the nucleation sites (where the crystals are starting to form from molecules) are disturbed resulting in delayed freezing. Therefore higher welding speeds and control of the solidification rate can be achieved. Evidence support grain refinement in both ferrous and non-ferrous materials. Two possible explanations on the grain refinement are a) the propagation of sonic disturbances through the molten pool that mechanically affect nucleation and its distribution; and b) pool turbulences break the tips off dendritic grains (tree-like structure of crystals growing as molten metal solidifies) that become sites for heterogeneous nucleation blocking further columnar growth. Repeated interruption of columnar growth then leads to formation of a region of equiaxed grains.

3.3 Pulsing Utilisation

Based on the aforementioned properties of pulsing currents, the author explored pulsing applications in both the ATLAS ITk cooling system development as well as applications in aerospace remanufacturing. Applications related to aerospace will be explored in detail in Chapters 4 and 5. In the following section the pulsing utilization in orbital welding for the joining of the ATLAS titanium cooling pipes is presented.

3.3.1 Orbital Welding

The process of welding tubes and pipes can be challenging depending on the working environment as well as the manufacturing application. In the case where the pipe is not fixed and therefore able to rotate, a traditional welding torch can be positioned stationary on top of the pipe (12 o'clock position – Figure 3.12). The pipe is then rotated, with the rotational speed adjusted accordingly in defining the arc travel speed. However, in cases where the pipes are not able to rotate, or in cases where restricted access does not allow the positioning of a stationary torch, orbital welding is utilised. Orbital welding may be defined as the welding process where the arc travels circumferentially around the external periphery of a fixed tube or pipe [62]. In order to achieve orbital welding, an automatic mechanism is required to rotate the welding torch around the pipe along a specific annular orbit [63]. With the pipe being fixed, it means the welding position changes along the weld seam from flat at 12 o'clock to vertical at 3 and 9 o'clock, overhead at 6 o'clock and inclined in-between (Figure 3.12). For this reason TIG welding is the process of choice in orbital welding as it is fully capable of consistent operation in all the welding positions [64]. Additionally, as TIG process uses non-consumable electrodes, it allows rotary and orbital welding heads to be easier developed than processes with consumable electrodes.

Orbital welding can be both autogenous or with filler wire, the latter requiring a wire-feeder regulating the feeding speed [65]. The option of autogenous welding translates also in less total heat input as the melting of added material is avoided, thus enabling higher welding speeds. In the case where the welded pipes are made of titanium, the orbital TIG process has the added advantage that the inert gas which is necessary for the fabrication also acts as the trailing shielding gas needed for protecting the seam from atmospheric air during cooling.

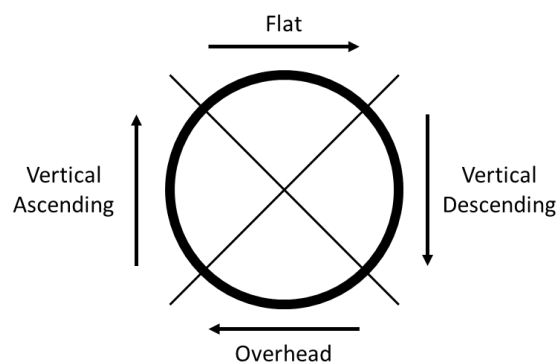


Figure 3.12 – Variations in the welding positions along an orbital welding path [66].

Commercial orbital TIG welding solutions are available for a variety of applications. For applications where the outer diameter of tubes does not exceed 200 mm enclosed-types welding heads are available where the autogenous welding is operated within the body of the enclosure. A fully shielded atmosphere is ensured with inert gas purged through the head around the outer weld seam as well as through the pipe. Since the shielding gas is already provided the only moving part is the electrode. For

larger pipes external mechanisms of geared rings are clamped on the pipe that drive complete welding torches with localised shielding, both autogenous and with filler metal. As seen in the previous section, pulsing currents have the advantage to significantly reduce the heat build-up in the welding component. This is of high importance in orbital welding as there is an overlap region at the end of the run where the arc overlaps the starting point of the weld seam. By utilising pulsed currents it is therefore enabled to reduce the residual heat build-up in a circumferential joint.

3.3.2 ATLAS ITk Development

The high level of robustness and quality required in operation under harsh conditions led to the selection of Ti CP2 and stainless-steel 316L as the materials of choice for the ATLAS ITk cooling system development. As presented in Chapter 2, the ultra-thin wall tubes are required to be welded in joints with each other as well as in joints with the ceramic electrical breaks in order to comprise the full assembly of the cooling system. Welding ultra-thin titanium components with repeatable results can be really challenging because of the multiple variables that require control during each part of the welding process. This challenge led to the formation of an industry-academia collaboration between the University of Sheffield and VBC Instrument Engineering Ltd. Utilizing the benefits of high frequency pulsed currents, modern control systems and existing commercial orbital welding tools, a low heat-input automatic orbital welding system was developed. This welding system provides new opportunities in applications where thin titanium alloys have proven to be an asset. Titanium's mechanical properties of high strength and good corrosion resistance allow the material use as tubing in cryogenic, aerospace, defence, energy and biomedical manufacturers.

Joining process

The orbital welding solution comprises of an InterPulse Heat Management System (IP50-HMS) and a commercial orbital welding head. Incorporating InterPulse technology, the IP50-HMS (Figure 3.13a) has the ability to produce accurate narrow bead welds on the circumference of tubes, leading to exceptional weld quality and control over the whole welding process [67]. The programmable unit gives the user a wide range of parameter setting freedom including control of welding currents and high frequency pulsing. Fostering the advantage of increased arc force due to the arc constriction the high frequency pulsing used by the system allows deeper penetration while using significantly lower input current. As a result, improved heat management is possible on these critical welds.

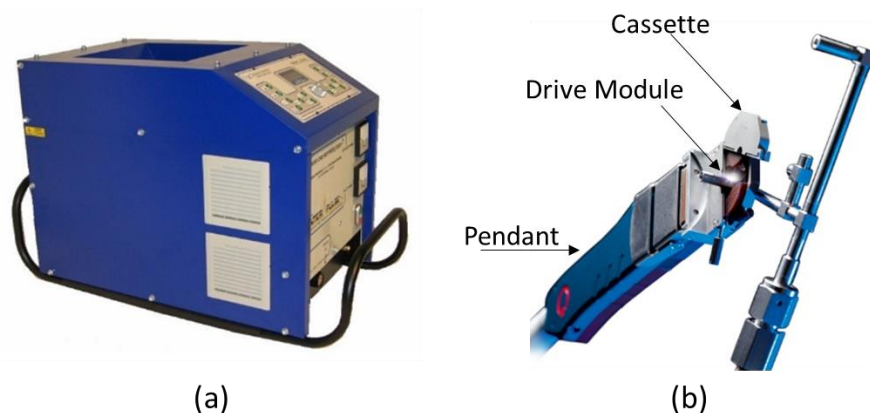


Figure 3.13 – (a) The VBCie HMS IP50 welding machine; (b) The Polysoude UHP closed chamber welding head. (Photo credits: VBCie Ltd and Polysoude S.A.S).

The orbital movement is achieved using a Polysoude Orbital Welding Head UHP 250-2 (Figure 3.13b). Its closed chamber welding head produces autogenous welds, while its compact design allows access to restricted areas with good shield gas coverage. The head comprises of three parts: the pendant which ensures connection with the power source; the drive module used to transmit both the motion and the welding current to the electrode; and the cassette used for the correct alignment of the tubes and positive polarity connection to the workpiece.

Welding of Pixel cooling loops

The Forward Pixel sensors of the ATLAS ITk will be cooled by semi-circular titanium loops embedded in a carbon fibre structure upon which the silicon detectors are mounted. In the first demonstration of the process for the application, orbital welding was performed on cooling loops prototypes [1]. Fitted ends were welded on bent tubes as shown in Figure 3.14. The welding head cassettes were used for fixturing and alignment and argon shielding gas was purged around and through the tube at monitored pressure.

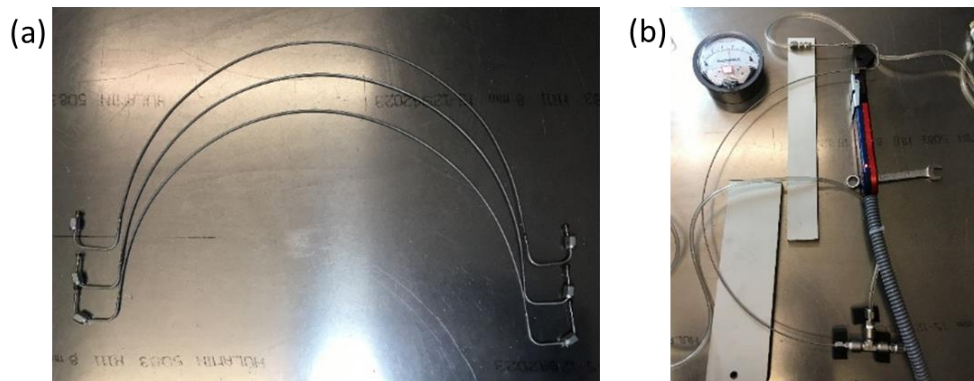


Figure 3.14 – (a) The Pixel cooling semi-circular loop demonstrator after welding, (b) Welding of the cooling loop using the Polysoude UHP closed chamber welding head.

Welding of the Strip Staves

Similarly to the Pixel detector, in the larger Strip detector the silicon sensors are mounted on a CFRP structure, the “Stave”. The elongated U-shaped titanium cooling loop embedded in the core was tested in orbital welding with the system developed. The initial results, after tensile destructive testing, showed that the mechanical properties of the final product were not acceptable for passing the QC. The reason was detected to be problems in the correct alignment of the tubes. The long size of the tubes, fixed and mounted using the cassettes of the welding head, were causing a slight misalignment altering the geometry of the welding joint.

In order to fix the misalignment problem the University of Sheffield designed and manufactured a custom alignment jig (Figure 3.15a). With the new jig structure, the long u-tubes are attached securely on the mounts and the welding head is inserted in position over the tube joint location (Figure 3.15b). The cassette part of the welding head is removed when the jig is used as the pipes are already aligned. A finished weld with the tube-to-tube joint fixed in position is shown in Figure 3.15c.

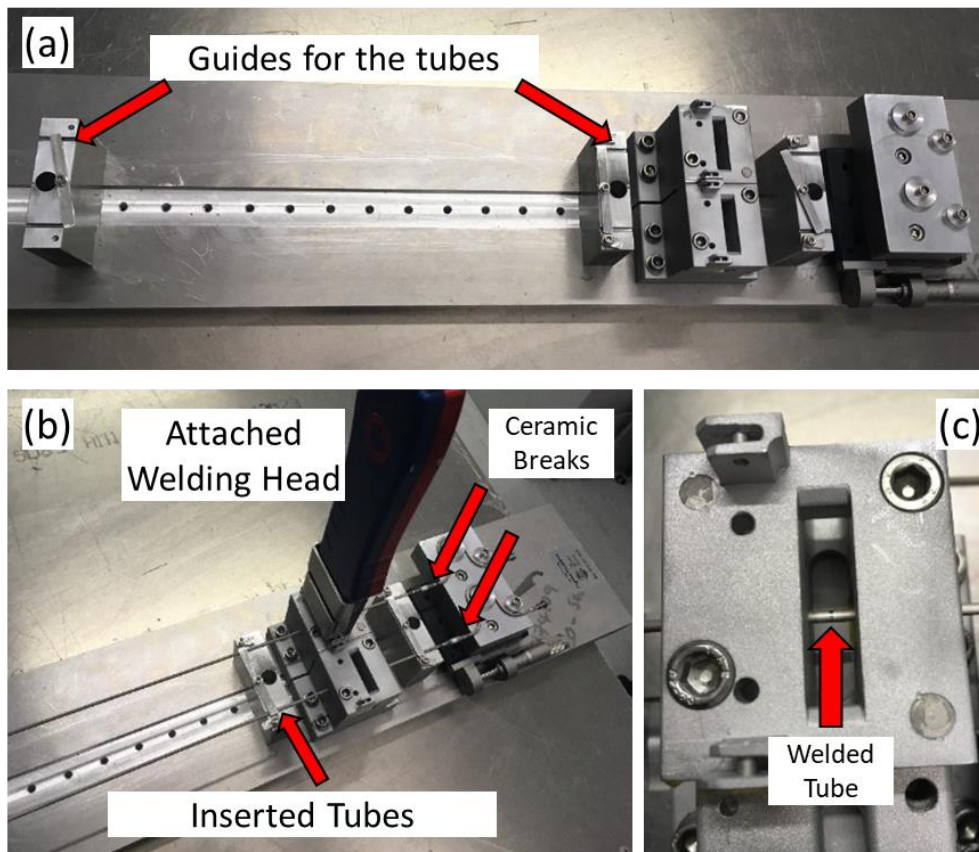


Figure 3.15 – a) Custom-build jig structure designed to support the cooling staves for the ATLAS ITk Strips to replace the cassettes to improve alignment; b) The welding head is entered and fixed precisely on the welding position of the alignment jig; c) Successful welding of the welding Strips U-shaped stave cooling loop tubes, correctly aligned on the jig.

Welding of the ceramic electrical break

When the weld joint is asymmetrical – as in different outer diameters between the two parts – different size of fixtures and electrode positioning are required. This is the case of the weld joint between the cooling tubes and the electrical isolator (Figure 3.16). The University of Sheffield ATLAS team, in a series of welding experimentations investigated the welding of the ceramic isolator to the titanium tubes in order to identify the optimal set of input parameters and setup. The dimensions of the ceramic break chosen allowed the titanium tube to be fitted inside the break. For the experimentation and the ongoing optimisation of the process, same-dimension titanium fittings are used for cost saving purposes. Two types of fixture cassettes were used to maintain the joints aligned and a custom-made sleeve guide was keeping the fitting in position to achieve repeatability. The published results revealed that the constricted arc achieved by high frequency pulsing allowed the successful joining of the ultra-thin titanium tubes to quality levels acceptable for the ATLAS ITk production [68]. The tensile strengths of the joints were found to exceed the tensile strength of the parent Ti CP2 and microstructure observations revealed weld grains of similar sizes with the ones of the parent metal. These findings confirm the effects of pulsing currents in terms of microstructure as presented in the Section 3.2.

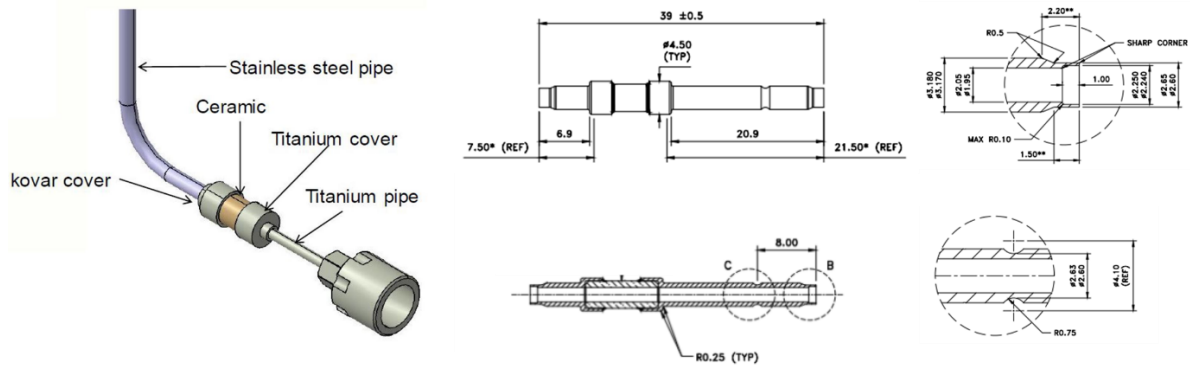


Figure 3.16 – Ceramic electrical isolator. Left: 3D schematic of the electrical breaks used in the IBL; Right: technical details of the electrical breaks to be used in the ATLAS ITk detector.

3.3.3 Welding Defects in Orbital Welding

The orbital welding process, though capable of producing repeatable quality results, can be susceptible to a variety of welding defects. Typical defects in orbital welding are the incomplete root fusion (lack of union at the root of a joint), the uneven penetration profile and the formation of root penetration concavities (shallow groove that may occur in the root of a butt weld) [51]. Since the process selected for development of the ATLAS ITk cooling system is fully automated, errors resulting from manual welding are avoided. Provided that the input parameters (e.g. current, voltage, travel speed) and welding conditions (e.g. inner tube pressure) are at optimal levels as defined by designed experiments, the majority of defects occurring in automatic TIG orbital welding can be traced back to:

- surface anomalies and pre-weld machining defects.
- improper surface preparation and contamination.
- interruptions of the shielding gas flow.
- errors in joint geometries from tube misalignments.
- electrode degradation.

The detection of such defects might not be possible by visual means at the time of production and may require further destructive or non-destructive testing to be detected. As seen in the previous section, during the welding of prototype Strip barrel cooling loops, slight misalignments were causing welds to underperform during tensile tests. These faulty welds were detected after the prototypes were completed which highlights the importance of developing a system capable of informing the operator of potential defects in the welds.

Following this need, the University of Sheffield developed a high-speed data acquisition system for monitoring the welding process. Work published by the author at the 70th International Institute of Welding Annual Assembly and Conference 2017 [1], describes how voltage and current measurements were gathered during the orbital welding process for tube-to-tube butt weld joining of the ATLAS titanium tubes. The measurements revealed changes in the voltage and subsequently the active power on two of the eight welds. The two welds where the disturbances were detected failed the subsequent destructive testing while the welds with undisturbed measurements passed. This gathering of valuable data during the welding process and the demonstrated detection of disturbances linked to defects in the weld joints enables the potential prediction of welding quality. The system, analysis methods and prediction methodologies will be in-depth presented in Chapter 6.

3.4 Conclusion

In this chapter an introduction to the arc welding processes was made and an overview of the forces contributing to the outcome of the weld was presented. The concept of pulsing welding currents was introduced followed by pulsing implementation in orbital welding. By utilising high frequency pulsing the joining of thin-walled titanium pipes was presented for the development of the cooling system of the ATLAS ITk detector. In the aspects of the presented work cooling loops prototypes were welded for the Pixel end-cap semi-circular loops and the Strip barrel staves. In order to detect faulty welds and contribute to the quality assurance, a welding monitoring system was introduced.

4 Welding-Based Additive Manufacturing

In this chapter the Wire Arc Additive Manufacturing process is presented, along with its benefits for the aerospace remanufacturing industry. Investigations on process and material performance in the controlling of desired bead geometry and heat affected zone are also presented followed by illustrations of dynamic competing phenomena identified in the melt pool. The majority of this work has been published in the Journal of Manufacturing Processes [7].

4.1 Additive Manufacturing and Remanufacturing

Components used in the aerospace industry are characterized by their high value, due to their manufacturing and evaluation processes combined with the use of specialized materials which results in high production costs. Because of this high value the remanufacturing and reuse of aerospace components is taking place where possible, resulting in significant savings. The term remanufacturing refers to "the rebuilding of a product to specifications of the original manufactured product using a combination of reused, repaired and new parts" [69]. Though remanufacturing engulfs various processes that lead to product recovery, the final outcome of a remanufactured product should match the same industry specifications as a new part. For this purpose remanufactured products undergo extensive testing and their performance is evaluated to be at least the same as their new counterparts.

As presented previously in Chapter 2.4, the benefits of additive manufacturing in terms of material, weight, and time savings have found extensive applications in the aerospace sector. Examples of AM applied in aerospace have been seen in both aircraft and spacecraft propulsion systems (e.g. aircraft titanium fuel nozzles, rocket engine regenerative-cooled nozzles, the pogo accumulator) and structural assemblies (e.g. Airbus A350 titanium brackets, waveguide brackets on NASA's JUNO spacecraft) [20], [70]. The AM benefits are also heavily explored and are expected to have widespread application in the aerospace maintenance, repair and overhaul industry (MRO), providing product regeneration with a reduced remanufacturing cost of 50% compared to conventional processes [71].

Mainly originating from welding technologies, there are different metal AM processes, each with its own advantages and disadvantages, making them suitable for specific applications. The AM processes are classified either by the form of the material feeding technology used, or by the form of heat source they utilize. Processes where the additive material is in the form of powder in a container with the heat applied directly on top of it are called "powder bed" ("bed" from here on) technologies, where the processes with powder delivered into the melt pool generated by the heat source are called "blown powder" or "powder-fed" technologies. In the cases where the additive material is provided in the form of a wire, the processes are characterised as "wire-fed" processes ("fed" from here on).

Hybrid AM systems also exist and can be either a "bed" or a "fed" system, combined with a milling machine. In "bed" and "fed" systems the additive material is being added layer by layer to form the final part, which is then moved outside the system and down the production line for post-processing, including milling and heat-treatment. In hybrid systems the milling process occurs within the system, resulting in a finished part that meets the geometrical requirements.

In order to fuse the additive metal material to the base material, welding techniques are employed. When classified by heat source used for the material melting, there are three main metal AM categories: electron beam based, laser based and electric arc based. The most commonly used

processes in AM are laser welding and electron beam welding (EB). Laser and EB present good dimensional properties in the shaping of parts, as a result of their very high energy density. On the downside, their material deposition rate is lower with big differences between laser and EB and their cost of equipment is high.

4.2 Wire Arc Additive Manufacturing

The process combining the wire feeding technology with an electric arc power source is usually called wire arc additive manufacturing (WAAM). Other names include welding shape deposition, 3D welding, shape metal deposition (SMD), shape welding and structural weld build-up [72]. WAAM uses an arc welding power source to melt the wire-shaped additive material which is guided by a motion platform and a digital control platform. Apart from its simplicity compared to other AM methods, WAAM provides a variety of other benefits. In particular it has the ability to manufacture large components, as opposed to powder bed and electron beam based AM methods where the manufacturing dimensions are restricted by the powder bed size and the vacuum chamber respectively [73]. This allows the manufacturing of larger aerospace frame components like wing spars resulting in additional cost savings both in weight and production time. Another benefit of the process is the minimal waste of feedstock compared to blown powder methods. The ability of the system to control the wire feed-rate and direct it to the weld pool provides high material consumption efficiency. WAAM has also the ability to deliver higher deposition rates compared to other AM processes [74]. Additional benefits of WAAM include the relatively low cost of equipment, high power efficiency (40%–90%) and larger selection of materials since welding is a more mature process than AM [75]–[77].

WAAM can be performed using three main types of welding technologies. The most frequently used is Metal Inert Gas (MIG), referred to as Gas Metal Arc Welding (GMAW) in Chapter 3.1. The main benefit of MIG used in WAAM is that the wire, which is also the consumable electrode that forms the arc, is positioned coaxially to the welding torch, which allows higher freedom of movement in contrast with the non-consumable electrode methods like Gas Tungsten Arc Welding (GTAW) and Plasma Arc Welding (PAW) where the filler wire is added sideways between the electrode and the workpiece. A modified MIG variant named Cold Metal Transfer (CMT) based on controlled dip transfer mode has been reported to provide weld beads of high quality and low thermal heat on aluminium and steel [78]. In CMT the filler wire is retracted in between the droplet transfers providing sufficient time for the weld to cool after receiving the next droplet. When applied to titanium, the process is unfortunately experiencing arc wandering resulting in increased surface roughness. Therefore GTAW and PAW are the processes of choice for WAAM of titanium alloys [79].

Since in GTAW the electrode is non-consumable, greater control over the electrode-workpiece distance can be achieved, resulting in greater arc stability than in processes with consumable electrodes. Additionally, GTAW can produce cleaner welds of greater finish than MIG, due to reduced spatter, as metal droplet transfer is better controlled. GTAW however, requires more time to complete a weld than MIG, and is regarded as a slower process [80]. The GTAW process can operate on both direct and alternating current depending of the application.

4.3 Desired bead geometry in Wire Arc Additive Manufacturing

WAAM is considered a Near Net Shape (NNS) process, meaning that the fabricated parts are close to their final geometries while still requiring further processing (e.g. machining, surface finishing) to reach their final geometry. In order to reach closer to net shape, an increase in the printing resolution

is required; the results vary from process to process. To achieve that level of printing accuracy in WAAM, proper control over penetration depth, weld cap reinforcement and bead width is required (Figure 4.1). Built-up passes may significantly differ from the root pass, where deep penetration with wide bead width is desired for a robust structural foundation. These demands require interchanging modes of operation in the same environment, provided either by different equipment or by a setup that can provide a variety of bead geometries.

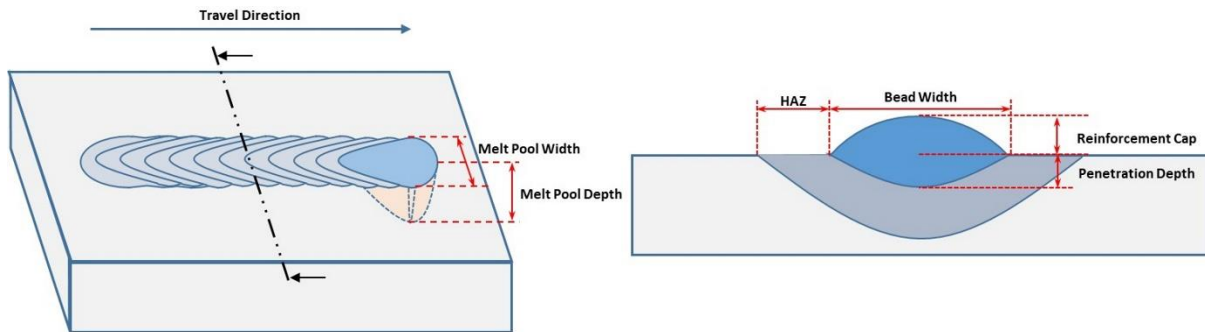


Figure 4.1 – Bead-on-plate welding process (left) with its corresponding cross section (right). The melt pool width corresponds to the width of the bead whereas the melt pool depth defines the penetration depth.

As seen in Chapter 3.2 pulsing currents affect the weld pool properties via changes in the forces dominating the welding process. It is therefore worthy to investigate changes in the weld bead geometry utilizing the variety of current modes provided by Pulsed-GTAW. In Figure 4.2a a cross section of a general weld bead geometry with high penetration is presented. While this geometry is ideal for the root pass on the substrate, it is not beneficial for the built-up passes, as high penetration depth liquefies the previous passes and reduces the existing wall height by widening the melt pool. By reducing the penetration depth and increasing the reinforcement cap, more flattened beads are formed (Figure 4.2b). Additional increase in the reinforcement cap results in more “bumpy” beads (Figure 4.2c) where the height of the reinforcement exceeds the depth of penetration. Finally, by reducing the bead width while increasing the reinforcement cap a more rounded ball-shaped bead is formed (Figure 4.2d).

Side-wall roughness should also be taken into consideration in wall build-ups, as a smoother surface closer to net shape will require less machining, while uneven surfaces will increase processing time and material waste. Successive layer depositions should ensure overlapping bead geometries to avoid undercuts that may result in cavity formation [81].

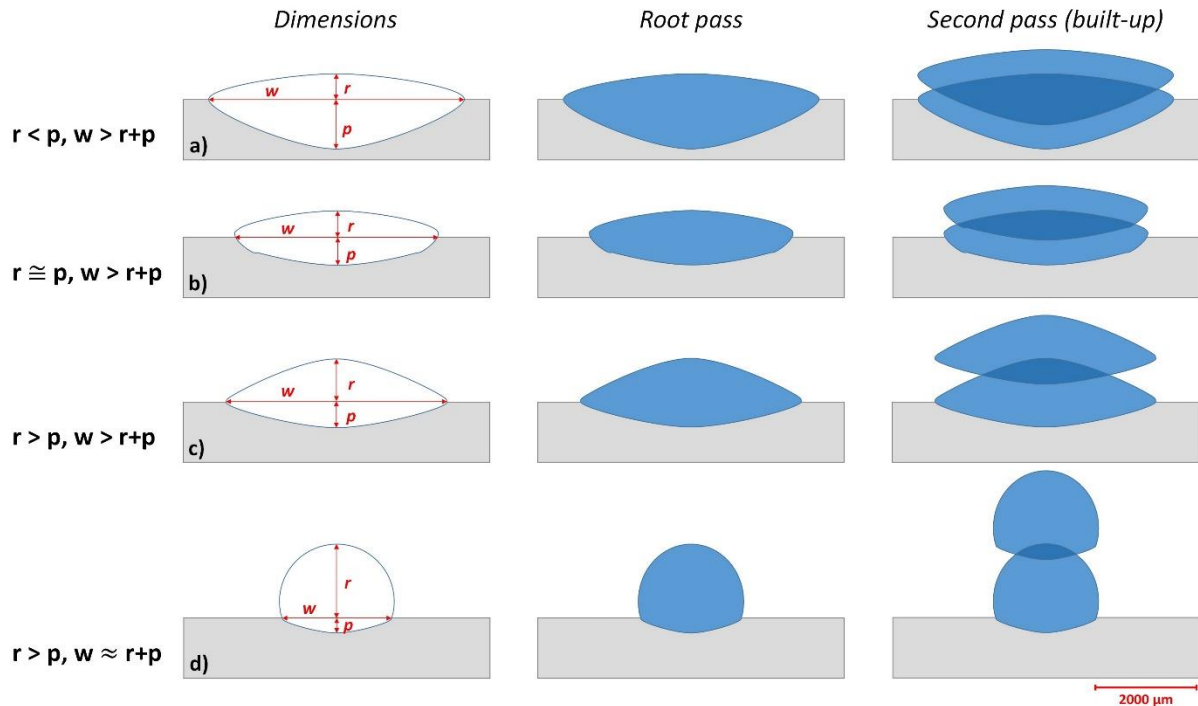


Figure 4.2 – Weld bead geometries characteristics for Wire Arc Additive Manufacturing (WAAM). The total bead height is defined by the reinforcement cap (r) and the penetration depth (p). Alterations in the ratios between bead height and width (w) can be utilised to form different bead geometries for root passes and secondary passes in WAAM.

4.4 Pulsed Wire Arc Additive Manufacturing

In the following work the author attempted the simultaneous control of penetration depth and bead width through alterations of pulsing modes and travel speeds in GTAW-based WAAM. The effects of the welding parameters on the weld bead geometry and heat affected zone of different current modes were investigated. Direct current, low frequency thermal pulsing, high frequency pulsing and a combination of both low and high frequency pulsing (double pulse) were applied in a series of experimental designs using filler wires of both titanium and nickel-based alloys used by the aerospace industry. The aim was to extract guidelines for parameter values and current modes utilizing the aforementioned properties of pulsing, to be used in WAAM aerospace component repair. The present work was performed at the Advanced Remanufacturing and Technology Centre (ARTC).

4.4.1 Materials and Methods

Experimental Setup

For this study an automatic welding system composed of a Pulsed-GTAW power source with the torch mounted on an industrial robotic arm was used to deliver beads-on-plate welds. The welding power source was an IE175i Heat Management System by VBC Instrument Engineering and the robotic arm used for the control and torch manipulation was an ABB IRB 2400/16 (Figure 4.3). The welding process was monitored using a sensor box custom-built by the University of Sheffield (more details in Chapter 6.3), connected to a Tektronix DPO 2022B Digital Oscilloscope, offering real-time weld current and voltage data.

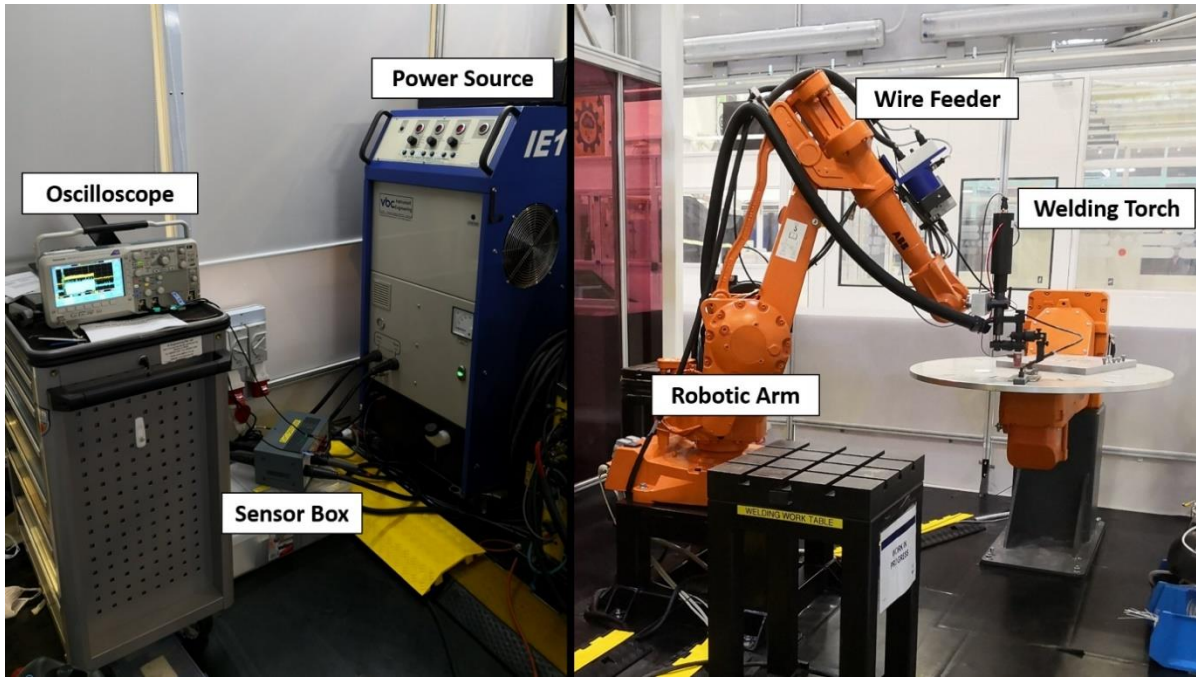


Figure 4.3 – Experimental setup used for GTAW-based WAAM.

Materials

The materials selected for the investigation were Inconel 718 (IN718) and Titanium alloy Ti-6Al-4V (Ti-6-4). These two materials are used in a variety of applications in the aerospace industry. IN718 is used in applications with elevated temperatures because of its superior mechanical properties and oxidation resistance in high temperature environments [82]. Applications include among others gas turbines, fuel tanks, heat exchangers, gas bottles for storage of high-pressure oxygen in space missions and outer casings of nickel-hydrogen cells for energy storage [83]. Ti-6-4 is considered the workhorse alloy of titanium responsible for 60% of the total titanium production [16]. It is used for its corrosion resistance, higher strength and creep resistance in a variety of applications including static and rotating components in jet engines, fasteners and airframes.

Two filler and plate material combinations were used in two different design of experiments which are presented below. In one set of experiments a combination of dissimilar metals was used to highlight the geometry boundaries of the additive material on the substrate after etching, while in the other one the same material was used as both substrate and additive wire, focusing on the weld heat affected zone. On the first experimental run AMS 5832G Inconel 718 wire (0.889 mm \varnothing) was used, delivering beads on Stainless Steel 316L (SS316L) 150 mm x 100 mm x 6 mm plates [84]. On the second one, AMS 4954J Ti-6Al-4V wire (1.143 mm \varnothing) was used to form beads on 150 mm x 100 mm x 3 mm plates of the same material [85]. The chemical compositions of the materials are presented in Table 4.1 and Table 4.2. Localized shielding gas environment was provided in all runs using pure argon at a flow rate of 17 l/min, delivered through the welding torch cup.

Current modes

In order to investigate changes in weld bead geometry for additive built-up applications, five welding parameters that contribute to the outcome of the welding process were selected. Three of them, namely Main Current (I_p), Background Current (I_b) and Delta Current (I_d), are directly related to the different current modes that were investigated, while the other two were the torch travel speed and the wire feeding rate. Four different current modes were used, as presented in Figure 4.4. Continuous

Current mode refers to direct current with no pulsing, maintaining the main value during the deposition. Slow Pulse Current mode refers to the thermal pulsing operation, where the current has the main value during the pulse duration (t_p) and the background value for the rest of the duty cycle (t_b). All the welds performed with slow pulse mode in this study had the same duty cycle $\delta = 50\%$, with both the t_p and t_b values at 0.3 s resulting in a 1.66 Hz pulsing frequency. In the InterPulse Current mode the frequency of the pulsing was set at 20,000 Hz, with the current values changing from Main to Delta every $t_D = 0.025$ ms. Finally, on the InterPulse Current with Slow Pulse mode, the two modes are combined providing both thermal and high frequency pulsing, resulting in current values between Main and Delta for the pulse duration (t_p), and values between Background and Delta for the remainder duty cycle (t_b). Mean current was calculated taking into consideration the current mode used in each weld, as presented in Figure 4.4.

Table 4.1 – Chemical composition of welding wire Inconel 718 (wt.%).

	Ni	Fe	Cr	Nb/Ta	Mo	Ti	Al	Co	Mn	Si	Cu	C	P	B	S
IN718	52.7	18.7	18.3	4.99	3.03	1.02	0.56	0.35	0.23	0.07	0.07	0.053	0.007	0.003	<0.002

Table 4.2 – Chemical composition of welding wire Ti-6-4 (wt.%).

	Ti	Al	V	C	Fe	H	N	O
Ti-6-4	Bal.	6.02	3.98	0.04	0.015	0.0125	0.02	0.13

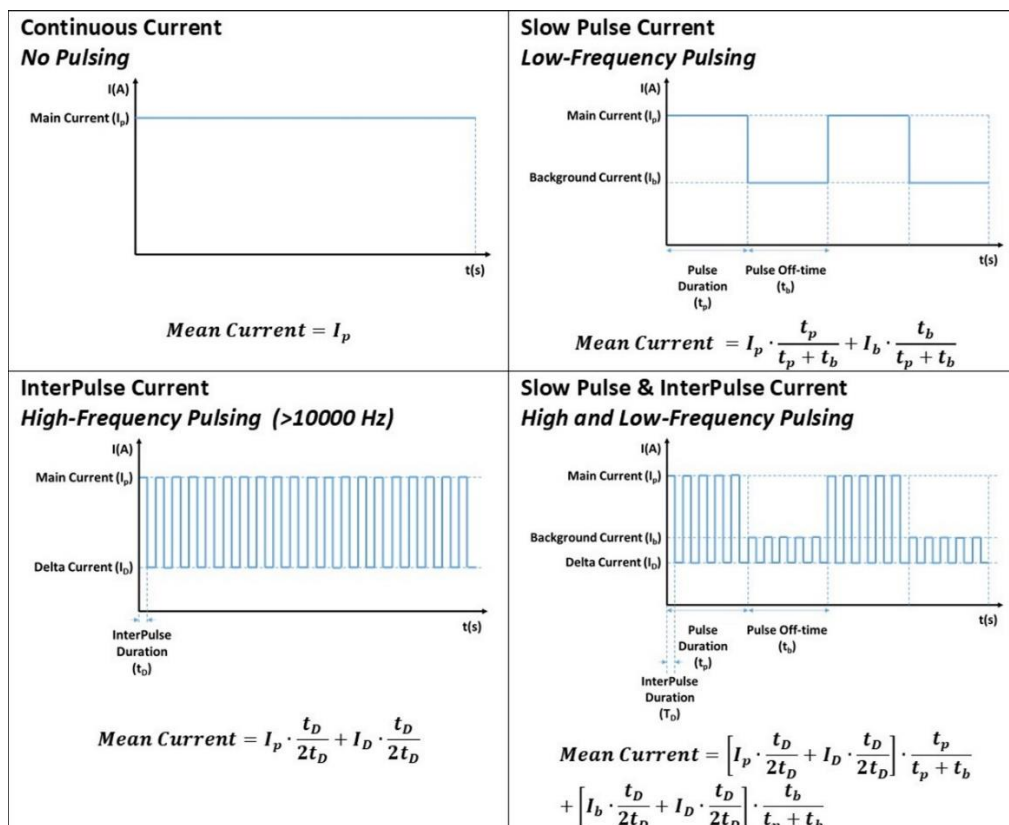


Figure 4.4 – Welding current modes with corresponding mean current calculations based on pulsing frequencies.

For a more clear representation in the comparison of different current modes and their effects on the weld, the heat input of each weld needed to be calculated, defined as the arc energy over the travel distance (Equation 4.1) [86], [87]. The welding machine used is characterized as a Constant Current

Power Source (CCPS), where the user presets the desired current output and the machine adjusts the voltage output based on the distance between the electrode and the workpiece. In the present work, a gauge was used to ensure the same electrode-workpiece distance in all the welds. Therefore the results related to the heat input are presented in the form of the electric charge input, defined as the charge delivered to the process per mm of travel distance (Equation 4.2). This simpler representation highlights the changes based on the input parameters of the operator related to the current and not on the machine-dependent (as electrode-workpiece distance was kept constant) or the process-dependent (TIG thermal efficiency) changes (Equation 4.3).

$$E(J/mm) = \frac{\text{Voltage (V)} \times \text{Current (A)} \times \text{Process Thermal Efficiency (\%)}}{\text{Travel Speed} \left(\frac{mm}{s}\right)} \quad (4.1)$$

$$\text{Electric Charge Input} \left(\frac{C}{mm}\right) = \frac{\text{Current (A)}}{\text{Travel Speed} \left(\frac{mm}{s}\right)} \quad (4.2)$$

$$E(J/mm) = \text{Electric Charge Input} \left(\frac{C}{mm}\right) \times \text{Voltage (V)} \times \text{Process Thermal Efficiency (\%)} \quad (4.3)$$

Design of Experiments

For the selection of the welding parameter values a Taguchi-inspired orthogonal array approach was followed. The Taguchi methods are a series of statistical method that are used to improve the quality of the outcome of a process, particularly manufacturing processes. In the Taguchi method with a fractional factorial design the main effects and the effects of the desired interaction are allowed to be studied in a minimum number of trials [88]. By incorporating noise factors and focusing on process robustness the need for the randomization needed in the classical Design of Experiments (DOE) approach is superseded. The Taguchi approach is frequently used in designing of welding experiments, in a variety of welding processes [89]–[91]. In the present case where the experiments implement switching between different current modes and are designed using an orthogonal array, the subsequent Taguchi analysis cannot be performed. This is because the array ceases to be orthogonal when the mean current values are calculated for a given duty cycle. In such cases a Taguchi-inspired methodology can be followed, where an initial investigation follows a fractional Taguchi design to identify contributing factors to the output and to verify a preliminary hypothesis [92]. This research stage is termed as “exploratory stage” and is followed by the “search stage” where subsequent experiments need to be run independently to establish the optimal levels of the contributing factors [92]. In this study the Taguchi approach was used with a partial factorial design as a guideline, in order to incorporate the different current modes in a single experiment. In this exploratory stage, for the five parameters selected (identified as factors in the design), three values (levels) were chosen for each experiment based on previous WPS for the selected materials. The two separate experimental runs followed the $L_{27}(3^5)$ Taguchi design (Table 4.3) with the values of each parameter presented on Table 4.4 for IN718 wire on SS316L plates and Table 4.5 for Ti-6-4 wire on Ti-6-4 plates.

Table 4.3 – DOE Partial Factorial L₂₇ Orthogonal Array

Weld Number	Welding Parameters (Levels) ¹				
	Main Current	Background Current	Delta Current	Travel Speed	Wire Feed rate
1	1	1	1	1	1
2	1	1	1	1	2
3	1	1	1	1	3
4	1	2	2	2	1
5	1	2	2	2	2
6	1	2	2	2	3
7	1	3	3	3	1
8	1	3	3	3	2
9	1	3	3	3	3
10	2	1	2	3	1
11	2	1	2	3	2
12	2	1	2	3	3
13	2	2	3	1	1
14	2	2	3	1	2
15	2	2	3	1	3
16	2	3	1	2	1
17	2	3	1	2	2
18	2	3	1	2	3
19	3	1	3	2	1
20	3	1	3	2	2
21	3	1	3	2	3
22	3	2	1	3	1
23	3	2	1	3	2
24	3	2	1	3	3
25	3	3	2	1	1
26	3	3	2	1	2
27	3	3	2	1	3

¹For the corresponding values of each parameter see Table 4.4 (IN718/SS316L) and Table 4.5 (Ti-6-4)

Table 4.4 – Welding input parameters for IN718 wire on SS316L plates.

Level	Factors				
	Main Current (A)	Background Current (A)	Delta Current (A)	Travel Speed (mm/s)	Wire Feed Speed (mm/s)
1	124	OFF	OFF	2	2
2	128	69	50	3	2.5
3	132	87	78	4	3

Table 4.5 – Welding input parameters for Ti-6-4 wire on Ti-6-4 plates.

Level	Factors				
	Main Current (A)	Background Current (A)	Delta Current (A)	Travel Speed (mm/s)	Wire Feed Speed (mm/s)
1	119	OFF	OFF	2	2.0
2	124	69	50	2.5	2.2
3	130	87	69	3	2.4

Optical microscopy and measurements

The welding samples were cold-mounted in epoxy resin (EpoKwick™) after being transversely sectioned using a water-cooled abrasive cutter. Gradual grinding was then performed using 180, 320, 400, 500 and 1000 Grit SiC abrasive papers sequentially. The samples were polished with 3 μm diamond suspension with the titanium samples getting an additional polishing step using colloidal silica suspension. Chemical etching was then introduced to reveal material contrasting on the Inconel/steel samples and the Heat Affected Zone on the titanium samples. The reagents used for etching the titanium samples and the Inconel/steel samples were Kroll's reagent and Kalling's reagent respectively [93]. The samples were observed and dimensions were measured using a Zeiss Axio Scope A1 microscope with AxioVision software and mosaic stitching.

4.4.2 Effects in Geometry and Heat Affected Zone

The experimental setup described was used to deliver linear bead-on-plate welds on both SS316L and Ti-6-4 plates. A total of 54 welds (27 for each material) were performed using an end effector⁴ tool path of 50 mm in length, maintaining the same electrode-workpiece distance. Representative examples for each current mode on both materials are presented in Figure 4.5.

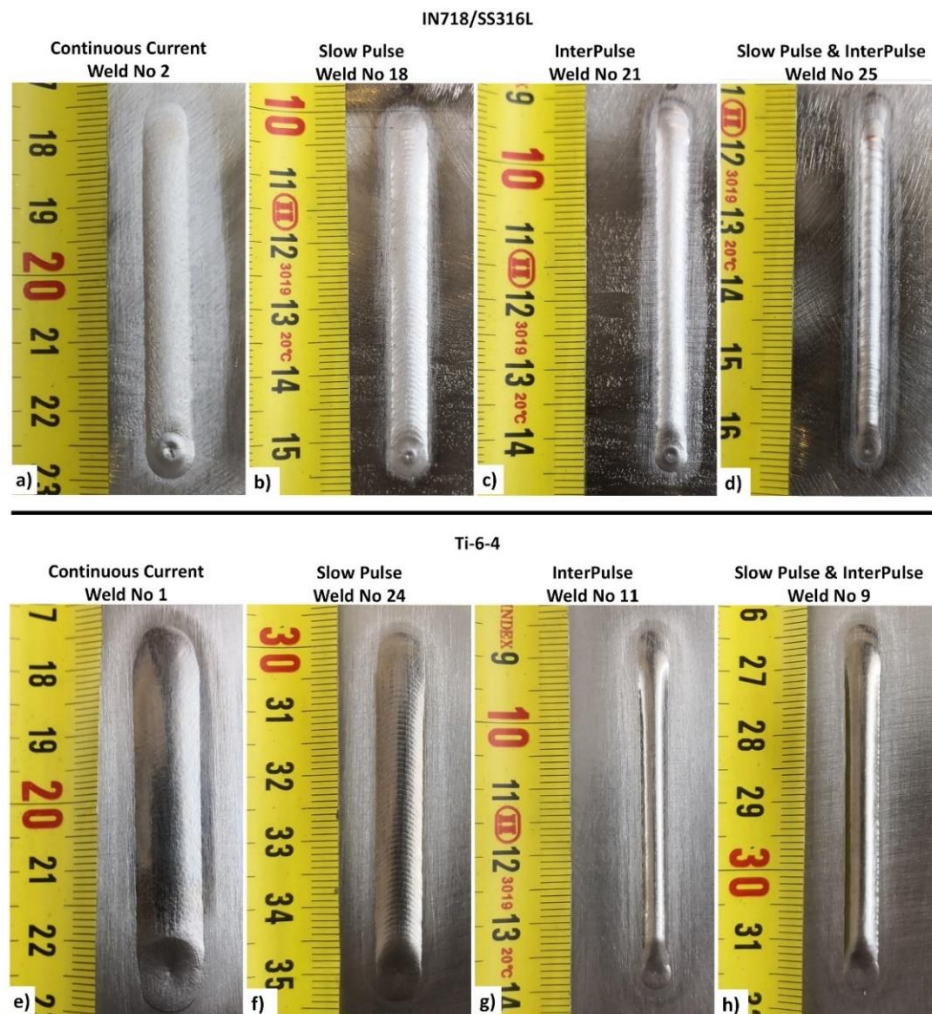


Figure 4.5 – Examples of linear bead-on-plate welds produced by each current mode. Top: IN718 wire on SS316L plates (a-d); Bottom: Ti-6-4 wire on Ti-6-4 plates (e-h).

⁴ See Glossary.

All the samples were prepared and chemically etched for metallography. The specimens corresponding to the welds in Figure 4.5 are shown in Figure 4.6 and Figure 4.7 for IN718/SS316L and Ti-6-4 respectively. Measurements were taken for determining the weld bead geometry and included weld bead width, penetration depth and weld cap reinforcement height. For the titanium samples, the penetration depth was not measured, as the additive material was the same with the substrate and the etching reagent used to reveal the HAZ did not provide clear boundaries of the bead edge. An estimation can be provided based on the changes in the microstructure, but for the purposes of this thesis penetration depth was measured only on IN718/SS316L.

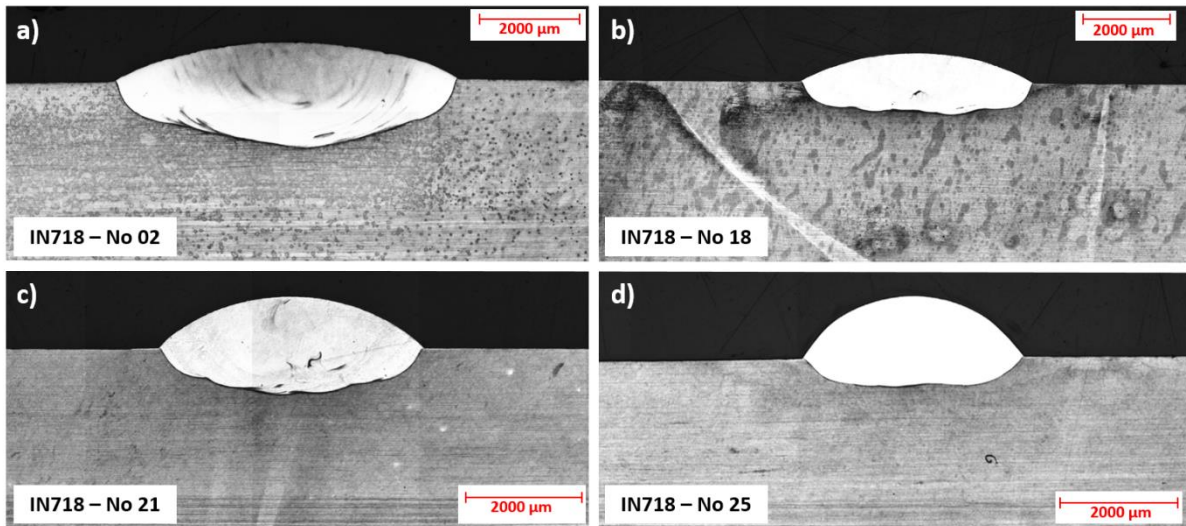


Figure 4.6 – Metallographic observations on etched cross sections of the IN718/SS316L linear welds from Figure 4.5.

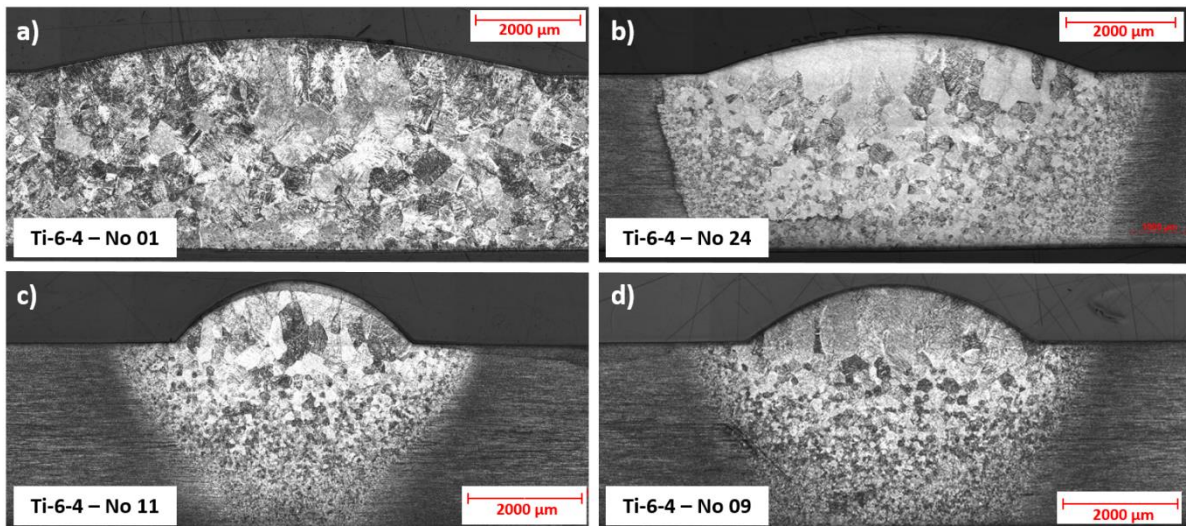


Figure 4.7 – Metallographic observations on etched cross sections of the Ti-6-4 linear welds from Figure 4.5.

4.4.2.1 Effects in geometry

From the initial post-weld visual inspections to the metallographic observations, significant changes were observed for different combinations of variables in both the weld geometries and dimensions. These changes, attributed to the variations in energy input as well as the variety of forces that contribute to the final output of the welding process, are presented.

Inconel 718

The aim of this research was to investigate the control over weld bead width simultaneously with the penetration depth. As presented in Figure 4.8, the experimental runs of IN718 on SS316L showed a linear correlation between the bead width and the penetration depth. Both the highest penetration depth and bead width were witnessed during the continuous current welds. The combination of the highest mean current with slow travel speed resulted in higher heat input and subsequently larger melt pool dimensions. When thermal pulsing was introduced, higher travel speeds with significantly lower mean currents reduced both the bead width and the penetration depth. Further manipulations of high frequency pulsing induced on the main current resulted in deeper penetration and wide beads for slower travel speeds and higher delta current, while showing both shallower penetration and narrow beads for higher speeds with low delta current. The combination of thermal and high-frequency pulsing, comprising the majority of the experimental runs, resulted in bead geometries grouped closer to the regression line in Figure 4.8. As presented in Figure 4.9, in the presence of high frequency pulsing, the bead width was significantly reduced compared to welds of similar heat input with only thermal pulsing. This is attributed to the arc constriction and arc root radius reduction associated with the high frequency pulsing.

Due to the fact that there were three welds for each current mode with the specific current values which differed only through the wire feed rate, the results were expected to show small groups of three points. In comparison with the results on the bead width, the penetration depth results (Figure 4.10) were more disperse in grouping, as wire feed rate alterations within each group were influencing the penetration depth. In the presence of thermal pulsing, the penetration depths of similar weld runs (differ only on wire feed speed) were more concentrated than those of high frequency pulsing and continuous current.

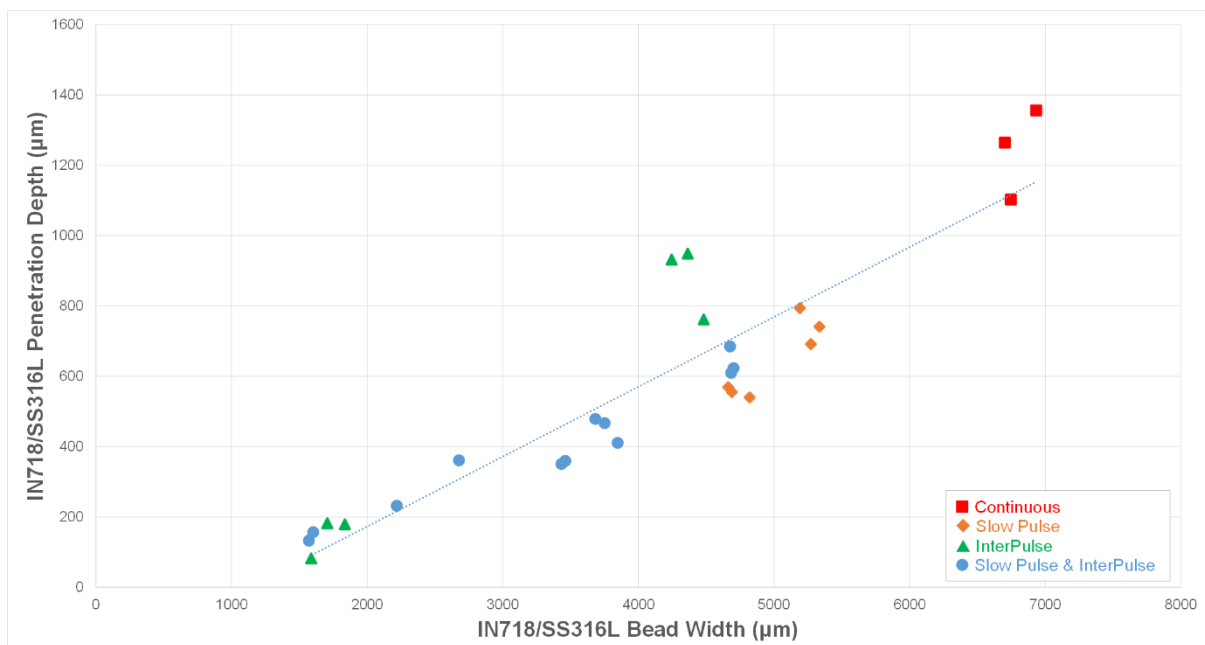


Figure 4.8 – Penetration depth versus bead width for IN718 on SS316L plates.

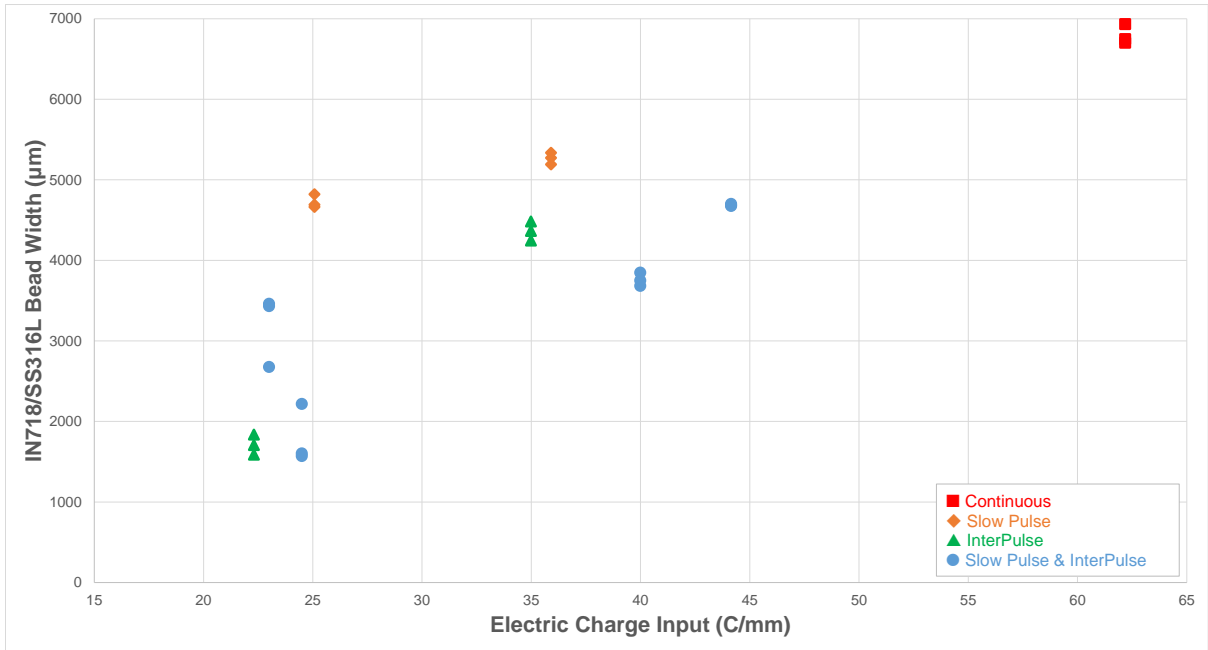


Figure 4.9 – Electric charge input versus bead width for IN718 on SS316L plates.

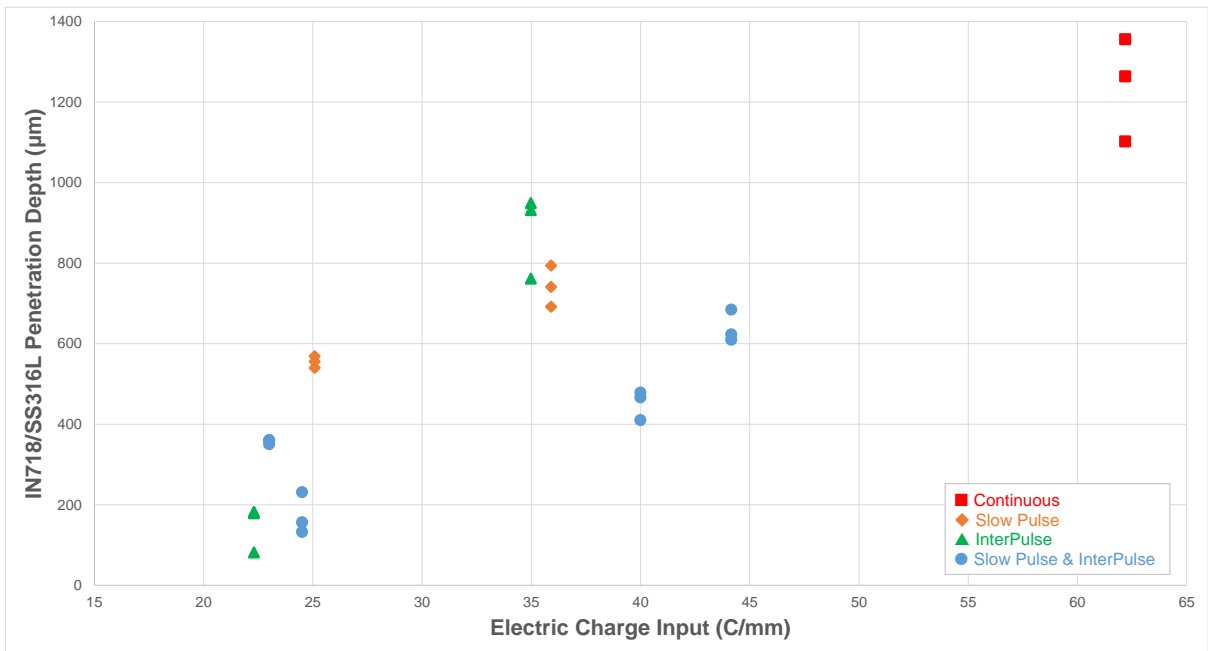


Figure 4.10 – Electric charge input results on penetration depth for IN718 on SS316L plates.

Measurements were also made on the weld reinforcement cap. In Figure 4.11 the resulting reinforcement to bead width ratio is presented. The more flattened beads (wide beads with short reinforcement cap) were obtained in the absence of delta current. Due to the arc constriction induced by the high frequency pulsing, narrowing of the bead width subsequently increased the reinforcement cap, creating more rounded beads with higher height-to-width ratios. Travel speed alterations and the combination of both thermal and high frequency pulsing allowed the formation of beads with a variety of height-to-width ratios.

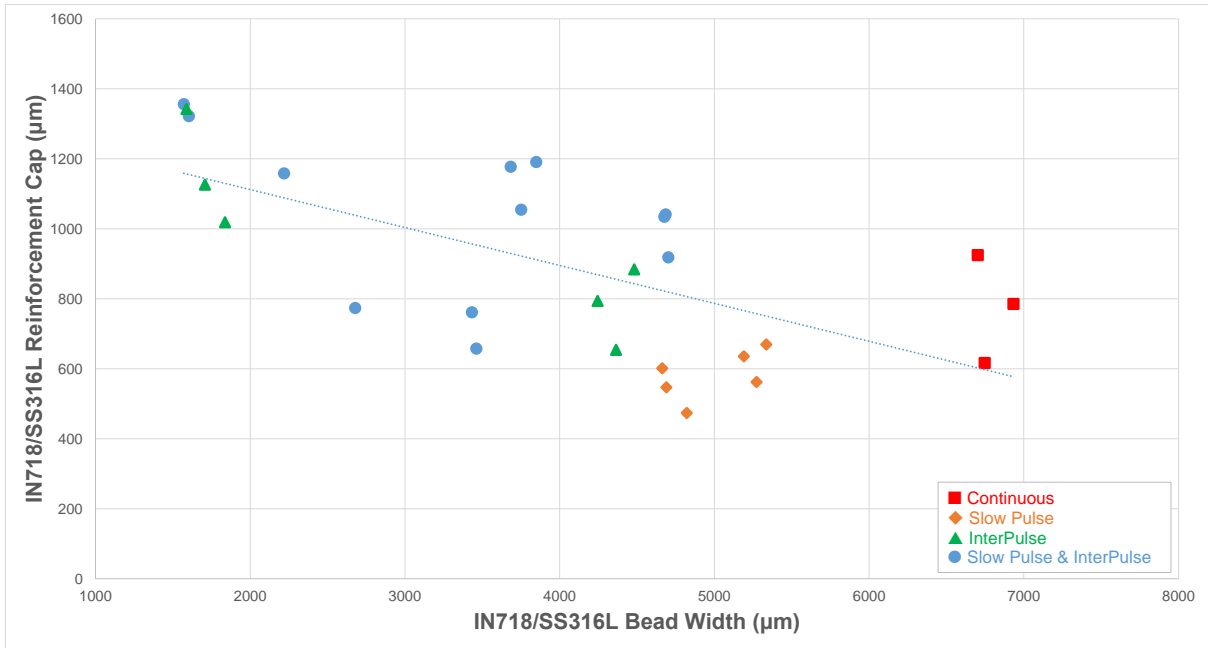


Figure 4.11 – Reinforcement cap and bead width for IN718 on SS316L plates.

In Figure 4.12 the effects on the total weld bead height – taking into consideration both the penetration depth and the reinforcement cap – are presented. The lowest total height to penetration depth ratios resulted from welds utilising continuous current (Figure 4.12a) while significantly higher ratios were obtained in welds with high frequency pulsing (Figure 4.12b). Flattened elongated welds with about 1:1 penetration depth to reinforcement cap ratio were witnessed on thermal pulsing welds (Figure 4.12c). On low heat inputs (Figure 4.13) the high frequency pulsing provided manyfold increases in the total-height-to-penetration depth ratio. As the heat input increases, when only one form of pulsing is utilised, the accumulated heat results in high penetration, subsequently resulting in lower ratios. When both thermal and high frequency pulsing are utilised, even on higher heat inputs the weld bead geometries maintain higher total-height-to-penetration ratios.

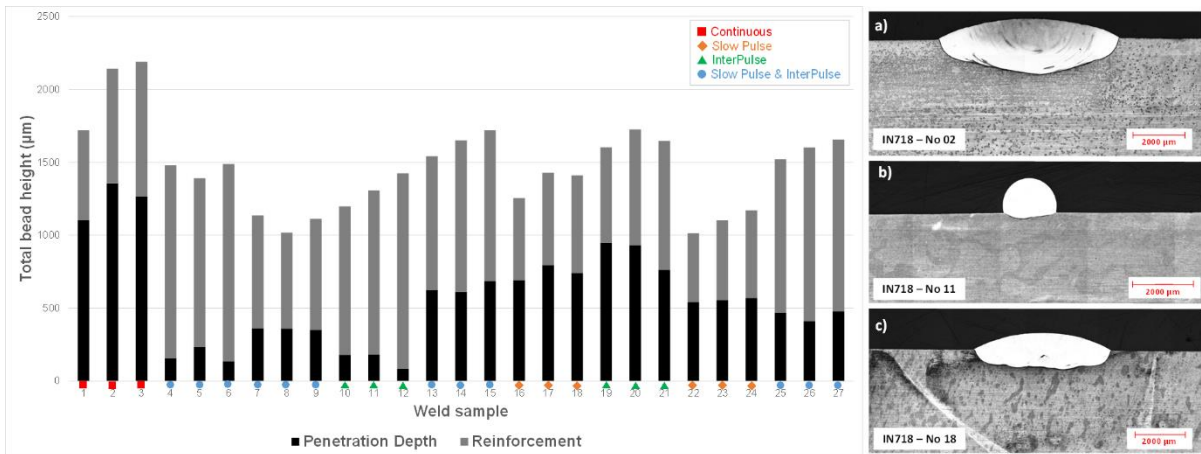


Figure 4.12 – Left: Total weld bead height as a combination of the penetration depth and the reinforcement cap for all the IN718 beads on SS316L plates. Right: Representative examples of bead geometries. Deep welds high penetration depth (a), high reinforcement cap with low penetration depth (b) and welds where the total height is evenly distributed between penetration depth and reinforcement cap (c).

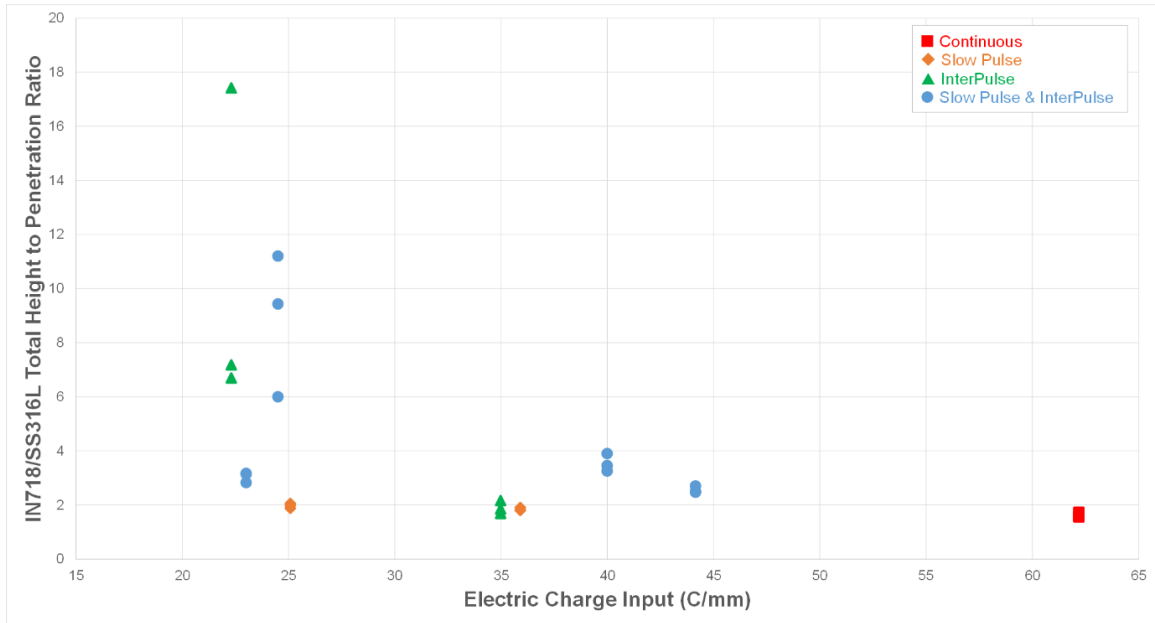


Figure 4.13 – Electric charge input versus total height-to-penetration ratio for IN718 on SS316L plates.

Titanium Ti-6-4

The effects on the weld bead geometry for the titanium samples were in general similar to those of Inconel. As presented in Figure 4.14, the resulting Ti-6-4 bead width changes in the experimental runs showed a response similar with IN718/SS316L. With the experiments following the same orthogonal array design, thermal pulsing and high frequency pulsing of similar heat input caused the same variations in the geometries. Changes to the bead size distribution in comparison with IN718/SS316L are mainly attributed to the different input parameter values between the two designs of experiments.

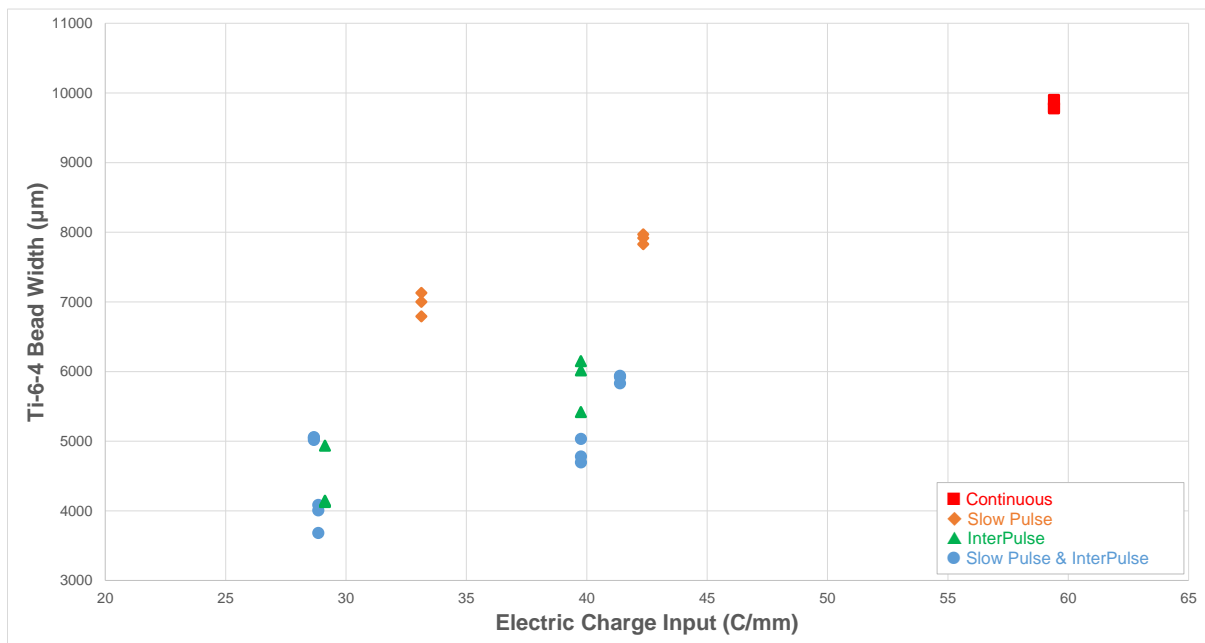


Figure 4.14 – Electric charge input versus bead width for Ti-6-4.

Similar results were also witnessed in the reinforcement cap measurements. The reinforcement to bead width ratio on Ti-6-4 followed the same type of distribution as the IN718/SS316L, with a slightly different trendline (Figure 4.15). The more rounded beads with high height-to-width ratios were again

witnessed in the presence of delta current while flattened beads were obtained in the absence of delta current, highlighting similar behaviour for both materials.

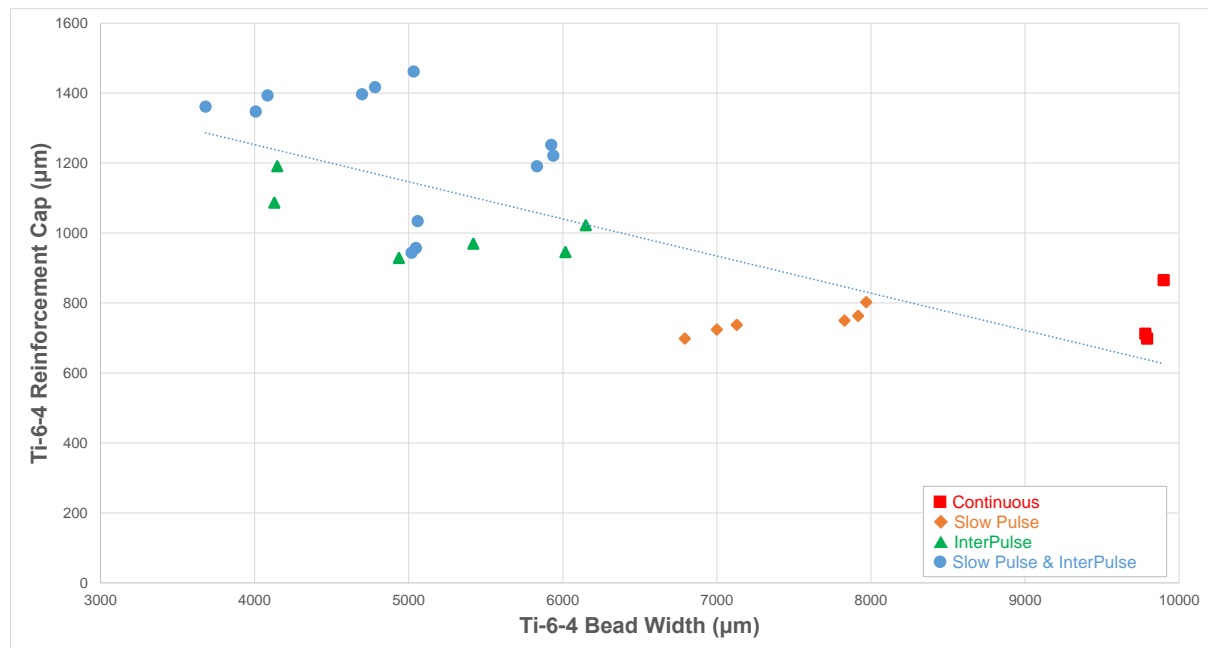


Figure 4.15 – Reinforcement cap and bead width for Ti-6-4.

4.4.2.2 Effects in heat affected zone

The titanium samples were etched in order to reveal the microstructure changes post-weld, and highlight the heat affected zone in each weld. The HAZ was measured only in width, as the heat affected regions were detected throughout the whole thickness of the material. To calculate the correct HAZ width on the titanium samples, measurements were taken from the center of the bead width to the edge of the affected zone following a subtraction of the actual bead width size (Figure 4.16).

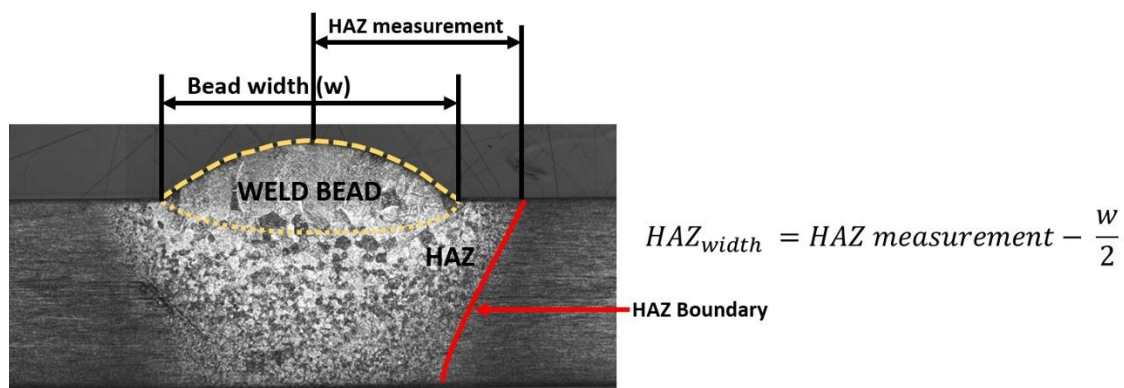


Figure 4.16 – HAZ measurements.

The HAZ width as a function of the heat input, shown in Figure 4.17, reveals a blend of HAZ width sizes through different heat inputs and current modes, with no clear indication of correlated changes. When focusing however on the cross-section arrangement and configuration of the HAZ and not only on the surface width measurement, there is a clear change in the shape and directionality of the high heat zone in the material. As presented in Figure 4.18, five main variations in shape were detected. The arc constriction and higher charge density induced by the high frequency pulsing allowed directionality in the heat distribution, resulting in an arrow-shaped heat affected region. The effects are more obvious

in welds of similar heat input (Figure 4.19) utilizing different current modes. On weld No 17 thermal pulsing resulted in a trapezoid-shaped heat affected region, whereas on weld No 15, the combination of thermal pulsing with InterPulse allowed a heat affected region with a narrower bottom and more notable sigmoid boundary lines.

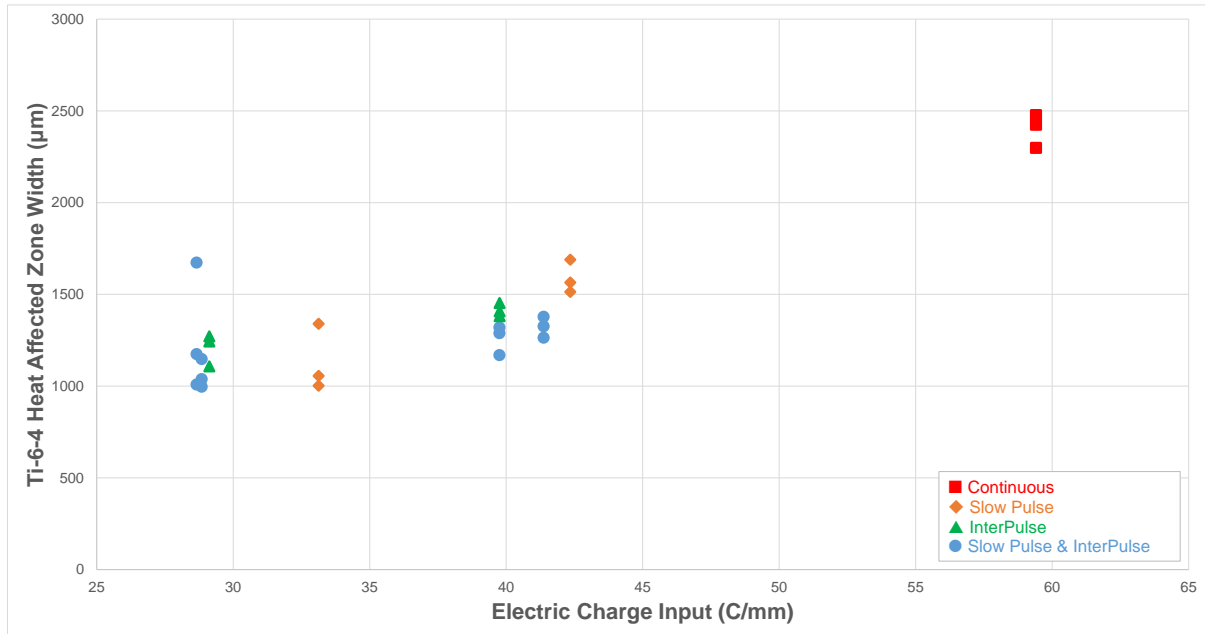


Figure 4.17 – Heat affected zone width results on Ti-6-4.

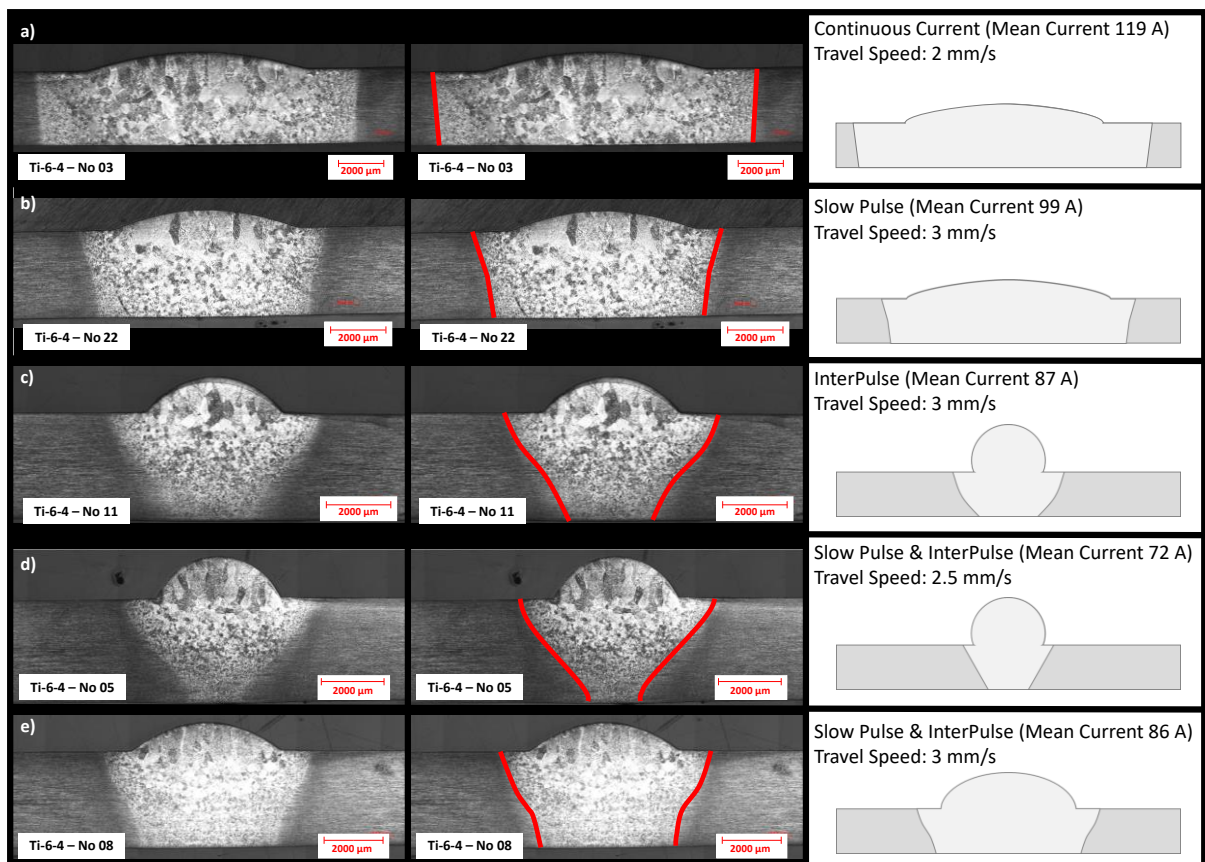


Figure 4.18 – Heat affected region shapes on different current modes. Changes in the directionality of the heat region resulted from introducing pulsed currents and simultaneously altering the travel speeds.

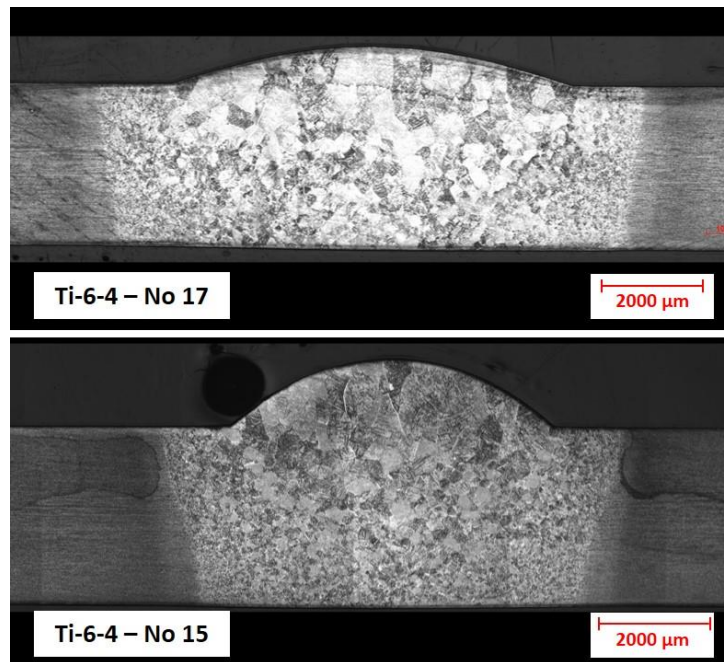


Figure 4.19 – Heat affected zone shape changes on weld with similar heat input. (Top: thermal pulsing, bottom thermal pulsing with InterPulse).

4.4.3 Current Mode Evaluation

In WAAM and AM in general the ideal weld bead would have been one that combines sufficient penetration, tall cap reinforcement and lower heat input for narrowing the HAZ and lowering residual stresses. The weld bead width would be selected depending on the application, however narrower beads result in higher printing resolution, allowing more manufacturing dexterity and builds closer to the net-shape than with wider beads. Therefore high height-to-width ratio is usually preferred.

From the measurements presented, the tallest cap reinforcement and the highest height-to-width ratio was achieved by the ball-shaped beads utilizing low InterPulse currents and high travel speeds. These welds however experienced the lowest penetration depth, and therefore could result in failures, jeopardizing structural integrity. Both high height-to-width ratio and tall weld cap reinforcement, while at the same time achieving moderate penetration depth was witnessed in welds No 25, No 26 and No 27. To fabricate these welds, that resulted in cardioid-shaped beads and sigmoid HAZ, the combination of high and low frequency pulsing was used with low travel speed.

When thermal pulsing was used without high frequency pulsing, high penetration and elongated beads were achieved, but with minimal cap reinforcement. By contrast, when InterPulse current was used without thermal pulsing the beads showed tall cap reinforcement with high height-to-width ratio.

When high and low frequency pulsing are used simultaneously, the mean current value can be reduced significantly compared to continuous current modes. This allows lower heat input and subsequently a reduction in the heat affected area, without compromising the weld specification. It is highlighted that welds No 25, No 26 and No 27 were fabricated using the second lowest mean current values of the whole DOE.

With regards to the process performance in relation with the material used, comparable bead geometries were witnessed in both the experimental runs for the same current modes (Figures 4.20

and 4.21). However, in order to get beads with desired dimensions on a specific material, individual Taguchi experiments with a single current mode should be performed for every material. In this way the subsequent Taguchi analysis will be enabled and this will provide the process optimization by means of variance analysis.

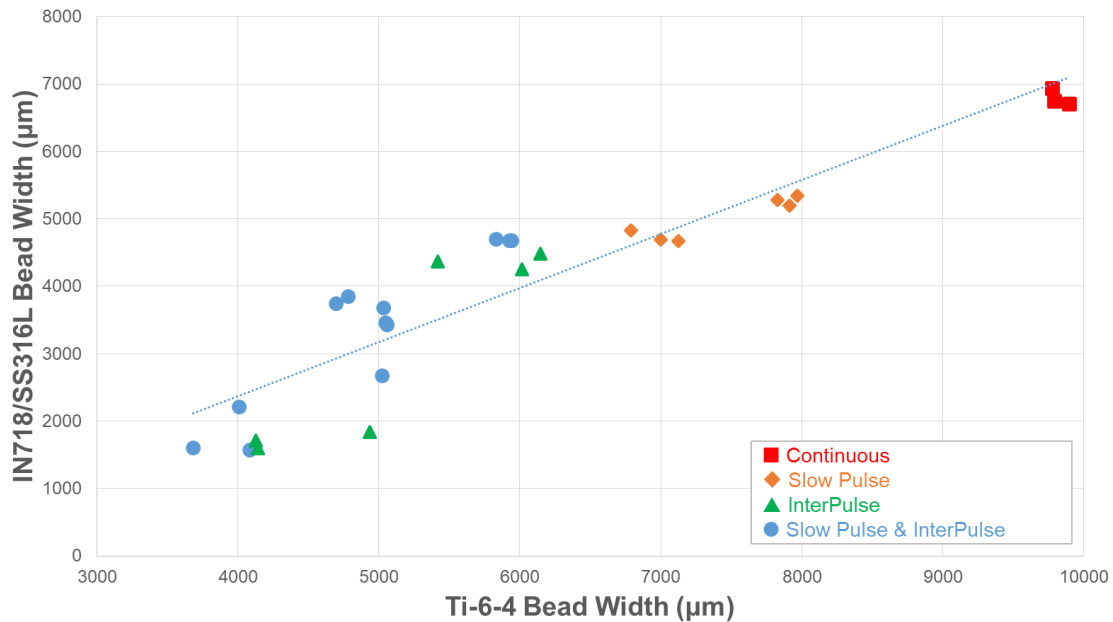


Figure 4.20 – Process outcome comparison on bead width for IN718/SS316L against Ti-6-4.

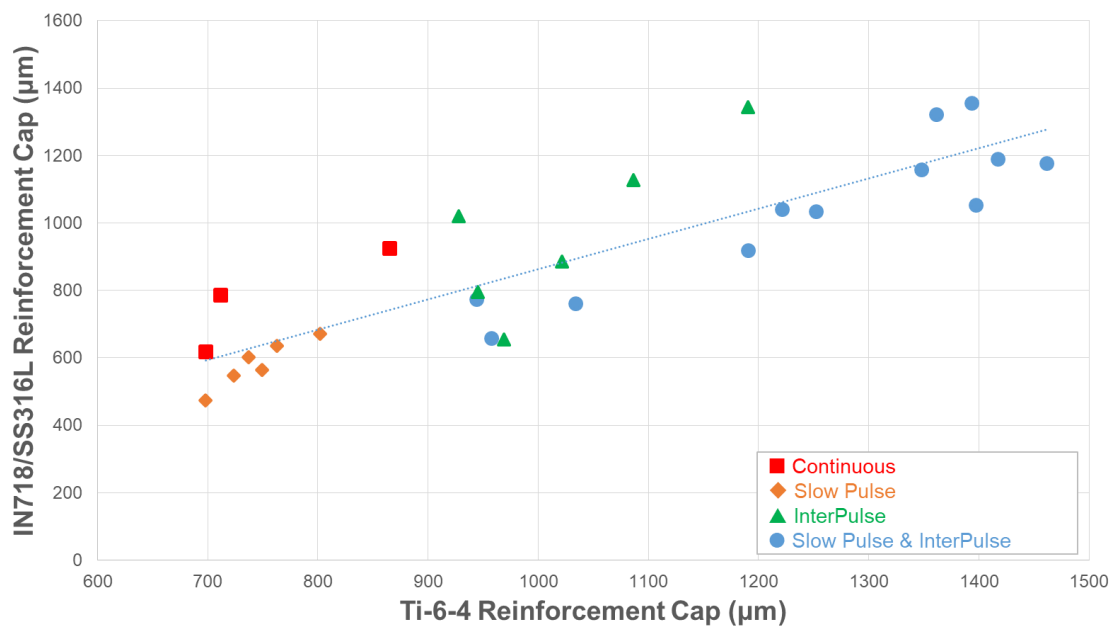


Figure 4.21 – Process outcome comparison on reinforcement cap for IN718/SS316L against Ti-6-4.

4.4.4 Pulsing Effects on Bead Shape and Weld Pool Dynamics

From the aforementioned investigation of pulsing currents in metal additive manufacturing notable weld pool dynamics were witnessed where competing phenomena altered the final outcome of the welding process. Figure 4.22 presents a series of different bead shapes that were identified post-weld by metallographic analysis. These changes occur from the combinations of changes in current modes

and torch travel speeds that result in variations in energy input as well as the variations in the applied welding forces.

a) Weld Nugget Shape

As presented in the previous section, the combination of both the continuous current and the slow travel speed resulted in the widest beads with the deepest penetration in the experiment due to the high heat input. These welds were characterized by a wide oval-like shaped bead, vertically asymmetrical with their penetration depth being larger than their cap reinforcement (Figure 4.22a).

b) Saucer shape

In the weld beads that presented the lowest height-to-width ratio, originating from low pulse current modes, elongated beads in the shape of a saucer were formed (Figure 4.22b). The higher travel speed and lower heat input compared to the welds with continuous current, resulted in shallow beads as the heat did not have sufficient time to penetrate deeper and spread wider. The elongated shape suggests higher forces in the outwards flow.

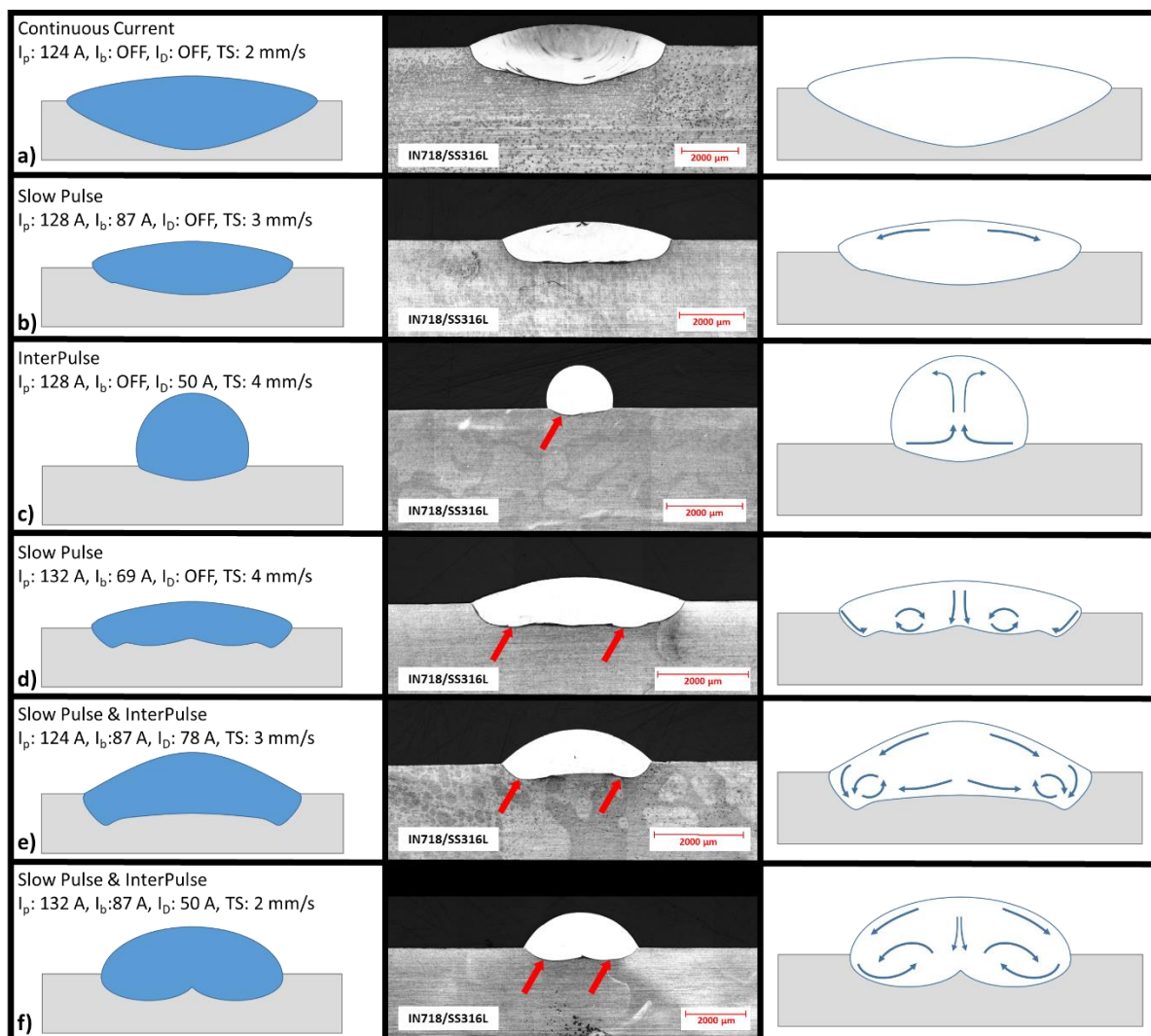


Figure 4.22 – Pulsing effects on bead shape and witnessed evidences of possible turbulences within the melt pool.

c) Ball shape

The combination of the low value of the high-frequency InterPulse current – which resulted in very low mean current – and the high travel speeds, allowed the formation of rounded ball-shaped beads

(Figure 4.22c). The arc constriction induced by the high frequency pulsing caused a significant reduction in the arc root radius, and the low heat input did not allow sufficient melting of the substrate, therefore penetration depth was minimal. Slight asymmetries witnessed at the root of the weld bead suggest intensive flows within the melt pool as the molten metal struggles to penetrate the substrate. The induced flows are therefore generating a form of turbulence, which is visible in the solidified bead. The shifting of the root from the central axis might suggest the possibility of the turbulence being induced by the Lorentz force and influenced by the magnetic field.

d) Saucer shape with root turbulences

Similarly with the saucer-shaped welds, thermal pulsed welding with lower background current and higher travel speeds – and therefore lower heat input – generated beads of saucer shapes but with two notable undulating curvatures at the root (Figure 4.22d). This again suggests the formation of turbulences within the melt pool as the low heat input is insufficient in excessive melting of the substrate. Colliding flows, likely originating from downward flows from the center and the outer regions of the weld, meet midway and form the undulating roots.

e) Bell shape

An unusual shape that resembles the figure of a bell was witnessed in dual pulsing combinations with high travel speeds. Higher height-to-weight ratios resulted in welds with tall reinforcement caps and – similarly with the previous example – two rounded beads were formed in the bottom (Figure 4.22e). It is likely that the outward flow at the root is greater than the inwards one, and therefore pushes the witnessed turbulences towards the outer regions of the root. This scenario might also be supported when the outwards flow on the surface – and subsequent edgy downward flow – is high enough to force the melting of the root at the outer regions of the weld, but the low total heat input is insufficient to melt the central root region. An explanation to this scenario might be that due to the arc constriction the aerodynamic drag force gets stronger, and – with the root radius reduced – the hotter liquid layers of the surface get pushed to the edges at higher rates. As a result the melting at the outer root region is occurring at a greater rate than at the central root. Therefore deeper penetration is achieved on the edges of the root compared to the center and the bell shape cross section is created.

f) Flatten cardioid shape

In welds with dual pulsing and lower travel speeds, higher heat input resulted in beads that resembled the shape of a slightly compressed cardioid (Figure 4.22f). It is likely that in continuation of the previous example, the higher heat input resulted in progressive melting of the edged regions with the turbulence getting bigger and reaching further closer to the central regions. With the total heat input still insufficient to melt the central root, two discrete rounded chunks are created by the turbulences, forming a cleft at their central joint.

From the variety of weld bead shapes that were identified in different current modes and pulsing combinations it is concluded that a series of competing phenomena are occurring within the melt pool. The main driver of these phenomena are both the forces induced by the plasma region as well as the four melt pool forces presented at Chapter 3.1: the aerodynamic drag, the Marangoni force, the buoyancy force and the Lorentz electromagnetic forces. The collective assembly of these forces leads to a high complexity in the weld pool dynamics, making the prediction of the final bead shape a challenging task. To this end extensive numerical models need to be formulated to correctly simulate the weld solidification process taking into consideration the physical mechanisms controlling the fluid

dynamics. Significant work is done in the field and experimental investigations using synchrotron X-ray beams have revealed flows in TIG spot melt pools that resulted in turbulences as the ones described above [94]. In order however to simulate the outcome of the constricted arc process, further understanding of the melt pool dynamics and their correlation with the pulsing modes is required. To this extent, evidence suggest that two circular flows should be considered in the weld pool [55]. As seen in Figure 4.23, different flows shall be considered for the top and bottom of the weld pool and this would be a candidate explanation for the formation of the circular turbulences witnessed via vortices.

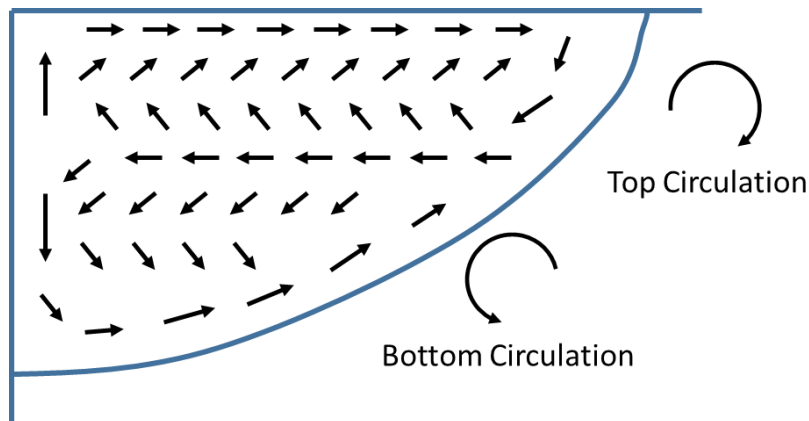


Figure 4.23 – Double circulation flow in melt pool as witnessed by Qi et al. [55].

To the author’s knowledge the aforementioned shapes are first-witnessed in research incorporating dual pulsing as no related literature was found with references in turbulences resulting in such weld bead formations. As no simulation and modelling work exists that takes into account high and low frequency pulsing effects in the solidification process, the author identifies the need of a renewed model that would explain and predict the weld shapes identified in the present research.

4.4.5 Application of the results in Wire Arc Additive Manufacturing

Implementations of the findings of this research was carried out in an initial step for the repair and re-manufacturing of aerospace components. Based on the aforementioned analysis, for the specific set of parameters, the current-mode of choice for the built-up of additive material via WAAM would be the combination of both high and low frequency pulsing. However, for achieving highest penetration on the substrate during the root pass and thus enabling a more stable structure to be built, the combination of a high-energy continuous current root pass followed by a series of built-up passes with high and low frequency current modulation was selected for the process. Using the welding parameters of Weld 3 and Weld 27, a series of linear welds were produced with Ti-6-4 successively, as presented in Figure 4.24. The high penetration of the root pass allowed the formation of a wide bead, eliminating the effect of undercut and preventing the formation of concavities. Subsequently, the combination of both high and low frequency pulsing allowed the formation of narrower beads with taller reinforcement caps and shallower penetration, resulting in beneficial geometries for built-up. Attributed to the dexterity on complementary shape-matching of the successive layers, no lack of fusion was witnessed, allowing smoother side-wall surfaces to be formed, reducing the uneven side-wall roughness that otherwise occurs. A series of root and built-up passes were also explored on circular paths. Circular motion is limited in GTAW when using a six-axis robotic arm and therefore an ABB IRBP A-250 industrial robot positioner was used in configuration with the robotic arm. In Figure 4.25 combinations of continuous and pulsing currents were used to deliver circular geometries.

Additional work is required to optimize the bead geometry for WAAM applications that will allow a greater number of successive layers and the opportunity to evaluate the pulsing effects in taller built-ups.

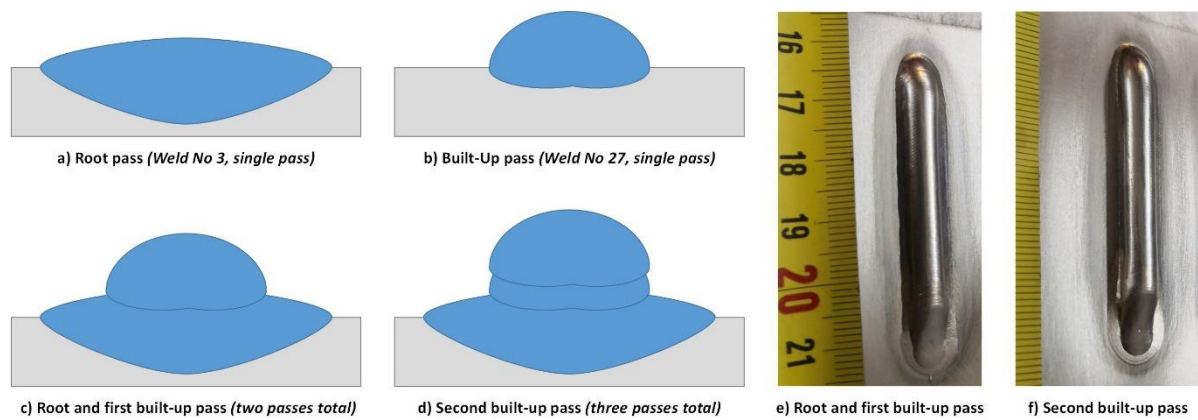


Figure 4.24 – Combination of continuous current root pass with pulsed-current build-up passes in WAAM (Ti-6-4).



Figure 4.25 – Circular root and built-up passes on wire arc additive manufacturing. The arrows mark the starting/ending point where passes overlap.

4.5 Conclusion

In this chapter the WAAM process was presented along with investigations made by the author on pulsing currents utilisation in the control of weld bead geometries and heat affected zones. The process provides the ability to achieve both deep penetration root passes and beads with higher height-to-width ratios in a single manufacturing setup. Metallographic observations revealed changes in the shape of the heat affected zones and competing phenomena were witnessed that influence the

bead shape. Initial steps in the application of the process for root and built-up passes were taken, allowing further development in the field of welding-based additive manufacturing.

5 Robotic Aerospace Remanufacturing System Development

The WAAM process was utilised in the development of a robotic system for the remanufacturing of aeroengine components. The system automated the tip-repair process of compressor blades regeneration implementing Industry 4.0 design principles. In this chapter the process management of the system is presented along with the system components configuration. Analysis of the first results and evaluation through in-line metrology and process monitoring are also presented. This chapter is the result of a series of publications related to the robotic system that the author co-authored [3]–[5].

5.1 Compressor Blades Regeneration

In an aircraft jet engine the operational process is divided in four main stages as illustrated in Figure 5.1: the intake stage, where atmospheric air enters the engine, the compression stage where the air is compressed to achieve higher pressures, the combustion where the compressed air is mixed with fuel and ignited, and the exhaust where the air exits the engine [95]. The gas turbine is placed between the combustion and the exhaust. These stages are grouped into cold stages and hot stages, with the cold section being prior to the combustion chambers and hot section from ignition and thereafter. In order for the intake air to be compressed, and the turbine to operate, various types of metal blades are used. Since the compressor and the gas turbine are positioned in the cold and the hot sections respectively, their corresponding blades are made of different materials. Compressor blades used to be made of steel alloys in early jet engine designs. Steel has now been replaced by titanium, due to the mechanical properties of titanium that allow weight savings, corrosion resistance and long operational service. Even with its high initial cost, titanium is the preferred material since the lighter rotor assembly reduces the forces on the engine structure, which in turn enables further weight reductions. The elevated temperatures in the hot section prohibit the use of titanium therefore nickel-based alloys are used for turbine blades.

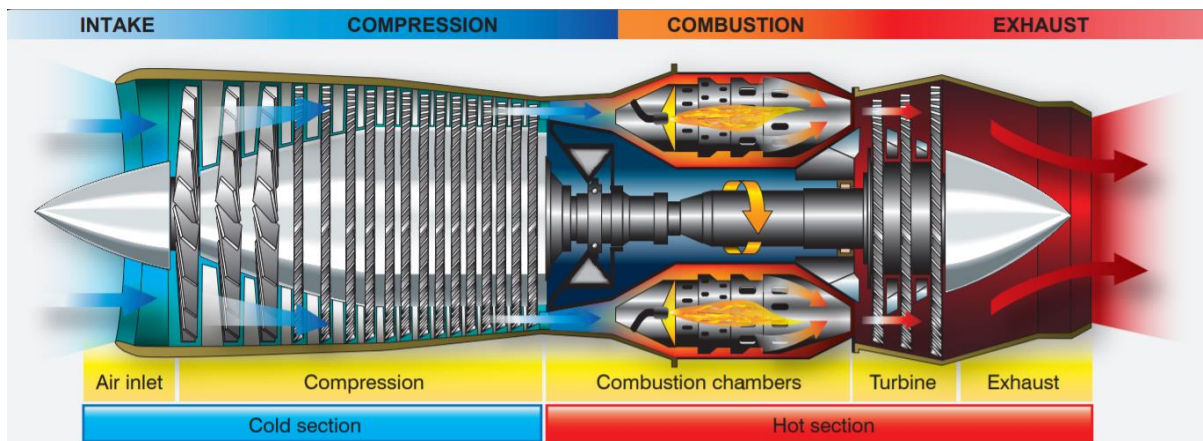


Figure 5.1 – Jet engine sections and stages [95].

Compressor blade wear and defects induced by extreme and prolonged operational conditions lower the engine's performance, increasing fuel consumption and reducing power output. Mitigation of operational safety risks, requires the need of maintenance, repair and overhaul of the engine to predetermined schedules. In order to decrease the MRO costs, engine manufacturers and MRO service providers minimize the replacement of such high value components by undertaking repair and remanufacturing where applicable.

After the blades are removed from service, they undergo inspection where their condition is assessed, identifying if their damage is repairable and the level of repair needed. Normally cracks presented on the blade's body are repaired via brazing or welding, depending on the defect's size. Plasma arc welding is employed for repairs where a patch-joint is required without additive material. Tip-repairs, as was already highlighted in Section 2.4, represent the majority of the restoration repairs. The tip restoration process is traditionally comprised of four processes: pre-treatment of each individual blade, repair via material deposition, re-contouring and post-treatment. In the pre-treatment stage the top layers of the blade are removed by means of subtractive machining (e.g. abrasive cutting), allowing the formation of a uniformly even top surface. The following process of material deposition may be carried out in a variety of ways and is depended upon the material of the blade and the repair required by each individual piece. It can be performed either via material cladding by laser welding, or via additive arc welding with filler material [27], [28], [30]–[32], [34]. Due to complex geometries and different repair requirements by each individual blade, the process is heavily dependent on manual welding performed by experienced welding engineers. However, while 80% of the recovered blades are repairable, the percentage that is successfully repaired is significantly lower, reported in the vicinity of 45%. Root causes of these rates of failure can be traced to errors originating from human input. In order to improve and increase the successful repair yield volume, human errors need to be avoided, and this can be achieved by automation of the repair process.

To automate the compressor blade regeneration process, the University of Sheffield further expanded the industry-academia collaboration with VBC Instrument Engineering Ltd, to develop a robotic additive manufacturing system based on arc welding. This robotic solution is focusing on the automation of the second stage of the regeneration process, the material deposition.

5.2 Benefits of the Robotic Solution

The proposed industrial system is characterized as “high-value”, for its strong potential for high economic value and its aim in advancing remanufacturing for the aerospace industry. The blade repairing process is of high cost, with a gas turbine blade repair ranging from £250 to £7000, depending on size and material. To highlight the amount of blades in a single engine, a Rolls-Royce Trent 1000 turbofan engine has approximately 600 blades. With a higher yield of successfully repaired blades, apart from the obvious savings in terms of the scrapped product cost, less time is spent on repairing with higher output of blades in a remanufacturing line. Additionally, with the aerospace alloys' high prices significant savings occur from less material wasting.

Apart from economic and environmental benefits, the advanced robotic solution was designed to provide valuable social gains in health and safety. As was highlighted in Chapter 2.4, the low heat input required in the process of blade regeneration and the titanium properties require the incorporation of GTAW (Figure 5.2). Ergonomic studies revealed a number of existing hazards in the manual GTAW process, which include among others, prolonged sitting periods, manual handling, wrist fatigue, cutaneous burns and eye damage [96]. By automating the process via the use of a collaborative robot and by engaging additional safety features, a safer working environment is ensured for the welding engineers.

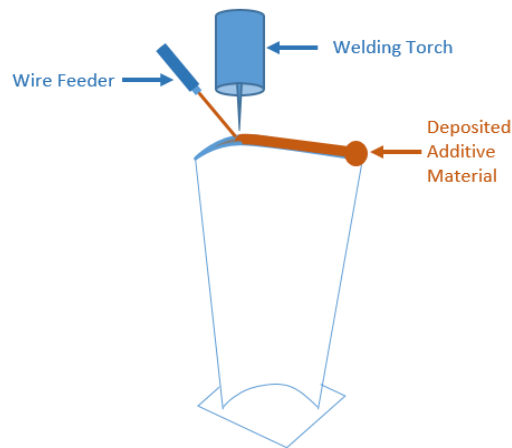


Figure 5.2 – Compressor blade tip-repair using GTAW-based material deposition.

5.3 Robotic System Development

The robotic remanufacturing system has a modular design, incorporating a variety of subsystems. These subsystems include a collaborative robot working with the peripheral systems used for characterization, inspection, monitoring and evaluation. The systems employ, among others, machine vision systems with advanced scanning and optical imaging capability combined with real-time monitoring sensors. Via means of process monitoring and post weld non-destructive testing, quality assurance that the repairs meet the acceptable mechanical properties of the product, is achieved. For successful automation of the system, numerous detailed databases are required, to assist in operation, safety monitoring, life cycle monitoring and logging. The welding system operating alongside the collaborative robot is composed of an advanced Heat Management System (HMS) with automatic filler material deposition, developed by VBC Instrument Engineering Ltd.

5.3.1 Designing of the System Process Management

The robotic concept is aiming to reduce the human impact on the re-manufacturing of compressor blades while achieving high rates of successful repairs. Based on these two goals the system was designed to receive pre-treated blades, characterize and intelligently inspect them, perform the tip-repair material deposition and deliver the finished product ready for re-contouring and post-treatment. The flow of the system process, as graphically presented in Figure 5.3, is explained in the following steps.

1. Blade detection

The blades arrive to the system loaded to trays in the loading bay. During the blade detection process the system checks for the presence of incoming blades and defines their position and orientation for pick-and-place operation.

2. Blade identification and properties definition

Once the position of a blade and its orientation are defined, the process of characterization of the blade takes place. This includes scanning of the blade manufacturers' code and shape definition. The type of the blade, the material and the original dimensions will be loaded from databases corresponding to either their embedded code or pattern recognition.

3. Loading for inspection

After the characterization of the blade the robot uses the information acquired from both scanning and databases to pick and place the blade, correctly attaching it to the tip-blade inspection site.

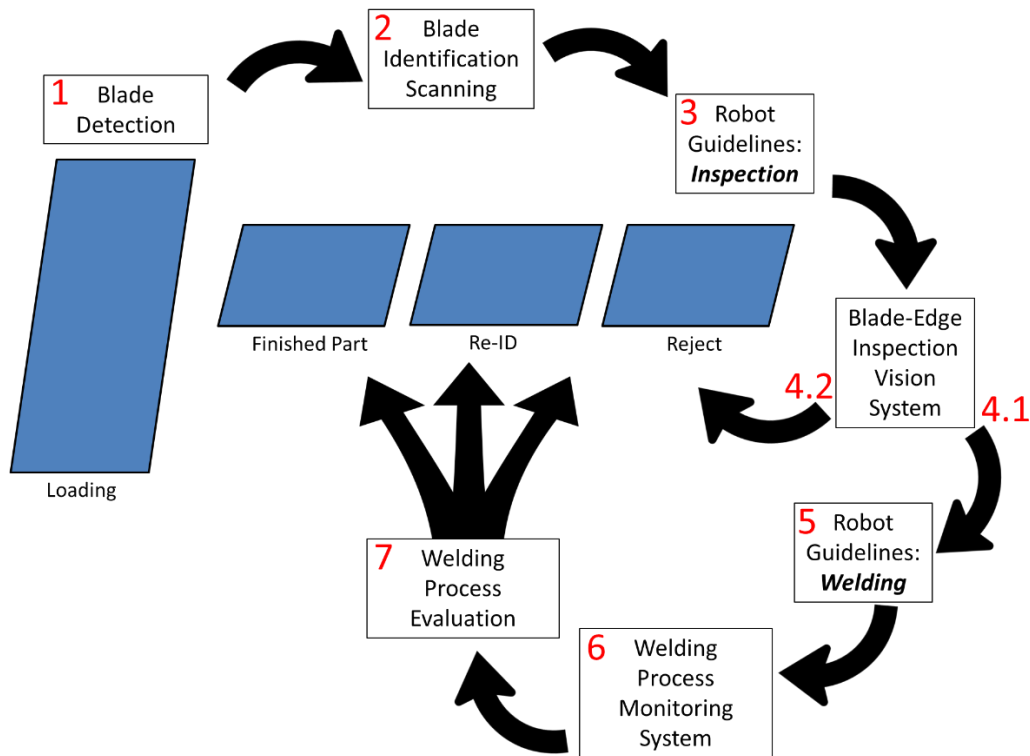


Figure 5.3 – The concept’s process flow for compressor blades re-manufacturing.

4. Pre-weld visual inspection

The machine vision system inspects the loaded sample defining its condition prior to welding. The system provides a pre-weld evaluation, defining if the blade is in an acceptable condition to proceed with material deposition. This ensures that oversights from the pre-treatment stage or defects that may occur during the transport and loading phase (e.g. surface contamination) are detected and avoided. If the blade is ready for repairing, then the welding input parameters are calculated and set in the WPS (Figure 5.3 – Step 4.1). If the blade is found in an improper condition for the system to proceed it is rejected (Figure 5.3 – Step 4.2).

5. WAAM Process

Based on the WPS provided by the inspection vision system, the robot’s toolpath guidelines are generated and the robotic system performs the operations for the material deposition.

6. Welding process monitoring

During the material deposition process, a high-speed data acquisition system performs measurements that are to be used for the creation of a database for post-weld evaluation. The welding monitoring system transfers both real-time electric measurements acquired by the DAQ system and live image feed, along with the rest operational parameters to the Graphical User Interface (GUI).

7. Weld Evaluation

Once the phase of material deposition is completed, the welded piece is evaluated based on the data acquired by the welding process monitoring system and post-weld visual inspection. Based on the evaluation the robot transfers the finished blade to the corresponding stages of either acceptance, further evaluation or rejection.

5.3.2 Industry 4.0 Design Principles

Industry 4.0, a term deriving from the German Industrie 4.0 conceived in 2011 at the Hannover Fair, relates to the context that acts as the driving force behind the ongoing fourth industrial revolution. It refers to the applications of cyber-physical systems (CPS) in the fields of manufacturing and production [97]. The goal of Industry 4.0 is to pave the way towards the “factory of the future”, turning organizations into truly digital enterprises utilizing industrial informatics and the networking of the Industrial Internet of Things (IIoT) in both their vertical and horizontal value chains.

To develop implementations of CPS in scenarios under the Industry 4.0 context, four main design principles are followed: interconnection, information transparency, decentralized decisions, and technical assistance [98]. These four principles are aiming to reshape the face of industry, advancing traditional manufacturing to futuristic “smart factories”.

A. Interconnection

Through the industrial adaption of the Internet of Things (IoT), the IIoT aims to connect people, machines, and products through communication technologies. Modules of standardized wireless communication devices (RFID, Bluetooth, Wi-Fi, etc) are being embedded, attached or connected on sensors, machines and equipment to allow real-time smooth exchange of information and enhance interoperability. Modularity and flexible adaptability is of high importance especially where manufacturing data are exchanged cross-disciplinarily along the product life-cycle. These characteristics are required not only on physical equipment but also on the software, where an adaptable code results in automatic re-configuration with less errors and transition time.

B. Information Transparency

With digitization at the core of the fourth industrial revolution, data acquired from sensors in the manufacturing plant are blended with software models to create virtual copies of the physical world (digital twins). Digital copies of manufactured products are created by the combination of pre-production fabrication guidelines, environmental and machine condition monitoring data, data from process monitoring during production and results from post-production of in-line metrology and quality assurance tests. These copies are then stored in databases both locally and in the cloud, with access to the respected parties involved, ensuring a digital trust between them. In order for this digital ecosystem to function properly, safety measures regarding cyber-security need to be taken. Clear guidelines on data integrity and digital security need to be applied not only for the data acquired during manufacturing but also for the communication data between the parties involved and the intellectual property surrounding the manufactured products.

C. Decentralized Decisions

The aforementioned design principles on interconnection and information transparency empower CPS with the ability to make decisions locally, without the need for approval from higher levels of hierarchy. Validation data required for the decision making can be provided between the interconnected parts, avoiding the cause of delays and bottleneck effects in a production line.

D. Technical Assistance

The term technical assistance in Industry 4.0 refers to the ability of CPS to support human actions in a production line. This assistance can be in the form of physical support, where difficult and hazardous tasks are performed by robotic systems, or in the form of comprehensive representation of complex

datasets via visualized information. The former protects the manual worker from work-related hazards and the latter ensures faster reactions and better decision making.

5.3.3 Implementation of the Design Principles

The autonomous re-manufacturing robotic solution was designed based on the aforementioned principles, and its development occurred driven by the advances that they enable. The collaborative robot that performs all the mechanical operations is connected with a variety of essential peripherals, forming the network that is presented in Figure 5.4. While this network reminds an old-fashioned representation of a centralized production line, the following expanded overview of the individual advances, illustrates the ongoing revolution in industrial automation. Each concept presented was designed accordingly in order to match the innovations and guidelines set by the Industry 4.0 principles.

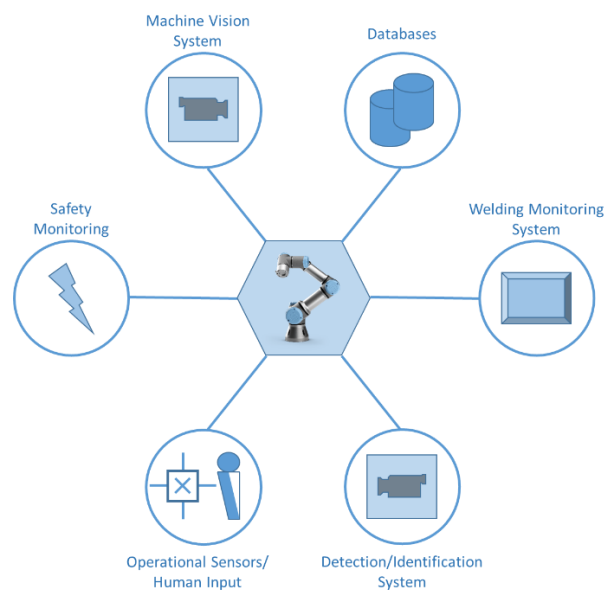


Figure 5.4 – Different modules and subsystem forming the network of the robotic solution.

Modularity and flexibility

Under the scope of the IIoT in a smart industrial environment, each product is able to present its history and find its way on a production and re-manufacturing supply chain. This concept is being adapted in the aerospace industry with this information being retrievable based on embedded serial numbers and codes. However, not all of the blades that are currently in use in operational gas turbines carry machine readable codes, and those who do have, carry them in a variety of ways: quick response codes (QR code), barcodes, embedded serial numbers, and embedded script codes. With modularity and flexibility in mind the detection-identification system is developed with the ability to detect and identify any kind of blade. Therefore, all the scanning, lighting and optical recognition elements are designed and developed to achieve this flexibility.

Sensor fusion

- *Sensor fusion in monitoring*

Advanced sensors that perform electric measurements on the welding equipment are transferring real-time data to the GUI. Live video feed is also presented on the remote GUI, acquired by the vision system. In this way direct visual contact with the bright welding light is avoided, eliminating eye-hazards during human-machine interaction and providing technical assistance. Remote monitoring

through sensor fusion on one monitoring platform improves interoperability by ensuring the ability to use a variety of devices and sensors.

- *Sensor fusion and machine vision in inspection*

A machine vision system that combines modules of advanced scanning and optical imaging equipment is utilized. The system is aiming to detect the position and wear of each individual blade, characterizing imperfections and calculating robot pathways. The system is designed to reject blades beyond the system's ability for remanufacturing and calculate the layers of linear weld required based on manufacturers' and new machine-created referencing databases. This decentralized decision aids in the QA and QC and avoids waste of materials on both faulty products and manual working.

- *Sensor fusion in final product evaluation and fault detection*

An advanced high-speed data acquisition system (DAQ) monitors the welding process, delivering real-time data regarding the input parameter and conditions during the welding. The system was developed by the University of Sheffield and has been proven able to detect malfunctions and flaws during the welding process. QA on the final product increases the product lifecycle since faults detected will lead to products which could go again in the repair cycle instead of unreparable waste.

- *Sensor fusion in safety*

A cluster of peripheral sensors are utilized for monitoring the whole process, ensuring human and equipment safety. The robot itself is designed to stop operation when an obstacle is opposing its actions, and the use of proximity sensors for collision avoidance is under evaluation. The safety features for the operation of the robot are also being evaluated, aiming to personalize clearance in order to ensure that usage by untrained personnel is avoided. These Industry 4.0 adaptations aid not only in machine and human safety, but also in Information Technology (IT) security since corporate intelligence will be available only for personnel with corresponding clearance.

Data management

Since information is the power that drives the modern industrial revolution, a number of databases are required for a smart factory to operate. The following databases are core elements in the developing system, providing information transparency and ensuring QC, QA, and IT safety, in parallel with the ability for further data analytics. Additionally, this abundance of wealthy information allows the creation of a "product ledger" which in turn enables a digital trust between suppliers, manufacturers and operators (Figure 5.5).

- *Database for blade-log:*

The complexity of the solution raises the need for flexible databases able to expand and adapt as the system progress. Existing data that are acquired by the blade manufacturers have to be combined with the data acquired by the system to create files corresponding to each blade. Apart from their type and origin the database must include a history of each blade when available, especially previous re-manufacturing history. If no data are available then a new data log has to be created.

- *Database for blade-type:*

Provided by the manufacturers the technical specifications for each type of blade has to be present in the system. These data are cross-referenced by the system on each blade for correct attachment and vision system positioning configuration. The size and shape of each blade will be used as a reference

for evaluation during inspection. Alongside, the vision acquired data will be used to define the robotic welding-path coordinates.

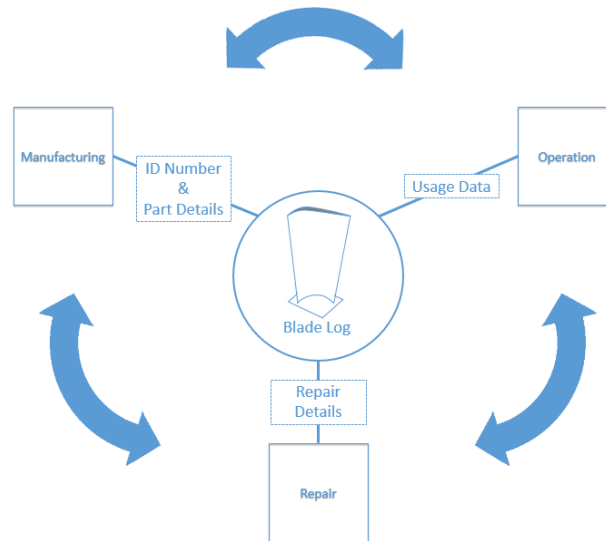


Figure 5.5 – Exchange of information between manufacturers, customers and service providers enables clearer transparency and builds additional trust in the service provided.

- *Database for weld evaluation and fault detection:*

Data from the high-speed DAQ system revealed that errors and malfunctions that occur during a welding process create variations in arc voltage measurements. These variations present themselves as repeatable patterns based on their nature and origin, resulting in the possibility to detect process variations in real-time. As the categorization and identification of each error in real-time is currently under further commercial development, plans of a software based system for this application are underway. The system will incorporate a database of known malfunctions and their electrical fingerprints and using pattern recognition in real-time data analytics will be able to distinguish and classify the error as it occurs.

- *Database for ID Clearance:*

In order to avoid untrained personnel use of the advanced remanufacturing system, and to protect classified commercial high-value information, access to the robot is limited. A security feature identifying the operator attached to the system, limits access to only persons that have the skills to interact with it. This platform can include simple security measures such as password protection, more advanced fingerprint sensors and facial recognition software. While the first one implemented for the prototype is an easy build, the others will require a safety database with the details required for login (facial recognition data, fingerprint data, etc.).

With all peripheral systems analysed and information exchange between the different modules presented, the centralised diagram from Figure 5.4 is expanding in the more complex network shown in Figure 5.6.

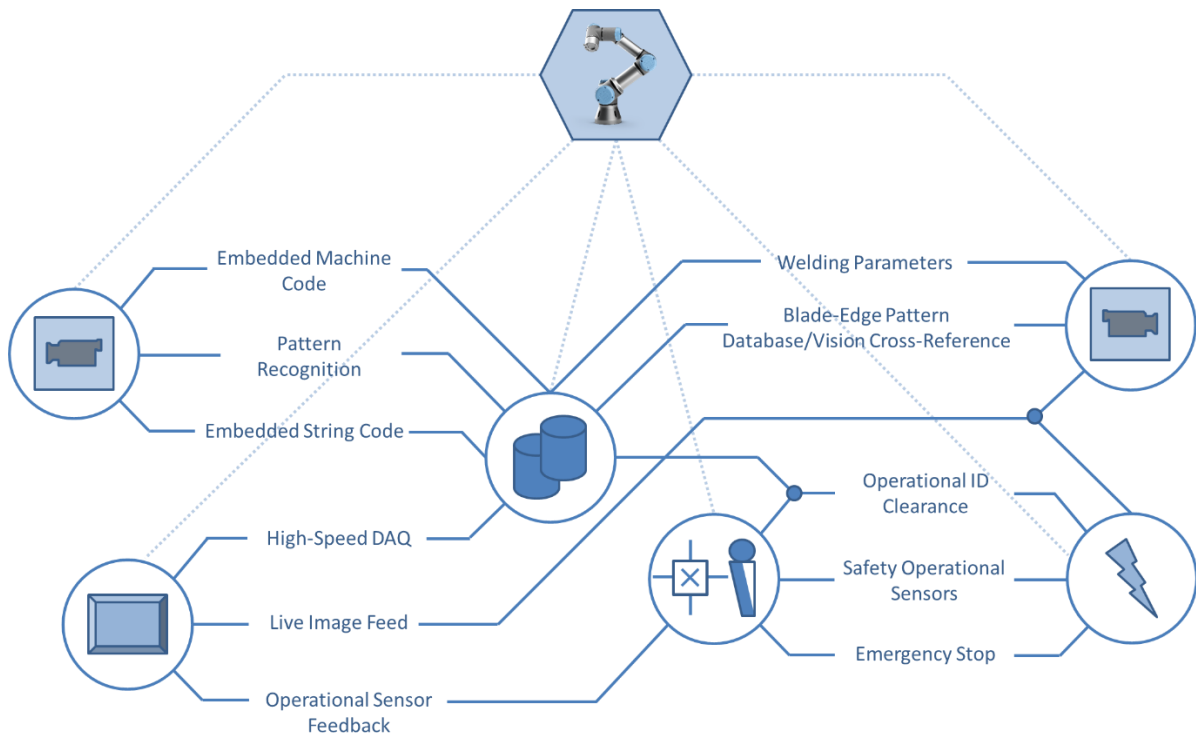


Figure 5.6 – Interconnection principle applied in the operational design of the robotic remanufacturing system.

5.4 Deposition Process

After the conceptual design based on regeneration process analysis and the implementation of the Industry 4.0 design principles, the prototype system development was initiated following concurrent engineering. In concurrent engineering, in contrast with traditional project execution, the development of a prototype follows continuous updates, with feedback received via trial and error. This project management method allows faster development as various components can be simultaneously built and adjusted accordingly further down the project timeline.

As already mentioned, when receiving the blades for material deposition, it is expected that the stage of pre-treatment has been completed. To ensure the surface quality meets the requirements for repair and to calculate in parallel the AM deposition path of the system, an intelligent 3D scanning system is used (Figure 5.7: Scanning Phase). After the scanning of the blade, the additive repair process is initiated. The system utilizes the pulsed GTAW-based WAAM technology that was described in Chapter 4. During the root pass, the first layer of the additive material is deposited and fused with the blade's base material. The heat generated from the arc and transferred to the blade plays a critical role in the success of the fusion. If the heat is insufficient, the additive material will not fuse with the base material, resulting in failure of the weld due to lack of fusion. If the heat is in excess, the thin tip of the blade will melt at a high rate, making challenging the control of material's build-up. As illustrated in Figure 5.7, the corners of the tip during scanning phase are sharp. Once the arc strikes, the heat distribution is limited due to the corner, which results in higher melting rate compared to the inner sections of the blade. This higher melting rate results in curved corners highlighted in Figure 5.7d. To fix this problem, the rate of feeding of the additive material (wire feed) is increased at the two corners of the blade. This results in excess of material at the beginning and the end of each pass, creating the "bumps" shown in the figure.

Once the root pass is completed, 3D scanning is confirming the material deposition and the path of the second root is calculated. Similar with the root pass, the corners melt faster than the tip interior, therefore the feed rate is readjusted to fill the generated gaps. The stages of scanning and deposition are repeated again until the deposited material exceeds the requirements for regaining the original shape (Figure 5.7e).

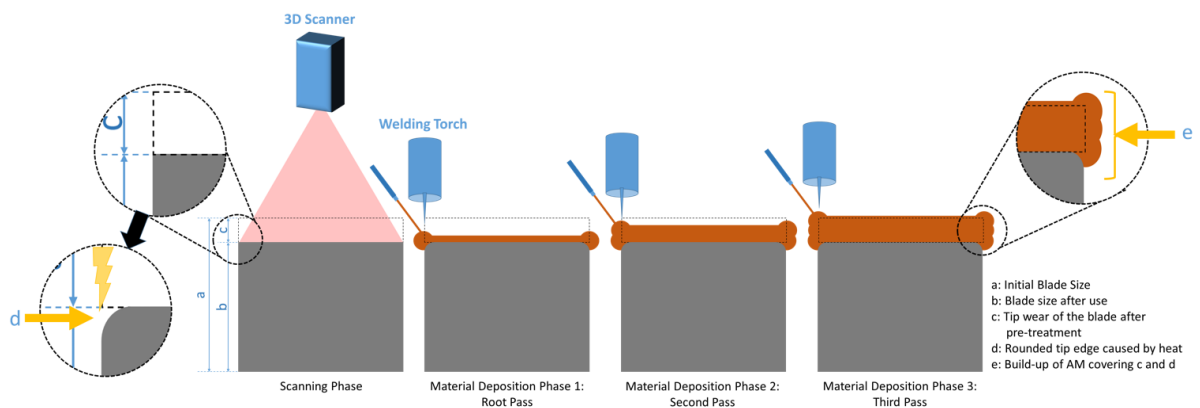


Figure 5.7 – Schematic representation of the AM build-up process for the regeneration of a compressor blade.

5.5 Welding Procedure Specifications

As seen in Chapter 3.1.4, the WPS provide the guidelines – the welding input parameters and conditions – that each specific welding operation should follow. For the blade regeneration process, the flexibility needed by the system to operate on various types and designs of blades, requires the ability to adjust the WPS accordingly.

Travel Speed and Torch Positioning Adaptation to Temperature

As highlighted previously, the temperature of the blade should be in a specific range in order to have a successful weld. To achieve the desired temperature, the welding travel speed is adjusted. At the beginning of the material deposition process, the blade temperature is in low levels, prohibiting the melting of the base material given the preselected current-voltage range limitations. To deal with this, the arc is used to heat the base material before the additive material is fed (Figure 5.8). Additionally, during the welding process the heat accumulated by the blade is increasing its temperature, resulting in faster rate of melting of the base material. To deal with this, the system is adjusting by increasing the travel speed as the temperature increases.

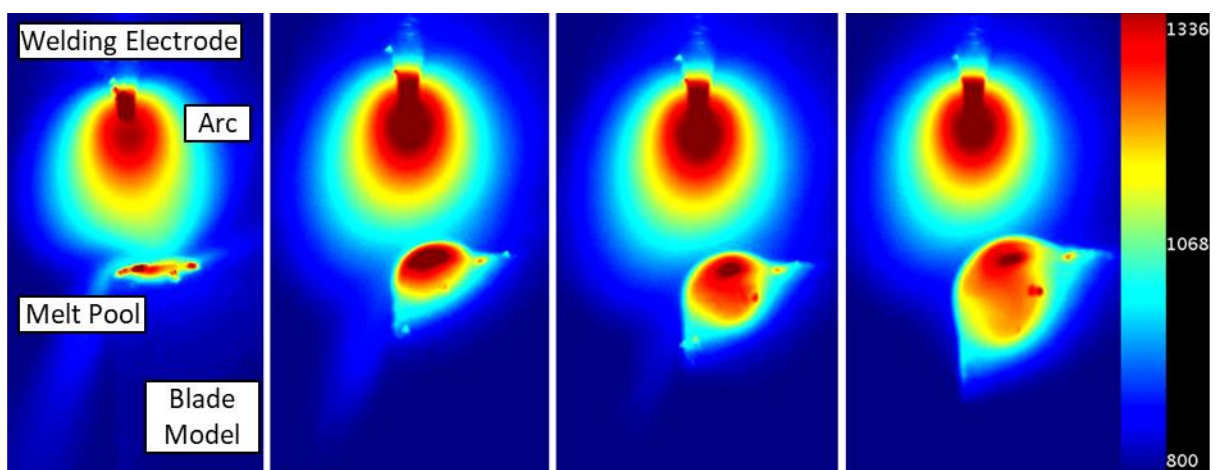


Figure 5.8 – A series of thermal camera images that illustrate the gradual accumulation of the arc heat by a model blade before feeding the additive material.

Wire Feed Adaptation to Temperature

Similar with the travel speed, the wire feeding also needs to be adapted to the temperature of the blade. The feed rate at the beginning of the weld is slower than the speed at the end, since the additive material needs to fill more area in a shorter amount of time. To achieve these alterations in the wire feed speeds a Wire Feed Controller module was developed and attached on the system.

Welding Current Adaptation for Build-Up

As the successful build-up of additive material increases, adaptations on the welding current need to be made. By gathering data from the scanning system between the different layers, the current output changes throughout the process. The current levels and rate of change results from experience of human welders, transferred to the WPS through experimental trials. Different WPS are to be followed on different types and shapes of blades and therefore current will accordingly be adjusted. An example of how voltage and current change along the welding path during a material deposition pass is presented in Figure 5.9. Current levels are set to specific levels for specific durations based on the blade. The transitions between the current levels can be either sudden or with up-slopes and down-slopes depending on the WPS.

Voltage Adaption to Power Variations

Variations occurring in the distance between the electrode and the workpiece (arc gap), correspond to changes in the voltage of the arc. By employing an electromechanical subsystem to maintain a pre-set arc, consistent voltage control is achieved. The Arc Voltage Controller (AVC) receives data from the process monitoring system, and positions the torch accordingly. By gaining greater control over the voltage, the amount of heat delivered to the workpiece is controlled providing a more stable welding process.

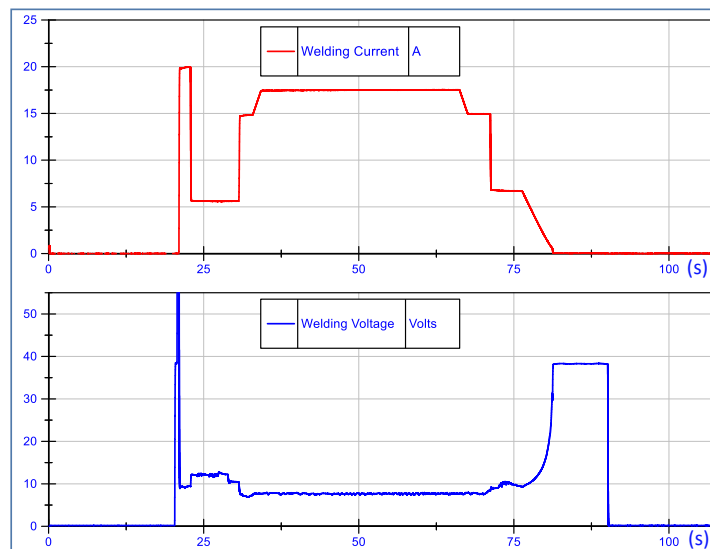


Figure 5.9 – Electric measurements during a material deposition pass. The system uses a constant-current power source, therefore the current (red) is operator inputted whereas the voltage (blue) is a response of the equipment used.

5.6 Evaluation of the First Results

Traversing through concept adaption and design phases, an operational robotic prototype was developed, delivering the first results in material deposition and therefore allowing process evaluation, systems performance assessment and optimisation. For the purposes of the presented

research, flat blade models made of SS316L were used in the welding trials for cost savings; a step prior to the transition on curved titanium blade models for final process optimization.

During the tip-repair material deposition step, the additive material is deposited on the edge of the compressor blade. In Figure 5.10 the result of the root pass with additive material deposited is shown. To ensure the successful sequential deposition, a series of visual inspection scans are performed intertwined with the deposition passes. A blade is scanned before and after the additive deposition process, resulting in a series of different 3D models which forms part of the QA and QC processes. These scans are performed using commercially available scanning systems that were integrated in the architecture of the system according to the interoperability principles of Industry 4.0. An example of such scanning series is presented in Figure 5.11. The blade models are initially scanned before the welding. The smooth surface of the refinished edge is identified with no variations on the height or the width of the edge (Figure 5.11a). After the root pass with the first material deposition is performed by means of WAAM, changes on the welded surface are detected on the scanned object (Figure 5.11c). The increase in the height of the blade, due to material deposition, is notable with different colouring according to the scale. In the event where the addition of material is obstructed (e.g. a mechanical malfunction in the wire feeder or not sufficient wire in the spool loaded), the welding process becomes autogenous. As a result, the welding arc melts the surface and therefore lower height is detected by the scanner (Figure 5.11b).

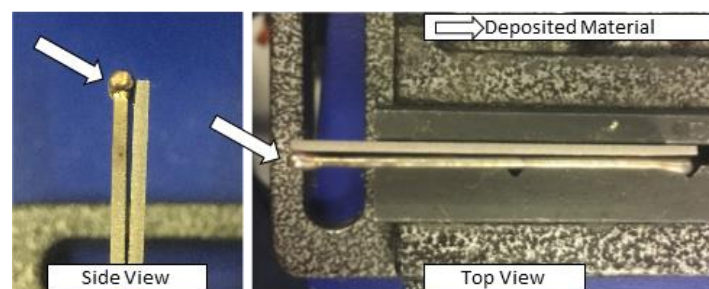


Figure 5.10 – Material deposition root pass of a blade model tip-repair. Side and top views of edge comparison with a non-welded blade model.

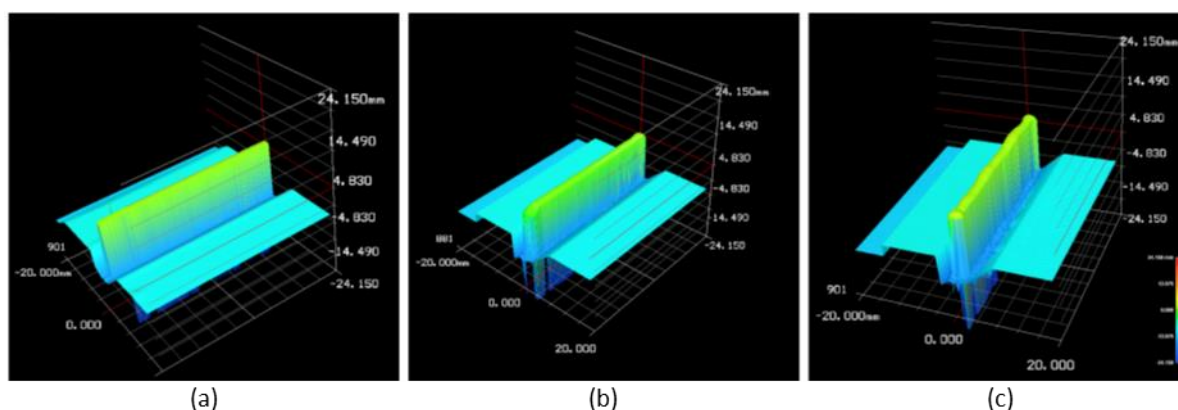


Figure 5.11 – 3D scanning modelling of a blade model: a) before welding, b) after welding without additive material, c) after welding with additive material.

Further expanding upon the utilisation of the inspection system for QA, the scanning of the blades prior to the initial deposition enables the detection of flaws on compressor blades that may have been incorrectly remanufactured or defects induced by other external factors (mishandling, contamination, etc.). In order to simulate and assess visual detection of such faults, a series of defects were

intentionally introduced on blade models. A large v-shaped cut was initially used to simulate blades bearing defects beyond the acceptable level of repair, presenting the scenario where a non-prepared blade arrives in the system. A smaller notch (<1 mm depth) was used to simulate defects occurring due to mishandling and a few drops of grease (~0.5 ml) to imitate contamination in a workshop environment. The blades were scanned with the inspection system prior to welding. In Figure 5.12 the images resulted from the 3D scanning of the flawed blade models are presented. As opposed to the flattened surface detected in the previous scanning example, blades that were not prepared correctly are characterised by electrical noise during scanning inspection, represented as spikes on the 3D scan image. The induced surface anomalies altered the 3D model of the scanner, from the initial baseline profile, allowing the visual representation of these defects.

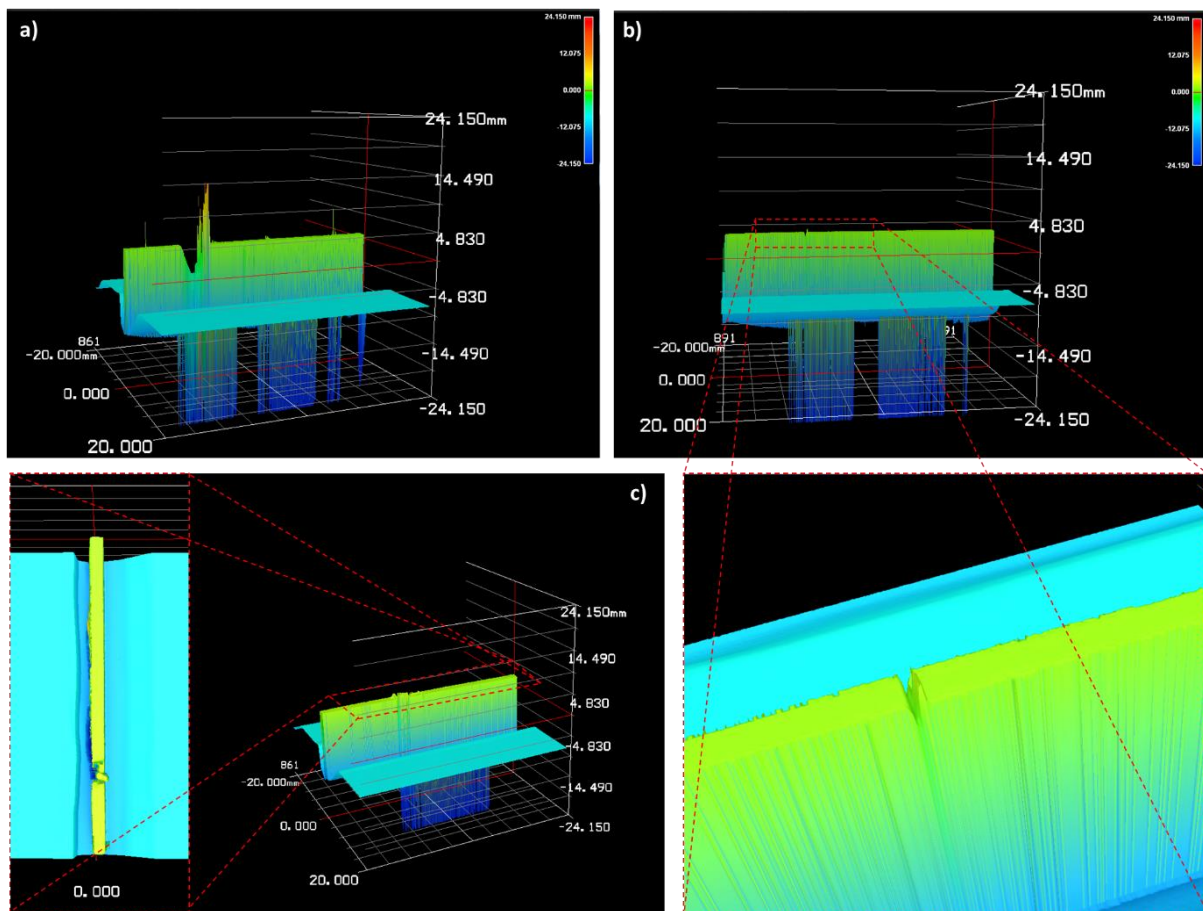


Figure 5.12 – 3D scanning of blade models, after introducing defects and contamination: a) Large V-cut on the blade edge, b) small notch on the blade edge, c) grease contamination.

Apart from the 3D scanning of the blades in between the passes, real-time monitoring of the welding process is also recruited for the evaluation of the finished part and QA. The high-speed DAQ system that was used to evaluate the welding operations for the ATLAS ITk detector that was presented in Chapter 3 is also used in the robotic solution, comprising a part of the system’s QA process. After introducing the structural defects (small notch) and contamination (grease) on the blade models described above, monitoring data (electric measurements of voltage and current) of the welding process were compared to those of welding of a non-defected blade model. While under visual inspection the welded blades appeared of normal quality without any defects, the acquired data revealed the detection of some disturbances – fluctuations on the arc power. These results highlight

the importance of a process monitoring system in maintaining the QA of the welding process, since a final product that would normally pass the visual inspection criteria, is now being flagged by the welding monitoring data for further inspection. In Figure 5.13a top views of the welded blades are presented, showing uniformly smooth surfaces with no variations, despite the presence of the induced defects. In contrast, in Figure 5.13b the acquired data from the monitoring system reveal the recorded fluctuations of the notch defect and grease contamination respectively. As these detections were initial trials on how the system responds to these welding condition alterations, further expansion of the detection is explored in Chapter 6.

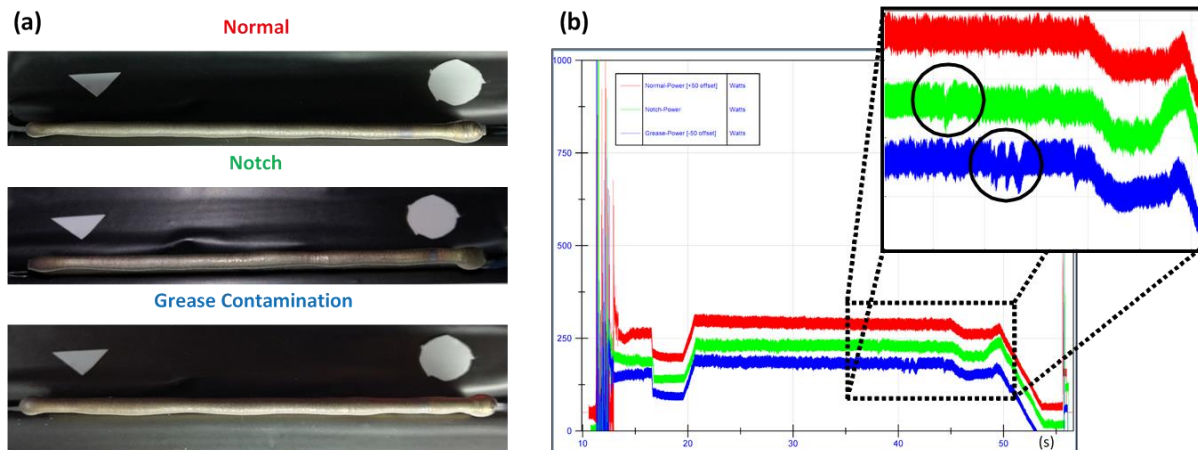


Figure 5.13 – a) Welded edge top view of turbine blade models on normal blade (top), blade with small notch (center) and blade with grease contamination (bottom). b) Power analysis from data received from the DAQ system during the welding process of the blades. Normal welding (red) and grease contamination (blue) have +50 and -50 Watts offset respectively, in order to separate the graphs. The two circles in the magnified section mark the fluctuations of the power signals caused by the notch (green) and grease contamination (blue).

5.7 Project Completion

In this aeroengine blade remanufacturing project the author’s engagement was limited to the steps discussed in the previous sections, as he went to undertake industrial secondment as part of his doctoral research while the project was still ongoing. The project continued and was successfully delivered by the ESIM team at the University of Sheffield in September 2018 without further involvement from the author. As per its design, the completed system successfully identifies the loaded blades and arranges their sequential delivery to the inspection and welding areas. Multi-layer material depositions have been achieved via adaptive welding procedure specifications while a series of pre-weld and post-weld inspections along with process monitoring ensure the quality of the remanufactured components.

5.8 Conclusion

In this chapter the steps taken towards the automation of a compressor blades re-manufacturing process, was presented. By implementing the design principles of Industry 4.0 an otherwise traditional process is evolving in a smart factory of the future. Pulsed GTAW-based WAAM is used as the process of choice to successfully deliver blade tip-repairs. Intelligent sensing and advanced monitoring modules, interconnected by the IIoT, enable fault detection and quality assurance while contributing to information transparency.

6 Welding Process Monitoring

In this chapter the concept of welding process monitoring is introduced and the various sensing technologies and methodologies utilized are presented. The benefits and limitations of each monitoring category allow varying implementation and further advances. Work undertaken by the author utilized the arc sensing methodology developed for the ATLAS ITk detector development to monitor the robotic GTAW process. Recorded data on welds of good quality were analyzed alongside welds with induced defects, time-domain features were extracted and machine learning was applied for classification of the weld quality.

6.1 Definition and Systems Classification

Welding process monitoring can be defined as the simultaneous measuring and monitoring of weld conditions and additional factors which contribute to the quality of a weld [40]. To understand the principles and explore the possibilities of real-time process monitoring in welding, the welding process needs to be considered as a complex system [99]. The adjustable welding parameters (also referred to as control variables) are the inputs of the system, whereas the properties of the generated weld and of the heat affected zone are some of the outputs. What defines the output, apart from the input parameters, are the pre-determined constants and processes that comprise the system, in this case the welding conditions. Welding conditions are parameters such as the chemical composition of the metals and the groove geometry, which are expected to remain constant throughout the process. On the contrary, inputs of the system such as current, voltage, heat input and travel speed are expected to vary throughout the process based on the desired output. However, controlling the welding conditions to their nominal values may not always be feasible, therefore fluctuations and variations from their expected values will occur. These disturbances of the system's conditions result in alterations of the output, and subsequently potentially undesired properties of the weld.

The uncertainty of the process' outcome highlights the need for monitoring, either by directly detecting the disturbances of the welding conditions or their effect on the system's output. The online monitoring of a welding process is an active area of research, mainly due to the complex physics underlying the process and the lack of commercially efficient and reliable solutions [100]. The repeatability of results in robotic welding highlights further the need for process monitoring as a human welder will be more likely to detect possible changes due to errors and try to fix them in the subsequent welds, whereas a robot would continue to repeat the process in the same way.

Studies performed in this area are revolving around the physical phenomena that are involved in the arc welding processes, particularly those related to the plasma arc and its effects on the weld pool properties. Proposed solutions in the field range from numerical simulations of the arc to vision systems with advanced image analysis, ultrasonic analysis and electromagnetic emission analysis [99], [101], [102]. Recent developments in the field of artificial intelligence see welding monitoring applications investigated by intelligent systems based on neural networks, machine learning and fuzzy logic [103].

Monitoring Classification

Process monitoring applications in welding are mainly classified based on the type of sensor and the physical phenomena they are monitoring. The sensor technologies used in research related to process monitoring are divided into four main categories: arc sensors, optical sensors, infrared sensors and

ultrasonic sensors. Additionally to these categories, research has been conducted in the fields of X-ray radiography, plasma emissions spectroscopy and acoustic emissions [99].

Independently of the sensor categorization, welding monitoring methods can also be classified at different levels according to the nature of the monitoring which relates to the type of measurements [99], [104]. At the lowest level (Level 1), inputs of the system are monitored, to ensure their correct values throughout the different stages of the process. At the mid-level (Level 2) the welding conditions (constants) of the process are monitored to ensure their nominal values are maintained at a constant (or within acceptable levels of variation). At the upper level (Level 3) variables that are affected by welding conditions and controlled by the welding parameters are monitored. These intermediate parameters (e.g. temperature gradient) are not the final output of the process but have a closer relationship with the result than individual welding parameters and conditions.

Welding monitoring systems can also be classified on three levels based on the system's ability to detect, identify and correct disturbances occurring in the process. On the lowest level (Level 1') the system is able to detect disturbances that occur in real-time. At the mid-level (Level 2'), the system has the ability not only to detect the disturbances but also to identify their origin, highlighting the malfunction in the process. At the highest level (Level 3') the system is equipped with a feedback mechanism that intervenes in the process correcting the disturbances [39].

6.2 Monitoring Sensor Technologies and Methodologies

As the welding processes are dominated by a variety of different physical phenomena, various emissions occur such as heat radiation, plasma optical radiation, audible sounds and ultrasonic waves, etc. These emissions can be used as indicators of certain properties that describe the state of the process [105] and form the core principle for welding process monitoring. Additionally unexpected disturbances occurring during the process are reflected in the measurements of these physical phenomena (e.g. magnetic field and electric field alterations, changes in temperature and sound pressure, shifts in the radiation emission, etc.) [39]. In order to detect these variations and extract useful information from the data collected during monitoring, several sensors governed by different technologies and methodologies are being used. In the following sections a brief presentation of these technologies follows, focusing on the principles behind their operation alongside with their advantages and limitations.

6.2.1 Arc Sensors

In arc welding processes, the arc itself can be used as a sensor. The principle that forms the backbone of this technology is the direct correlation that exists between the arc voltage and the arc length (the distance between the welding torch (electrode) and the workpiece) [106]. It is therefore possible to estimate the position of the torch based on the voltage/current measurements, as well as to control the voltage by adjusting the position of the torch relative to the workpiece.

Arc sensing is the working principle upon which Automatic Voltage Control (AVC) systems are built. Disturbances in the measurements of voltage correspond to changes in the gap between the electrode and the workpiece, altering the overall length of the arc. To maintain control over these changes, an electromechanical system is used for adaptive control of the voltage via altering the distance between the electrode and the workpiece. Similarly, the relationship of the arc length and the voltage measurements can be used for tracking the seam and correct positioning of the welding torch. As an

example the variation of the arc length between the edges and the center of a V-shaped groove can be used to identify the torch position and alignment related to the joint (Figure 6.1). When the arc length reaches its highest value, the torch is positioned over the center of the joint, whereas the lowest value corresponds to the torch positioned over the edge of the joint groove.

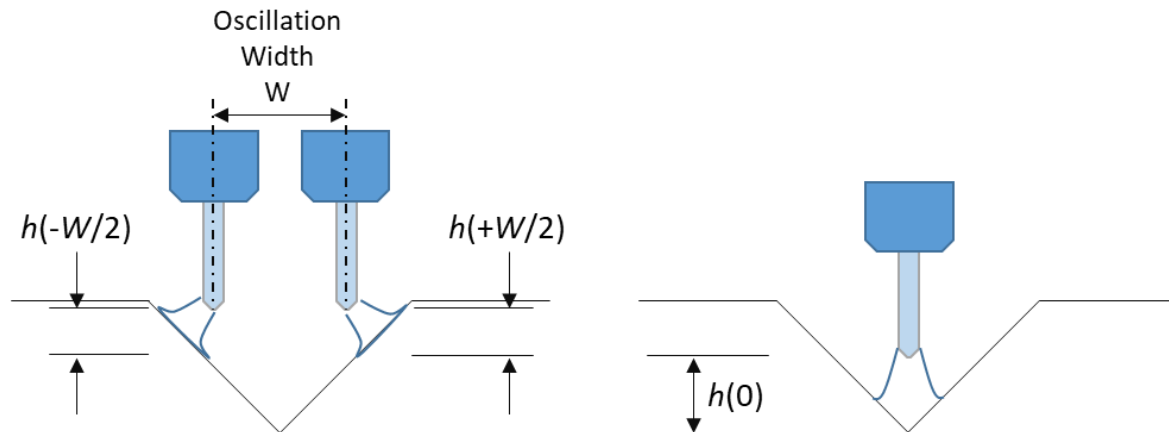


Figure 6.1 – Torch position sensing by through-the-arc electrical arc signal variations [106].

The welding current can also be used as reference signal to determine the stability of a welding process due to its sensitivity in changes occurring in the process. Arc measurements have been used as indicators in a variety of welding processes. Examples include correlations reported on arc measurements with the penetration depth in GMAW fillet welds [107], defect detection on robotic GMAW [108], [109], and weld-pool oscillation monitoring on GTAW [110].

The major benefit for using arc sensing in real-time process monitoring, is that there is usually no extra investments in expensive equipment, since arc measurements are most of the times already provided within modern commercial welding power sources [106], [107]. Additionally, the arc sensing does not require fragile components susceptible to electromagnetic arc emissions and the harsh welding environment in the vicinity of the arc. This also increases the freedom of movement of the torch as opposed to other techniques that require additional bulky components on the workbench or attached to robotic arms limiting their operational freedom [104]. However, while electric measurements are very reliable on detecting defects occurred by deviations of current and voltage parameters the detection of flaws like plate mismatches and perturbations of the gas flow may be difficult [100]. Current and voltage measurements are also not sufficient to completely characterize the welding process and identify the detected defects [111].

6.2.2 Vision-Based Systems

Vision has been the natural way of monitoring and controlling the manual welding process. In order to implement machine vision ability to robotic welders a variety of methods and applications have been investigated and developed, classified in different ways based both on the technology used and the methodology to extract features from the weld. Monitoring systems based on observations performed in the visible spectrum of light utilize various types of sensors. The main optical sensor categories are the electro-optic sensors (photoresistors, photodiodes, etc.), Charge-Coupled Device (CCD) sensors and Complementary Metal–Oxide–Semiconductor (CMOS) sensors. Their working principles vary technologically, and this is not covered in the scope of the present work, rather focusing on the methods of monitoring using optical systems. There are three main categories of

vision-based welding process monitoring: stroboscopic video cameras, structured light systems and stereovision (Figure 6.2) [112]. According to the type of image lighting source used the methods can be classified into active methods (external illumination source is required for the imaging) and passive methods (imaging is done only with the arc illumination) [113]. Additionally, the methods can be described as either top-side or back-side sensing according to the position of the sensor related to the workpiece and the welding torch. Back-side refers to the monitoring of the bottom of the weld joint by positioning the vision system below the workpiece [110].

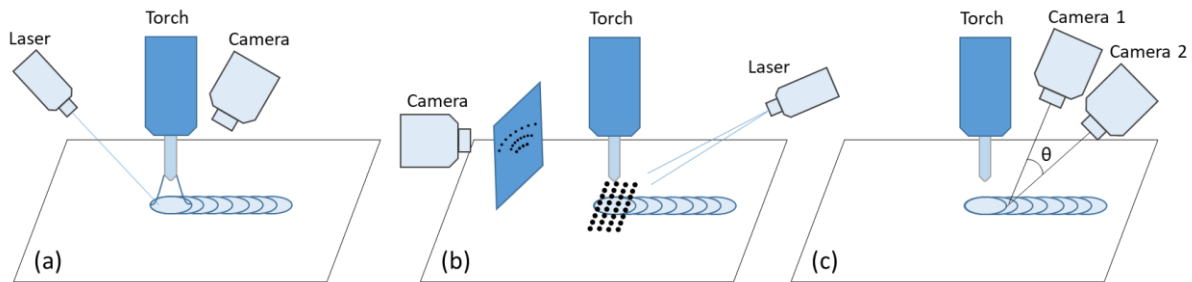


Figure 6.2 – Vision systems in welding monitoring. a) Stroboscopic Video Camera, b) Structured Light System, c) Stereovision. See text for details.

Stroboscopic Video Camera

In stroboscopic vision the camera is used to capture video images using light of high intensity originating from a strobe illumination unit (e.g. a laser source) (Figure 6.2a) [112]. The system is usually comprised of the external illumination source (laser) and a camera. By applying a spectral filtering consistent with the laser's wavelength, the rest of the arc spectrum is blocked including the intense spectral lines that can damage the camera electronic sensors. The outcome of these systems is usually monochromatic images revealing the 2D boundaries of the weld pool and the 3D pool surface morphology [102], [114].

Structured light system

In the structured light monitoring methodologies, patterns of light (lines, grid, dots, etc.) are projected on the welding surface at a known angle and a sensor is used to detect the deformation of the pattern (Figure 6.2b). Just like in the previous case, the laser wavelength is selected based on the arc light spectrum and an appropriate band-pass filter is used centered at that specific wavelength. The image can be acquired by the camera either directly from the weld pool or through an imaging plane where the projected pattern is reflected. With structured light projections, the shape and dynamic characteristics of the weld pool can be observed. Dimensional properties can then be extracted based on the pattern deformation and defects such as misalignments and undercuts can be detected [107], [115].

Stereovision System

An optical monitoring method of the welding process that is more closely related to the human vision, is the stereoscopic vision method. A stereovision system is composed of two separate cameras positioned at the same level (distance from the weld pool) with a separation similar to the human eyes (Figure 6.2c). With the use of image processing algorithms the images acquired by both cameras are merged and, benefiting from the binocular disparity resulting from their horizontal separation, 3D images are produced revealing the weld geometries. This allows to detect porosity, undercut and perform quantitative evaluation of the weld appearance [116].

Weld Pool Oscillations Monitoring

Additional from the aforementioned uses of vision-based systems, it is worth mentioning the use of optical sensors for weld pool oscillation detection in GTAW. The surface of the weld pool acts as a mirror, reflecting the arc-emitted light. This specular reflection contains information regarding oscillations in the melt pool, which can be used to monitor and control the welding process, as correlation has been established between the penetration status and the oscillations [112].

While visual inspection is the most used post-weld diagnostic method, real-time optical process monitoring is challenging. The major advantage of vision systems is that the sensors used can operate at a distance from the workpiece, not requiring physical contact with it or with the weld pool. This eliminates problems arising from parts being affected by the high temperatures that govern the process. However, when vision-based sensing is used for direct monitoring of the weld pool geometry, strong emissions across a wide spectrum from the arc light, could result in damages of the equipment [117]. As previously mentioned, optical filters are employed to protect the inspection sensors [107].

Another obstacle in the adoption of vision for welding process monitoring is the need for complex image processing algorithms and high processing power to extract useful information. The algorithms are often limited to a specific use as different joints and geometries require different approaches. An additional barrier is that the equipment employed (such as high-speed cameras and lasers) is usually very expensive. Methods using low-cost photodiodes or based on passive sensing have been explored in order to minimize the applications cost [100], [108].

6.2.3 Infrared Sensors

Since arc welding is itself a thermal process, infrared sensing is a natural choice [118]. During the welding process, parameters such as welding speed, voltage and current, and material properties of the weld (e.g. surface tension and thermal conductivity) determine the temperature distribution within the material. It is therefore possible to determine some of the weld characteristics by tracking and monitoring thermal distributions [119]. Infrared (IR) sensing refers to the non-contact thermal measuring that is based on the emissions in the infrared region of the electromagnetic spectrum (700 nm – 1 mm) [120]. The working principle of infrared sensing is based on the intrinsic electromagnetic radiation that any body with a temperature above absolute zero is emitting. Part of this radiation is emitted in the infrared spectrum, and can be used to measure the temperature of the object [121].

Infrared sensing for welding process monitoring dates back to 1963, where thermistors and Lead Sulphide-based (PbS) scanning sensors were used in GTAW and GMAW. Since then silicon photodiodes, optical pyrometers and thermographic infrared cameras have been used to monitor and control four weld characteristics: bead width, penetration depth, weld position and cooling rate. As presented in the sections below, both top-side and back-side techniques have been used for IR monitoring, with many setup variations to avoid arc plasma interferences.

Infrared Monitoring of the Torch Positioning

Nagarajan et al. used infrared thermography for topside sensing on GTAW performed on butt joints of steel plates [122]. By misaligning the welding torch path from parallel to cross-joint, it was found that the thermal profiles of the welds were changing relative to the torch position. When the torch was on-joint (over the center of the joint), the isotherms of the thermal profile were symmetrical, whereas in off-joint position (offset from joint center), the thermal profiles had asymmetrical patterns. Therefore using the information acquired from the isotherm radii, the arc position relative to the joint

could be identified. Subsequently, this relation was further investigated to detect and correct in real-time initial positioning errors on butt welds of both fitted joints and joints with gaps [123]. Additionally, on joints with a gap, the infrared intensity distributed on a line transverse to the torch displacement direction revealed notable temperature drop over the joint gap. This drop is mainly attributed to the lower thermal conductivity of the gap relative to the plates, and the difference in emissivity of the joints [119].

Infrared Monitoring of the Weld Pool Size and Penetration Depth

Single-element detectors alongside chromatic filtering were used to monitor and determine the weld pool size in laser welding [124]. Changes in the size of the thermal radiation source (in this case the welding pool) were detected utilizing the changes on the field of view introduced by the chromatic aberration. Changes in the temperature distribution have been associated to changes in the joint penetration depth originating from variations of the input parameters [125]. On butt-joint welds performed with GMAW on steel plates, a linear relationship between the infrared thermal image profile width and the weld bead width was established. Further metallographic techniques to measure the joint penetration and actual bead width resulted in an exponential relationship of the penetration depth with the measured surface temperature profile at the center of the weld pool. The authors concluded that this correlation can be investigated to implement feedback controlled joint penetration using IR thermography in GMAW.

Infrared Monitoring of the Cooling rate and Defect Detection

Changes in the thermal cycles (heating and cooling rate) of the workpiece affect directly its mechanical properties, especially in the HAZ, via changes in the materials' microstructure. It is therefore important to monitor and control the cooling rate post-weld. Infrared sensing is best suited for weld cooling rate measurements, because of its sensitivity, fast response and non-contacting nature [119]. On both GTAW and GMAW IR thermography is used to monitor the cooling rate and successfully produce welds with high yield strengths [126]. Sreedhar et al., developed a monitoring system of detecting welding defects based on spatial and temporal surface temperature distributions [118]. A stationary infrared camera was used to generate thermal images of GTAW welds on rotating propellant tanks. The image acquisition was focused on the solidified region of the weld, right after the torch pass. Using threshold-based processing and decision making the system was able to detect the significant defects that were radiographically assessed post-weld. The actual cooling rate was later determined numerically and experimentally using the same system [120]. Yu et al., also developed a low-cost system based on infrared sensing to detect perturbations of the GMAW process on aluminium alloy plates [121]. By using a single point infrared sensor and a galvanometer scanning mirror, temperature profile measurements were performed on a line transverse to the weld seam. In the presence of defects (humping, undercut and lack of fusion) the temperature profile showed asymmetries compared to welds of good quality, allowing real-time quality assessment.

Infrared Sensing for Arc Monitoring

Another approach to defect detection in GTAW process uses an infrared sensor to directly monitor the arc status and consequently extract information related to the quality of the weld [39]. The output of the sensor (voltage) is changing in relation to the length of the arc, which is susceptible to perturbations of the process (e.g. arc length disturbance, presence of contaminants, absence of shielding gas). In a later work the same approach employed a Field Programmable Gate Array-based (FPGA) system for in-situ changes detection [127].

The depth and breadth of applications and the non-contacting nature of the infrared sensing allow a wide implementation of these technologies in welding process monitoring. Infrared sensing is the most extensively used sensor category for monitoring and control of the weld process [119]. It is frequently used in applications that combine more than one methods of detection. With sensor fusion, infrared sensors have been combined with arc sensors, acoustic emissions sensing, optical vision system and ultrasonics [39], [105], [116]. Similarly image processing techniques can be used to merge images from both optical and infrared cameras, enabling features to be studied in parallel and correlated with arc sensing data [107].

The main limitation to the wide industrial adoption of infrared sensing is the difficulty of attaching the sensors on challenging setups. It usually results in bulky equipment in the torch vicinity, confining the space and limiting the freedom of movement. Moreover, in applications where the welding torch is not in a fixed position, matching the sensor to the movement of the welder is challenging [110]. An additional barrier in the implementation of infrared thermography is that the estimated temperature is a function of the surface emissivity which varies with the material, the surface preparation and the surface temperature itself [125]. Therefore every application must rely on relative rather than absolute temperature measurements.

6.2.4 Ultrasonic Sensors

Ultrasonic testing (UT) is the most widely used NDT technique for inspecting a variety of manufactured components, developed to replace the hazardous radiography. The term ultrasound refers to sound waves (mechanical vibrations) that have a frequency greater than 20 kHz, which makes them undetectable by humans (20 Hz – 20 kHz). In ultrasonic testing, a variety of sensors are used to create and detect these mechanical waves. These can be piezoelectric, capacitive, Electromagnetic Acoustic Transducers (EMAT), ultrasonic phased-arrays and laser ultrasonic sensors, with piezoelectric and EMAT being the most commonly used [128].

Two techniques of UT commonly used in welding are the pulse-echo and the transmitted compression (time-of-flight). In the former, the waves are introduced by a transducer into a medium and echoes (reflections) are returning to a receiver whereas in the latter, the propagated signals are refracted, diffracted or attenuated from structural changes within the medium. By analyzing the signals received by the sensors these methods allow to visualize the inner structure uniformity, size and condition of a material. Ultrasonic testing is widely used for locating cracks, inclusions, porosity, lack of fusion and other defects in fusion welds [110].

Ultrasonic Monitoring of the weld pool geometry and defect detection

In order to use ultrasonic testing in-situ during the welding process, Stares et al., used a combination of ultrasonic compression and shear wave on steel root butt welds produced in GTAW [129]. Shear waves transducers used pulse-echo technique and transmitted compression technique was used on ultrasonic compression waves (Figure 6.3). Their probe array was able to determine the lateral width of the weld pool and changes occurring to its dimensions due to changes in the welding parameters. At the same time, the system was able to detect and characterize various welding defects such as porosity, inclusions and lack of fusion, in real-time. It was found that fluctuations in ultrasonic intensity were attributed to the presence of porosity and a reduction in the intensity was caused by inclusions and lack of fusion. The experimental results showed better sensitivity and performance of the transmitted compression waves over shear waves.

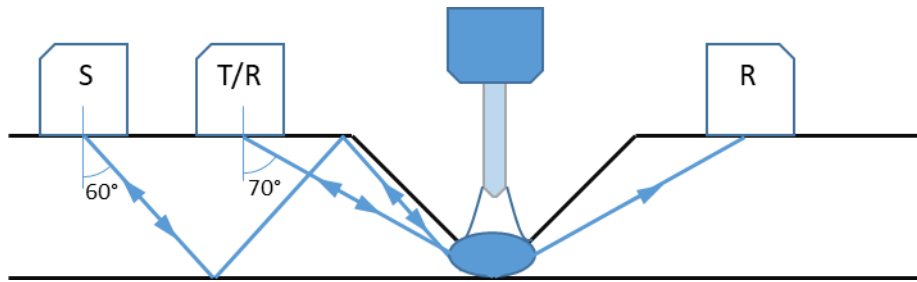


Figure 6.3 – Diagram of ultrasonic probes arrangement used to monitor root-pass welds; S is pulse-echo shear probe, T/R is pulse-echo compression probe and R is transmission receiver probe (compression) [129].

Contactless Ultrasonics for Welding Monitoring

For proper functionality of UT the transducers need to be in contact with the material, and this is achieved with the use of a couplant (a medium for the sound wave to travel through). This requirement confines the wider industrial implementation of ultrasonics in welding monitoring, because the high temperatures involved and the moving parts of the process make maintaining the transducer-workpiece contact challenging. To solve this challenge in the previous example Stares et al., used water as a couplant through an irrigation system and kept the transducer constantly aligned with the welding torch. With the established ability to generate ultrasounds using pulsed Nd:YAG (neodymium-doped yttrium aluminum garnet) lasers and the emergence of the new field of laser ultrasonics, contactless UT sensing was enabled (Figure 6.4). Pulsed lasers allow the generation of all type of waves (compression, shear, surface and guided) by ablation or through thermoelastic process. To detect such waves without physical contact, laser interferometers are employed. These operate either by measuring the surface displacement through interference with a reference beam, or by detecting changes in the frequencies of scattered/reflected light [128]. Lower sensitivity was however reported with laser-ultrasonic non-contact detection when compared to other ultrasonic techniques in GTAW monitoring [116].

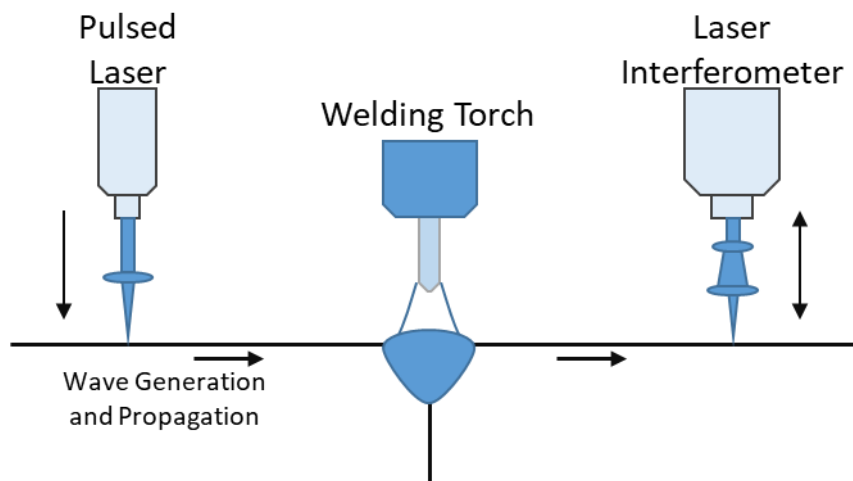


Figure 6.4 – Laser ultrasonic used for online inspection of a welding process [128].

Further investigations for contactless UT include the use of Electro-Magnetic Acoustic Transducer (EMAT) as a receiver of ultrasound signal from a pulsed laser [130] [131]. Studies were performed on steel plates welded via GMAW process and in both cases correlation between the measured time of flight and weld penetration depth was established, allowing the ability to monitor, predict and control the weld quality in real-time. However, since the EMAT use is based on magnetic fields, its application

is limited to ferromagnetic materials (e.g. not applicable for materials with very weak magnetic properties such as titanium).

Ultrasonics for Resistance Welding Monitoring

While resistance welding is a pressure-based process and therefore not covered in the present work, it is worth mentioning the application of ultrasonic monitoring in resistance spot welding. By introducing resistance welding electrodes with embedded ultrasonic transducers, online monitoring and measuring of the weld bead size was achieved [132]. Since by nature spot welding has stationary parts and electrodes with no need for moving parts during welding, the application of ultrasonics was easier compared to fusion welding. With the ultrasound transducer positioned inside the top electrode, the transmitted signal gets four reflections: one from the top plate surface, one from the nugget's top edge, one from the bottom edge and one from the bottom plate surface (Figure 6.5). With these reflections, it is possible to calculate the size of the nugget and the penetration depth of the weld. The system was successfully tested on a variety of materials including aluminium alloys and mild steel [132], [133].

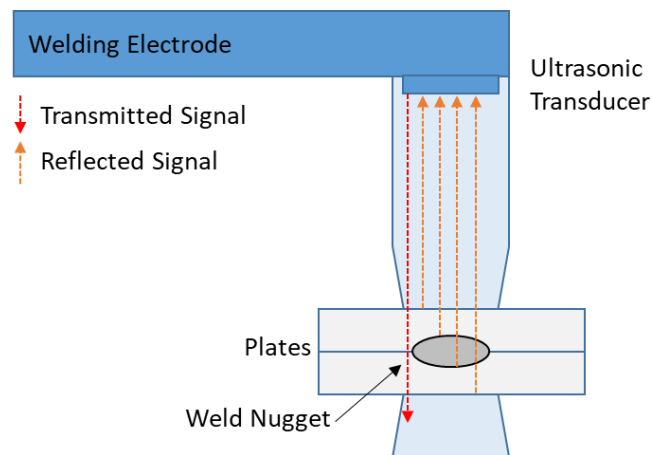


Figure 6.5 – Ultrasonic reflections in resistance spot welding [132].

The properties of ultrasonic monitoring of the welding process that were presented highlight the ability of the method to provide representative information of the weld pool size and bead formation in real time. However, industrial implementation of this monitoring method is restricted due to the need for the transducers to be in constant contact with the workpiece via a couplant. The high temperatures, the industrial environment quality standards to be followed, and the complexity of process setups with moving parts make the use of contact-based transducers extremely challenging [130]. Solutions explored with EMAT sensors and ultrasonic lasers have demonstrate the ability of contactless operation, there are however extreme increases in the cost of such equipment and more complex interpretation methods [128].

6.2.5 Other Process Monitoring Techniques

The aforementioned four sensor categories comprise the main welding process monitoring techniques. There are however other monitoring methods that share some characteristics with the aforementioned categories, but are different in terms of working principles and equipment, hence their separation from the previous section.

6.2.5.1 Spectroscopy

Spectrometry describes a set of techniques that are used to measure the electromagnetic spectrum resulting from emission, absorption or diffraction of electromagnetic radiation by molecules or atoms [103]. By applying emission spectroscopy to arc welding monitoring, information can be analyzed qualitatively and quantitatively. In the former, the elements which exist in the plasma are revealed, whereas in the latter the intensities of each different wavelength of the plasma radiation are measured yielding information such as electron temperature and plasma density [39]. It is therefore possible to detect anomalies in the plasma properties corresponding to process disturbances and sources of defects.

Ancona et al., used a miniature spectrometer to calculate the axial electron temperature of arc plasma during GTAW root passes on carbon steel pipes [134]. Changes in the electron temperature were found in correspondence to a series of defects (porosity, drop-out, hollow cavers, tungsten inclusions and undercut) induced by insufficient shielding gas, unskilled filling wire manipulation, electrode contact with the weld pool or torch misalignment. In a similar setup of GTAW the electron temperature was also used to detect seam oxidation on Stainless Steel 304 [100]. In GMAW used to deliver bead-on-plate welds on steel plates, iron and manganese electronic temperatures were used as indicators of changes in quality, successfully detecting induced defects such as grease contamination, oxidation, slag inclusion and lack of penetration [103]. Defects of seam oxidation (due to non-cleaned and oil-contaminated surface) and simulated disturbances due to unstable wire feed speed and step-changed welding current were also studied through spectroscopy on aluminum alloy by analyzing the radiation of selected spectrum of interest [135]. In order to discriminate in real-time the weld defects, statistical features were extracted from the spectral curves. The system was tested in Pulsed-GTAW, where feature parameters variance and kurtosis have shown great sensitivity to seam oxidation.

The two main benefits of spectroscopy in welding process monitoring is its immunity to the strong electromagnetic interference of arc welding (since optical fibers can be used to keep sensitive equipment away from the welding torch) and the versatile ability to perform analysis of different chemical species that participate in the plasma. This enables defect characterization and identification far better than other techniques [100]. However the cost of professional spectrometers is huge barrier to the adoption of spectroscopy in the welding industry. Moreover, the varying spectral lines between different processes, setups and materials require constant-reconfiguration alongside with advanced technical expertise.

6.2.5.2 Acoustic Emissions

In the welding process, both during the melting and solidification phases, weld plastic deformation, fracture, martensitic transformation and crack formation generate acoustic emissions, providing a potential means of monitoring and characterizing the weld quality. Acoustic emissions are elastic waves caused by rapid energy release from sources within a material. Similar to ultrasounds, acoustic emissions can be detected using a variety of sensors like piezoelectric sensors and laser interferometers. While the detection methods are the same, what differentiates acoustic emissions monitoring from ultrasonic monitoring is the origin of the waves: acoustic emission monitoring is a passive method detecting waves originating from the welding process itself whereas in UT the waves are externally induced.

During the welding process, generated sounds in the audible to human frequency spectrum, (referred as arc sound signals or arc acoustics), are used by experienced welders to evaluate the welding process [136]. While the features of the sound in the time domain represent no obvious correlation with the welding state, transformation to the frequency domain is used to extract further information. Research shows that the frequency bands 2 kHz – 3 kHz, 17kHz – 19 kHz and 30 kHz – 35 kHz are highly correlated with weld state [105]. Experimentally, the weld penetration depth was found to be closely related to welding sounds in GTAW [136], Pulsed-GMAW [54] and in laser welding [105]. Acoustic emissions sensing has been proven more reliable than other sensors technologies in the detection of specific perturbations (ferric chloride contamination) and weld penetration monitoring [39], [54].

The adoption of acoustic emissions in welding process monitoring can be relatively easy to achieve and inexpensive, but demanding analysis algorithms are required to achieve weld characterization. In order to extract useful information based on the features of sound signals, wavelet analysis (simultaneous representation of both time and frequency domains) and wavelet packet decomposition offer a more flexible and broad field of analysis, as opposed to the limited resolution of Fourier transformations [136].

6.2.5.3 *X-ray Radiography*

In radiography the inspected object is irradiated with X-rays (120 eV – 120 keV). The high energy allows them to penetrate through a material, enabling a series of options for characterization of the internal structure of materials (X-ray scattering, X-ray diffraction/crystallography, etc.). This penetrative ability of X-rays is utilized in welding-related research to reveal phase transformations during the process and to study weld pool dynamics as presented in Chapter 4.4.4. Elmer et al., in a series of experiments using Synchrotron-based X-Ray diffraction performed in-situ monitoring of the phase transformations, and with spatially resolved X-ray diffraction (SRXRD) they were able to present the first in-situ mapping of phase boundaries occurring in fusion welds [137]–[140]. Their experimental setup was applied to various materials including low carbon and medium carbon steels, commercially pure titanium grade 2 and grade 4, and Ti-6-4.

X-ray radiography is the preferred method used for post-weld inspection and NDT of fusion welding, under the concept of industrial radiography. Two-dimensional images from radiography and 3D images from X-ray Computed Tomography (CT) scans of welded workpieces are used to provide details of defects present in both the weld and the HAZ. A series of experiments were performed by Rokhlin and Guu in the late 80s and early 90s, investigating the use of radiography for real-time monitoring of submerged arc and GTAW welding processes [141]–[144]. An image intensifier for image acquisition was located on the opposite site of the workpiece, relative to the X-ray source. Their system was able to detect defects occurring in real-time and feed back through a decision algorithm to the welding parameters and correcting the process. An experimental setup employing a balancing scale allowed monitoring the arc force in addition to the radiography. During these studies the weld pool depression by the arc force was associated with weld penetration.

6.2.6 *Industrial Adoption Barriers*

Despite the fact that the aforementioned welding monitoring technologies have been an active field of research for more than 30 years and have demonstrated sufficient abilities in in-situ defect detection, these technologies have not been widely adopted in the industry. A notable recent example highlighting the lack of industrial implementation is the Subaru recall of 2,100 brand-new vehicles

back in July 2019 due to faulty welds impacting the vehicle's body strength [145]. This situation is mainly attributed to the variety and complexity of the welding processes, which complicates the assessment of the suitability of monitoring methods [117]. Additional obstacles that monitoring systems developers need to overcome include the high initial costs, fragile and sensitive equipment operating in harsh industrial environments (e.g. contact-requiring sensors in high temperatures, fumes and spatter), arc radiation interference, restricted access in the welding area and weight limitations preventing the attachment of bulky components to the welding torch [134].

6.3 Welding Monitoring for ATLAS and Aerospace Remanufacturing

Building on the knowledge extracted from the literature review presented in the previous section, it follows that the selection of a monitoring technology should be based on the specific application. For the ATLAS ITk development, parts of the cooling loops will be welded in a laboratory and the rest will be welded in-situ. Therefore the system selected should be able to operate in a confined space. Additionally, the rotating parts of orbital welding alongside the small size of the cooling pipes restrict the use of sensors close to the operating area. Based on these limitations the monitoring via arc sensing was the most suitable choice.

The electric measurements DAQ system mentioned in the previous sections was developed by University of Sheffield. As seen in Figure 6.6 the measurements are performed by redirecting the power cables that connect the power source to the welding torch and the workpiece through a sensor box. Inside the box two separate systems measure current and voltage using Hall-effect-based sensors. The information is then carried outside the sensor box to be recorded by the DAQ system. The metallic frame hosting the diagnostics and all electronic equipment is grounded to prevent external factors from affecting the measurements.

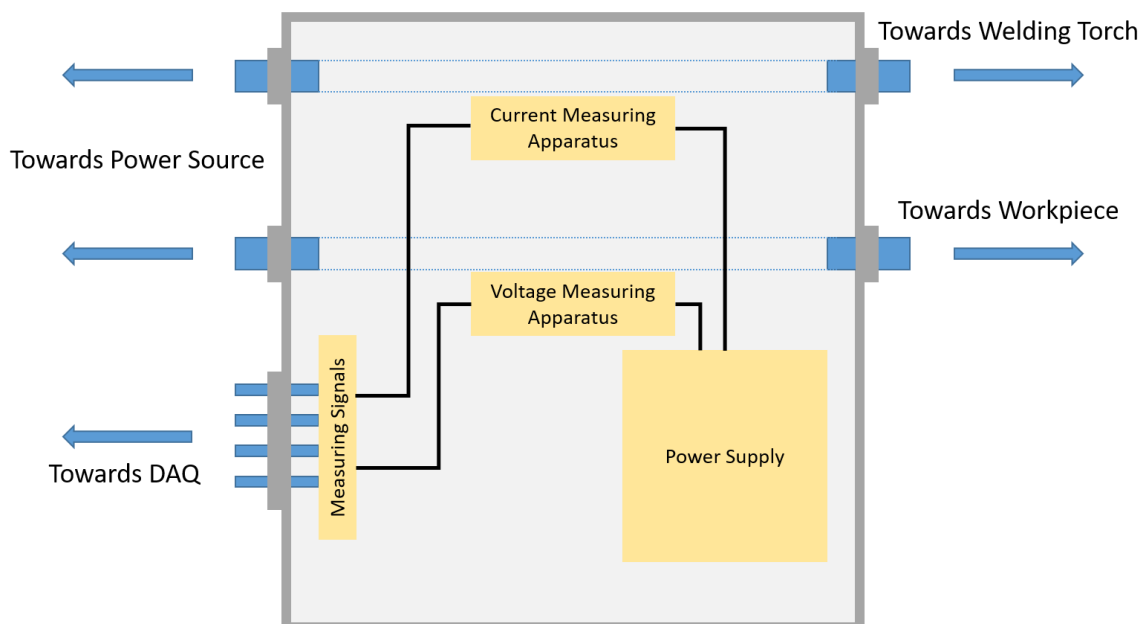


Figure 6.6 – Sensor box used for welding current and voltage measurements. The connecting cables between the power source and the torch/workpiece are redirected through the box in order to perform the measurements.

The major benefit of this setup is that it can be applied without changes to several GTAW applications. The same sensor boxes were used within the scopes of the present work on manual welding, orbital

welding for the tube-to-tube joining (ATLAS ITk), orbital tube-to-tubesheet welds (Chapter 7.2), robotic beads-on-plates welds, robotic butt-joints welds and the compressor blade tip-repair process.

When the system was utilized in gathering data from industrial robotic welding, the possibility to position the sensor box away from the workbench provided less interference with the intense arc radiation that may otherwise threaten sensitive electronics. Since no additional equipment is needed in the vicinity of the arc the robot movements are not limited by the monitoring process.

One unexpected problem arose when using the system with the VBCie IE175 HMS/ABB robot setup and the Automatic Voltage Controller (AVC) enabled. The problem was tracked to the power source systems architecture as the addition of the measuring parallel resistance in the sensor box was affecting the response of the AVC controller. The AVC electrode touchdown could not retract as the signal sent wasn't recognized by the controller. The problem was solved by increasing the measuring resistance but at the cost of lowering the measuring sensitivity on the voltage transducer. Therefore whenever possible the AVC function was not utilized, keeping the original measuring resistance and maintaining the high sensitivity.

6.4 Fault Detection and Quality Assurance

The author was involved in a number of welding monitoring investigations and applications using the monitoring setup presented in the previous section. As shown in Chapter 3, the monitoring setup was used to evaluate orbital welding on titanium tubes for the ATLAS ITk development. Similarly in Chapter 5, monitoring the welding process allowed quality assurance and control in the development of the compressor blade repair robotic solution.

In an attempt to further expand on the implementation of the monitoring setup in robotic welding processes, a series of investigations were performed by the author at the Advanced Remanufacturing and Technology Centre. The basis for these investigations was that as welding process monitoring is advancing in the context of Industry 4.0, the need for complex data analytics is emerging. In order for a system to be able to detect and advance in characterizing disturbances, machine learning algorithms are employed to "teach" a monitoring system how to predict the quality of a weld.

In line with this rationale, a series of welding trials were performed to gather welding data under normal and disturbed welding conditions. The recorded data were analyzed to establish correlations between the disturbances and the extracted features from the signals. The features were then used as inputs in a supervised machine learning algorithm to classify the welding quality.

6.4.1 Materials and Methods

Experimental Setup

For the welding trials presented in this section the same Gas Tungsten Arc Welding experimental setup that was presented in Chapter 4.4.1, consisting of an ABB IRB 2400/16 robotic arm connected with a VBCie IE175i Heat Management System power source, was used.

Materials

The robotic welding setup was utilized to deliver a variety of welds both on SS316L and Ti-6-4 substrate plates. In the case of butt-welds the welding-seam sectioning was performed using AgieCharmilles CUT 300 Sp wire Electric Discharge Machining (EDM) and plate fixing was done by means of manual spot TIG welding (Figure 6.7). The welding parameter selection for the seam welding was based on

prior DOEs that followed both Taguchi full and partial factorial analysis that monitored high penetration and wide reinforcement cap. In the case of beads-on-plates InterPulse welding current was used, benefiting from the high height-to-width ratio. An example of welding parameters used for delivering beads-on-plates linear welds on SS316L plates is presented in Table 6.1.

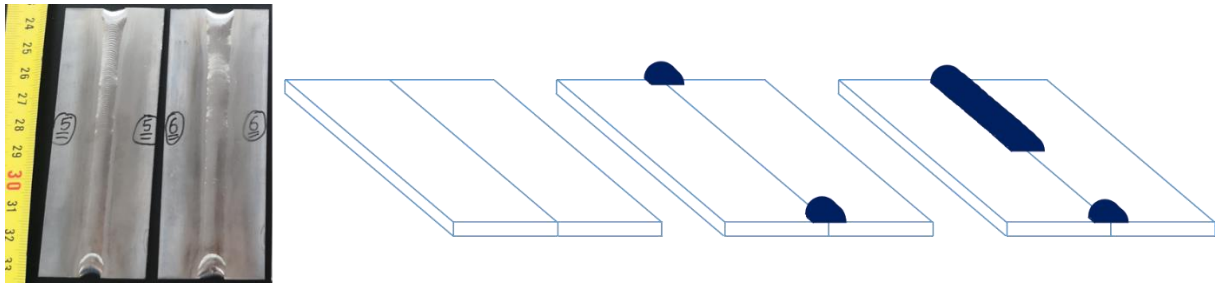


Figure 6.7 – Examples of square butt welds. Spot welds are introduced at the edges prior to seam welding to avoid mismatching due to plate deformation from heat accumulated as the weld progresses.

Table 6.1 – Experiment Welding Parameters

Parameter	Value
Current and polarity	InterPulse Direct Current – Electrode Negative
Main welding current	126 A
Delta Current	53 A
AVC function	OFF
Shielding gas	Pure Argon
Shielding gas flow rate	17 L/min
Feeding wire	Inconel 718, 0.889 mm
Wire feeder speed	18 mm/s
Torch travel speed	3.3 mm/s

Disturbances and Design of Experiment

In order to simulate potential undesired disturbances that could occur in a welding workshop, three welding conditions were altered. Surface integrity was disturbed by machined notches on the plates perpendicular to the weld seam, to simulate improper surface preparation and material handling. V-shaped notches were machined using a Proxxon Milling Machine controlling the depth and width of notches as illustrated in Figure 6.8.

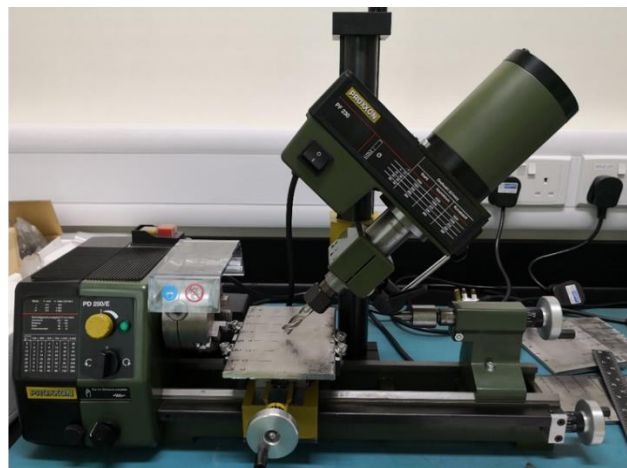
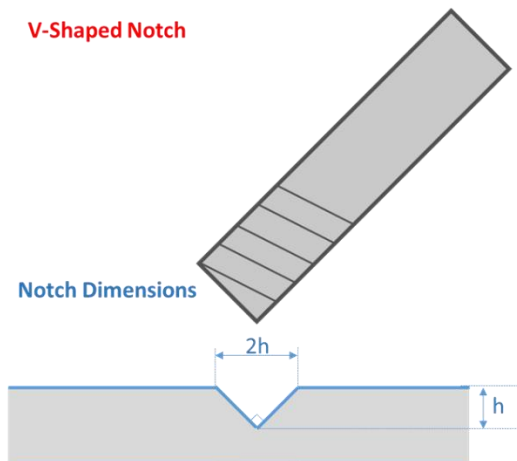


Figure 6.8 – Introducing Notches on SS316L plates using milling machining to simulate compromised surface integrity.

Shielding gas flow disturbances were introduced by manual flow rate reduction from a brass ball valve, simulating potential regulator failures and accidental hose step-on. Grease applied on the welding path simulated surface contamination (Figure 6.9). All three disturbances were introduced in controlled ways in order to have quantified disturbance levels. In the example presented in Table 6.2 the three disturbances were introduced in three levels (0, 1 and 2) resulting in 27 combinations. This composes an L₂₇ full-factorial orthogonal array. Level 0 represents the optimal condition in which the system is expected to perform normally. This translates into no contamination, no notch or in the nominal value of the shielding gas flow rate. Level 1 represents a “small” disturbance, which was simulated by 0.1 ml of grease, a V-shaped notch of 0.2 mm depth and 0.4 mm width, or a gas flow reduced by 15%. Level 2 represents a “bigger” disturbance, simulated by 0.2ml of grease, a V-shaped notch of 0.6 mm depth and 1.2 mm width, or a gas flow reduced by 75% (Table 6.3).

Table 6.2 – DOE Full Factorial L₂₇ Orthogonal Array.

Weld Number	Disturbances (Levels) ¹		
	Notch	Grease Contamination	Gas Disturbances
1	0	0	0
2	0	0	1
3	0	0	2
4	0	1	0
5	0	1	1
6	0	1	2
7	0	2	0
8	0	2	1
9	0	2	2
10	1	0	0
11	1	0	1
12	1	0	2
13	1	1	0
14	1	1	1
15	1	1	2
16	1	2	0
17	1	2	1
18	1	2	2
19	2	0	0
20	2	0	1
21	2	0	2
22	2	1	0
23	2	1	1
24	2	1	2
25	2	2	0
26	2	2	1
27	2	2	2

¹For the corresponding values of each level see Table 6.3

Table 6.3 – Disturbance levels.

Level	Disturbances		
	Gas Disturbances (%)	Grease Contamination (ml)	Notch Depth (mm)
0	0	0	0
1	-15	0.1	h = 0.02
2	-75	0.2	h = 0.06

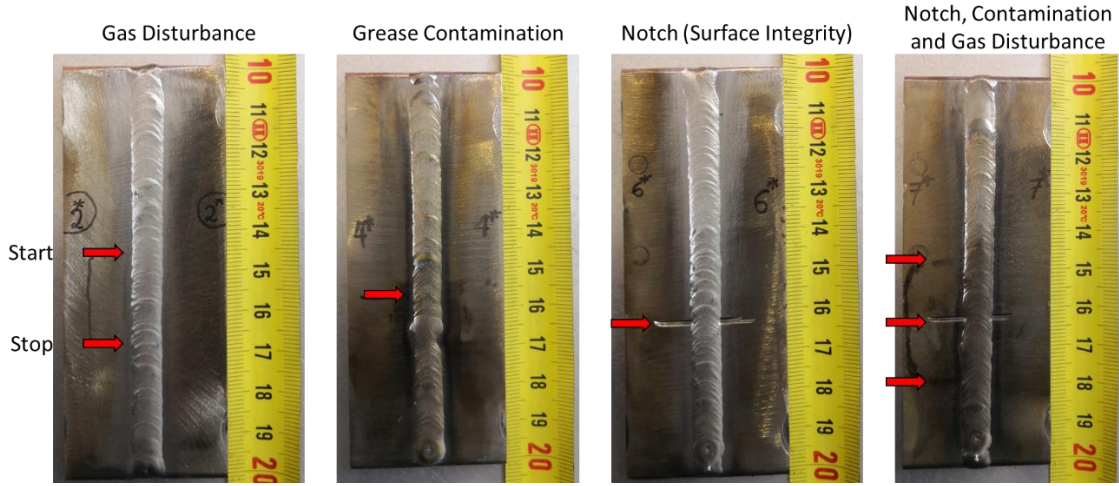


Figure 6.9 – Welding conditions disturbances on SS316L square butt welds.

Data Analytics

The data acquired were analysed in order to extract time-domain features including the first four statistical moments (mean, variance, skewness and kurtosis). A total of 15 features were extracted for each acquired signal (Table 6.4) [146].

Table 6.4 – Definitions of Time-domain features.

Feature	Definition
Mean (average amplitude)	$p_1 = \frac{1}{k} \sum_{i=1}^k s(i)$
Variance (standard deviation)	$p_2 = \left(\frac{\sum_{i=1}^k (s(i) - p_1)^2}{k-1} \right)^{1/2}$
Root-mean-square amplitude (RMS)	$p_3 = \left(\frac{1}{k} \sum_{i=1}^k s(i)^2 \right)^{1/2}$
Square of mean of rooted absolute amplitude (SMRA)	$p_4 = \left(\frac{1}{k} \sum_{i=1}^k \sqrt{ s(i) } \right)^2$
Peak value	$p_5 = \max s(i) $
Skewness coefficient	$p_6 = \frac{\sum_{i=1}^k (s(i) - p_1)^3}{(k-1)p_2^3}$
Kurtosis coefficient	$p_7 = \frac{\sum_{i=1}^k (s(i) - p_1)^4}{(k-1)p_2^4}$
Peak factor (crest factor)	$p_8 = \frac{p_5}{p_3}$
Margin factor	$p_9 = \frac{p_3}{p_4}$
Waveform factor	$p_{10} = \frac{p_3}{\frac{1}{k} \sum_{i=1}^k s(i) }$
Impulse factor	$p_{11} = \frac{p_5}{\frac{1}{k} \sum_{i=1}^k s(i) }$
Min amplitude	$p_{12} = \min(s(i))$
Max amplitude	$p_{13} = \max(s(i))$
Max – Min	$p_{14} = p_{13} - p_{12}$
Peak – Mean	$p_{15} = p_5 - p_1$

It should be highlighted that the features were extracted only for the welding time interval where stable conditions are expected (Figure 6.10). The pre- and post-weld zones are the areas of signal recorded prior and after the welding process and therefore are not of interest in this investigation. In

the arc initiation phase is also excluded as high frequency high voltage is applied between the electrode and the workpiece in order to ionize the gas and form the arc. After the arc is established, the robotic arm movement is initiated and the welding is performed, forming the welding zone in the recorded signal. Once the welding is finished the torch stops travelling and the arc is extinguished in the arc turn-off zone.

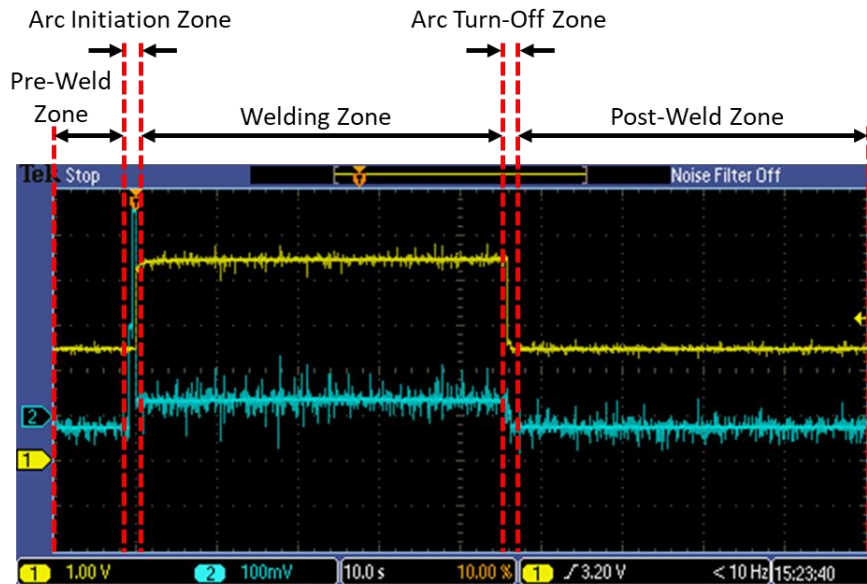


Figure 6.10 – Zones within a recorded welding signal corresponding to the different stages of the process.

Each welding zone signal was segmented into 1562 parts and the values of the time-domain features were calculated. The extracted features were subsequently used in supervised machine learning for weld classification. The machine learning method chosen was the ExtraTreesClassifier [147]. ExtraTreesClassifier is an ensemble method (combining predictions of several base estimators to improve generalizability and robustness compared to a single estimator) fundamentally based on Decision Trees. ExtraTreesClassifier is similar to the Random Forest where an estimator fits a number of Decision Tree classifiers of several subsets from a dataset, improving the predictive accuracy and controlling the over-fitting by using the subset average [148]. What differentiates ExtraTreesClassifier is that thresholds are drawn at random for each candidate feature (instead of looking for the most discriminative thresholds) and the best of these randomly-generated thresholds is picked as the splitting rule [149]. This additional randomness allows further reduction to the model's variance, at the expense of a slightly greater increase in bias. This bias-variance trade-off is preferred in welding monitoring as small fluctuations on the monitored signals are expected and therefore overfitting on noise of training data should be avoided.

6.4.2 Extracted Features Correlations

In order to evaluate the features as potential disturbance detectors – and subsequently as disturbance identifiers – analysis was first performed on data corresponding to individual disturbances. By plotting together each group of similar disturbances, correlations were studied for each feature. In Figure 6.11 the correlations of the first statistical moment (mean) on both current and voltage signals are seen for the welds where the disturbances were individually introduced to the welds. The voltage signal mean increased in the presence of grease and with the decrease of shielding gas flow rate, and decreased in the presence of surface marks. The current mean, decreased in the presence of contamination and increased in the presence of surface marks. While a higher value variation was recorded during

shielding gas flow disturbances, not sufficient correlation was established on the mean values, possibly attributed to uneven quantification of the disturbance (manual brass-valve).

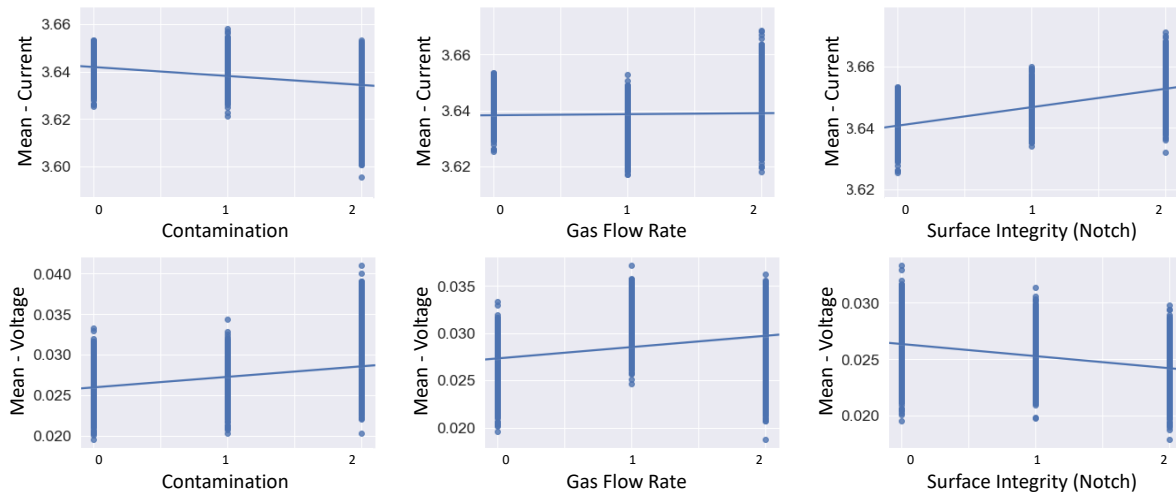


Figure 6.11 – Current and voltage measurement mean values for individual welding condition disturbances (C = contamination, GF = gas flow, N = notch). Left: C:0-2, GF:0, N:0; Middle: C:0, GF: 0-2, N:0; Right: C:0, GF:0, N:0-2.

Of the 15 different time-domain features that were extracted, some showed higher correlations than others in different conditions of disturbances. In current measurements the features that presented the highest correlation level on all three disturbances were the “squared mean of rooted absolute amplitude (SMRA)” and the “waveform factor” (Figure 6.12). In voltage measurements higher correlations were found on the “peak mean” and “standard deviation (variance)” (Figure 6.13).

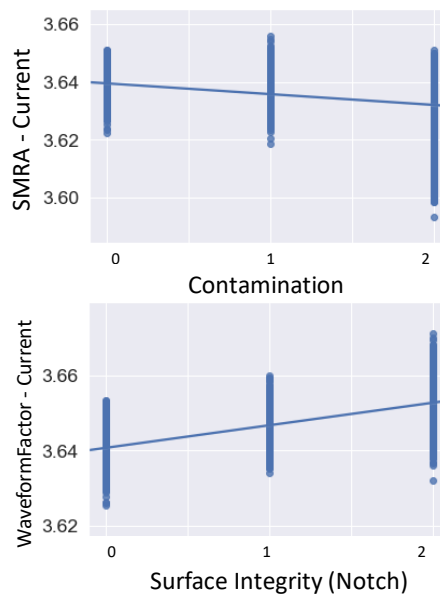


Figure 6.12 – Examples of SMRA (top) and Waveform factor (bottom) of current signals for individually induced disturbances.

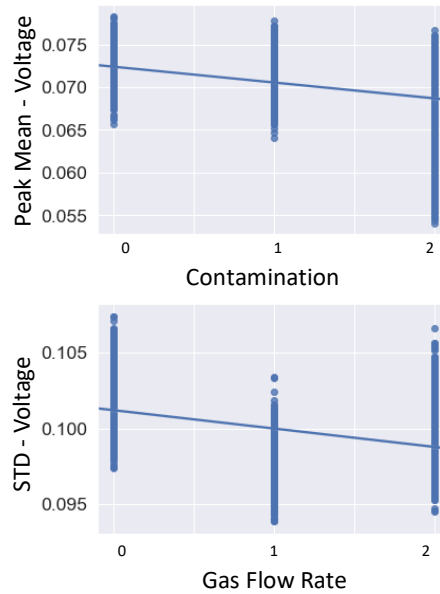


Figure 6.13 – Examples of voltage peak mean (top) and standard deviation (bottom) values for individually induced disturbances.

Detection and characterization of the disturbances become more complicated when two or three types of disturbances are simultaneously introduced to the weld. From Figure 6.11 it is extracted that voltage in welds with simultaneous contamination and gas flow rate disturbances will show sufficient correlation levels. However, when these disturbances are occurring in the presence of a notch, it is expected that the correlation in the measurements will not be so clear since the effects of the different disturbances to the measurements are opposite. As a result, when the time-domain features are collectively analyzed for all of the 27 welds simultaneously, the correlation levels are reduced compared to the individual disturbances (Figure 6.14).

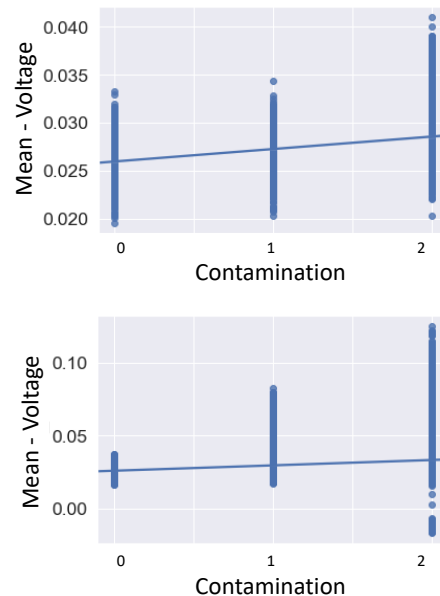


Figure 6.14 – Voltage mean value vs. contamination (Top: C:0-2, GF:0, N:0; Bottom: C:0-2, GF: 0-2, N:0-2).

6.4.3 Supervised Classification

After studying correlations, the extracted features of the segmented signals were used as inputs in training a quality prediction model based on ExtraTreesClassifier. The training was performed using

function $fit()$ by marking each set of features as “Good Weld” or “Bad Weld” based on the absence or presence of an induced disturbance. A series of good welds were fed in the model along with the 27 welds from the orthogonal array and cross-validation was used in-between the samples. The quality prediction was performed using function $predict()$, which is essentially performing a prediction for each test instance. The results as presented in Figure 6.15 reveal a prediction accuracy⁵ level of greater than 92% except from one case of a weld with no disturbance with an accuracy of 78%. Since the quality of all the welds with induced disturbances were predicted with more than 92% accuracy, the possibility that a disturbance may have indeed occurred in the outlier “good weld” further enhances the confidence to rely on the system for quality assurance.

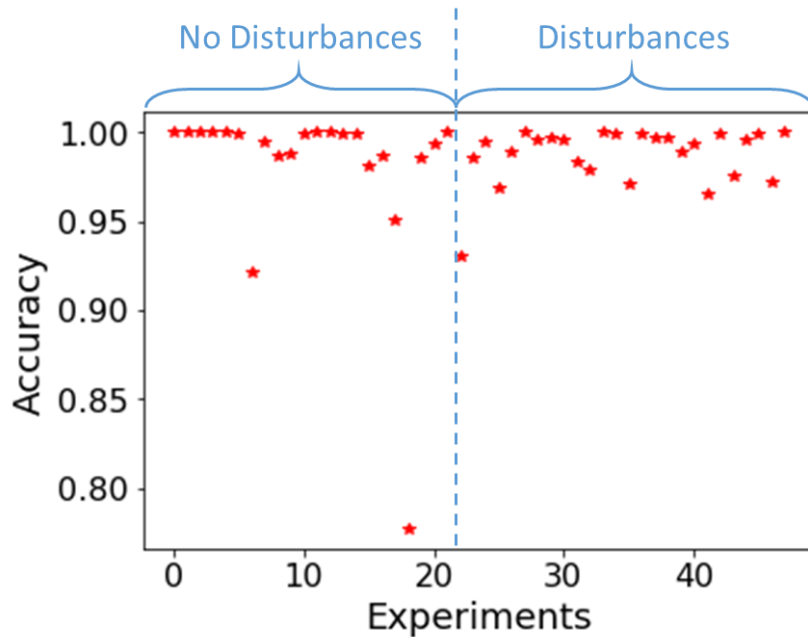


Figure 6.15 – Quality prediction accuracy on welds with and without induced disturbances.

What should be highlighted is that all the data used in the previous classification experiment were related to the same category of welds (beads-on-plates), where the electronic signal is expected to be the same. This corresponds also to the same sampling rate on data acquisition. Since the data collection was done using an oscilloscope the storage limitation allows only a specific area for capturing. If the time-scale is to be increased (for example on welds of longer seams or with slower travel speeds) the sampling rate will change to fit the allowed data range on the oscilloscope. In an attempt to investigate the same model on signals with varying sampling rate the 27 welds from the previous orthogonal array (one good weld and 26 with disturbances) were down-sampled and used in the model. As seen in Figure 6.16 the new model marks the down-sampled data as disturbances and the welds with no down-sampling as good welds. The good weld at Experiment position 0 since it is down-sampled like the faulty welds is classified 100% as a weld with disturbances resulting in 0 prediction accuracy. It is therefore concluded that welds with different sampling rates should not be used in the same model.

⁵ See Glossary.

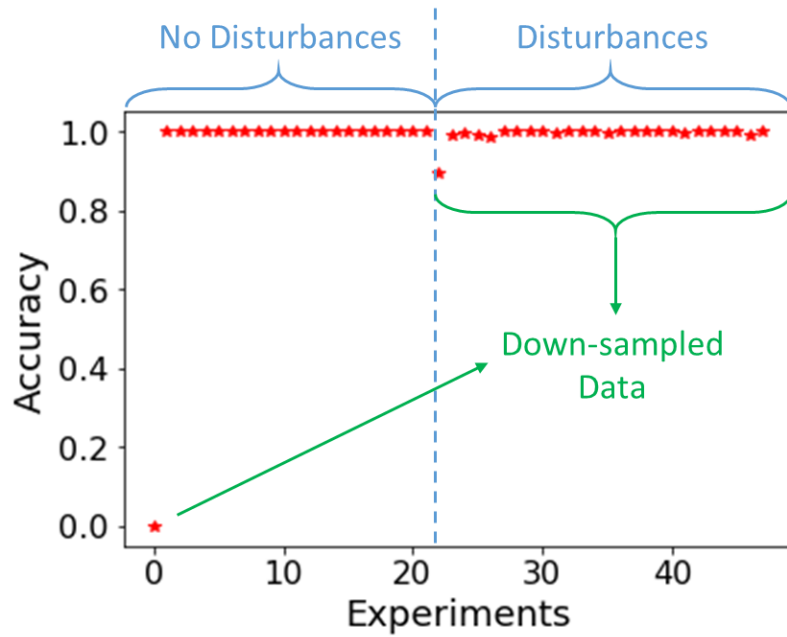


Figure 6.16 – Quality prediction accuracy with down-sampled signals. Data of different sampling rates fed in the prediction model result in false indicators of quality.

6.5 Conclusion

In this chapter the main welding process monitoring methodologies were reviewed along with their advantages and limitations. Benefiting from adaptability and ease of application arc sensing was selected as the method of choice for monitoring the ATLAS ITk weld development and further investigations were conducted on robotic arc welding. Extracted time-domain statistical features from the acquired signals were used to establish correlations with induced disturbances. The features were used as inputs in supervised learning for weld quality classification. The results revealed a disturbance prediction accuracy of greater than 92%.

7 Technology Transfer

The term “Technology Transfer” refers to the migration of results from scientific and technological research to applications in commercial markets and the wider public. This transfer can occur in a variety of ways, spanning from the actual research findings to skills and procedures, knowledge and expertise, manufacturing methods and technologies, etc. By transferring the advanced technical knowledge accessible only by a handful of experts to different “actors”, a continuation and wider application of the results to benefit society is ensured. Technology transfer allows the results from research not to be relegated to academic journals and libraries, and by guiding the scientists via structured processes and procedures (Figure 7.1), ensures the smooth transition to the market.

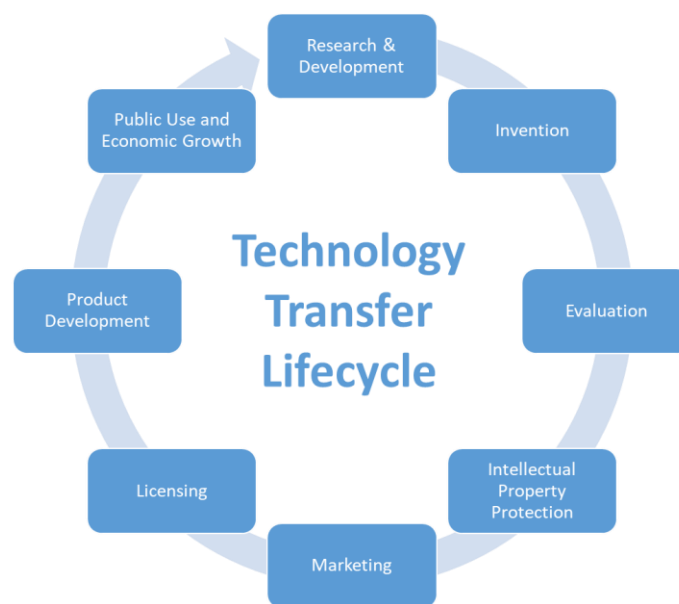


Figure 7.1 – Schematic representation of the technology transfer lifecycle.

The author’s engagement with the various aspects of research that were presented in the previous chapters allowed him to identify and take part in actions that enable wider implementations of findings and ideas. Towards this goal, three areas that will benefit from implementing welding process monitoring are covered in the following sections.

The first area is related to advancing the welding industrial process by applying the Industry 4.0 design principles and means of process monitoring to welding equipment. This set of ideas, highlighting the ongoing technological developments in the field, was part of an article presented at the Intelligent Welding Manufacturing Special Session during the 2019 IEEE 15th International Conference on Automation Science and Engineering (IEEE-CASE) [6].

The second area relates to the application of the welding monitoring setup to a different welding process and in an industry other than the ones already presented. Using the DAQ system – during the early stages of this research project – the University of Sheffield team performed welding trials at the Nuclear Advanced Manufacturing Research Centre (Nuclear AMRC) on defect detection during manual welding and tube-to-tubesheet orbital welding for nuclear power reactor manufacturing. These findings were published as a Chapter in the book “Advances in Ergonomics of Manufacturing: Managing the Enterprise of the Future” [2].

The third area for technology transfer relates to the process monitoring applications for in-space manufacturing. With welding being the first manufacturing process performed in the outer space back in 1969, the author identified the increasing need for process monitoring in space missions of the near future and presented this need at the 2019 70th annual International Astronautical Congress (IAC) [8].

7.1 Welding 4.0 – The Future of Welding

As was described in Chapter 5.3, the context of Industry 4.0 has been shaping the global manufacturing industry. Industrial applications of Cyber-Physical Systems (CPS) are enabling the digital transformation of traditional production lines, shaping the path towards the “Factory of the Future”. Organizations are transforming into truly digital enterprises where abundance of data disrupts existing practices and bring holistic changes in both vertical and horizontal chains.

7.1.1 Red Queen Hypothesis

In Lewis Carroll’s 1871 book “Through the Looking-Glass”, the Red Queen provides an explanation to Alice regarding the nature of the glass-land, which came to be known as the Red Queen Hypothesis [150]. “Now, here, you see, it takes all the running you can do, to keep in the same place” [151]. In an evolutionary race between prey and predators the ability to move fast and adapt to a dynamically changing environment ensures the survival of a species. Fast-forwarding to the 21st century, this analogy is applied in the field of manufacturing where companies that can quickly adapt to the fast-moving digital industrial ecosystem will stay competitive, whereas companies lose their customers when they can’t anticipate demands for connected products and services [152].

In the “2016 Global Industry 4.0 Survey”, responses were collected from over 2,000 participants from nine major industrial sectors and twenty four countries [153]. The results revealed that Industry 4.0 is no longer considered as a future trend revolving around a “buzzword”, but companies have moved from talk to action. About 33% of the participants classified their companies’ current level of digitization and integration as high level, whereas 72% expect a high level of digitization in five years. To achieve that level, the companies are heavily investing in Industry 4.0. As extracted from the survey, global industrial products companies are investing US\$907 billion per year through to 2020, with an average of 5% investment as a percentage of their annual revenue. 55% of the participants expect return of investment within two years. These investments are not only towards digital technologies (e.g. sensors and connectivity solutions) and software applications (e.g. modelling software, manufacturing execution systems), but also on training of their employees, since the lack of digital skills was found to be the biggest challenge in Industry 4.0 implementation.

7.1.2 Applied Industry 4.0 Principles

The welding industry is being affected by the ongoing manufacturing trends which are driven by the Red Queen Hypothesis in manufacturing. The implementation of CPS in welding power sources and related equipment enables the utilisation of industrial informatics gathered during the welding process for further development. By implementing the four basic design principles of Industry 4.0 the otherwise traditional process of welding is being transformed into the so-called Welding 4.0.

Interconnection in Welding

As seen in Section 5.3.2, the design principle of interconnection allows the extensive communication between people, equipment and products while ensuring the smooth exchange of information between them.

- Recent developments on applied interconnection in welding applications are focusing on human/machine communication that enables the remote control of welding parameters. Wireless foot-pedals and controls with operational frequencies in the industrial, scientific and medical (ISM) radio bands are already available in the market, with applications of voice-activated controls embedded on the helmet being taken into consideration [154].
- Wireless Bluetooth 4.0 communication (also in the ISM radio bands) between the helmet and the power source is also an option explored. Signals for the arc status are used to control the auto-darkening shades of the helmet's visor, ensuring the safety of the welder [155].
- Modern welding power sources are expected to have the ability to connect to computers and the internet. Subsequently, information from each welding station is provided with details of the usage, arc status and values of welding parameters, enabling remote monitoring and asset utilization management [156], [157].

Information Transparency in Welding

With the concept of digital twins and the wealth of information characterising the fourth industrial revolution, an abundance of opportunities arise for further expanding the welding process.

- Data collected from the variety of sensors involved in welding process monitoring are merged with the data collected from the power sources to create detailed performance documentation for each weld. These data, need to be securely stored with access only to respective stake-holders. Therefore not only strong foundations of digital trust are established between the manufacturer and the customer but also their reliability and reputation is ensured in case faulty products require further investigations.
- In areas where post-production testing is a requirement, the test-results can be linked and stored alongside with the collected process data.

Decentralized Decisions in Welding

The ability of cyber-physical systems to undertake decisions in a decentralized way allows greater flexibility and shifter reaction, increasing production efficiency.

- The most important feature of real-time welding process monitoring systems is their ability to detect, identify and classify disturbances, parameter variations, process interruptions and malfunctions as they occur. With decentralized decisions, modern welding systems are expected to have the authority not only to automatically readjust parameters and alter conditions but also to intervene with process interruptions when deemed necessary. To achieve such high level of automation, the monitoring systems should be equipped with advanced data analytics employing machine learning and predictive models, while maintaining fast data transfer and high processing power. As the number of monitoring parameters is increasing and the predictive models become more complex, more processing power will be required, hence the potential need for intelligent sensors with embedded processors.
- In cases where complex geometries of welded products proscribe the use of a feedback mechanism, or in cases where the system's response time forbids a Level 3' monitoring system (Section 6.1), the analyzed data can be used in post-weld evaluation to ensure the weld quality. This solution reduces the cost both in terms of time spent from waiting the results of a Non-Destructive Testing (NDT), as well as in terms of money to perform the NDT.

Technical Assistance in Welding

Robotic welding has been around from the very beginning of the third industrial revolution. Since the 1960s when industrial robots were introduced, the welding processes have grown to be the most common applications on industrial robots worldwide [158]. Apart from reducing processing time, improving productivity and obtaining high quality welds, among the benefits of the robotic welding there is also the reduction of exposure of human welders to the hazardous welding environment [159]. Risks emerging from arc radiation exposure, fumes, extreme temperatures and prolonged sitting positions have been reduced, and the concept of technical assistance has been incorporated for years in the welding industry. There are however cases where robotic welding cannot be applied, as in products with complex geometries limiting robotic movement and access. Manual welding isn't predicted to be completely replaced in the near future, raising the need for technical assistance to be provided in additional ways.

- Advances in monitoring technologies have been applied to welding wearables, attaching sensors and display screens on welding helmet. Arc sensors detect and register arc initiations and welding durations, projecting information to the welder about total arc time [154]. This development can also be used in predictive maintenance, calculating the electrode replacement based on the operational time recorded.
- Another way of visualizing information to the welder can be by applying augmented reality technologies in the welding helmet. This innovating technology will transform manual tasks and with significant options for applications in welding. Apart from the projection of welding parameters and conditions on the welder's field of view, process monitoring systems can visualize corrections to ensure quality. Vision systems and arc sensors used for torch position identification can be utilized to guide the welder towards correct positioning while infrared thermography can be utilized to project to the welder isothermal images marking potential defects.
- Under the concept of "Virtual Welding" the welding process and the welders are modelled in the virtual world. This digitization allows programmers to check the robot movement for correct torch positioning, avoiding unnecessary rejects that lead to wastes. Additionally it helps human welders in training, allowing them to practice virtual welds holding dummy welding torches, avoiding exposure to hazards and eliminating materials and consumables wastes. Both augmented reality and virtual reality training modules are already available [160], [161].
- Modern welding power sources with embedded barcode scanners allow product identification. Pre-stored welding procedure specifications are guiding the welding engineer on how to successfully deliver the weld, minimizing time in training and allowing greater adaptability with less time in workpiece transitioning [157].

7.2 Nuclear Reactor Pressure Vessels Fabrication

At the very early stages of the author's involvement with the collective research that was presented, a series of welding trials were performed at the Nuclear Advanced Manufacturing Research Centre (NAMRC) in collaboration with the Department of Physics and Astronomy of the University of Sheffield. The welding trials were aiming to demonstrate real-time process monitoring capabilities during the fabrication of critical nuclear power reactor components in order to detect flaws in weld quality that could compromise the integrity of such components.

Using a highly skilled welding engineer based at the NAMRC, manual and automated welding was performed on common tube to plate joints found in nuclear reactor pressure vessels. For the automatic orbital welding the power supply was controlled using an AMI Model 227 programmable GTAW portable pipe welding power supply designed for automatic orbital welding applications. The programming feature of this machine allowed control of both continuous or pulsed current, current amplitude, and rotation speed. During this research, the Model 96 weld head -pneumatically operated, specifically designed for single and multi-pass automatic welds- was used because of the self-supporting tube-to-tubesheet setup. The manual welding equipment used was the Miller Dynasty 350 TIG GTAW AC/DC inverter based power supply. The power source was used in conjunction with a conventional TIG welding torch and wireless foot control pedal. Using the real-time data acquisition alongside the sensing equipment that was presented in the previous sections data were recorded on a series of welds.

Automatic welds were performed on an 11-x-19 tube-to-plate worksheet found in nuclear heat exchangers using the automatic orbital welder. A series of good welds were made in accordance with British Standard 3915:1965 [162], followed by a second series of welds with deliberate induced defects (grease contamination, notches and gas perturbations). All of the weld samples have been welded using a qualified WPS designed and proprietary to the NAMRC and carried out under controlled environmental conditions.

Measurements taken from the test sample (Figure 7.2) represent the correct welding conditions with no introduced disturbances. The measurements were taken simultaneously on both voltage and current for both the power demand of the machine and the power delivered to the arc.

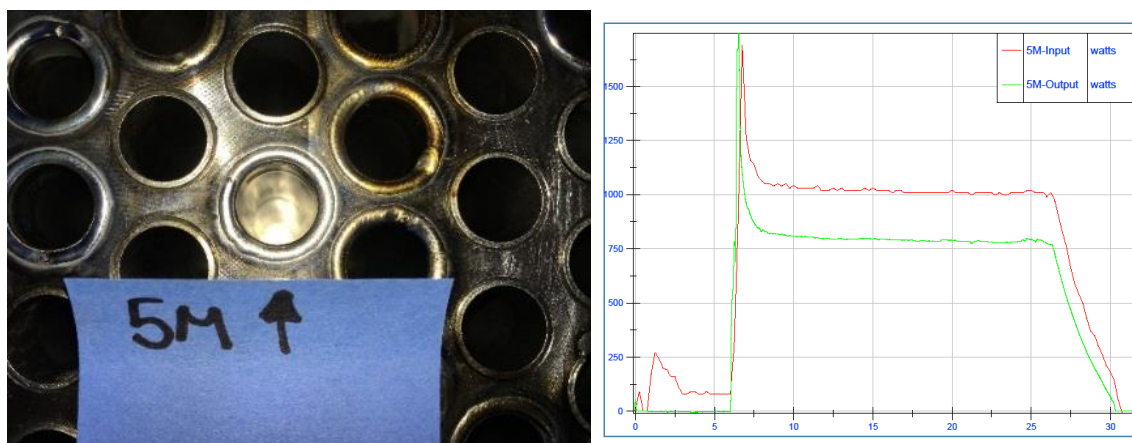


Figure 7.2 – Left: Picture of a good (no induced disturbances) tube-to-tubesheet weld of a 316L test structure representing the heat exchanger component found in a nuclear reactor construction; Right: Power demanded by welding machine (red) and power delivered to weld (green).

One notch was cut into three test samples at a fixed point creating a defective joint. Visual inspection of the completed weld shows the presence of a pinhole (or lack of fusion) at the notch location. The active power deposited on the test sample (Figure 7.3) revealed two peaks on the curve with their location representing the exact time where the electrode was travelling on top of the notch. Figure 7.3 highlights the two peaks on the power delivered to the test sample (green curve). These two peaks are less noticeable on the power demand of the welding system (red curve) because the measurement frequency of the power input is lower than the high-speed DAQ, just 4 samples/second.

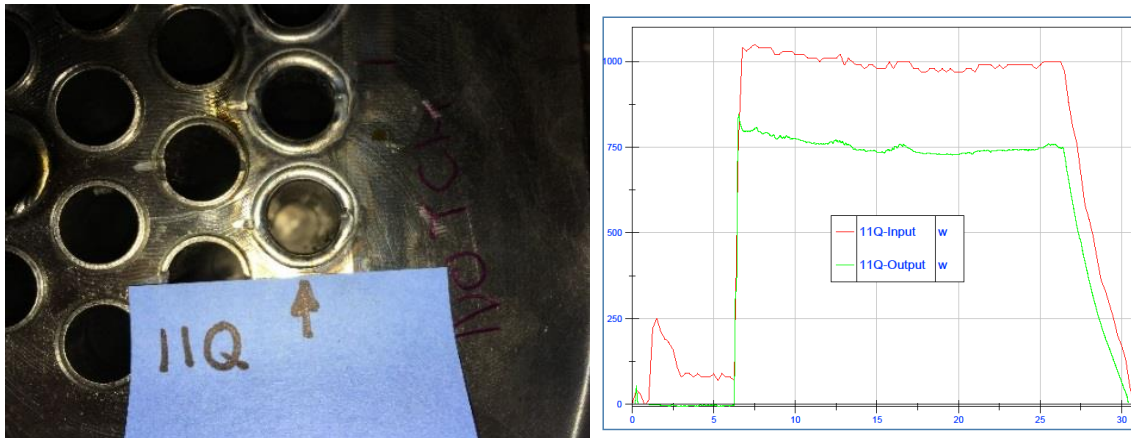


Figure 7.3 – Left: Picture of a defected (notch) tube-to-tubesheet weld of a 316L test structure representing the heat exchanger component found in a nuclear reactor construction; Right: Power demanded by welding machine (red) and power delivered to weld (green).

A small amount of grease was introduced on the surface of the welding area in order to simulate possible contamination that can occur in a workshop. Evaluating the data received from the welding of the contaminated area revealed a clear change in both, welding voltage and current that effects the arc power (Figure 7.4). Visually the test sample shows black colouring and pinholes where the grease contamination was located.

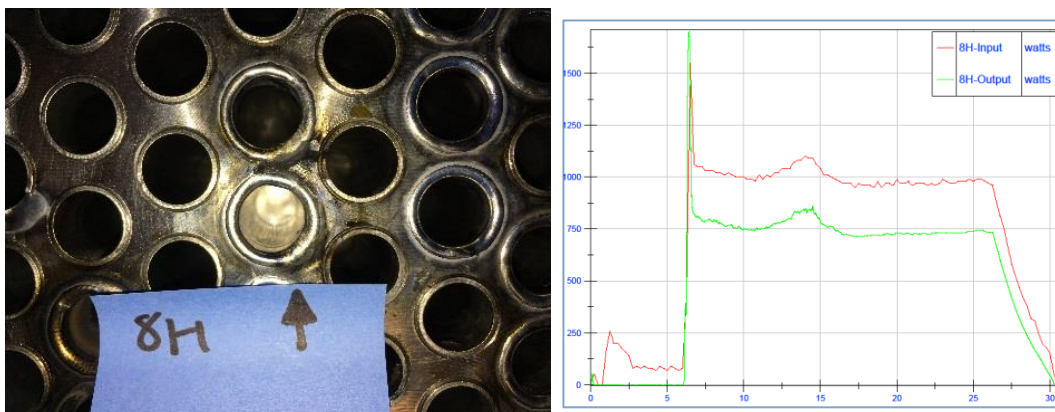


Figure 7.4 – Left: Picture of a defected (grease contamination) tube-to-tubesheet weld of a 316L test structure representing the heat exchanger component found in a nuclear reactor construction; Right: Power demanded by welding machine (red) and power delivered to weld (green).

Inert shield gas flow disturbances by introducing air were made to simulate variations that occur during welding, either by mechanical malfunction or human factors interrupting the flow. A fast time change to gas concentration was introduced five seconds after the arc strike with a short burst of compressed air. Data analysis of the welds revealed a voltage peak at the start of the arc air perturbation attributed to arc blown and subsequently larger arc length. A noise-like perturbation was also notable in the welding current measurement. As a result, the power output delivered to the sample test is higher than other variations (Figure 7.5). Visually, a bad weld, dark in colour, and pinholes are observed at the end of the weld.

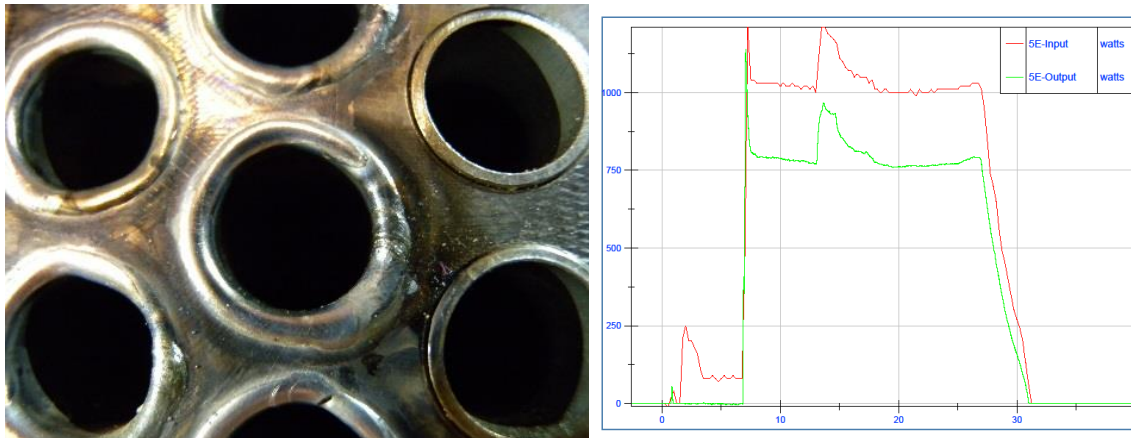


Figure 7.5 – Left: Picture of a defected (gas disturbances) tube-to-tubesheet weld of a 316L test structure representing the heat exchanger component found in a nuclear reactor construction; Right: Power demanded by welding machine (red) and power delivered to weld (green).

A series of manual welds were also performed on 316 stainless steel plates. Using the same conditions and parameters for the automatic welding described previously, the aim of the trials was to simulate errors which occur during manual welding of nuclear industry components. This would be evidenced by the data generated and used in the identification and prevention of such flaws in the final products. Simulated errors comprised of using the wrong filler wire material and surface contamination. Wrong filler wire selection occurs through poor human judgment based on accidental selection due to similar visual appearance. Surface contamination occurs in the workshop due to substances like grease or debris. The data acquired from the defective welds were compared with data acquired from identical weld produced correctly following nuclear standards.

There were no visible defects on a well prepared steel plate when using the correct filler wire. However, when using a carbon filler wire on a steel plate more power was required to obtain correct penetration or fusion (Figure 7.6).

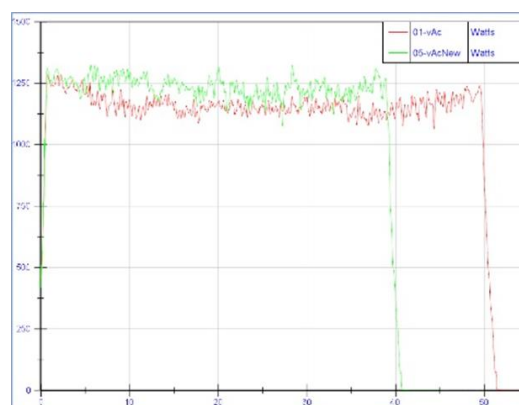


Figure 7.6 – Welding power of test sample (no contamination) using the right filler wire (red) and using a wrong filler wire (green).

When welding the contaminated steel plate using a carbon filler wire the arc power presented higher fluctuations than when using steel filler wire on a dirty material. This is attributed to the welding machine trying to maintain stable arc and power outputs which can compensate for the contamination and the wrong filler wire. Similar differences between welding speeds are witnessed when welding with the wrong filler wire (Figure 7.7). Furthermore, welding the contaminated material took approximately 35% longer than welding the non-contaminated plate.

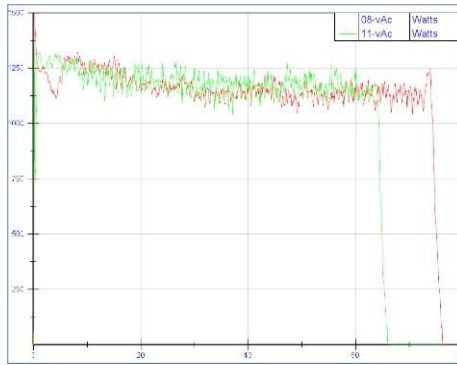


Figure 7.7 – Welding power of contaminated test sample using the right filler wire (red) and using a wrong filler wire (green).

The presented results was the first work undertaken by the University of Sheffield in transferring the monitoring methodology that was developed for the ATLAS ITk development to different industries and applications. The demonstrated ability of the system to operate on different machines and processes under varying conditions highlights the modularity and adaptability required by the industry for monitoring the arc welding processes. The work was further refined through the systematic, in-depth studies that were later performed in ARTC.

7.3 The Need for Process Monitoring in In-Space Manufacturing

Proposed scenarios of manned missions to the Moon and Mars rely on automated processes that prepare the environment prior to the humans' arrival, either by harnessing and transforming local resources (e.g. producing fuel and oxygen) or by building habitats and infrastructures. Additional to the in-situ resource utilization, long-duration space missions require astronauts to build structures and create tools and spacecraft components away from the surface of the Earth.

The status of in-space manufacturing has evolved from the first welding experiments upon Soyuz 6 in 1969, to the installation of the first 3D printer on the International Space Station (ISS) in 2014. Its descendant "Additive Manufacturing Facility" installed on ISS in 2016 has printed in-orbit more than 200 objects to date.

However, the flexibility to create critical components and spare parts on-demand raises another need. When aerospace components are manufactured on Earth, they undergo thorough examination and non-destructive testing to ensure their properties are within acceptable safety standards. These methods of quality assurance may not be an option when the components are printed in-orbit or on the surface of another celestial body, due to the lack of either human presence or specialized testing equipment. Therefore automatic process monitoring evaluation tools and analysis techniques are required, ensuring the manufacturing conditions and additional factors that contribute to the product's quality were maintained within acceptable limits throughout the production process.

The recent developments and applications of in-process metrology utilizing the IIoT in Industry 4.0 that were presented in the previous sections can pave the way to non-destructive evaluation in in-space manufacturing. To this extent, since the subject is not directly related to the present work but was inspired by the developments on welding process monitoring, the author includes in APPENDIX A a review of in-space manufacturing and highlights the need for process monitoring associated with monitoring of additive manufacturing.

8 Conclusions

8.1 Overview and Project Outcomes

The need for higher energies and higher collision rates at particle physics research pushes the boundaries of engineering to develop large-scale complex particle detectors. Their high performance hinges on silicon sensors operating in low temperature environments. To achieve the low temperatures at the new ATLAS Inner Tracker detector being developed for operation at the High-Luminosity upgrade of the Large Hadron Collider at CERN, an evaporative CO₂ cooling system will be employed. The heat accumulated in the detector is removed by coolant transported via thin titanium cooling pipes. Precision control of the heat input is required in joining these pipes, minimizing the microstructure changes and the effects on the material's properties that could imply risks to the detector's operation.

Gas Tungsten Arc Welding is a fusion welding process where an arc is formed between a non-consumable electrode and the workpiece. By using pulsing modulation in the welding currents greater control of the heat delivered to the weld is achieved. Low frequency pulsing enables thermal control and low heat accumulation whereas high-frequency pulsing affects the dynamics of the plasma region and agitates the melt pool. By applying pulsing currents in orbital welding the joining of the thin titanium cooling tubes for the ATLAS ITk detector has been demonstrated.

The low heat input benefits of pulsing welding currents are also utilised in aerospace remanufacturing. Wire arc additive manufacturing is employed to remanufacture aerospace components providing successive material deposition on a layer-upon-layer manner. By using combinations of thermal and high frequency pulsing it has been demonstrated that control over bead geometries and heat affected zones is possible. This provides the ability to perform on the same manufacturing setup root passes with wide beads of high penetration depth and built-up passes with lower penetration depth and higher height-to-width ratios. During these investigations, metallographic observations revealed evidence of dynamic turbulence formations within the agitated melt-pool during welding utilising pulsing currents.

Further expanding on aerospace remanufacturing, during the regeneration process of aeroengine compressor blades, the stage of tip-repairing depends on material deposition by means of welding processes. Following design principles set by the Industry 4.0 context of the fourth industrial revolution, a bespoke robotic system was developed aiming to automate the process and increase the yield of successful blades repaired with high frequency pulsing currents. Modularity and interoperability allowed flexibility and adaptability of the process while inline metrology and non-destructive evaluation generate a wealth of information further expanding the shift towards the factory of the future and digital manufacturing.

In order to ensure the quality of a weld, monitoring methodologies are implemented overseeing the welding process. Monitoring is performed to ensure the guidelines provided by the welding procedure specifications are followed throughout the process and the welding conditions are maintained within acceptable limits. A high-speed data acquisition system was developed by the University of Sheffield to perform current and voltage measurements during the welding process. The acquired data allow assessment of the welding quality to be performed by data comparison between faulty welds and welds of good quality. The system was successfully demonstrated in detecting failures in welds on the

ATLAS ITk cooling pipes due to misalignments. Further implementation of the system in robotic welding revealed measurements in correlation with welding condition disturbances such as surface contamination and gas perturbations. By utilising time-domain features extracted from the recorded signals, supervised machine learning was enabled, classifying welds with induced disturbances with an accuracy higher than 92%.

Under the context of technology transfer, welding process monitoring was implemented for disturbances detection in tube-to-tubesheet automatic welding and manual welding in nuclear engineering. Inspired by the outcomes of this project further implementations were identified in the area of Welding 4.0, guiding the future of the welding industry. Additionally, the need for process monitoring in in-space manufacturing was identified, with potentials of benefiting from the recent developments of in-line metrology and additive manufacturing quality assurance.

8.2 Outcome of Industry-Academia collaboration

The presented work is partially a result of a collaboration between the Department of Physics and Astronomy of the University of Sheffield, UK and the Agency for Science, Technology and Research (A*STAR) Singapore through its Advanced Remanufacturing and Technology Centre (ARTC). Under the A*STAR Research Attachment Programme (ARAP) students from member universities are undertaking extensive placements in A*STAR Research Institutes.

The benefits to the researcher of this specific collaboration was the transition from an academic research environment to an industry-driven workplace. During the secondment, trainings are undertaken focusing on industry-specific needs and actively applied in ongoing projects. Involvement in a variety of projects enhances the learning through experience process, builds “hands-on” experience and provides an extensive inventory of skills and expertise that enables an easier transition in the industrial workforce upon the project completion.

While there are many similarities in conducting research in academia and industry, what is different is learning to follow a business way of thinking. The researcher mindset shifts and expands from doing research simply for knowledge expansion to finding practical implementations of research findings by providing solutions to problems or improving existing processes. Similarly, practicality is of essence and terms like cost justification and return on investment are more frequently used.

Another difference highlighted is the confidentiality that needs to be followed when presenting research findings that resulted from industry-related projects. Non-disclosure agreements, intellectual property of the hosting organisation or clients and potential commercialization of research solutions can often be barriers in open communication, publication and outreach.

Of additional benefit from the author’s personal point of view is the broad cultural and geographical exposure as a side effect of the intercontinental transfer. Apart from building an extensive professional network it also expands one’s horizons, perception and character.

8.3 Future Work

“The more I learn, the less I realize I know” is a phrase that is often attributed to the Greek philosopher Socrates. Similarly in scientific research, answers to questions reveal more questions that need answers. As some of the work presented in this thesis was of exploratory nature the author identifies and highlights potential future work that can be undertaken in line with the research outcomes:

- *Wire Arc Additive Manufacturing* – Utilising the benefits that result from dual pulsing, wire arc additive manufacturing process can be further expanded to have varying geometries close to near net shape with adaptive control input following the changes in the heat transfer mechanisms as deposited material increases in height.
- *Weld pool dynamics identification and modelling* – The weld bead shapes that were identified while utilising high and low frequency pulsing require further investigation to identify the underlying mechanisms that generate the flows resulting in the witnessed evidence of turbulences.
- *Weld microstructure and heat affected zone properties* – The mechanisms that truncates columnar growth to equiaxed grains in high frequency pulsing can be further investigated along with its effects on shaping the heat affected zone.
- *Design of Experiments* – A new design of experiments can be investigated that can solve the problem of performing process optimisation in a setup that utilises different current modes. The rationale behind this proposal would be to find the optimum welding procedure specifications in a new workpiece without having to perform separate experiments for each current mode.
- *Weld quality prediction* – The monitoring classification algorithm used in the present work underperforms when signals of different sampling rates are used simultaneously. Further research could establish a system that can exploit learning from various signals allowing a wealth of information to be built and therefore better prediction accuracy.
- *Predictive maintenance* – The tungsten electrode degradation due to oxidation requires frequent changes in order to avoid defect formation. Possible correlations of signals recorded via process monitoring system with the electrode degradation could lead to potential maintenance prediction. This can be further explored by comparing the signals from electric measurements with quantitative spectroscopy.

Publications

Author's Publications to Date

M. Benakis, D. Costanzo, and A. Patran, "Current mode effects on weld bead geometry and heat affected zone in pulsed wire arc additive manufacturing of Ti-6-4 and Inconel 718," *J. Manuf. Process.*, vol. 60, no. December 2020, pp. 61–74, Dec. 2020, doi: 10.1016/j.jmapro.2020.10.018.

M. Benakis, "The need for process monitoring in in-space manufacturing," in *Proceedings of the International Astronautical Congress, IAC, 2019, Oct. 2019.*

M. Benakis, C. Du, A. Patran, and R. French, "Welding process monitoring applications and industry 4.0," *IEEE Int. Conf. Autom. Sci. Eng.*, vol. 2019-Augus, 1755–1760, Aug. 2019, doi: 10.1109/COASE.2019.8843319.

R. French, **M. Benakis**, and H. Marin-Reyes, "Process monitoring and industrial informatics for online optimization of Welding Procedure Specifications (WPS) in Gas Tungsten Arc Welding (GTAW) – Industry 4.0 for robotic additive remanufacturing of aeroengine components," in *ICARM 2018 – 2018 3rd IEEE International Conference on Advanced Robotics and Mechatronics, 2019, 812–817*, doi: 10.1109/ICARM.2018.8610808.

R. French, H. Marin-Reyes, and **M. Benakis**, "Transfer Analysis of Human Engineering Skills for Adaptive Robotic Additive Manufacturing in the Aerospace Repair and Overhaul Industry", vol. 793. 2019.

R. French, **M. Benakis**, and H. Marin-Reyes, "Intelligent sensing for robotic re-manufacturing in aerospace – An industry 4.0 design based prototype," in *Proceedings – 2017 IEEE 5th International Symposium on Robotics and Intelligent Sensors, IRIS 2017, 2018, vol. 2018-Janua, pp. 272–277*, doi: 10.1109/IRIS.2017.8250134.

R. French, H. Marin-Reyes, and **M. Benakis**, "Advanced real-time weld monitoring evaluation demonstrated with comparisons of manual and robotic TIG welding used in critical nuclear industry fabrication", vol. 606. 2018.

R. French, H. Marin-Reyes, and **M. Benakis**, "Real-time welding evaluation system assessment using the TIG orbital welding process on ultra-thin wall tube joints in titanium & stainless steel," in *70th IIW Annual Assembly and International Conference, 2017.*

Glossary of Terms, Abbreviations and Acronyms

A*STAR	Agency for Science, Technology and Research
ALICE	A Large Ion Collider Experiment
AM	Additive Manufacturing
AMRC	Advanced Manufacturing Research Centre
AMS	Aerospace Material Specifications
ARTC	Advanced Remanufacturing and Technology Centre
ASICs	Application-Specific Integrated Circuits
ATLAS	A Toroidal LHC ApparatuS – Large general-purpose particle detector experiment
Buy-to-Fly Ratio	The weight of the raw material purchased to make an aerospace component, compared to the weight of the final part.
CCD	Charge-Coupled Device
CCPS	Constant-Current Power Source
CERN	European Organization for Nuclear Research
CFRP	Carbon Fibre Reinforced Polymers
CMOS	Complementary Metal–Oxide–Semiconductor
CMS	Compact Muon Solenoid experiment
CMT	Cold Metal Transfer
CPS	Cyber-Physical Systems
CT	Computed Tomography
DAQ	Data Acquisition
DC	Direct Current
DOE	Design Of Experiments
EB	Electron-Beam
EDM	Electric Discharge Machining
EMAT	Electro-Magnetic Acoustic Transducer
End Effector	The device at the end of a robotic arm. For welding robots the end effector is the welding torch/gun.
ESIM	Enabling Sciences for Intelligent Manufacturing
FE	Front-End
FPGA	Field-Programmable Gate Array
GMAW	Gas Metal Arc Welding
GTAW	Gas Tungsten Arc Welding
GTCAW	Gas Tungsten Constricted Arc Welding
GUI	Graphical User Interface
HAZ	Heat Affected Zone
HL-LHC	High-Luminosity Large Hadron Collider
HMS	Heat Management System
IBL	ATLAS Insertable B-Layer
IIoT	Industrial Internet of Things
IN718	Inconel 718
IoT	Internet of Things
IR	Infrared
IT	Information Technology
ITk	ATLAS Inner Tracker
LHC	Large Hadron Collider
LHCb	Large Hadron Collider beauty experiment

Luminosity	A luminosity L provides a reaction rate of $\sigma \cdot L$ per second for a process of cross-section σ (in $\text{cm}^2 \text{s}^{-1}$)
MIG	Metal Inert Gas
MRO	Maintenance Repair and Overhaul
NAMRC	Nuclear Advanced Manufacturing Research Centre
NDE	Non-Destructive Evaluation
NDT	Non-Destructive Testing
OD	Outer Diameter
PAW	Plasma Arc Welding
Prediction Accuracy	Presented as the fraction of correct predictions (All correct =1, All incorrect = 0).
QA	Quality Assurance
QC	Quality Control
QR	Quick Response
RFID	Radio-Frequency Identification
SAW	Submerged Arc Welding
SCT	Semi-Conductor Tracker
SMAW	Shielded Manual Arc Welding
SMD	Shape Metal Deposition
SRXRD	Spatially-Resolved X-ray Diffraction
SS	Stainless Steel
SS316L	Stainless Steel 316 Low Carbon
TBO	Time Between Overhauls
Ti CP2	Titanium Commercially Pure Grade 2
Ti-6-4	Titanium Alloy (Ti-6Al-4V)
TIG	Tungsten Inert Gas
UHP	Ultra High Purity, closed chamber welding head
UT	Ultrasonic Testing
VBCie	VBC Instrument Engineering Ltd
VCR Connector	Fittings for metal-to-metal seal, providing leak-tight service from vacuum to positive pressure.
WAAM	Wire Arc Additive Manufacturing
WPS	Welding Procedure Specifications

References

- [1] R. French, H. Marin-Reyes, and M. Benakis, "Real-time welding evaluation system assessment using the TIG orbital welding process on ultra-thin wall tube joints in titanium & stainless steel," in *70th IIW Annual Assembly and International Conference*, 2017.
- [2] R. French, H. Marin-Reyes, and M. Benakis, *Advanced real-time weld monitoring evaluation demonstrated with comparisons of manual and robotic TIG welding used in critical nuclear industry fabrication*, vol. 606. 2018.
- [3] R. French, M. Benakis, and H. Marin-Reyes, "Intelligent sensing for robotic re-manufacturing in aerospace - An industry 4.0 design based prototype," in *Proceedings - 2017 IEEE 5th International Symposium on Robotics and Intelligent Sensors, IRIS 2017*, 2018, vol. 2018-Janua, pp. 272–277, doi: 10.1109/IRIS.2017.8250134.
- [4] R. French, M. Benakis, and H. Marin-Reyes, "Process monitoring and industrial informatics for online optimization of Welding Procedure Specifications (WPS) in Gas Tungsten Arc Welding (GTAW) - Industry 4.0 for robotic additive remanufacturing of aeroengine components," in *ICARM 2018 - 2018 3rd International Conference on Advanced Robotics and Mechatronics*, 2019, pp. 812–817, doi: 10.1109/ICARM.2018.8610808.
- [5] R. French, H. Marin-Reyes, and M. Benakis, *Transfer Analysis of Human Engineering Skills for Adaptive Robotic Additive Manufacturing in the Aerospace Repair and Overhaul Industry*, vol. 793. 2019.
- [6] M. Benakis, C. Du, A. Patran, and R. French, "Welding process monitoring applications and industry 4.0," *IEEE Int. Conf. Autom. Sci. Eng.*, vol. 2019-Augus, pp. 1755–1760, Aug. 2019, doi: 10.1109/COASE.2019.8843319.
- [7] M. Benakis, D. Costanzo, and A. Patran, "Current mode effects on weld bead geometry and heat affected zone in pulsed wire arc additive manufacturing of Ti-6-4 and Inconel 718," *J. Manuf. Process.*, vol. 60, no. December 2020, pp. 61–74, Dec. 2020, doi: 10.1016/j.jmapro.2020.10.018.
- [8] M. Benakis, "The need for process monitoring in in-space manufacturing," in *Proceedings of the International Astronautical Congress, IAC*, 2019, vol. 2019-Octob.
- [9] D. H. Perkins, *Introduction to High Energy Physics, 4th Edition Introduction to High Energy Physics*, 4th Editio. Cambridge University Press, 2000.
- [10] X. Ρούτση Ευαγγελίδη, *Εισαγωγή στη Φυσική Υψηλών Ενέργειών*. Xanthi, Greece: Democritus University of Thrace, 2006.
- [11] A. ATLAS Collaboration, "The ATLAS experiment at the CERN large hadron collider," *J. Instrum.*, vol. 3, p. S08003, 2008.
- [12] A. ATLAS Collaboration, "Technical Design Report for the ATLAS Inner Tracker Strip Detector," *Cern. ; Atlas-Tdr-025*, vol. I, no. April, 2017.
- [13] A. ATLAS Collaboration, "Technical Design Report for the ATLAS Inner Tracker Pixel Detector," *Atlas-Tdr-030*, 2017.
- [14] "International Titanium Association (ITA)." [Online]. Available: www.titanium.org. [Accessed: 09-Dec-2019].

- [15] R. R. Boyer, "Titanium for aerospace: Rationale and applications," *Adv. Perform. Mater.*, vol. 2, no. 4, pp. 349–368, 1995, doi: 10.1007/BF00705316.
- [16] R. R. Boyer, "An overview on the use of titanium in the aerospace industry," *Mater. Sci. Eng. A*, vol. 213, no. 1–2, pp. 103–114, 1996, doi: 10.1016/0921-5093(96)10233-1.
- [17] S. Seong, O. Younossi, B. Goldsmith, T. Lang, and M. Neumann, *Titanium: Industrial Base, Price Trends, and Technology Initiatives*. 2018.
- [18] R. E. Crandall, "Where Will Additive Manufacturing Take Us ?," *APICS*, 2013. [Online]. Available: <https://www.apics.org/apics-for-individuals/apics-magazine-home/magazine-detail-page/2013/01/28/where-will-additive-manufacturing-take-us->. [Accessed: 16-Aug-2020].
- [19] B. A. Szost *et al.*, "A comparative study of additive manufacturing techniques: Residual stress and microstructural analysis of CLAD and WAAM printed Ti-6Al-4V components," *Mater. Des.*, vol. 89, pp. 559–567, Jan. 2016, doi: 10.1016/j.matdes.2015.09.115.
- [20] B. Barroqueiro, A. Andrade-Campos, R. A. F. Valente, and V. Neto, "Metal additive manufacturing cycle in aerospace industry: A comprehensive review," *J. Manuf. Mater. Process.*, vol. 3, no. 3, pp. 1–21, 2019, doi: 10.3390/jmmp3030052.
- [21] "SmarTech Analysis: Opportunities in Additive Manufacturing for Civil Aviation Parts Production, 2019-2029," 2019.
- [22] G. J. Schiller, "Additive manufacturing for Aerospace," *IEEE Aerosp. Conf. Proc.*, vol. 2015-June, 2015, doi: 10.1109/AERO.2015.7118958.
- [23] L. Nickels, "AM and aerospace: An ideal combination," *Met. Powder Rep.*, vol. 70, no. 6, pp. 300–303, 2015, doi: 10.1016/j.mprp.2015.06.005.
- [24] M. Attaran, "The rise of 3-D printing: The advantages of additive manufacturing over traditional manufacturing," *Bus. Horiz.*, vol. 60, no. 5, pp. 677–688, 2017, doi: 10.1016/j.bushor.2017.05.011.
- [25] T. Wohlers, "Making products by using: Additive manufacturing," *Manuf. Eng.*, vol. 146, no. 4, pp. 70–77, 2011.
- [26] D. Van, G. P. Dinda, J. Park, J. Mazumder, and S. H. Lee, "Enhancing hardness of Inconel 718 deposits using the aging effects of cold metal transfer-based additive manufacturing," *Mater. Sci. Eng. A*, vol. 776, no. January, p. 139005, 2020, doi: 10.1016/j.msea.2020.139005.
- [27] B. Denkena, V. Boess, D. Nesper, F. Floeter, and F. Rust, "Engine blade regeneration: a literature review on common technologies in terms of machining," *Int. J. Adv. Manuf. Technol.*, vol. 81, no. 5–8, pp. 917–924, 2015, doi: 10.1007/s00170-015-7256-2.
- [28] O. Yilmaz, N. Gindy, and J. Gao, "A repair and overhaul methodology for aeroengine components," *Robot. Comput. Integr. Manuf.*, vol. 26, no. 2, pp. 190–201, 2010, doi: 10.1016/j.rcim.2009.07.001.
- [29] Pratt & Whitney Customer Service, "Fashionably late doesn't apply to your engine TBO," 2018. [Online]. Available: <https://www.pwc.ca/en/airtime-blog/articles/technical-tips/fashionably-late-does-not-apply-to-your-engine-tbo---here-is-why>. [Accessed: 20-Dec-2019].

- [30] J. Geng, X. Tian, M. Bai, X. Jia, and X. Liu, "A design method for three-dimensional maintenance, repair and overhaul job card of complex products," *Comput. Ind.*, vol. 65, no. 1, pp. 200–209, 2014, doi: 10.1016/j.compind.2013.08.008.
- [31] Z. Zhang, G. Liu, Z. Jiang, and Y. Chen, "A cloud-based framework for lean maintenance, repair, and overhaul of complex equipment," *J. Manuf. Sci. Eng. Trans. ASME*, vol. 137, no. 4, pp. 1–11, 2015, doi: 10.1115/1.4030619.
- [32] E. Uhlmann, M. Bilz, and J. Baumgarten, "MRO - Challenge and chance for sustainable enterprises," *Procedia CIRP*, vol. 11, pp. 239–244, 2013, doi: 10.1016/j.procir.2013.07.036.
- [33] T. J. Carter, "Common failures in gas turbine blades," *Eng. Fail. Anal.*, vol. 12, no. 2, pp. 237–247, 2005, doi: 10.1016/j.engfailanal.2004.07.004.
- [34] Rolls-Royce Plc, "Compressor blades repair and overhaul (Internal Report)," 2002.
- [35] "Private Communication, January 25th, 2018".
- [36] R. C. Creese, *Introduction to manufacturing processes and materials*. 2017.
- [37] British Standards Institution, "BSI Standards Publication: Welding terms and symbols - BS 499-1:2009," 2009.
- [38] V. Merchant, "Laser beam welding," in *New Developments in Advanced Welding*, 2005, pp. 81–112.
- [39] S. C. A. Alfaro, "Sensors for quality control in welding," *Soldag. Inspeção*, vol. 17, no. 3, pp. 192–200, 2012, doi: 10.1590/s0104-92242012000300003.
- [40] P. Huot, "The Basics of Weld and Process Monitoring," *Quality*, vol. 54, no. 4, pp. 6–8, 2015.
- [41] J. Beddoes and M. J. Bibby, *Principles of Metal Manufacturing Processes*. Elsevier ButterNorth-Heinemann, 2003.
- [42] M. Tanaka, H. Terasaki, M. Ushio, and J. J. Lowke, "A unified numerical modeling of stationary tungsten-inert-gas welding process," *Metall. Mater. Trans. A Phys. Metall. Mater. Sci.*, vol. 33, no. 7, pp. 2043–2052, 2002, doi: 10.1007/s11661-002-0036-2.
- [43] L. Sansonnens, J. Haidar, and J. J. Lowke, "Prediction of properties of free burning arcs including effects of ambipolar diffusion," *J. Phys. D. Appl. Phys.*, vol. 33, no. 2, pp. 148–157, 2000, doi: 10.1088/0022-3727/33/2/309.
- [44] M. Yang, B. Qi, B. Cong, F. Liu, Z. Yang, and P. K. Chu, "Study on electromagnetic force in Arc plasma with UHFP-GTAW of Ti-6Al-4V," *IEEE Trans. Plasma Sci.*, vol. 41, no. 9, pp. 2561–2568, 2013, doi: 10.1109/TPS.2013.2274810.
- [45] M. Tanaka, "An introduction to physical phenomena in arc welding processes," *Weld. Int.*, vol. 18, no. 11, pp. 845–851, 2004, doi: 10.1533/wint.2004.3342.
- [46] K. C. Mills, B. J. Keene, R. F. Brooks, and A. Shirali, "Marangoni effects in welding," *Philos. Trans. R. Soc. A Math. Phys. Eng. Sci.*, vol. 356, no. 1739, pp. 911–925, 1998, doi: 10.1098/rsta.1998.0196.
- [47] B. J. Keene, K. C. Mills, J. W. Bryant, and E. D. Hondros, "Effects of interaction between surface active elements on the surface tension of iron," *Can. Metall. Q.*, vol. 21, no. 4, pp. 393–403, 1982, doi: 10.1179/cm.1982.21.4.393.

- [48] J. Norrish, *Advanced Welding Processes*. Woodhead Publishing Limited, 2006.
- [49] P. K. Ghosh, *Pulse Current Gas Metal Arc Welding*. Springer Singapore, 2017.
- [50] S. J. A, *Pulsed Arc Welding*. Abington Publishing, 1990.
- [51] W. Lucas, *TIG and Plasma welding*. 1990.
- [52] Q. Wu, Z. Ma, G. Chen, C. Liu, D. Ma, and S. Ma, "Obtaining fine microstructure and unsupported overhangs by low heat input pulse arc additive manufacturing," *J. Manuf. Process.*, vol. 27, pp. 198–206, 2017, doi: 10.1016/j.jmapro.2017.05.004.
- [53] N. Ahmed, "Direct metal fabrication in rapid prototyping: A review," *J. Manuf. Process.*, vol. 42, no. May, pp. 167–191, 2019, doi: 10.1016/j.jmapro.2019.05.001.
- [54] K. Pal and S. K. Pal, "Effect of pulse parameters on weld quality in pulsed gas metal arc welding: A review," *J. Mater. Eng. Perform.*, vol. 20, no. 6, pp. 918–931, 2011, doi: 10.1007/s11665-010-9717-y.
- [55] B. J. Qi, M. X. Yang, B. Q. Cong, and F. J. Liu, "The effect of arc behavior on weld geometry by high-frequency pulse GTAW process with 0Cr18Ni9Ti stainless steel," *Int. J. Adv. Manuf. Technol.*, vol. 66, no. 9–12, pp. 1545–1553, 2013, doi: 10.1007/s00170-012-4438-z.
- [56] M. Yang, L. Li, B. Qi, and H. Zheng, "Arc force and shapes with high-frequency pulsed-arc welding," *Sci. Technol. Weld. Join.*, vol. 22, no. 7, pp. 580–586, 2017, doi: 10.1080/13621718.2016.1277625.
- [57] E. G. Cook and H. E. D. E. H. Eassa, "The Effect of High-Frequency Pulsing of a Welding Arc," *IEEE Trans. Ind. Appl.*, vol. IA-21, no. 5, pp. 1294–1299, 1985, doi: 10.1109/TIA.1985.349557.
- [58] M. Yang, H. Zheng, and L. Li, "Arc shape characteristics with ultra-high-frequency pulsed arc welding," *Appl. Sci.*, vol. 7, no. 1, 2017, doi: 10.3390/app7010045.
- [59] Y. M. Zhang, C. Pan, and A. T. Male, "Solidification behavior of Al-Mg aluminum alloy using double-sided arc welding process," *J. Mater. Sci. Lett.*, vol. 19, no. 10, pp. 831–833, 2000, doi: 10.1023/A:1006764826566.
- [60] W. Kurz, C. Bezençon, and M. Gäumann, "Columnar to equiaxed transition in solidification processing," *Sci. Technol. Adv. Mater.*, vol. 2, no. 1, pp. 185–191, 2001, doi: 10.1016/S1468-6996(01)00047-X.
- [61] S. A. David and J. M. Vitek, "Correlation between solidification parameters and weld microstructures," *Int. Mater. Rev.*, vol. 34, no. 1, pp. 213–245, 1989, doi: 10.1179/imr.1989.34.1.213.
- [62] P. W. Muncaster, "Practical TIG (GTA) welding," p. 131, 1991.
- [63] P. D. Zhemanyuk, I. A. Petrik, and S. L. Chigileychik, "Using orbital welding in the manufacture and repair of thin wall pipelines," *Weld. Int.*, vol. 30, no. 8, pp. 649–652, 2016, doi: 10.1080/09507116.2016.1140424.
- [64] W. C. for M. J. T. Twi, "Guide to best practice, 'WELDING TITANIUM', A DESIGNERS AND USERS HANDBOOK," p. 5,20,24, 1999.
- [65] A. C. DAVIES, *The science and practice of welding. Volume 2 - Practice of welding*. 1993.

- [66] E. J. Lima, G. C. F. Torres, I. Felizardo, F. A. Ramalho Filho, and A. Q. Bracarense, "Development of a robot for orbital welding," *Ind. Rob.*, vol. 32, no. 4, pp. 321–325, 2005, doi: 10.1108/01439910510600182.
- [67] VBCie, "InterPulse 50 Automatic Welder and Welding Head - Operating Instructions Manual." VBC Instrument Engineering.
- [68] L. Cooper *et al.*, "In situ micro gas tungsten constricted arc welding of ultra-thin walled 2.275 mm outer diameter grade 2 commercially pure titanium tubing," *J. Instrum.*, vol. 15, no. 6, 2020, doi: 10.1088/1748-0221/15/06/P06022.
- [69] M. R. Johnson and I. P. McCarthy, "Product recovery decisions within the context of Extended Producer Responsibility," *J. Eng. Technol. Manag. - JET-M*, vol. 34, pp. 9–28, 2014, doi: 10.1016/j.jengtecman.2013.11.002.
- [70] National Research Council, Committee on Space-Based Additive Manufacturing, Aeronautics and Space Engineering Board, National Materials and Manufacturing Board, and Division on Engineering and Physical Sciences, *3D Printing in Space*. 2014.
- [71] S. M. Yusuf, S. Cutler, and N. Gao, "Review: The impact of metal additive manufacturing on the aerospace industry," *Metals (Basel)*, vol. 9, no. 12, 2019, doi: 10.3390/met9121286.
- [72] W. Jin, C. Zhang, S. Jin, Y. Tian, D. Wellmann, and W. Liu, "Wire Arc Additive Manufacturing of Stainless Steels: A Review," *Appl. Sci.*, vol. 10, no. 5, p. 1563, 2020, doi: 10.3390/app10051563.
- [73] C. R. Cunningham, J. M. Flynn, A. Shokrani, V. Dhokia, and S. T. Newman, "Invited review article: Strategies and processes for high quality wire arc additive manufacturing," *Addit. Manuf.*, vol. 22, no. June, pp. 672–686, 2018, doi: 10.1016/j.addma.2018.06.020.
- [74] F. Li, S. Chen, Z. Wu, and Z. Yan, "Adaptive process control of wire and arc additive manufacturing for fabricating complex-shaped components," *Int. J. Adv. Manuf. Technol.*, vol. 96, no. 1–4, pp. 871–879, 2018, doi: 10.1007/s00170-018-1590-0.
- [75] B. Wu *et al.*, "A review of the wire arc additive manufacturing of metals: properties, defects and quality improvement," *Journal of Manufacturing Processes*, vol. 35. Elsevier Ltd, pp. 127–139, 01-Oct-2018, doi: 10.1016/j.jmapro.2018.08.001.
- [76] F. Xu *et al.*, "Realisation of a multi-sensor framework for process monitoring of the wire arc additive manufacturing in producing Ti-6Al-4V parts," *Int. J. Comput. Integr. Manuf.*, vol. 31, no. 8, pp. 785–798, 2018, doi: 10.1080/0951192X.2018.1466395.
- [77] Y. M. Zhang, Y. Chen, P. Li, and A. T. Male, "Weld deposition-based rapid prototyping: A preliminary study," *J. Mater. Process. Technol.*, vol. 135, no. 2-3 SPEC., pp. 347–357, 2003, doi: 10.1016/S0924-0136(02)00867-1.
- [78] S. Selvi, A. Vishvakshan, and E. Rajasekar, "Cold metal transfer (CMT) technology - An overview," *Def. Technol.*, vol. 14, no. 1, pp. 28–44, 2018, doi: 10.1016/j.dt.2017.08.002.
- [79] S. W. Williams, F. Martina, A. C. Addison, J. Ding, G. Pardal, and P. Colegrove, "Wire + Arc additive manufacturing," *Mater. Sci. Technol. (United Kingdom)*, vol. 32, no. 7, pp. 641–647, 2016, doi: 10.1179/1743284715Y.0000000073.
- [80] P. K. Baghel and D. S. Nagesh, "Pulse TIG welding: Process, Automation and Control," *J. Weld. Join.*, vol. 35, no. 1, pp. 43–48, 2017, doi: 10.5781/jwj.2017.35.1.43.

- [81] D. Ding, Z. Pan, D. Cuiuri, and H. Li, "A multi-bead overlapping model for robotic wire and arc additive manufacturing (WAAM)," *Robot. Comput. Integr. Manuf.*, vol. 31, pp. 101–110, 2015, doi: 10.1016/j.rcim.2014.08.008.
- [82] H. C. Chen, A. J. Pinkerton, and L. Li, "Fibre laser welding of dissimilar alloys of Ti-6Al-4V and Inconel 718 for aerospace applications," *Int. J. Adv. Manuf. Technol.*, vol. 52, no. 9–12, pp. 977–987, 2011, doi: 10.1007/s00170-010-2791-3.
- [83] K. Sajun Prasad, S. K. Panda, S. K. Kar, M. Sen, S. V. S. N. Murty, and S. C. Sharma, "Microstructures, Forming Limit and Failure Analyses of Inconel 718 Sheets for Fabrication of Aerospace Components," *J. Mater. Eng. Perform.*, vol. 26, no. 4, pp. 1513–1530, 2017, doi: 10.1007/s11665-017-2547-4.
- [84] SAE International, "AMS5832G: AEROSPACE MATERIAL SPECIFICATION - Nickel Alloy, Corrosion and Heat Resistant, Welding Wire 52.5Ni - 19Cr - 3.0Mo - 5.1Cb(Nb) - 0.90Ti - 0.50Al - 18Fe Consumable Electrode or Vacuum Induction Melted," 2020.
- [85] SAE International, "AMS4954J: AEROSPACE MATERIAL SPECIFICATION - Titanium Alloy, Welding Wire 6Al - 4V," 2009.
- [86] E. O. Ogundimu, E. T. Akinlabi, and M. F. Erinosh, "An Experimental Study on the Effect of Heat Input on the Weld Efficiency of TIG-MIG Hybrid welding of Type 304 Austenitic Stainless Steel," *J. Phys. Conf. Ser.*, vol. 1378, no. 2, 2019, doi: 10.1088/1742-6596/1378/2/022075.
- [87] J. I. Ruiz-Vela, J. J. Montes-Rodríguez, E. Rodríguez-Morales, and J. A. Toscano-Giles, "Effect of cold metal transfer and gas tungsten arc welding processes on the metallurgical and mechanical properties of Inconel® 625 weldings," *Weld. World*, vol. 63, no. 2, pp. 459–479, 2019, doi: 10.1007/s40194-018-0661-z.
- [88] J. Antony, *Design of Experiments for Engineers and Scientists*. Elsevier Science and Technology Books, 2003.
- [89] C. Schneider, C. Lisboa, R. Silva, and R. Lermen, "Optimizing the Parameters of TIG-MIG/MAG Hybrid Welding on the Geometry of Bead Welding Using the Taguchi Method," *J. Manuf. Mater. Process.*, vol. 1, no. 2, p. 14, 2017, doi: 10.3390/jmmp1020014.
- [90] N. Guo, Q. Cheng, Y. Fu, Y. Du, X. Zhang, and J. Feng, "Investigation on the mass transfer control, process stability and welding quality during underwater pulse current FCAW for Q235," *J. Manuf. Process.*, vol. 46, no. 2, pp. 317–327, 2019, doi: 10.1016/j.jmapro.2019.08.022.
- [91] V. Prajapati, Dinbandhu, J. J. Vora, S. Das, and K. Abhishek, "Study of parametric influence and welding performance optimization during regulated metal deposition (RMD™) using grey integrated with fuzzy taguchi approach," *J. Manuf. Process.*, vol. 54, no. February, pp. 286–300, 2020, doi: 10.1016/j.jmapro.2020.03.017.
- [92] D. Trietsch, "A Proposal to Apply Taguchi-Inspired Methods to the Reduction of Machining Variance," *Dept Adm. Sci. Nav. Postgrad. Sch.*, vol. NPS-AS-92-, no. September 1992, pp. 1–30, 1992.
- [93] W. H. Tarn and P. Walker, *Handbook of Metal Etchants*. CRC Press, 1991.
- [94] L. Aucott *et al.*, "Revealing internal flow behaviour in arc welding and additive manufacturing of metals," *Nat. Commun.*, vol. 9, no. 1, pp. 1–7, 2018, doi: 10.1038/s41467-018-07900-9.

- [95] Federal Aviation Administration, *FAA-H-8083-3B Airplane Flying Handbook*. 2016.
- [96] R. French and H. Marin-Reyes, "High value intelligent aerospace turbofan jet engine blade re-manufacturing system," *Adv. Intell. Syst. Comput.*, vol. 490, pp. 241–252, 2016, doi: 10.1007/978-3-319-41697-7_22.
- [97] B. Vogel-Heuser and D. Hess, "Guest Editorial Industry 4.0-Prerequisites and Visions," *IEEE Trans. Autom. Sci. Eng.*, vol. 13, no. 2, pp. 411–413, 2016, doi: 10.1109/TASE.2016.2523639.
- [98] M. Hermann, T. Pentek, and B. Otto, "Design principles for industrie 4.0 scenarios," *Proc. Annu. Hawaii Int. Conf. Syst. Sci.*, vol. 2016-March, pp. 3928–3937, 2016, doi: 10.1109/HICSS.2016.488.
- [99] Y. M. Zhang, "An analysis of welding process monitoring and control," in *Real-Time Weld Process Monitoring*, 2008, pp. 1–11.
- [100] J. Mirapeix, R. Ruiz-Lombera, J. J. Valdiande, L. Rodriguez-Cobo, F. Anabitarte, and A. Cobo, "Defect detection with CCD-spectrometer and photodiode-based arc-welding monitoring systems," *J. Mater. Process. Technol.*, vol. 211, no. 12, pp. 2132–2139, 2011, doi: 10.1016/j.jmatprotec.2011.07.011.
- [101] M. Tanaka and J. J. Lowke, "Predictions of weld pool profiles using plasma physics," *J. Phys. D. Appl. Phys.*, vol. 40, no. 1, 2007, doi: 10.1088/0022-3727/40/1/R01.
- [102] R. Kovacevic and Y. M. Zhang, "Real-Time Image Processing for Monitoring of Free Weld Pool Surface," *J. Manuf. Sci. Eng. Trans. ASME*, vol. 119, no. 2, pp. 161–169, 1997, doi: 10.1115/1.2831091.
- [103] S. C. A. Alfaro, D. de S. Mendonça, and M. S. Matos, "Emission spectrometry evaluation in arc welding monitoring system," *J. Mater. Process. Technol.*, vol. 179, no. 1–3, pp. 219–224, 2006, doi: 10.1016/j.jmatprotec.2006.03.088.
- [104] P. Kah, P. Layus, E. Hiltunen, and J. Martikainen, "Real-time weld process monitoring," *Adv. Mater. Res.*, vol. 933, no. May 2014, pp. 117–124, 2014, doi: 10.4028/www.scientific.net/AMR.933.117.
- [105] P. Zhang, L. Kong, W. Liu, J. Chen, and K. Zhou, "Real-time Monitoring of Laser Welding Based on Multiple Sensors," in *Chinese Control and Decision Conference*, 2008, pp. 1746–1748.
- [106] G. E. Cook, A. M. Strauss, D. H. Lammlein, and P. A. Fleming, "Arc sensors in weld monitoring," in *Real-Time Weld Process Monitoring*, 2008, pp. 15–44.
- [107] A. E. Öberg and F. Sikström, "Barriers for industrial implementation of in-process monitoring of weld penetration for quality control," *Int. J. Adv. Manuf. Technol.*, vol. 91, no. 5–8, pp. 2427–2434, 2017, doi: 10.1007/s00170-016-9894-4.
- [108] C. S. Wu, J. Q. Gao, and J. K. Hu, "Real-time sensing and monitoring in robotic gas metal arc welding," *Meas. Sci. Technol.*, vol. 18, no. 1, pp. 303–310, 2007, doi: 10.1088/0957-0233/18/1/037.
- [109] A. Mazlan, H. Daniyal, A. I. Mohamed, M. Ishak, and A. A. Hadi, "Monitoring the quality of welding based on welding current and ste analysis," *IOP Conf. Ser. Mater. Sci. Eng.*, vol. 257, no. 1, 2017, doi: 10.1088/1757-899X/257/1/012043.
- [110] R. Kovacevic, Y. Zhang, and L. Li, "Monitoring of Weld Joint Penetrations Based on Weld Pool

- Geometrical Appearance," *Welding Journal-Including Welding Research Supplement*, vol. 75, no. 10. pp. 317–329, 1996.
- [111] K. Pal and S. K. Pal, "Monitoring of weld penetration using arc acoustics," *Mater. Manuf. Process.*, vol. 26, no. 5, pp. 684–693, 2011, doi: 10.1080/10426910903496813.
- [112] G. M. Saeed and H. Song, "Optical sensors in welding," in *Real-Time Weld Process Monitoring*, 2008, pp. 45–73.
- [113] S. B. Chen, Y. J. Lu, L. Wu, and D. B. Zhao, "Intelligent Methodology for Sensing, Modeling and Control of Pulsed GTAW: Part I - Bead-On-Plate Welding," *Weld. Res. Suppl.*, pp. 151–163, 2000.
- [114] R. Kovacevic, Y. M. Zhang, and S. Ruan, "Sensing and control of weld pool geometry for automated GTA welding," *J. Manuf. Sci. Eng. Trans. ASME*, vol. 117, no. 2, pp. 210–222, 1995, doi: 10.1115/1.2803297.
- [115] Z. Wang, "Monitoring of GMAW weld pool from the reflected laser lines for real-time control," *IEEE Trans. Ind. Informatics*, vol. 10, no. 4, pp. 2073–2083, 2014, doi: 10.1109/TII.2014.2349360.
- [116] Y. Fujita, T. Ogawa, S. Asai, S. Yamamoto, T. Ohdake, and M. Ochiai, "Development of a welding monitoring system for in-process quality control of thick walled pipe," *Weld. World*, vol. 56, no. 11–12, pp. 15–25, 2012, doi: 10.1007/BF03321391.
- [117] B. M. Abdullah, J. S. Smith, W. Lucas, J. Lucas, and F. Malek, "Monitoring of TIG welding using laser and diode illumination sources: A comparison study," *2008 Int. Conf. Electron. Des. ICED 2008*, pp. 4–7, 2008, doi: 10.1109/ICED.2008.4786739.
- [118] U. Sreedhar, C. V. Krishnamurthy, K. Balasubramaniam, V. D. Raghupathy, and S. Ravisankar, "Automatic defect identification using thermal image analysis for online weld quality monitoring," *J. Mater. Process. Technol.*, vol. 212, no. 7, pp. 1557–1566, 2012, doi: 10.1016/j.jmatprotec.2012.03.002.
- [119] H. Yang, H. C. Wickle, S. Nagarajan, M. Johnson, P. Banerjee, and B. A. Chin, "Infrared sensors in welding," in *Real-Time Weld Process Monitoring*, 2008, pp. 74–103.
- [120] S. Unnikrishnakurup, C. V. Krishnamurthy, and K. Balasubramaniam, "Monitorowanie spawania z nietopliwą elektrodą wolframową w osłonie gazów obojętnych z użyciem termografii – symulacje i eksperymenty," *Prz. Elektrotechniczny*, vol. 92, no. 4, pp. 6–9, 2016, doi: 10.15199/48.2016.04.02.
- [121] P. Yu, G. Xu, X. Gu, G. Zhou, and Y. Tian, "A low-cost infrared sensing system for monitoring the MIG welding process," *Int. J. Adv. Manuf. Technol.*, vol. 92, no. 9–12, pp. 4031–4038, 2017, doi: 10.1007/s00170-017-0515-7.
- [122] S. Nagarajan, W. Chen H., and B. A. Chin, "Infrared sensing for adaptive arc welding," *Weld. J.*, vol. 68, no. 11, pp. 462–466, 1989.
- [123] S. M. Govardhan, H. C. Wickle, S. Nagarajan, and B. A. Chin, "Real-time welding process control using infrared sensing," *Proc. Am. Control Conf.*, vol. 3, pp. 1712–1716, 1995, doi: 10.1109/acc.1995.529801.
- [124] C. Kim, M. Kim, and K. Kim, "Size variation monitoring of an extended thermal radiation source by chromatic filtering," *Opt. Commun.*, vol. 152, no. July, pp. 239–242, 1998, doi:

- 10.1016/S0030-4018(98)00185-0.
- [125] B. A. Chin and W. Chen, "Monitoring joint penetration using infrared sensing techniques," *Weld. J.*, vol. 69, no. 4, pp. 181s-185s, 1990.
- [126] W. E. Lukens and R. A. Morris, "Infrared Temperature Sensing of Cooling Rates for Arc Welding Control.," *Weld. J. (Miami, Fla)*, vol. 61, no. 1, pp. 27–33, 1982.
- [127] C. H. Llanos, R. H. Hurtado, and S. C. A. Alfaro, "FPGA-based approach for change detection in GTAW welding process," *J. Brazilian Soc. Mech. Sci. Eng.*, vol. 38, no. 3, pp. 913–929, 2016, doi: 10.1007/s40430-015-0371-z.
- [128] J. Shao and Y. Yan, "Ultrasonic sensors in welding," in *Real-Time Weld Process Monitoring*, 2008, pp. 104–128.
- [129] I. J. Stares, C. Duffil, J. A. Ogilvy, and C. B. Scruby, "On-line weld pool monitoring and defect detection using ultrasonic," *NDT Int.*, vol. 23, no. 4, pp. 195–200, 1990, doi: 10.1016/0308-9126(90)91601-O.
- [130] M. Miller, B. Mi, A. Kita, and I. C. Ume, "Development of automated real-time data acquisition system for robotic weld quality monitoring," *Mechatronics*, vol. 12, no. 9–10, pp. 1259–1269, 2002, doi: 10.1016/S0957-4158(02)00028-4.
- [131] B. Mi and C. Ume, "Real-time weld penetration depth monitoring with laser ultrasonic sensing system," *J. Manuf. Sci. Eng. Trans. ASME*, vol. 128, no. 1, pp. 280–286, 2006, doi: 10.1115/1.2137747.
- [132] W. P. Regalado, A. M. Chertov, and R. G. Maev, "Real time ultrasonic aluminum spot weld monitoring system," *AIP Conf. Proc.*, vol. 1211, pp. 1152–1158, 2010, doi: 10.1063/1.3362181.
- [133] A. F. Andreoli, A. M. Chertov, and R. G. Maev, "Correlação entre teste de destacamento e teste ultrassônico em tempo real para diagnóstico da qualidade em soldagem a ponto," *Soldag. e Insp.*, vol. 21, no. 3, pp. 282–289, 2016, doi: 10.1590/0104-9224/SI2103.04.
- [134] A. Ancona, P. M. Lugarà, F. Ottonelli, and I. M. Catalano, "A sensing torch for on-line monitoring of the gas tungsten arc welding process of steel pipes," *Meas. Sci. Technol.*, vol. 15, no. 12, pp. 2412–2418, 2004, doi: 10.1088/0957-0233/15/12/010.
- [135] Z. Zhang, H. Yu, N. Lv, and S. Chen, "Real-time defect detection in pulsed GTAW of Al alloys through on-line spectroscopy," *J. Mater. Process. Technol.*, vol. 213, no. 7, pp. 1146–1156, 2013, doi: 10.1016/j.jmatprotec.2013.01.012.
- [136] J. F. Wang, H. D. Yu, Y. Z. Qian, R. Z. Yang, and S. B. Chen, "Feature extraction in welding penetration monitoring with arc sound signals," *Proc. Inst. Mech. Eng. Part B J. Eng. Manuf.*, vol. 225, no. 9, pp. 1683–1691, 2011, doi: 10.1177/0954405411405108.
- [137] J. W. Elmer, J. Wong, M. Fröba, P. A. Waide, and E. M. Larson, "Analysis of heat-affected zone phase transformations using in situ spatially resolved X-ray diffraction with synchrotron radiation," *Metall. Mater. Trans. A Phys. Metall. Mater. Sci.*, vol. 27, no. 3, pp. 775–783, 1996, doi: 10.1007/BF02648965.
- [138] J. W. Elmer, T. A. Palmer, and J. Wong, "In situ observations of phase transitions in Ti-6Al-4V alloy welds using spatially resolved x-ray diffraction," *J. Appl. Phys.*, vol. 93, no. 4, pp. 1941–1947, 2003, doi: 10.1063/1.1537464.

- [139] J. W. Elmer and T. A. Palmer, "In-Situ Monitoring Of Phase Transformations During Welding Of Steels Using Synchrotron-Based X-Ray Diffraction Techniques," *Proc. IMECE04 2004 ASME Int. Mech. Eng. Congr. Expo.*, pp. 1–10, 2004.
- [140] J. W. Elmer, T. A. Palmer, W. Zhang, and T. DebRoy, "Advanced techniques for in-situ monitoring of phase transformations during welding using synchrotron-based x-ray diffraction," *ASM Proc. Int. Conf. Trends Weld. Res.*, vol. 2005, pp. 901–910, 2005.
- [141] S. I. Rokhlin, A. C. Guu, and K. Cho, "Closed-Loop Radiographic Process Control of ARC Welding," *Rev. Prog. Quant. Nondestruct. Eval.*, pp. 2173–2180, 1989, doi: 10.1007/978-1-4613-0817-1_276.
- [142] A. C. Guu and S. I. Rokhlin, "Computerized radiographic weld penetration control with feedback on weld pool depression," *Mater. Eval.*, vol. 47, no. 10, pp. 1204–1210, 1989, doi: 10.1016/0963-8695(96)84922-x.
- [143] A. C. Guu and S. I. Rokhlin, "REAL-TIME RADIOGRAPHIC INVESTIGATION OF WELD POOL DEPRESSION," *Rev. Prog. Quant. Nondestruct. Eval.*, vol. 10B, pp. 2209–2216, 1991.
- [144] S. ROKHLIN and A. GUU, "A study of arc force, pool depression, and weld penetration during gas tungsten arc welding," *Weld. Journal(USA)*, vol. 72, no. 8, p. 381, 1993.
- [145] "Subaru welding fail means brand-new cars need to be repaired or replaced," *NBC News*. [Online]. Available: <https://www.nbcnews.com/business/autos/subaru-welding-fail-means-thousands-new-cars-are-headed-scrap-n1030316>. [Accessed: 20-Dec-2020].
- [146] Q. Wu, X. Yang, and Q. Zhou, "Pattern Recognition and Its Application in Fault Diagnosis of Electromechanical System," *J. Inf. Comput. Sci.*, vol. 9, no. 8, pp. 2221–2228, 2012.
- [147] "ExtraTreesClassifier Documentation." [Online]. Available: <https://scikit-learn.org/stable/modules/generated/sklearn.ensemble.ExtraTreesClassifier.html>. [Accessed: 15-Nov-2020].
- [148] "RandomForestClassifier Documentation." [Online]. Available: <https://scikit-learn.org/stable/modules/generated/sklearn.ensemble.RandomForestClassifier.html>. [Accessed: 15-Nov-2020].
- [149] "Ensemble Methods." [Online]. Available: <https://scikit-learn.org/stable/modules/ensemble.html>. [Accessed: 15-Nov-2020].
- [150] R. Dawkins and J. R. Krebs, "Arms races between and within species," *Proc. R. Soc. London - Biol. Sci.*, vol. 205, no. 1161, pp. 489–511, 1979, doi: 10.1098/rspb.1979.0081.
- [151] L. Carroll, *Through the Looking-Glass*, The Millen. Project Gutenberg, 1871.
- [152] R. Geissbauer, S. Eddy, B. Jaruzelski, and M. Mueller, "New strategies for IoT investment," 2018.
- [153] PWC, "2016 Global Industry 4.0 Survey," 2016.
- [154] "MillerWelds." [Online]. Available: <http://www.millerwelds.com>. [Accessed: 09-Jan-2019].
- [155] E. Helmut, B. Jürgen, and P. Gerhard, "Industry 4.0 in Welding," 2018.
- [156] "Fronius." [Online]. Available: <http://www.fronius.com/en/>. [Accessed: 08-Jan-2019].

- [157] "EWM Welding 4.0." [Online]. Available: <https://www.ewm-group.com/en/innovation-research/welding-4-0.html>. [Accessed: 06-Apr-2019].
- [158] K. Zhou, X. Li, Z. Xia, X. Cui, and S. Wang, "A platform design of networked service in industrial robot welding," *Proc. - 2016 9th Int. Congr. Image Signal Process. Biomed. Eng. Informatics, CISP-BMEI 2016*, pp. 1892–1896, 2017, doi: 10.1109/CISP-BMEI.2016.7853026.
- [159] A. G. Dharmawan, A. A. Vibhute, S. Foong, G. S. Soh, and K. Otto, "A survey of platform designs for portable robotic welding in large scale structures," *2014 13th Int. Conf. Control Autom. Robot. Vision, ICARCV 2014*, pp. 1683–1688, 2014, doi: 10.1109/ICARCV.2014.7064569.
- [160] "Soldamatic." [Online]. Available: <http://www.soldamatic.com/>. [Accessed: 05-Apr-2019].
- [161] "Lincoln Electric." [Online]. Available: www.lincolnelectric.com. [Accessed: 05-Apr-2019].
- [162] British Standards Institution, "BSI Standards Publication: Specification for Carbon and low alloy steel pressure vessels for primary circuits of nuclear reactors - BS 3915:1965," 1965.

Appendix A: The Need for Process Monitoring in In-Space Manufacturing

A.1 Introduction

In-space manufacturing, as the name suggests, refers to the production of goods by means of labour, machining and chemical and biological processes, outside of the atmosphere of the earth. As no clear boundary exist as of where the edge of space starts, Earth's Kármán line which lies 100 km above sea level will be used as point of reference in this article. Therefore, in-space manufacturing may include production and manufacturing of goods from as low as Low Earth Orbit – where conditions of microgravity and outer space vacuum (hard vacuum) exist – up to the surface of other celestial bodies – where gravity and atmospheres do exist.

In the present article, a brief history of in-space manufacturing is presented in Section A.2, alongside with examples and the benefits of utilizing manufacturing in space. The need for process monitoring and its applications in in-space manufacturing processes are highlighted in Section A.3, where the current state of process monitoring in additive manufacturing is presented in Section A.4.

A.2 In-Space Manufacturing

The idea of in-space manufacturing precedes spaceflight itself, with the most notable example the Wernher von Braun's technical book *Das Marsprojekt* (The Mars Project), where he envisioned a fleet of enormous spaceships being manufactured in orbit using materials supplied from earth via reusable space shuttles [A1].

The first manufacturing experiments that were performed in space, were carried out on 16th October 1969 by cosmonaut Valery Kubasov onboard Soyuz 6, during the ambitious "Troika" flight [A2]. The experiment involved a welding unit named "Vulkan" that was prepared by scientists at the Paton Institute and was composed of three welding processes: low-pressure compressed arc, electron beam and fusible electrode; carried out in vacuum conditions. The experiments were designed on the assumption that constructing future space stations would require mastering the art of in-space welding and was reported that only the electron beam welding was a complete success [A3].

A few years later, between May 1973 and February 1974, a series of manufacturing experiments were carried out onboard Skylab space station including metal melting, exothermic brazing and electron beam welding, as well as investigations of solidification phenomena on sphere forming and gallium-arsenide crystal growth [A4].

On 25th July 1984, during the Salyut 7 – EP4 expedition, cosmonauts Svetlana Savitskaya and Vladimir Dzhanibekov performed welding, cutting, soldering and spraying experiments during an extravehicular activity (EVA) outside of the Salyut 7 space station [A5].

Numerous manufacturing and materials science experiments were carried out afterwards, both on standalone flights (e.g. Spacelab, Wake Shield Facility) and space stations (e.g. Mir, ISS). The more recent experiments are focusing on the emerging field of additive manufacturing (also known as 3D printing), where parts are manufactured layer by layer, enabling the creation of shapes and forms that traditional manufacturing processes cannot deliver. On 24th November 2014, the first part was 3D-printed in space using the Made In Space's Zero-G printer [A6]. In March 2016, Made In Space's second

3D printer named Additive Manufacturing Facility (AMF) was launched to the ISS and has printed more than 200 tools and parts to date [A7].

A.2.1 Benefits of in-space manufacturing

Manufacturing goods, materials and parts in space can be beneficial due to a variety of factors. At first, dimension limitations related to the cargo volume allowed in a launcher, require compact size-restricted spacecraft and parts. By manufacturing the final product in space using materials supplied either from earth or another source, the ability to create massive superstructures previously unavailable can be achieved. An experimental work done by Grumman Aerospace in the late 1970s, had a Space Fabrication Demonstration System (named “Beam Builder (B2)”) built and successfully tested in the underwater EVA simulator at Marshall Space Flight Centre. Though the automated machine was never flown to space, it demonstrated the ability to generate beams from aluminium rolls, by bending and welding them with cross braces [A8].

The microgravity environment experienced away from Earth’s atmosphere allows manufacturing of materials not possible done before. Different physics applied to the crystal growth, heat transfer mechanisms and liquids’ surface tension that unlocks endless possibilities for new materials, spanning from bulk metallic glasses [A9], to fiber optics with lower insertion loss [A10] and 3D DNA Origami crystals [A11]. In fact there are currently more than 25 companies, from major multinational organisations to newly formed start-ups, who are actively working towards utilizing space’s microgravity environment for commercial manufacturing [A12].

Space’s extreme conditions, namely the high temperature difference between shades and sun-lighted areas and the hard vacuum, allow a variety of tasks to be carried out simultaneously in the same place, something troublesome if carried out on Earth. Additional to this, operations with potential hazards can be carried out with fewer precautions than on Earth, provided they lie within the applicable international space laws.

On-demand manufacturing, a term referring to the ability of producing single customised products only when they are needed, is enabled in space with the current developments in additive manufacturing. Success of long-term space missions, as well as operations of current and future space stations, are heavily relied on sufficient spare parts inventory, to deal with both emergency and routine repairs. The ability to produce spare parts and tools while in orbit, providing to the facility only the raw material, reduces dramatically the launch costs in terms of both fuel and volume.

In-situ resource utilization (ISRU) refers to the practice of collecting and utilizing materials on other celestial bodies, such as asteroids, natural satellites and other planetary surfaces. Proposed scenarios for humans returning to the Moon and going to Mars, are heavily depending on the ability to utilize the local resources, both for the construction of habitats and facilities, as well as for the production of oxygen, water and fuel. For example, in the Mars Direct mission concept, the Earth Return Vehicle (ERV) is equipped with a chemical plant that harnesses the carbon dioxide gas (CO₂) from Mars’ atmosphere and combines it with liquid hydrogen (H₂) brought from Earth to produce methane (CH₄) – that can be used as fuel – and water (H₂O), through a process called methanation (Sabatier reaction) [A13].

A.2.2 Manufacturing product verification

When products are manufactured on Earth, they undergo a series of tests that contribute to the process quality assurance and quality control output, to match the corresponding industrial standards. These tests may include destructive testing of randomly selected samples from a yield of products, as well as a series of non-destructive testing where applicable and needed. Especially in industries like aerospace, where each manufacturing component is marked as critical and human lives as well as millions of dollars' worth of equipment rely on it, the non-destructive quality assurance tests are rigorous and mandatory. However, when the product is to be in-space manufactured, the lack of bulky and advanced equipment due to size limitations, alongside the lack of personnel (either on a standalone machine – as the Mars Direct ERV plant described above – or crew time constraints), these quality assurance tests cannot be performed prior to the products use. This way of qualification and certification, described during NASA's Small Business Innovation Research 2018 Phase I Solicitation as "traditional", can be replaced with online quality control, where an automated qualification process is superimposed in-situ to the original process to ensure the quality of the outcome [A14]. This qualification process can be composed of condition and process monitoring, in-line metrology as well as post-process inspection and verification methods.

A.3 Process Monitoring

Process monitoring can be defined as the simultaneous measuring of the input parameters and additional factors that contribute to the quality of the process' outcome. A simplified example of such process is welding, where current, voltage, shielding gas and travel speed are the input parameters and material composition and groove shape are additional factors that influence the quality of the weld [A15]. By monitoring these aforementioned parameters and factors, direct correlation to the process output can be established, therefore enabling a quality prediction and assurance by means of monitoring.

A huge variety of different techniques and technologies can be implemented, depending of the nature of the process. Optical metrology systems, acoustic and ultrasonic emissions sensors, vibration sensing, temperature recorders, infrared thermographs and x-ray detectors are some of the sensors and systems implemented for quality assurance through process monitoring.

A.3.1 Process Monitoring in In-Space Manufacturing

As described in Section A.2, the benefits of in-space manufacturing are enabling manufacturing techniques and ISRU previously unavailable. It is however very challenging to ensure the process' quality through in-situ monitoring. In fact, the European Space Agency (ESA) alongside UK-based company Metalysis, launched in 2018 their Grand Challenge, offering €500,000 to the successful participant who can implement process monitoring on electrochemical cells aimed to be used for ISRU [A16]. Metalysis' cells are converting refined oxides and ores that will be extracted from celestial bodies, into metal alloy powders that can be used in additive manufacturing for aerospace applications.

A similar ISRU system, though for different application, unofficially named "dust-to-thrust factory" is being developed by the Swamp Works Lab at NASA's John F. Kennedy [A17]. A combination of a Sabatier reactor, heating ovens and mining rovers called RASSOR, the system has demonstrated on Earth the ability to extract water from regolith mockup, electrolyze it into H₂ and O₂, collect CO₂ from the atmosphere and produce methane fuel. However, if this system is to be deployed on Mars, a whole new level of autonomy needs to be achieved, and the means to do it is through process monitoring.

The need for process monitoring on an ISRU system has also been highlighted by AI SpaceFactory, the winner of the NASA's 3D Printed Habitat Challenge. Earlier in 2019, AI SpaceFactory was awarded \$500,000 by NASA for the construction of their 15-foot tall 3D-printed Mars habitat prototype named MARSHA [A18]. While their prize was awarded based on the most autonomous process throughout the contestants, they had to manually intervene several times and change process parameters and robot-path directions. In their own words "3D-printed construction is far from a fully autonomous process and requires human eyes on the print, practice, and improvisation" [A19]. It is therefore a necessity for a process monitoring system to be developed, with the ability to feedback the necessary adjustments.

Similarly, process monitoring becomes a necessity on in-orbit construction and fabrication of large-sized structures. Two conceptual projects are presented here, SpiderFab and Archinaut, which are exploring the feasibility of assembling large, hundred-meters-to- kilometers-sized structures in orbit.

Archinaut, a project carried out by a collaboration between Made In Space, Inc, Northrop Grumman Corporation and Oceaneering International, Inc, is developing additive manufacturing technologies for construction of large structures in space [A20]. Initially the project is aiming on constructing antenna reflectors and fabricating solar arrays for satellites. Future expansions may include additional robotic arms for the decommissioning and recycling of decaying satellites.

Similarly, by combining additive manufacturing technologies with robotic assembly technologies, the SpiderFab effort by Tethers Unlimited, Inc demonstrated conceptual implementation of in-orbit fabrication of both support trusses for large solar arrays and spacecraft components such as antenna reflectors [A21]. Accurate measurements were found to be essential to the success of such fabrications, therefore metrology techniques need to be implemented in two scales: macro-scale metrology, for assuring that the overall shape will meet the system's requirements, and micro-scale metrology, for enabling accurate positioning of material feeders in respect to the material substrate. Stereo-optic imagers, structured-light mapping and Light Detection and Ranging (LIDAR) technologies were proposed as solutions, where a structured light scanner was used as proof-of-concept.

A.4 Additive Manufacturing and Process Monitoring

As mentioned in Section 2, additive manufacturing, (also known as direct manufacturing, 3D-printing or rapid prototyping) is the manufacturing of parts direct from a CAD model, by the successive addition of material layer-by-layer. Though the concept of additive manufacturing dates back to the 1970s, the process became more popular in the 2000s, with a lot of research currently ongoing in the field.

The flexibility and benefits that additive manufacturing is providing, notably the ability to create lighter components using structures previously unable to be produced through subtractive manufacturing, has attracted interest from aerospace companies, where weight reductions result in significant savings. The first 3D-printed parts in an operational spacecraft was flown to space on August 5th, 2011, onboard NASA's Juno space probe [A8]. These waveguide brackets, parts of the spacecraft's microwave communications system, were manufactured by Lockheed Martin and were installed on the spacecraft during its assembly.

Since then a variety of components and parts are implemented in space missions and launchers. A notable example is Relativity Space's 3D-printer named Stargate, a selective laser sintering system

which is regarded the largest metal 3D-printer in the world. The company aims in producing at least 95% of their launcher, inclusive of the engines, via additive manufacturing [A22].

However, the aforementioned manufactured parts are all produced on Earth, where again, they undergo extensive quality testing prior their installation and use in space. Moving a metal additive manufacturing facility in space requires overcoming of significant challenges. The Committee on Space-Based Additive Manufacturing by the National Academy of Sciences, highlighted in their report “3D Printing in Space” these challenges, which include among others considerations of the microgravity, vacuum and thermal environment, platform stability, infrastructure and support facilities, autonomy and lack of human presence, communication and data telemetry, and quality verification and validation [A8]. A dynamic system control based on process monitoring through a variety of sensors can aid in overcoming some of these barriers, increasing autonomy and ensuring final product quality.

Under the context of Industry 4.0, the driving force of the ongoing fourth industrial revolution, a variety of sensors are implemented in every step of a manufacturing process, recording data and generating digital twins. This unison of cyber-physical systems enables process optimization, better asset utilization, information transparency and decentralized decisions through interconnection. This interconnection is achieved via the Industrial Internet of things (IIoT), where the modular components of separate systems in a manufacturing facility are connected to a local network, which is subsequently connected to the Internet and the cloud. The abundance of collected industrial data leads to subsequent complex data analysis from where information are extracted and shared to respected stakeholders and subsystems, enabling actions previously unavailable.

Additive manufacturing processes are heavily influenced by this digitization, with ongoing research on monitoring technologies that can result in closed-loop systems, which in turn will result in completely autonomous systems. A variety of monitoring technologies and sensors have emerged, with some products already commercialized and available for implementation. Optical systems have been developed for processes like direct energy deposition, electron beam melting, and laser powder bed fusion. These systems have been tested on materials used in the aerospace industry, including stainless steel, titanium and nickel alloys. However, variations in the powder chemistry and particle size distribution due to the lack of certified materials measurement methods prohibits a universal feedback mechanism that allows real-time adjustments [A23].

- ARCAM LayerCam is used for quality assurance, detecting defects by measuring the porosity layer-by-layer [A24].
- QM Meltpool 3D combines a camera with a photodiode, allowing simultaneous monitoring of the meltpool intensity and measuring of the meltpool area. The systems can be linked as feedback signal to alter the laser power [A25].
- EOSTATE MeltPool similarly measures the meltpool area, where hardware separates the reflected light from the process light and software creates 2D and 3D representations, highlighting abnormalities that may occur through the process [A26].
- PrintRite3D is another multi-sensor monitoring system where thermal energy density is combined with geometrical meltpool data measured in-situ to generate reports based on data analytics and quality metrics. It is reported that further advances of the system are under ongoing development for a closed-loop control [A27].

Further to the above commercialized solutions, ongoing research involves acoustic emissions signals that detect crack propagation signals and calculate the time and location of the cracks [A23], as well as built-height and depth measurements by means of inline coherent imaging and high-speed CCD cameras [A28].

It is worth highlighting that while a lot of sensing technologies can provide invaluable information related to the product quality, the analysis of these information is of uttermost importance, as the analytics techniques used might not reveal an existing flaw. Multiple signal analyses combining features extracted from both the time and the frequency domains may reveal a more detailed representation. However, sampling rates, processing power capabilities, time restrictions and data handling should be considered, alongside bandwidth limitations by the system's architecture.

A.5 Conclusion

In-space manufacturing is essential to the success of long-term space missions, as it allows the fabrication of large structures in space and the ability to create essential parts on demand, options previously unavailable. Additionally, it enables the application of in-situ resource utilization, upon which future manned exploration missions are heavily depending. In order to ensure the quality of a manufacturing process in space, process monitoring implementation is essential. While conceptual developments of monitoring systems are being implemented in current studies related to future in-space manufacturing projects, completely autonomous systems of additive manufacturing are still not available. Commercial process monitoring equipment is readily available, however, the complexity of the processes and the variations in both applications and materials hamper the development of closed-loop control systems.

References (Appendix A)

- [A1] W. von Braun, *The Mars Project* (2nd ed.), University of Illinois Press, 1991 [1952], ISBN 978-0-252-06227-8.
- [A2] C. Burgess, R. Hall, "The First Soviet Cosmonaut Team", Springer-Praxis, 2009, ISBN 978-0-387-84823-5.
- [A3] "SALYUT: Soviet Steps Toward Permanent Human Presence in Space—A Technical Memorandum", Washington, D.C.: U.S. Congress, Office of Technology Assessment, OTATM-STI-14, December 1983.
- [A4] R.W. Newkirk, I.D. Ertel, C.G. Brooks, *Skylab – A Chronology*, NASA, 1977.
- [A5] American Welding Society, "Welding in Space", 22 July 2015, <https://awo.aws.org/2015/07/welding-in-space/>, (accessed 05/10/19).
- [A6] Made In Space, "History", <https://madeinspace.us/about/#timeline>, (accessed 05/10/19).
- [A7] Made In Space, "Additive Manufacturing in Space", <https://madeinspace.us/capabilities-and-technology/additive-manufacturing-facility/>, (accessed 05/10/19).
- [A8] Committee on Space-Based Additive Manufacturing, "3D Printing in Space", The National Academy Press, 2014, ISBN 978-0-309-31008-6.
- [A9] D.C. Hofmann, S.N Roberts, "Microgravity metal processing: from undercooled liquids to bulk metallic glasses", *npj Microgravity*, 2015; doi: 10.1038/npjmgrav.2015.3.
- [A10] D. Starodubov, K. McCormick, M. Delloso, E. Erdelyi, L. Volfson, "Facility for orbital material processing," *Proc. SPIE 10641, Sensors and Systems for Space Applications XI*, 106410T (2 May 2018); doi: 10.1117/12.2305830.
- [A11] DNA Origami, <https://space-origami.com/>, (accessed 05/10/19).

- [A12] Factories in space, <https://www.factoriesinspace.com/manufacturing-companies>, (accessed 05/10/19).
- [A13] R. Zubrin, "The Case for Mars", Simon & Schuster, 1996, ISBN: 9780684819303.
- [A14] NASA SBIR 2018 Phase I Solicitation, H7.02, "In-situ monitoring and development of in-process quality control for in-space manufacturing (ISM) applications", 2018.
- [A15] M. Benakis, C. Du, A. Patran, R. French, "Welding process monitoring applications and industry 4.0.", in: 2019 IEEE 15th International Conference on Automation Science and Engineering (CASE). 22-26 Aug 2019, Vancouver, BC, Canada. Institute of Electrical and Electronics Engineers (IEEE).
- [A16] ESA Grand Challenge, "Metalysis—ESA Grand Challenge launched", 26 July 2018, https://www.esa.int/About_Us/Business_with_ESA/ESA_Grand_Challenge/Metalysis_ESA_Grand_Challenge_launched, (accessed 05/10/19).
- [A17] K.W. Leucht, "From Dust to Thrust", IEEE Spectrum, 11.18, pp. 32-37, 2018.
- [A18] R. Parikh, "AI SpaceFactory wins NASA's 3D Printed Habitat Challenge", 06 May 2019, <https://www.aispacefactory.com/post/ai-spacefactory-wins-1st-place-prize-for-nasa-3d-printing-habitat-challenge>, (accessed 05/10/19).
- [A19] D. Malott, "So how autonomous is 3D printed construction, really?", 20 May 2019, <https://www.aispacefactory.com/post/so-how-autonomous-is-3d-printed-construction-really>, (accessed 05/10/19).
- [A20] Project Archinaut, www.projectarchinaut.com, (accessed 05/10/19).
- [A21] R. Hyot, J. Cushing, J. Slostad, "SpiderFab: Process for On-Orbit Construction of KilometerScale Apertures", Final Report, NASA, 2013.
- [A22] D. Mosher, "Defectors from SpaceX, Blue Origin, and Tesla are developing a remarkable technology called 'Stargate' to help colonize other planets", <https://www.businessinsider.com/relativity-space-3d-printed-rockets-mars-2018-10>, (accessed 05/10/19).
- [A23] Q.Y. Lu, C.H. Wong, "Additive manufacturing process monitoring and control by non-destructive testing techniques: challenges and in-process monitoring", Virtual and Physical Prototyping, 13:2, 39-48, 2018. doi: 10.1080/17452759.2017.1351201.
- [A24] Arcam EBM, "Arcam Validation Tools", <http://www.arcam.com/technology/electron-beam-melting/process-validation-tools/>, (accessed 05/10/19).
- [A25] ConceptLaser, "QM Meltpool 3D", <https://www.concept-laser.de/en/products/quality-management.html>, (accessed 05/10/19).
- [A26] EOS, "EOSTATE MeltPool: Real-time process monitoring for EOS M 290" <https://www.eos.info/software/monitoring-software/meltpool-monitoring>, (accessed 05/10/19).
- [A27] Sigma Labs, "PrintRite3D: In-Process Control and Quality Assurance Software for Additive Manufacturing, <https://sigmalabsinc.com/products/>, (accessed 05/10/19).
- [A28] S.K. Everton, M. Hirsch, P. Stravroulakis, R.K. Leach, A.T. Clare, "Review of in-situ process monitoring and in-situ metrology for metal additive manufacturing", Materials & Design, Volume 95, 2016, Pages 431-445, ISSN 0264-1275, doi:10.1016/j.matdes.2016.01.099.